

Advances

in Clinical and Experimental Medicine

MONTHLY ISSN 1899-5276 (PRINT) ISSN 2451-2680 (ONLINE)

advances.umw.edu.pl

2024, Vol. 33, No. 9 (September)

Impact Factor (IF) – 2.1
Ministry of Science and Higher Education – 70 pts
Index Copernicus (ICV) – 171.00 pts



WROCLAW
MEDICAL UNIVERSITY

Advances
in Clinical and Experimental
Medicine



Advances in Clinical and Experimental Medicine

ISSN 1899-5276 (PRINT)

ISSN 2451-2680 (ONLINE)

advances.umw.edu.pl

MONTHLY 2024
Vol. 33, No. 9
(September)

Advances in Clinical and Experimental Medicine (*Adv Clin Exp Med*) publishes high-quality original articles, research-in-progress, research letters and systematic reviews and meta-analyses of recognized scientists that deal with all clinical and experimental medicine.

Editorial Office

ul. Marcinkowskiego 2–6
50-368 Wrocław, Poland
Tel.: +48 71 784 12 05
E-mail: redakcja@umw.edu.pl

Editor-in-Chief

Prof. Donata Kurpas

Deputy Editor

Prof. Wojciech Kosmala

Managing Editor

Marek Misiak, MA

Statistical Editors

Wojciech Bombała, MSc

Łucja Janek, MSc

Anna Kopszak, MSc

Dr. Krzysztof Kujawa

Jakub Wronowicz, MSc

Manuscript editing

Marek Misiak, MA

Paulina Piątkowska, MA

Publisher

Wrocław Medical University
Wybrzeże L. Pasteura 1
50-367 Wrocław, Poland

Online edition is the original version
of the journal

Scientific Committee

Prof. Sandra Maria Barbalho

Prof. Antonio Cano

Prof. Chong Chen

Prof. Breno Diniz

Prof. Erwan Donal

Prof. Chris Fox

Prof. Yuko Hakamata

Prof. Carol Holland

Prof. Sabine Bährer-Kohler

Prof. Markku Kurkinen

Prof. Christos Lionis

Prof. Raimundo Mateos

Prof. Zbigniew W. Raś

Prof. Jerzy W. Rozenblit

Prof. Silvina Santana

Prof. Sajee Sattayut

Prof. James Sharman

Prof. Jamil Shibli

Prof. Michał J. Toborek

Prof. László Vécsei

Prof. Cristiana Vitale

Prof. Hao Zhang

Section Editors

Basic Sciences

Prof. Iwona Bil-Lula

Prof. Bartosz Kempisty

Dr. Wiesława Kranc

Dr. Anna Lebedeva

Clinical Anatomy, Legal Medicine, Innovative Technologies

Prof. Rafael Boscolo-Berto

Dentistry

Prof. Marzena Dominiak

Prof. Tomasz Gedrange

Prof. Jamil Shibli

Laser Dentistry

Assoc. Prof. Kinga Grzech-Leśniak

Dermatology

Prof. Jacek Szepietowski

Emergency Medicine, Innovative Technologies

Prof. Jacek Smereka

Gynecology and Obstetrics

Prof. Olimpia Sipak-Szmigiel

Histology and Embryology

Dr. Mateusz Olbromski

Internal Medicine

Angiology

Dr. Angelika Chachaj

Cardiology

Prof. Wojciech Kosmala

Dr. Daniel Morris

Endocrinology

Prof. Marek Bolanowski

Gastroenterology

Assoc. Prof. Katarzyna Neubauer

Hematology

Prof. Andrzej Deptała
Prof. Dariusz Wołowicz

Nephrology and Transplantology

Prof. Mirosław Banasik
Prof. Krzysztof Letachowicz

Pulmonology

Prof. Anna Brzecka

Microbiology

Prof. Marzenna Bartoszewicz
Assoc. Prof. Adam Junka

Molecular Biology

Dr. Monika Bielecka

Neurology

Assoc. Prof. Magdalena Koszewicz
Assoc. Prof. Anna Pokryszko-Dragan
Dr. Masaru Tanaka

Neuroscience

Dr. Simone Battaglia
Dr. Francesco Di Gregorio

Oncology

Prof. Andrzej Deptała
Prof. Adam Maciejczyk
Prof. Hao Zhang

Gynecological Oncology

Dr. Marcin Jędryka

Ophthalmology

Dr. Małgorzata Gajdzis

Orthopedics

Prof. Paweł Reichert

Otolaryngology

Assoc. Prof. Tomasz Zatoński

Pediatrics

Pediatrics, Metabolic Pediatrics, Clinical Genetics, Neonatology, Rare Disorders

Prof. Robert Śmigiel

Pediatric Nephrology

Prof. Katarzyna Kiliś-Pstrusińska

Pediatric Oncology and Hematology

Assoc. Prof. Marek Ussowicz

Pharmaceutical Sciences

Assoc. Prof. Marta Kepinska
Prof. Adam Matkowski

Pharmacoeconomics, Rheumatology

Dr. Sylwia Szafraniec-Buryło

Psychiatry

Dr. Melike Küçükkarapınar
Prof. Jerzy Leszek
Assoc. Prof. Bartłomiej Stańczykiewicz

Public Health

Prof. Monika Sawhney
Prof. Izabella Uchmanowicz

Qualitative Studies, Quality of Care

Prof. Ludmiła Marcinowicz

Radiology

Prof. Marek Szaśiadek
Prof. Paweł Gać

Rehabilitation

Dr. Elżbieta Rajkowska-Labon

Surgery

Assoc. Prof. Mariusz Chabowski
Assoc. Prof. Mirosław Kozłowski
Prof. Renata Taboła

Telemedicine, Geriatrics, Multimorbidity

Assoc. Prof. Maria Magdalena
Bujnowska-Fedak

Editorial Policy

Advances in Clinical and Experimental Medicine (Adv Clin Exp Med) is an independent multidisciplinary forum for exchange of scientific and clinical information, publishing original research and news encompassing all aspects of medicine, including molecular biology, biochemistry, genetics, biotechnology and other areas. During the review process, the Editorial Board conforms to the "Uniform Requirements for Manuscripts Submitted to Biomedical Journals: Writing and Editing for Biomedical Publication" approved by the International Committee of Medical Journal Editors (www.ICMJE.org). The journal publishes (in English only) original papers and reviews. Short works considered original, novel and significant are given priority. Experimental studies must include a statement that the experimental protocol and informed consent procedure were in compliance with the Helsinki Convention and were approved by an ethics committee.

For all subscription-related queries please contact our Editorial Office: redakcja@umw.edu.pl
For more information visit the journal's website: advances.umw.edu.pl

Pursuant to the ordinance of the Rector of Wrocław Medical University No. 37/XVI R/2024, from March 1, 2024, authors are required to pay a fee for each manuscript accepted for publication in the journal Advances in Clinical and Experimental Medicine. The fee amounts to 1600 EUR for all types of papers.

Advances in Clinical and Experimental Medicine has received financial support from the resources of Ministry of Science and Higher Education within the "Social Responsibility of Science – Support for Academic Publishing" project based on agreement No. RCN/SP/0584/2021.



Ministry of Education and Science
Republic of Poland

Czasopismo Advances in Clinical and Experimental Medicine korzysta ze wsparcia finansowego ze środków Ministerstwa Edukacji i Nauki w ramach programu „Społeczna Odpowiedzialność Nauki – Rozwój Czasopism Naukowych” na podstawie umowy nr RCN/SP/0584/2021.



Ministerstwo
Edukacji i Nauki

Indexed in: MEDLINE, Science Citation Index Expanded, Journal Citation Reports/Science Edition, Scopus, EMBASE/Excerpta Medica, Ulrich's™ International Periodicals Directory, Index Copernicus

Typographic design: Piotr Gil, Monika Kołęda

DTP: Wydawnictwo UMW

Cover: Monika Kołęda

Printing and binding: PRINT PROFIT Sp. z o.o., Koźmin 27, 59-900 Zgorzelec

Contents

Editorials

- 905 Andrea Porzionato, Rafael Boscolo-Berto
Assessing violent mechanical asphyxia in forensic pathology: State-of-the-art and unanswered questions

Original papers

- 909 Cemile Idiz, Ufuk Oguz Idiz
Illuminating insights: Exploring the effect of 16/8 intermittent fasting on serum cytokine levels in overweight adults
- 915 Muammer Çelik, Adnan Karabacak, Tuğçe Açıköz, Feyzullah Yavuz Atabay, Gamze Helvacı, Ahmad Nejat Ghaffari, Çağlar İrmak, Hacer Ceylan Çimendağ, Figen Coşkun, Vildan Avkan-Oğuz
Infectious diseases and clinical microbiology consultations in the emergency department: A cross-sectional study at a tertiary-care hospital
- 921 Bing Song, Xiangyue Chen, Kun Pan, Xiaowei Chen
Unraveling the role of collateral circulation and serum ELAVL1 in carotid atherosclerosis and ischemic stroke: Insights from clinical observations
- 929 Qinghua Ding, Hongbin Gao, Xianghui Hu, Weilu Gao
HGFN deficiency exacerbates spinal cord injury by promoting inflammation and cell apoptosis through regulation of the PI3K/AKT signaling pathway
- 941 Jiaying Zou, Yue Peng, Yue Wang, Shouzhu Xu, Chuandao Shi, Qiling Liu
Icariin ameliorates osteoporosis by activating autophagy in ovariectomized rats
- 953 Hualing Li, Zhiyi Zhen, Junjie Wei, Xianxian Fan, Pengfei Cao, Yitang Zhang, Yali Chen, Yue Li, Yifan Zhu, Rui Wang, Xingjie Ma
Endogenous hsa-circ_0007113 binds hsa-miR-515-5p to regulate senescence in human embryonic lung fibroblasts
- 965 Pengfei Yu, Zhijia Ma, Hong Jiang, Jintao Liu, Hongwei Li
Sinapine thiocyanate alleviates intervertebral disc degeneration by not regulating JAK1/STAT3/NLRP3 signal pathway

Reviews

- 979 Sergio Charifker Ribeiro Martins, Marcio da Costa Marques, Michael Gomes Vidal, Pedro Henrique Moreira Paulo Tolentino, Roberto Galvão Dinelli, Gustavo Vicentis de Oliveira Fernandes, Jamil Awad Shibli
Is the facial bone wall critical to achieving esthetic outcomes in immediate implant placement with immediate restoration? A systematic review
- 999 Yuejia Qin, Linhui Pan
Prebiotics and sepsis in infants: An updated systematic review and meta-analysis
- 1007 Paulina Sokółowska, Layla Bleibel, Jacek Owczarek, Anna Wiktorowska-Owczarek
PPAR γ , NF- κ B and the UPR pathway as new molecular targets in the anti-inflammatory actions of NSAIDs: Novel applications in cancers and central nervous system diseases?

Research letters

- 1023 Marta Nowakowska-Kotas, Adrian Korbecki, Sławomir Budrewicz, Joanna Bładowska
Investigation of cerebellar damage in adult amyotrophic lateral sclerosis patients using magnetic resonance imaging and diffusion tensor imaging

Assessing violent mechanical asphyxia in forensic pathology: State-of-the-art and unanswered questions

Andrea Porzionato^D, Rafael Boscolo-Berto^{A,D}

Department of Neurosciences, Institute of Human Anatomy, University of Padova, Italy

A – research concept and design; B – collection and/or assembly of data; C – data analysis and interpretation;

D – writing the article; E – critical revision of the article; F – final approval of the article

Advances in Clinical and Experimental Medicine, ISSN 1899–5276 (print), ISSN 2451–2680 (online)

Adv Clin Exp Med. 2024;33(9):905–908

Address for correspondence

Rafael Boscolo-Berto

E-mail: rafael.boscoloberto@unipd.it

Funding sources

None declared

Conflict of interest

None declared

Received on May 1, 2024

Reviewed on June 2, 2024

Accepted on August 11, 2024

Published online on September 20, 2024

Abstract

Mechanical asphyxiation has been a common method used to commit homicide, including femicide, throughout history. A recent report by the United Nations has shed light on the issue of misidentification and concealment of gender-related killings, which makes it difficult to effectively fight against it. Forensic pathologists are frequently asked to examine cases involving suspected asphyxia to determine whether other persons have been involved. Therefore, medicolegal experts must look for signs of occlusion of the oral/nasal orifices, compression of the neck, or specific signs such as the “facie sympathique”. There are situations where the physical signs are not distinctive enough to diagnose asphyxia, especially in cases where the individual has limited ability to resist external compression. In such cases, judicial autopsies should include an anatomical dissection of the neck structures through a layer-by-layer progression. It is important to search for the Amussat’s sign, e.g., as part of a Forensic Clinical Anatomy approach. Additionally, individual anatomical variations, age or artefactual modifications, must be considered for the correct interpretation of findings. Microscopic examinations could aid in the diagnosis by providing additional findings, and several attempts have been made to identify unique markers of asphyxia through various laboratory techniques such as biochemistry, radiology and miRNA studies. However, no single finding or method has been identified as definitive. In the future, biomedical-legal sciences will have to rely on scientific research and the retrospective case series to provide a scientific framework on which to base their hypothesis, giving weight to evidence in the trial.

Key words: asphyxia, autopsy, cadaver, forensic pathology, forensic clinical anatomy

Cite as

Porzionato A, Boscolo-Berto R. Assessing violent

mechanical asphyxia in forensic pathology:

State-of-the-art and unanswered questions.

Adv Clin Exp Med. 2024;33(9):905–908.

doi:10.17219/acem/192226

DOI

10.17219/acem/192226

Copyright

Copyright by Author(s)

This is an article distributed under the terms of the

Creative Commons Attribution 3.0 Unported (CC BY 3.0)

(<https://creativecommons.org/licenses/by/3.0/>)

Introduction

Forensic medicine has seen a growth in subdisciplines, leading to increased scientific contributions in forensic pathology in developed countries.^{1,2} One of the emerging topics is the use of scientific evidence to consistently identify murderers.³ A common historical method for committing homicide, including femicide, is mechanical asphyxiation.^{4–6} The issue of gender-based violence is a global concern and has been discussed at the United Nations General Assembly through a special report analyzing its causes and consequences. The report highlights the emerging issue of misidentification, concealment and underreporting of gender-related killings, which hinders the effective fight against this type of crime.⁷

Classification of asphyxias

Asphyxia is the acute respiratory failure caused by the arrest of pulmonary ventilation following actions that act directly on the respiratory system, preventing the penetration of air into the lungs, and we refer specifically to violent mechanical asphyxiation for our purposes. It is classified into internal and external asphyxia based on the location of the obstruction. Internal asphyxia occurs due to the failure of oxygen to bind to hemoglobin or the inability of hemoglobin to release oxygen to tissues. Notable examples include carbon monoxide poisoning and the increasingly prevalent sodium nitrite poisoning. External asphyxia is defined as the inability of oxygen to reach the alveoli. It can be further classified into several types including environmental asphyxia that results from a lack of oxygen in the inhaled air, impaired chest expansion due to intrinsic pathologies or external compression (also referred to as positional asphyxia), and upper airway obstruction caused by an internal blockage (e.g., obstruction of the oronasal orifices or food blockage) or external compression. External compression asphyxia can present more pronounced autopsy signs, both at the external orifices and the neck. The direct signs of external asphyxia include abrasions or bruises at the external orifices and neck, and rope marks in cases of hanging. Indirect signs include facial congestion and cyanosis, petechiae in the conjunctivae and serous membranes, and dark-blue livor mortis.⁸

Forensic pathologists are frequently requested by judicial authorities to examine cases involving suspected asphyxia. This is aimed to clarify whether other individuals may have played a role in causing the victim's death. While circumstantial evidence collected during a death investigation can offer some insight, it is essential to remember that such evidence is just one factor among many to consider.⁹ Additionally, this evidence can sometimes be misleading if it is the result of tampering with the crime scene or an attempt to conceal the murder. Therefore, medicolegal experts must look for signs of any external/

internal occlusion of the oral/nasal orifices or compression of the neck.^{10,11} Nevertheless, there are only a few rare cases where the physical signs present on the body are not distinctive of an asphyxia diagnosis. In certain situations, individuals who are vulnerable and have limited ability to resist external compression, such as infants, elderly individuals as well as people under the influence of psychoactive substances may become victims of strangulation or suffocation.^{12,13} Also, in infant homicides, or in decomposed bodies, autoptic findings can be of very little help to pathologists.^{14,15} In such cases, external signs may not be evident because only slight compression of the neck or orifices is sufficient to interrupt the oxygen supply to the body. At any rate, to differentiate between homicidal and pretended suicidal, genuine suicidal or accidental asphyxia, it is of utmost importance to conduct a comprehensive examination of the skin, soft tissues, muscles, vessels and other internal structures of the neck.

Autopsy technique and autopsy findings

In suspected asphyxia deaths, the examination will help identify any signs of trauma, fractures, bleeding or modifications that may suggest vitality. In most cases, signs can be observed that replicate the mechanism causing the constriction. A typical sign of hanging is the ligature furrow, which varies in direction and characteristics depending on the type of hanging and the position of the knot and the body.¹⁶ In manual strangulation, marks are often visible at the base of the mouth or neck, or in other areas of the body resulting from the immobilization of the victim. Finally, in ligature strangulation, there are signs that need to be differentiated from those in hanging. In cases of hanging, the anatomical structures of the neck require careful dissection to find even discrete injuries. To this end, the soft tissues of the neck, particularly the neck muscles, need to be dissected under artificial bloodlessness in a layered procedure. In this sense, judicial autopsies for supposed asphyxia should be integrated by anatomical dissection of the neck structures through layer-by-layer progression, according to a Forensic Clinical Anatomy approach.^{17,18} The topographic complexity of the neck region needs an anatomical methodological approach to fully ascertain and evaluate all the findings useful to clarify pathophysiologic mechanisms of injury and to permit medicolegal diagnosis. The context of individual anatomy such as variations, age, disease/surgery-related modifications,¹⁹ as well as the possibility of artefactual modifications, have also to be considered for correct interpretation of findings, as also stressed in Del Balzo et al.²⁰ A particular finding among the others is the unilateral miosis with or without ptosis at the opposite side from the knot, the so-called "facie sympathique".²¹ What is most relevant, the medicolegal diagnosis could benefit from additional findings collected

through microscopic examinations aimed at ascertaining the pathophysiologic chain involved in the mechanism of death, as well as estimating the time of death.⁸ On this point, the literature primarily refers to the presence of hemorrhagic infiltration in skin injuries caused by the means used to induce asphyxia. For instance, vital signs in hanging include the transverse laceration of the intimal layer of carotid arteries, the so-called Amussat's sign, whose vitality could also be checked by the analysis of the glycophorin A.^{8,20,22}

Ongoing research topics, unanswered questions and future perspectives

In most of cases, it can be difficult to distinguish between asphyxia and natural death, often of cardiac origin, when the microscopic pathology is inconclusive. Therefore, the forensic pathologist should examine alternative markers during investigations and, in some cases, consider contextual information. Several attempts have been made to identify unique markers of asphyxia using laboratory techniques such as biochemistry, radiology and miRNA studies,^{15,20,23–25} and the research paper by Del Balzo et al. is aligned with this direction.²⁰ Unfortunately, although many of them can support the hypothesis of asphyxia, no single finding or method has been identified as definitive. Finding future autopsy markers that are not influenced by body decomposition, unlike classic external signs, will be a challenge for forensic pathology, as this remains an unresolved issue to date and is still a topic of ongoing research. The issue related to circumstantial data is still controversial. In fact, it is believed that circumstantial data, also referred to as context information, should be considered by the forensic pathologist during the autopsy.²⁶ Contextual data are very useful in investigative reasoning, whereas criteria are stricter in evaluative reasoning due to the high risk of bias. The forensic pathologist's opinion should be mainly based on forensic pathology evidence, such as the number, location and types of wounds.²⁷ However, especially in cases where findings may be subtle and non-indicative, circumstantial data must be considered and evaluated to formulate a hypothesis. For a correct evaluation of circumstantial data to be incorporated into forensic reasoning, close collaboration between the forensic pathologist performing the scene investigation and autopsy, and the police handling the scene, is crucial for obtaining an accurate multidisciplinary assessment that considers all collected evidence.


In criminal proceedings, forensic pathologists are required to present all the evidence that supports the hypothesis of asphyxia. They must also evaluate their observations against the backdrop of 2 or more alternative hypotheses, as usually performed in medical malpractice

and forensic clinical anatomy.¹⁸ To do this, they need to be in a situation where all the elements that support or refute the hypothesis can be weighed, and this evaluation should not be based solely on their personal experience. Forensic pathology, particularly the study of violent asphyxiations, seems slow to adopt these principles, unlike other medico-legal branches, such as forensic genetics. In the future, biomedical-legal sciences, including forensic pathology, will need to strive through scientific research and the study of retrospective cases to give weight to scientific evidence, providing a logically sound framework on which to base the strength of their hypothesis.

In the context of modern forensic investigations, distinguishing between violent asphyxia death without any external signs of compression and sudden death is an intricate task during a trial. It is especially challenging for forensic pathologists to provide evidence that supports a homicidal dynamic over an accidental one. In some instances, it may be impossible for the pathologist to provide conclusive evidence to the trier-of-fact. As a result, circumstantial data that may fall outside the narrow expertise of a pathologist, often plays a crucial role in trials involving asphyxia. This could prove to be a critical factor. For all these reasons, future scientific research must focus on identifying indicative signs of asphyxia, rather than solely relying on the evaluator's experience.

ORCID iDs

Andrea Porzionato  <https://orcid.org/0000-0003-3025-4717>

Rafael Boscolo-Berto  <https://orcid.org/0000-0001-7556-1943>

References

1. Viel G, Boscolo-Berto R, Cecchi R, Bajanowski T, Vieira ND, Ferrara SD. Bio-medicolegal scientific research in Europe: A country-based analysis. *Int J Legal Med.* 2011;125(5):717–725. doi:10.1007/s00414-011-0576-3
2. Boscolo-Berto R, Viel G, Cecchi R, et al. Journals publishing bio-medicolegal research in Europe. *Int J Legal Med.* 2012;126(1):129–137. doi:10.1007/s00414-011-0620-3
3. Ferrara SD, Bajanowski T, Cecchi R, Boscolo-Berto R, Viel G. Bio-medicolegal scientific research in Europe: A comprehensive bibliometric overview. *Int J Legal Med.* 2011;125(3):393–402. doi:10.1007/s00414-010-0538-1
4. Thomsen AH, Leth PM, Hougen HP, Villesen P. Asphyxia homicides in Denmark 1992–2016. *Int J Legal Med.* 2022;136(6):1773–1780. doi:10.1007/s00414-022-02787-0
5. Fong WL, Pan CH, Lee JCI, Lee TT, Hwa HL. Adult femicide victims in forensic autopsy in Taiwan: A 10-year retrospective study. *Forensic Sci Int.* 2016;266:80–85. doi:10.1016/j.forsciint.2016.05.008
6. Giorgetti A, Fais P, Giovannini E, et al. A 70-year study of femicides at the Forensic Medicine department, University of Bologna (Italy). *Forensic Sci Int.* 2022;333:111210. doi:10.1016/j.forsciint.2022.111210
7. Šimonović D. *Report of the Special Rapporteur on Violence against Women, Its Causes and Consequences on Online Violence against Women and Girls from a Human Rights Perspective.* New York, USA: United Nations (UN); 2018:21. <https://digitallibrary.un.org/record/1641160?v=pdf>.
8. Dettmeyer RB, Verhoff MA, Schütz HF. *Forensic Medicine: Fundamentals and Perspectives.* Berlin–Heidelberg, Germany: Springer Berlin Heidelberg; 2014. doi:10.1007/978-3-642-38818-7
9. Leković A, Živković V, Nikolić S. Subendocardial hemorrhages in a case of crush asphyxia. *J Forensic Leg Med.* 2023;95:102506. doi:10.1016/j.jflm.2023.102506

10. Leković A, Živković V, Nikolić S. Commentary on the “Entrapment within an ottoman storage bed: an unusual accidental asphyxial death”: The complex asphyxiation. *Forensic Sci Med Pathol.* 2022;18(3): 382–384. doi:10.1007/s12024-022-00500-6
11. Cinquetti A, Franchetti G, Fichera G, Giraud C, Viel G, Cecchetto G. Entrapment within an ottoman storage bed: An unusual accidental asphyxial death. *Forensic Sci Med Pathol.* 2022;18(2):176–181. doi:10.1007/s12024-022-00473-6
12. Pelletti G, Garagnani M, Rossi F, Roffi R, Banchini A, Pelotti S. Safe drugs in drug facilitated crimes and acute intoxications in Northern Italy. *Forensic Sci Med Pathol.* 2018;14(4):442–449. doi:10.1007/s12024-018-0010-y
13. Živković V, Leković A, Nikolić S. Hyposphagma, positional asphyxia, and acute intoxication with psychoactive substances. *J Forensic Sci.* 2022;67(6):2492–2496. doi:10.1111/1556-4029.15141
14. Galante N, Blandino A, Disegna M, Franceschetti L, Casali MB. Intentional child and adolescent homicides in Milan (Italy): A 30-year interdisciplinary study. *Leg Med (Tokyo).* 2024;68:102433. doi:10.1016/j.legalmed.2024.102433
15. Giovannini E, Franchetti G, Ridolfi M, et al. An unusual case of corpse concealment driven by emotional distress. *Leg Med (Tokyo).* 2024;67: 102379. doi:10.1016/j.legalmed.2023.102379
16. Leković A, Vukićević A, Nikolić S. Assessing the knot in a noose position by thyrohyoid and cervical spine fracture patterns in suicidal hangings using machine learning algorithms: A new insight into old dilemmas. *Forensic Sci Int.* 2024;357:111973. doi:10.1016/j.forsciint.2024.111973
17. Porzionato A, Macchi V, Stecco C, Loukas M, Tubbs RS, De Caro R. Forensic clinical anatomy: A new field of study with application to medicolegal issues. *Clin Anat.* 2017;30(1):2–5. doi:10.1002/ca.22796
18. Porzionato A, Macchi V, Stecco C, et al. Clinical anatomy and medical malpractice: A narrative review with methodological implications. *Healthcare (Basel).* 2022;10(10):1915. doi:10.3390/healthcare10101915
19. Porzionato A, Macchi V, Mazzarolo C, Morra A, Sanudo J, De Caro R. Symmetrical apophyses on the posterior margins of the thyroid cartilage: A previously undescribed anatomical variation with potential forensic implications. *Am J Forensic Med Pathol.* 2019;40(1):84–88. doi:10.1097/PAF.0000000000000452
20. Del Balzo G, Pelletti G, Raniero D, et al. Forensic value of soft tissue detachments from the hyoid bone in death due to strangulation asphyxia [published online as ahead of print on April 29, 2024]. *Adv Clin Exp Med.* 2024. doi:10.17219/acem/186560
21. Marchetti D, Santoro L, Mercuri G. The “facie sympathique” sign in hanging: Historical background, forensic review, and perspectives. *Forensic Sci Med Pathol.* 2023;20(1):261–267. doi:10.1007/s12024-023-00603-8
22. Crudele L, Graziano D, Graziano, et al. The forensic application of the glycophorin A on the Amussat’s sign with a brief review of the literature. *J Forensic Leg Med.* 2021;82:102228. doi:10.1016/j.jflm.2021.102228
23. Zhang K, Liu R, Tuo Y, et al. Distinguishing asphyxia from sudden cardiac death as the cause of death from the lung tissues of rats and humans using Fourier transform infrared spectroscopy. *ACS Omega.* 2022;7(50):46859–46869. doi:10.1021/acsomega.2c05968
24. Ikematsu K, Takahashi H, Kondo T, Tsuda R, Nakasono I. Temporal expression of immediate early gene mRNA during the supravital reaction in mouse brain and lung after mechanical asphyxiation. *Forensic Sci Int.* 2008;179(2–3):152–156. doi:10.1016/j.forsciint.2008.05.007
25. Scopetti M, Padovano M, Manetti F, et al. Molecular autopsy in asphyxia deaths: Diagnostic perspectives of miRNAs in the evaluation of hypoxia response. *Int J Med Sci.* 2023;20(6):749–753. doi:10.7150/ijms.79539
26. De Boer HH, Fronczek J, Berger CEH, Sjerps M. The logic of forensic pathology opinion. *Int J Legal Med.* 2022;136(4):1027–1036. doi:10.1007/s00414-021-02754-1
27. Irmici M, D’Aleo M, Pelletti G, et al. Homicide or suicide? A probabilistic approach for the evaluation of the manner of death in sharp force fatalities. *J Forensic Sci.* 2024;69(1):205–212. doi:10.1111/1556-4029.15413

Illuminating insights: Exploring the effect of 16/8 intermittent fasting on serum cytokine levels in overweight adults

Cemile Idiz^{1,A–F}, Ufuk Oguz Idiz^{2,3,A–D,F}

¹ Division of Endocrinology and Metabolism, Department of Internal Medicine, Faculty of Medicine, Istanbul University, Turkey

² Department of General Surgery, Istanbul Training and Research Hospital, Turkey

³ Department of Immunology, Aziz Sancar Institute of Experimental Medicine (DETAE), Istanbul University, Turkey

A – research concept and design; B – collection and/or assembly of data; C – data analysis and interpretation;

D – writing the article; E – critical revision of the article; F – final approval of the article

Advances in Clinical and Experimental Medicine, ISSN 1899–5276 (print), ISSN 2451–2680 (online)

Adv Clin Exp Med. 2024;33(9):909–914

Address for correspondence

Cemile Idiz

E-mail: cemileidiz@gmail.com

Funding sources

None declared

Conflict of interest

None declared

Received on June 3, 2023

Reviewed on July 31, 2023

Accepted on October 10, 2023

Published online on December 12, 2023

Abstract

Background. The immune system's pivotal role extends to numerous diseases, and maintaining a balance between dietary and consumed energy is vital for preventing chronic illnesses and increasing life expectancy. Intermittent fasting (IF), a dietary approach typically implemented through time restrictions, exerts positive effects on the immune system and shows promising outcomes in managing various diseases.

Objectives. To evaluate the effectiveness of IF on the immune system with a wide cytokine panel.

Materials and methods. A total of 21 volunteers with body mass index (BMI) between 25 and 30 were included in the study. Fasting was applied for 16 h in a day to the volunteers, and they were free to consume food for the rest of the day. The weight, BMI, interleukin (IL)-1 β , interferon (IFN)- α 2, IFN- γ , tumor necrosis factor (TNF)- α , monocyte chemoattractant protein (MCP)-1, IL-6, IL-8, IL-10, IL-12p70, IL-17A, IL-18, IL-23, and IL-33 values were measured using flow cytometry and compared before and after 21 days follow-up.

Results. The mean age of study participants was 37.76 \pm 8.06 years and weight loss of the volunteers was 3.35 percentile compared to the values obtained before fasting. The pro-inflammatory cytokines decreased, while anti-inflammatory cytokines increased after fasting; there was a significant difference in TNF- α , MCP-1, IL-6, IL-8, and IL-33 values. Also, IL-1 β , IL-8 and IL-12p70 had moderately positive, IL-33 had strongly negative, and IL-10 had moderately negative correlation with the BMI change over time.

Conclusions. Intermittent fasting has positive effects on obesity-induced inflammation and promotes decrease in proinflammatory cytokines and increase in IL-33 values, which is known to have a protective effect on fat-associated inflammation.

Key words: obesity, inflammation, cytokine, IL-33, intermittent fasting

Cite as

Idiz C, Idiz UO. Illuminating insights: Exploring the effect of 16/8 intermittent fasting on serum cytokine levels in overweight adults. *Adv Clin Exp Med.* 2024;33(9):909–914. doi:10.17219/acem/173585

DOI

10.17219/acem/173585

Copyright

Copyright by Author(s)

This is an article distributed under the terms of the Creative Commons Attribution 3.0 Unported (CC BY 3.0) (<https://creativecommons.org/licenses/by/3.0/>)

Background

It is believed that maintaining a balance between dietary energy intake and energy expenditure plays a crucial role in preventing chronic diseases and increasing life expectancy.¹ Indeed, reports indicate that a long-term positive energy balance can lead to metabolic disorders caused by excessive weight gain and diseases such as type 2 diabetes mellitus, cardiovascular disorders, and low-grade inflammation-related diseases.² Additionally, it is hypothesized that lifelong reduction in food consumption (calorie restriction) significantly affects aging and lifespan in animals.³

Intermittent fasting (IF) regimens involve limited feeding periods and have historical roots in religious and spiritual traditions. Today, IF is regarded as a dietary intervention for weight loss and metabolic control.¹ Over recent years, numerous physiological effects of IF have been documented in studies involving rodents, monkeys and humans.⁴ Notably, these effects include increased life expectancy, decreased mortality rates from cancers and cardiovascular diseases, improved insulin sensitivity, and reduced oxidative stress and inflammation.^{5–8} Moreover, IF has been shown to significantly suppress inflammatory biomarkers such as interleukin (IL)-6 and C-reactive protein (CRP).^{9,10}

Intermittent fasting and energy-restricting diets (ERDs) have the potential to partially slow down the aging process by mitigating systemic inflammatory status.¹¹ They achieve this primarily through diminishing the production of reactive oxygen species (ROS) and inhibiting gene expression linked to inflammatory responses at the tissue level.^{12,13} Diets that simulate fasting i.e., fasting-mimicking diets (FMDs) have demonstrated beneficial effects in inflammatory diseases, such as rheumatoid arthritis, by regulating gastrointestinal microbiota, metabolism, and mitochondrial modulation throughout the day.¹⁴

Objectives

There are studies indicating that IF could reduce inflammation. However, these studies typically use only a few proinflammatory cytokines as markers. The aim of our study was to investigate the effects of IF on the immune system through a large group of cytokines that play a role in inflammation in order to explain the benefits of IF in many diseases.

Materials and methods

Patients

Following the approval of the Istanbul Training and Research Hospital Clinical Research Ethics Committee (approval No. 2534) for this observational cohort study, a public trial system application was submitted, and

informed content was obtained from all volunteers (who were working in a hospital as healthcare workers). Participants volunteered to fast for 16 h a day and have an 8-h eating window between April 15, 2021, and May 5, 2021 (for a period of 21 days). Individuals with a body mass index (BMI) between 25 and 30 were included in the study during the month of Ramadan. According to the study protocol, volunteers fasted for 16 h between 04:00 AM and 08:00 PM and were permitted oral intake between 08:00 PM and 04:00 AM.

None of the volunteers participating in the study were subjected to any special diet program or calorie restrictions, and they were allowed to consume as much food as they wanted without any restrictions. The exclusion criteria were having known diabetes, cancer, immunodeficiency, or chronic inflammatory disease. The female volunteers were included in the study just after the end of their menstruation period, which resulted in the study lasting 21 days. Twenty volunteers were required for the study based on the power analysis, with a type 1 error as low as 0.05, a power as high as 0.95 and an effect size of 1.13, which was calculated from the expected BMI change.

Data collection and cytokine measurement

Volunteers were asked to note their food intake for the 3 days before starting the study and during the last 3 days of the study. Subsequently, the calorie intake and the amount and percent of carbohydrate, fat and protein they consumed before and during the IF period were calculated using the BeBis 8 computer program (EBISpro for Windows; EBISpro, Stuttgart, Germany). Their weight and height were measured, and blood samples were collected before and on the 21st day of the study. Blood samples were centrifuged at 1,800 rpm for 5 min to separate the serum. The levels of IL-1 β , interferon (IFN)- α 2, IFN- γ , tumor necrosis factor (TNF)- α , monocyte chemoattractant protein-1 (MCP-1), IL-6, IL-8, IL-10, IL-12p70, IL-17A, IL-18, IL-23, and IL-33 were measured in pg/mL using a Cube 8TM flow cytometer (Sysmex, Kobe, Japan; cat. No. CY-S-3068R_V3) and a LEGENDplexTM Human Inflammation Panel 1 cytokine measurement kit (BioLegend, San Diego, USA; cat. No. 740808) to assess the inflammation status as primary outcomes. The weight, BMI, consumed food components, and cytokine values were compared before and after the 21 days of IF.

Patient follow-up

Daily face-to-face communication was established with the volunteers to assess whether they continued to meet the study conditions. At the beginning of the study, 27 volunteers were included. However, during the study, 1 volunteer contracted coronavirus disease-19 (COVID-19), and 5 did not fulfill the fasting criteria for 1 or more days, resulting in 6 volunteers being excluded from the study.

Statistical analyses

Data analysis employed IBM SPSS v. 26.0 (IBM Corp., Armonk, USA), with the Shapiro–Wilk test assessing the normality of the distribution of the differences. If the differences were normally distributed, they were expressed as mean ± standard deviation (M ± SD), otherwise as median and interquartile range (IQR). In the analysis, paired t-tests compared dependent and normally distributed differences, and Wilcoxon’s signed-rank test evaluated dependent and non-normally distributed differences. Pearson’s correlation coefficients examined BMI change. The interpretations of the correlation analysis were very weak (0.00–0.19), weak (0.20–0.39), moderate (0.40–0.59), strong (0.60–0.79), or very strong (0.80–1.0). The statistical significance level of the data was accepted as $p < 0.005$.

Results

The mean age of the volunteers was 37.76 ± 8.06 years, and the mean BMI was 27.93 ± 1.12 . The study comprised 9 women and 12 men. After 21 days, the volunteers had lost $3.35 \pm 1.29\%$ of their weight, which was significant compared to pre-IF levels ($p < 0.001$). Additionally, there were significant reductions in energy intake and the amounts of carbohydrate, protein, and fat intake at the end of the study ($p < 0.001$ for all) (Table 1).

It was determined that the TNF- α , MCP-1, IL-6, and IL-8 values were significantly lower after the IF period, while IL-33 concentration was significantly higher compared to the pre-IF values ($p = 0.022$, $p = 0.030$, $p = 0.025$, $p = 0.004$, $p = 0.0017$, and $p = 0.011$, respectively). Furthermore, IL-10 levels were slightly higher, and IFN- α 2, IL-12p70, and IL-18 measurements were slightly lower.

Table 1. Evaluation of daily energy and macronutrient intake and weight-BMI status before and after 21 days of follow-up

Parameters	Before fasting	After fasting	p-value	95% CI of the difference (lower)–(upper)	t or Z value
Weight (kg) (M ± SD)	83.81 ± 10.71	81.00 ± 10.42	<0.001 ^a	(2.31)–(3.30)	11.94 [#]
BMI (M ± SD)	27.93 ± 1.12	26.98 ± 0.87	<0.001 ^a	(0.76)–(1.12)	11.01 [#]
Energy intake (kcal) (M ± SD)	2443.18 ± 352.55	1846.69 ± 359.12	<0.001 ^a	(473.61)–(719.37)	10.12 [#]
Carbohydrate intake (g) (M ± SD)	300.64 ± 66.39	226.79 ± 65.42	<0.001 ^a	(54.09)–(93.61)	7.79 [#]
Carbohydrate intake (%) (M ± SD)	50.14 ± 7.65	49.38 ± 7.57	0.576 ^a	(–2.03)–(3.55)	0.56 [#]
Protein intake (g) (median – IQR)	82.40–33.60	66.20–20.45	<0.001 ^b	(0.00)–(0.13)	–4.01 [*]
Protein intake (%) (M ± SD)	13.57 ± 2.69	14.67 ± 1.90	0.083 ^a	(–2.34)–(0.15)	–1.82 [#]
Fat intake (g) (M ± SD)	98.16 ± 21.14	73.09 ± 14.09	<0.001 ^a	(16.34)–(33.79)	5.99 [#]
Fat intake (%) (M ± SD)	35.96 ± 7.23	35.85 ± 6.55	0.932 ^a	(–2.19)–(2.38)	0.08 [#]

^a paired sample t test; ^b Wilcoxon signed-rank test; [#] t value; ^{*} Z value; 95% CI – 95% confidence interval; M ± SD – mean ± standard deviation; BMI – body mass index; IQR – interquartile range; df is 20 for all the variables.

Table 2. Comparison of blood cytokine values before and after 21 days of follow-up

Parameters	Before fasting	After fasting	p-value	95% CI of the difference (lower)–(upper)	t or Z value
IL-1 β pg/mL (M ± SD)	58.87 ± 36.03	53.94 ± 48.05	0.470 ^a	(–9.02)–(18.88)	0.73 [#]
IFN- α 2 pg/mL (median – IQR)	1.82–3.14	1.59–1.47	0.205 ^b	(0.02)–(0.35)	–1.26 [*]
IFN- γ pg/mL (median – IQR)	1.11–9.51	1.20–2.91	0.244 ^b	(0.02)–(0.35)	–1.16 [*]
TNF- α pg/mL (median – IQR)	29.00–38.44	0.02–18.17	0.022 ^b	(0.00)–(0.13)	–2.29 [*]
MCP-1 pg/mL (median – IQR)	312.50–354.26	286.56–198.12	0.030 ^b	(0.00)–(0.13)	–2.17 [*]
IL-6 pg/mL (M ± SD)	5.89 ± 5.06	4.66 ± 3.74	0.028 ^a	(0.15)–(2.31)	2.37 [#]
IL-8 pg/mL (M ± SD)	39.03 ± 28.23	21.46 ± 22.30	0.003 ^a	(6.52)–(28.62)	3.16 [#]
IL-10 pg/mL (median – IQR)	3.91–4.57	4.27–6.30	0.108 ^b	(0.00)–(0.22)	–1.60 [*]
IL-12p70 pg/mL (median – IQR)	2.39–4.50	2.08–1.27	0.289 ^b	(0.02)–(0.35)	–1.06 [*]
IL-17A pg/mL (median – IQR)	0.11–0.45	0.10–0.36	0.390 ^b	(0.17)–(0.58)	–0.85 [*]
IL-18 pg/mL (median – IQR)	172.74–117.38	161.87–148.48	0.394 ^b	(0.31)–(0.73)	–0.85 [*]
IL-23 pg/mL (median – IQR)	10.03–26.92	8.20–19.27	0.065 ^b	(0.00)–(0.13)	–1.84 [*]
IL-33 pg/mL (median – IQR)	31.32–119.53	81.34–276.07	0.011 ^b	(0.00)–(0.13)	–2.55 [*]

^a paired sample t test; ^b Wilcoxon signed-rank test; [#] t value; ^{*} Z value; 95% CI – 95% confidence interval; M ± SD – mean ± standard deviation; IL – interleukin; IFN – interferon; TNF – tumor necrosis factor; MCP – monocyte chemoattractant protein; IQR – interquartile range; df is 20 for all the variables.

Table 3. The correlation results of % change of the parameters according to % BMI change after 21 days of intermittent fasting

Parameters	Correlation (p, r)	
	p-value	r-value
Weight	1.000	0.000
IL-1 β	0.009	0.553
IFN- α 2	0.078	0.393
IFN- γ	0.115	0.354
TNF- α	0.145	0.329
MCP-1	0.055	0.424
IL-6	0.624	-0.114
IL-8	0.018	0.510
IL-10	0.024	-0.490
IL-12p70	0.046	0.440
IL-17A	0.115	0.354
IL-18	0.113	0.357
IL-23	0.160	0.318
IL-33	<0.001	-0.729
Energy intake	<0.001	0.749
Carbohydrate (g)	0.012	0.539
Carbohydrate (%)	0.837	0.048
Protein (g)	0.095	0.374
Protein (%)	0.200	-0.291
Fat (g)	0.004	0.601
Fat (%)	0.483	0.162

BMI – body mass index; IL – interleukin; IFN – interferon; TNF – tumor necrosis factor; MCP – monocyte chemoattractant protein.

However, these differences were not statistically significant (Table 2).

The correlation analysis of BMI changes revealed that IL-1 β , IL-8, IL-12p70, and the amount of carbohydrate intake had a moderate positive correlation, while energy intake and the amount of fat intake exhibited a strong positive correlation, IL-33 showed a strong negative correlation, and IL-10 demonstrated a moderate negative correlation (Table 3).

Discussion

Excessive caloric intake and subsequent development of obesity are characterized by a chronic state of inflammation involving increased levels of circulating proinflammatory cytokines, described as “low-grade inflammation.”¹⁵ In this situation, a 2-to-3-fold increase in systemic concentrations of TNF- α , IL-1 β and IL-6 is typically observed,¹⁶ which may contribute to the induction of autoimmune diseases such as rheumatoid arthritis and inflammatory conditions, including atherosclerosis, insulin resistance, cardiovascular diseases, and tissue damage associated with many types of cancer.¹⁷

There are numerous publications examining the effects of IF on serum cytokines, with most reporting a decrease in proinflammatory cytokines. Furthermore, IL-1 β , IL-6, and TNF- α have been shown to significantly decrease after Ramadan fasting (RF), which serves as an IF model.¹⁷ Additionally, significant decreases in body weight, BMI, IL-2, IL-8, and TNF- α have been reported in obese men after RF, not just in men with a normal BMI.¹⁸ Another study states that RF can significantly reduce all anthropometric parameters, IL-6, and CRP in patients with nonalcoholic fatty liver disease.¹⁹ In our study, we observed a significant regression of proinflammatory TNF- α , IL-6, and IL-8 after IF, although IL-1 β decreased by an insignificant amount. Moreover, we found a moderate positive correlation between the decrease in BMI and IL-1 β and IL-8 values.

There are studies reporting an increase in IL-10 after IF, which plays an anti-inflammatory role. One such study reported that, while proinflammatory cytokines decreased during a 4-week RF, the IL-10 value increased significantly.²⁰ Another study found a significant increase in IL-10 levels after RF.²¹ In our study, we observed an increase in IL-10 levels after IF, although it was not statistically significant. Additionally, this increase showed a moderate negative correlation with BMI.

The MCP-1 is a crucial chemokine that plays a significant role in many diseases. It binds to C-C chemokine receptor type 2 (CCR2), activating signaling pathways that regulate leukocyte migration. Studies have reported higher MCP-1 levels in patients with obesity than in lean individuals.^{22,23} However, there are few studies in the literature evaluating the effect of IF on MCP-1. In an animal study, mice were subjected to a high-fat diet for 3 days, followed by 1 day of fasting for 7 or 14 weeks. They were compared with rats that received a continuous high-fat diet, and it was observed that MCP-1 levels decreased significantly in both the 7- and 14-week IF groups compared to the continuous high-fat diet group.²⁴ In obese mice, calorie restriction has been shown to significantly reduce messenger ribonucleic acid (mRNA) expression levels of several inflammatory cytokines and chemokines in white adipose tissue, including MCP-1.²⁵ In our study, we observed a significant decrease in MCP-1 levels after IF-induced weight loss.

Interleukin 17A, released from T-helper 17 (Th17 cells), and IL-23, an important cytokine for Th17 development, are related to autoimmunity. Evidence suggests that the Th17 cell number increases while regulatory cells decrease in obesity.²⁶ However, there are very few studies evaluating IL-17 and IL-23 values in obesity and the effect of IF on these cytokines. Some studies have reported higher IL-17 and IL-23 levels in obese individuals,²⁷ and it has been observed that IL-23 values significantly decrease after an intermittent ERD.²⁸ We found that the IL-17A and the IL-23 values decreased after IF; however, these differences did not reach statistical significance. This lack of significance could be attributed to the relatively short duration of the IF period or only including overweight individuals.

Interleukin 33 is a cytokine belonging to the IL-1 family that induces type 1 and type 2 immune responses by binding to the tumor necrosis factor receptor 2 (TNFR2) receptor. The literature reports that IL-33 has a protective effect on adipose tissue, shielding it from inflammation.²⁹ In a study by Hasan et al., who investigated the relationship between serum IL-33 levels and BMI of lean and obese individuals, overweight study participants had lower serum IL-33 levels than lean individuals, and a negative correlation was observed between IL-33 and BMI.³⁰ There is only 1 study investigating the effect of intermittent ERD on IL-33 values, which reported that IL-33 values were significantly lower in intermittent ERD patients. However, our study found that IL-33 values increased significantly after IF, and there was a strong negative correlation with the change in BMI, suggesting that the increase in IL-33 may be linked to its inflammation-reducing effect on adipose tissue.

In the literature, there are only a few studies evaluating the effects of IF on IL-12p70, IL-18, IFN- γ , and IFN- α 2 serum levels. In a study of 28 obese patients divided into 2 groups, 1 group was administered on a 3 nonconsecutive day intermittent ERD for 12 weeks, during which the patients consumed 550 kcal/day for women and 650 kcal/day for men. The other group received a continuous ERD with a low-calorie diet (LCD) of 33% energy restriction. Among the groups, IFN- γ , IL-18 and IL-23 values were significantly lower in patients on an intermittent ERD.²⁸ Our study found that IL-12p70, IL-18, IFN- γ , and IFN- α 2 decreased after IF; however, these differences did not reach statistical significance.

Limitations

Study limitations include the limited number of volunteers, not comparing the volunteers with different BMI categories, using kit-dependent cytokine measurements within specific intervals, and only evaluating a 3-week period. Additionally, no special diet program or calorie restriction was applied to any volunteers participating in the study. While this situation might suggest that the results could be influenced by variations in food intake among individuals, efforts were made to address this concern by setting up each volunteer with their own control.


Conclusions

The immune system plays the most important role in many diseases. There are publications discussing the benefits of IF on cancer and various diseases, but the impact of IF on the immune system remains unclear in explaining the benefits of IF on these conditions. Our study is one of the rare investigations evaluating the effects of IF on the immune system. According to our results, IF led to a significant decrease in proinflammatory cytokines and a significant increase in IL-33 levels, which is known

to have protective effects against inflammation in adipose tissue. These findings support that IF is an effective dietary approach that promotes weight loss and could potentially reduce obesity-related inflammation by decreasing BMI; long-term studies are needed on this subject.

ORCID iDs

Cemile Idiz  <https://orcid.org/0000-0001-6635-5996>

Ufuk Oguz Idiz  <https://orcid.org/0000-0002-8462-7809>

References

- Santos HO, Macedo RCO. Impact of intermittent fasting on the lipid profile: Assessment associated with diet and weight loss. *Clin Nutr ESPEN*. 2018;24:14–21. doi:10.1016/j.clnesp.2018.01.002
- Kahn SE, Hull RL, Utzschneider KM. Mechanisms linking obesity to insulin resistance and type 2 diabetes. *Nature*. 2006;444(7121):840–846. doi:10.1038/nature05482
- Weindruch R, Sohal RS. Caloric intake and aging. *N Engl J Med*. 1997;337(14):986–994. doi:10.1056/NEJM199710023371407
- Varady KA, Hellerstein MK. Alternate-day fasting and chronic disease prevention: A review of human and animal trials. *Am J Clin Nutr*. 2007;86(1):7–13. doi:10.1093/ajcn/86.1.7
- Mattson M, Wan R. Beneficial effects of intermittent fasting and caloric restriction on the cardiovascular and cerebrovascular systems. *J Nutr Biochem*. 2005;16(3):129–137. doi:10.1016/j.jnutbio.2004.12.007
- Varady KA, Roohk DJ, McEvoy-Hein BK, Gaylinn BD, Thorner MO, Hellerstein MK. Modified alternate-day fasting regimens reduce cell proliferation rates to a similar extent as daily calorie restriction in mice. *FASEB J*. 2008;22(6):2090–2096. doi:10.1096/fj.07-098178
- Lu J, EL, Wang W, et al. Alternate day fasting impacts the brain insulin-signaling pathway of young adult male C57BL/6 mice. *J Neurochem*. 2011;117(1):154–163. doi:10.1111/j.1471-4159.2011.07184.x
- Castello L, Froio T, Maina M, et al. Alternate-day fasting protects the rat heart against age-induced inflammation and fibrosis by inhibiting oxidative damage and NF- κ B activation. *Free Radic Biol Med*. 2010;48(1):47–54. doi:10.1016/j.freeradbiomed.2009.10.003
- Brannon S, Gozansky W, Donahoo W, Melanson E, Cage C, Coussons-Read M. 13. Obesity and inflammation: Effects of short-term fasting on IL-6 and relationship to diurnal cortisol. *Brain Behav Immun*. 2009;23:528. doi:10.1016/j.bbi.2009.06.018
- Aksungar FB, Topkaya AE, Akyildiz M. Interleukin-6, C-reactive protein and biochemical parameters during prolonged intermittent fasting. *Ann Nutr Metab*. 2007;51(1):88–95. doi:10.1159/000100954
- González O, Tobia C, Ebersole J, Novak M. Caloric restriction and chronic inflammatory diseases. *Oral Dis*. 2011;18(1):16–31. doi:10.1111/j.1601-0825.2011.01830.x
- Chung HY, Cesari M, Anton S, et al. Molecular inflammation: Underpinnings of aging and age-related diseases. *Ageing Res Rev*. 2009;8(1):18–30. doi:10.1016/j.arr.2008.07.002
- Clément K, Viguerie N, Poitou C, et al. Weight loss regulates inflammation-related genes in white adipose tissue of obese subjects. *FASEB J*. 2004;18(14):1657–1669. doi:10.1096/fj.04-2204.com
- Silwal P, Kim J, Yuk JM, Jo EK. AMP-activated protein kinase and host defense against infection. *Int J Mol Sci*. 2018;19(11):3495. doi:10.3390/ijms19113495
- Fontana L, Eagon JC, Trujillo ME, Scherer PE, Klein S. Visceral fat adipokine secretion is associated with systemic inflammation in obese humans. *Diabetes*. 2007;56(4):1010–1013. doi:10.2337/db06-1656
- Petersen AMW, Pedersen BK. The anti-inflammatory effect of exercise. *J Appl Physiol*. 2005;98(4):1154–1162. doi:10.1152/jappphysiol.00164.2004
- Faris MAIE, Kacimi S, Al-Kurd RA, et al. Intermittent fasting during Ramadan attenuates proinflammatory cytokines and immune cells in healthy subjects. *Nutr Res*. 2012;32(12):947–955. doi:10.1016/j.nutres.2012.06.021
- Ünalacak M, Kara İH, Baltacı D, Erdem Ö, Bucaktepe PGE. Effects of Ramadan fasting on biochemical and hematological parameters and cytokines in healthy and obese individuals. *Metab Syndr Relat Disord*. 2011;9(2):157–161. doi:10.1089/met.2010.0084

19. Aliasghari F, Izadi A, Gargari BP, Ebrahimi S. The effects of ramadan fasting on body composition, blood pressure, glucose metabolism, and markers of inflammation in NAFLD patients: An observational trial. *J Am Coll Nutr.* 2017;36(8):640–645. doi:10.1080/07315724.2017.1339644
20. Madkour MI, Malhab LJB, Abdel-Rahman WM, Abdelrahim DN, Saber-Ayad M, Faris ME. Ramadan diurnal intermittent fasting is associated with attenuated *FTO* gene expression in subjects with overweight and obesity: A prospective cohort study. *Front Nutr.* 2022;8:741811. doi:10.3389/fnut.2021.741811
21. Faris MAIE, Madkour MI, Obaideen AK, et al. Effect of Ramadan diurnal fasting on visceral adiposity and serum adipokines in overweight and obese individuals. *Diabetes Res Clin Pract.* 2019;153:166–175. doi:10.1016/j.diabres.2019.05.023
22. Panee J. Monocyte chemoattractant protein 1 (MCP-1) in obesity and diabetes. *Cytokine.* 2012;60(1):1–12. doi:10.1016/j.cyto.2012.06.018
23. Catalán V, Gómez-Ambrosi J, Ramirez B, et al. Proinflammatory cytokines in obesity: Impact of type 2 diabetes mellitus and gastric bypass. *Obes Surg.* 2007;17(11):1464–1474. doi:10.1007/s11695-008-9424-z
24. Chen Y, Su J, Yan Y, et al. Intermittent fasting inhibits high-fat diet-induced atherosclerosis by ameliorating hypercholesterolemia and reducing monocyte chemoattraction. *Front Pharmacol.* 2021;12:719750. doi:10.3389/fphar.2021.719750
25. Zhou RH, Wang Q, Hu XM, Liu M, Zhang AR. The influence of fasting and caloric restriction on inflammation levels in humans: A protocol for systematic review and meta analysis. *Medicine.* 2021;100(15):e25509. doi:10.1097/MD.00000000000025509
26. Tsigalou C, Vallianou N, Dalamaga M. Autoantibody production in obesity: Is there evidence for a link between obesity and autoimmunity? *Curr Obes Rep.* 2020;9(3):245–254. doi:10.1007/s13679-020-00397-8
27. Sumarac-Dumanovic M, Stevanovic D, Ljubic A, et al. Increased activity of interleukin-23/interleukin-17 proinflammatory axis in obese women. *Int J Obes.* 2009;33(1):151–156. doi:10.1038/ijo.2008.216
28. Castela I, Rodrigues C, Ismael S, et al. Intermittent energy restriction ameliorates adipose tissue-associated inflammation in adults with obesity: A randomised controlled trial. *Clin Nutr.* 2022;41(8):1660–1666. doi:10.1016/j.clnu.2022.06.021
29. de Oliveira MFA, Talvani A, Rocha-Vieira E. IL-33 in obesity: Where do we go from here? *Inflamm Res.* 2019;68(3):185–194. doi:10.1007/s00011-019-01214-2
30. Hasan A, Al-Ghimlas F, Warsame S, et al. IL-33 is negatively associated with the BMI and confers a protective lipid/metabolic profile in non-diabetic but not diabetic subjects. *BMC Immunol.* 2014;15(1):19. doi:10.1186/1471-2172-15-19

Infectious diseases and clinical microbiology consultations in the emergency department: A cross-sectional study at a tertiary-care hospital

Muammer Çelik^{1,A–F}, Adnan Karabacak^{1,B,E,F}, Tuğçe Açıkgöz^{2,B,D–F}, Feyzullah Yavuz Atabay^{1,B,E,F}, Gamze Helvacı^{1,B,D–F}, Ahmad Nejat Ghaffari^{1,B,E,F}, Çağlar İrmak^{1,B,E,F}, Hacer Ceylan Çimendağ^{1,B,E,F}, Figen Coşkun^{2,A,D–F}, Vildan Avkan-Oğuz^{1,A,C–F}

¹ Department of Infectious Diseases and Clinical Microbiology, Faculty of Medicine, Dokuz Eylül University, Izmir, Turkey

² Department of Emergency Medicine, Faculty of Medicine, Dokuz Eylül University, Izmir, Turkey

A – research concept and design; B – collection and/or assembly of data; C – data analysis and interpretation;

D – writing the article; E – critical revision of the article; F – final approval of the article

Advances in Clinical and Experimental Medicine, ISSN 1899–5276 (print), ISSN 2451–2680 (online)

Adv Clin Exp Med. 2024;33(9):915–920

Address for correspondence

Muammer Çelik

E-mail: muammer4677@yahoo.com

Funding sources

None declared

Conflict of interest

None declared

Received on April 3, 2023

Reviewed on June 23, 2023

Accepted on October 9, 2023

Published online on December 6, 2023

Cite as

Çelik M, Karabacak A, Açıkgöz A. Infectious diseases and clinical microbiology consultations in the emergency department: A cross-sectional study at a tertiary-care hospital. *Adv Clin Exp Med.* 2024;33(9):915–920. doi:10.17219/acem/173557

DOI

10.17219/acem/173557

Copyright

Copyright by Author(s)

This is an article distributed under the terms of the Creative Commons Attribution 3.0 Unported (CC BY 3.0) (<https://creativecommons.org/licenses/by/3.0/>)

Abstract

Background. Although there is limited data about the role of infectious diseases and clinical microbiology (IDCM) consultations in the Emergency Department (ED), they have a key role in deciding on hospitalization and appropriate use of antibiotics.

Objectives. To evaluate demographic and clinical characteristics of patients who visited the ED of our hospital and underwent an IDCM consultation.

Materials and methods. In this cross-sectional study, we reviewed the medical records of adult patients who visited the ED of our hospital between May and August 2021 and needed IDCM consultation. The demographic data, the date and time of admission and consultation, the departments that were consulted before IDCM, laboratory results, diagnosis, and outcome were recorded.

Results. Out of 42,116 ED visits, 1,007 (2.4%) IDCM consultations were requested. The median time between admission and IDCM consultation was 239 min (150.0–373.5). Before 56.9% of IDCM consultations, pre-consultations were requested from other departments, and the time interval was significantly longer. The median age of patients was 68 years (51–77 years). Infections were confirmed by the IDCM physician in 79.6% of the consultations. The most diagnosed infections were urinary tract infections (32.4%), skin-soft tissue infections (16.9%) and lower respiratory tract infections (10.3%), whereas 9.3% of the consultations resulted in hospitalization to the infection ward, 25.1% to other wards, and 5% to the intensive care unit (ICU).

Conclusions. Two of 3 consultations resulted in hospitalization in other wards, and this shows that IDCM consultations are beneficial for managing patients with infectious diseases hospitalized in other departments. Communication between IDCM specialists and ED colleagues is important, especially in the management of elderly patients who require a multidisciplinary approach.

Key words: consultation, emergency department, infectious diseases and clinical microbiology, tertiary-care hospital

Background

Infectious diseases and clinical microbiology (IDCM) consultations are vital for improving the clinical management of patients with suspected infectious diseases and increasing the rational usage of antibiotics.^{1–4} Due to the unavailability of culture results, antimicrobial susceptibility tests, and other serological or molecular diagnostic tests in the Emergency Department (ED), most decisions are based on clinical symptoms and findings resulting in empirical therapy. Moreover, it is difficult to diagnose infectious diseases in the ED because of the heavy workload, heterogeneous presentation of infections, and varying host characteristics (elderly patients, children and/or immunosuppressed patients). The absence of typical infection signs and symptoms, and the presence of comorbid diseases, such as malignancy, make it difficult to interpret the clinical picture, especially in elderly patients.⁵ In the elderly patients, the prevalence of bacterial colonization risk factors, including frequent hospitalization, antibiotic use, invasive devices such as urinary catheters, and residency in long-term care facilities, make the differential diagnosis of infectious diseases more challenging.^{6,7}

Although there is limited data on the role of IDCM consultations in the ED, they are critical when deciding on hospitalization and the appropriate use of antibiotics. The implementation of IDCM consultations for the early management of patients with severe sepsis/septic shock in the ED reduces mortality.⁸ In a Canadian study, automatic IDCM consultations for patients admitted to the ED with cellulitis were beneficial for differential diagnosis, reducing recurrence and preventing hospital admissions.⁹

Objectives

This study aimed to evaluate the contribution of IDCM consultations by determining the demographic and clinical characteristics of patients who were consulted in the ED.

Materials and methods

Study design and population

The study was designed as a retrospective, cross-sectional study. Dokuz Eylül University Hospital in Izmir, Turkey, is a tertiary care reference hospital with a 1,100-bed capacity. The ED of our hospital has 45 beds and receives approx. 120,000 admissions annually. After triage, the patient is examined by the resident physician of the ED and evaluated alongside the senior assistant or emergency medicine specialist. If necessary, a consultation is requested from the relevant departments. Infectious diseases and clinical microbiology consultation is requested for ED

patients suspected of having infectious diseases and who require an expert opinion.

The inpatient service of the IDCM Department has 14 beds and was not accepting patients other than those with coronavirus disease 2019 (COVID-19) between March 2020 and May 2021 due to the heavy workload and staff shortages caused by the pandemic. After the necessary conditions were met, non-COVID-19 patients were accepted from May 1, 2021. The IDCM consultations are evaluated by a designated consultant during working hours, while IDCM residents and specialists are on duty outside working hours.

All patients older than 18 years who presented to the ED between May 1 and August 31, 2021, and required IDCM consultation, were included in this study.

Data collection and analysis

Data on patients and consultations were accessed through the computerized hospital management system. The first consultations requested on the patient's admission to the ED were considered new admissions. Those who revisited the ED at least 72 h after being discharged and were consulted were also considered new admissions. If the patient had repeated consultations during their stay in the ED or revisited within 72 h of discharge from the ED, the requested consultations were considered a re-consultation. Consultations requested from other departments before IDCM were defined as pre-consultations.

Since some patients had more than 1 admission at different times, demographic data were evaluated on the number of patients and other clinical or laboratory data on the number of admissions. The demographic data of each patient were recorded. The admission and consultation time, reason for admission, departments for which pre-consultation was requested, laboratory data, diagnosis, recommendations, and results were recorded for each application. Infectious disease was diagnosed based on symptoms such as fever, nausea, vomiting, cough, dysuria, abdominal pain, physical examination findings, laboratory results (high C-reactive protein (CRP) and/or procalcitonin, leukocytosis/leukopenia, the presence of pyuria), and/or radiological findings (system-specific findings such as pneumonic infiltration) compatible with an infection. A diagnosis of infection was excluded based on patients having no symptoms, physical examination findings, supportive laboratory and/or radiological findings compatible with an infection, and another acute condition that would explain their clinical situation.

Statistical analyses

Statistical analysis employed IBM SPSS v. 24.0 (IBM Corp., Armonk, USA). Categorical variables are presented as numbers and percentages. The normality of continuous variables was assessed using the Shapiro–Wilk test and

histograms. The homogeneity of variance was evaluated with the Levene’s test. The results of assumption verification for test applications are given in the Supplementary Table (<https://doi.org/10.5281/zenodo.8410371>). Based on the results of the normality tests, non-parametric statistical tests were utilized. Numerical data were summarized using median values and interquartile range (IQR), which was defined as the 1st quartile (Q1) to the 3rd quartile (Q3). The Mann–Whitney U test compared differences between 2 independent groups, while the Kruskal–Wallis test assessed significant differences in a continuous dependent variable of a categorical independent variable (with 3 or more groups), followed by Dunn’s post-hoc test. The statistical significance limit was accepted as 0.05 (p-value).

Ethics statement

The Non-Interventional Research Ethics Committee of the Dokuz Eylül University (Izmir, Turkey) approved the study on November 24, 2021 (No. 2021/34-06). Necessary permissions were obtained from the hospital management and the Department of Emergency Medicine of the Dokuz Eylül University.

Results

Between May 1 and August 31, 2021, there were 42,116 admissions to the ED of our hospital, and 1,007 (2.4%) consultations were requested from the Department of IDCM for 808 patients. Of the consultations, 853 (84.7%) were new admissions, and 154 (15.3%) were re-consultations. Forty-four (5.4%) patients had multiple admissions to the ED at different times. During the study period, at least 1 consultation was requested from the ED every day except for 2 days. The median number of daily consultations was 8 (6–10), with the distribution of consultations based on hourly intervals during the day given in Fig. 1.

In 56.9% (485/853) of the admissions, a pre-consultation was requested from other departments before IDCM, and the median number of pre-consultations per admission was 1 (0–2). Pre-consultations were primarily requested from the following departments: Nephrology (13.5%, n = 115), Pulmonology (9.6%, n = 82), Oncology (8%,

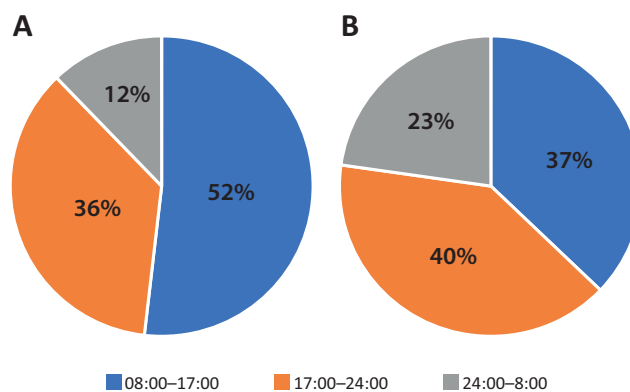


Fig. 1. A. Percentage of admissions to the Emergency Department (ED) according to working hours; B. Percentage of Department of Infectious Diseases and Clinical Microbiology (IDCM) consultations according to working hours

n = 68), Gastroenterology (6.6%, n = 56), Cardiology (6%, n = 51), Orthopedics and Traumatology (5.7%, n = 50), and Neurology (4.1%, n = 35).

The median time between admission to the ED and IDCM consultation was 239 min (150.0–373.5; 3 h and 59 min), ranging between 6 and 4718 min (78 h and 38 min). The median time was 287 min (183.0–444.5; 4 h 47 min) for those with pre-consultation and 185 min (122.0–269.5; 3 h and 5 min) for those without pre-consultation (p < 0.001; U = 53719.5). As the number of departments requested for pre-consultation increased, the time until the IDCM consultation increased (p < 0.001; Kruskal–Wallis test) (Table 1,2). The median response time of the IDCM to the consultation was 96 min (64.0–138.5).

The median age of the patients was 68 years (51–77), and 53.25% of patients were 65 and older. Distribution of the patients according to age group is given in Fig. 2. Of the patients, 50.7% (n = 410) were men. The most common symptom on admission was fever (21.5%, n = 183), with the other symptoms given in Table 3. After evaluation by an IDCM physician, infections were diagnosed in 79.6% (n = 679) of the consultations. The diagnoses of infectious diseases are given in Table 4.

Sampling for blood cultures was done in 50.9% (434/835) of ED admissions, with no growth in 61.1% (265/434) of the blood cultures. Of the blood culture results, 19.4% (84/434) were compatible with contamination (most commonly coagulase-negative staphylococci), and 19.5%

Table 1. The time interval between the patient’s arrival at the emergency department and the infectious diseases consultation based on the number of pre-consultations

Number of pre-consultations	n	Time [min] (median, IQR)	Kruskal–Wallis H test	df	p-value
0	368	184.5 (122.0–269.5)	133.515	2	<0.001
1	360	258.5 (158.7–402.0)			
≥2	125	403 (269.5–635.5)			
Total	853	239 (150.0–373.50)			

IQR – interquartile range; Kruskal–Wallis test was used; n – number; df – degrees of freedom.

Table 2. The p-values of post hoc comparisons for variables between the groups

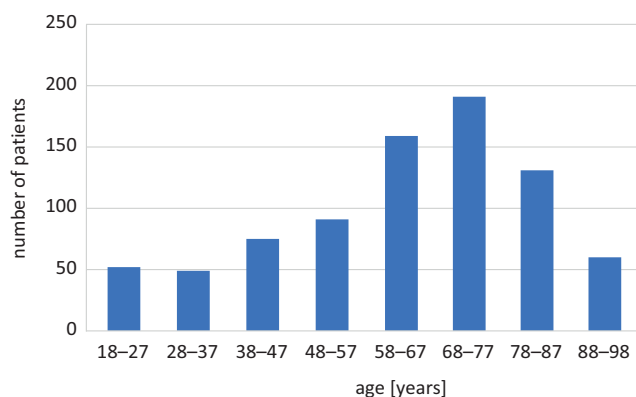
Pairwise comparisons	p-value
0 vs 1 pre-consultation	<0.001
0 vs ≥2 pre-consultations	<0.001
1 vs ≥2 pre-consultations	<0.001

The Kruskal–Wallis test and the Dunn's post hoc test were used.

Table 3. Symptoms of the patients at presentation

Symptom	n (%)
Fever	183 (21.5)
Cutaneous symptoms (erythema, edema, swollen, tenderness, infected wound/ulcer, rash, etc.)	167 (19.6)
General systemic symptoms (weakness, fatigue, loss of appetite, myalgia, confusion, headache, etc.)	130 (15.2)
Gastrointestinal symptoms (abdominal pain, nausea, vomiting, diarrhea, etc.)	109 (12.8)
Genitourinary symptoms (dysuria, frequency, urgency, cloudy urine, flank pain, penile/vaginal discharge, etc.)	94 (11.0)
Pulmonary symptoms (coughing, sputum, shortness of breath, chest pain)	90 (10.5)
Others (joint pain, seizure, altered mental status, behavioral changes, postvaccination reaction, etc.)	80 (9.4)
Total	853 (100.0)

n = number.

**Fig. 2.** The distribution of patients across different age groups

(85/434) were accepted as an infectious agent. The most frequently isolated microorganisms in blood cultures were *Escherichia coli* (41.2%, 35/85), *Staphylococcus aureus* (13.0%, 11/85) and *Klebsiella pneumoniae* (8.2%, 7/85).

Urine cultures were obtained from patients in 52.4% (447/853) of the ED admissions, with no growth in 40.0% (179/447). In 16.5% (74/447) of urine cultures, more than 3 microorganisms were isolated, which were considered contamination. The most common agents isolated in urine cultures were *E. coli* (21.0%, 94/447), *K. pneumoniae* (10.5%, 47/447) and *Pseudomonas aeruginosa* (3.8%, 17/447).

Of all consultations, 9.2% (n = 78) resulted in admission to the IDCM ward. The most common diagnoses for hospitalization were urinary tract infection (43.6%,

Table 4. Diagnosis of infectious diseases

Diagnosis, n (%)	n (%)
UTI	220 (32.4)
upper UTI	176 (25.9)
lower UTI	44 (6.5)
SSTI	115 (16.9)
cellulitis	72 (10.6)
complicated SSTI	32 (4.7)
abscesses	11 (1.6)
LRTI	70 (10.3)
pneumonia	46 (6.8)
empyema	2 (0.3)
COVID-19	22 (3.2)
Bloodstream infection	24 (3.5)
bacteremia	12 (1.8)
central line-associated bloodstream infection	9 (1.3)
endocarditis	3 (0.4)
Central nervous system infection	7 (1.0)
Gastrointestinal system infection	61 (9.0)
acute gastroenteritis	33 (4.9)
cholecystitis – cholangitis	11 (1.6)
peritonitis	8 (1.2)
intra-abdominal infection	8 (1.2)
esophagitis	1 (0.1)
Musculoskeletal system infection	49 (7.2)
diabetic foot infection	24 (3.5)
septic arthritis/arthritis	17 (2.5)
prosthesis infection	7 (1.1)
osteomyelitis	1 (0.1)
Fever	67 (10.0)
fever of unknown origin	43 (6.3)
neutropenic fever	24 (3.5)
Sepsis of unknown origin	28 (4.1)
Other*	38 (5.6)
Total	679 (100.0)

*Herpes zoster, HIV, Orf, infectious mononucleosis, lymphadenitis, malaria, tetanus, Crimean-Kongo hemorrhagic fever, sexually transmitted diseases. UTI – urinary tract infection; LRTI – lower respiratory tract infection; SSTI – skin-soft tissue infection; COVID-19 – coronavirus disease 2019.

n = 34), skin-soft tissue infection (23.1%, n = 18), central nervous system infection (7.7%, n = 6), bloodstream infection (7.7%, n = 6), acute gastroenteritis (6.4%, n = 5), herpes zoster (3.8%, n = 3), and other (7.7%, n = 6), such as diabetic foot infection, fever of unknown origin, human immunodeficiency virus (HIV) infection, malaria, tetanus, and Crimean-Kongo hemorrhagic fever.

Of all ED visits, 25.1% (n = 214) of patients were admitted to other services, and 80.8% (n = 173) had accompanying infectious diseases. Of the ED visits, 5% (n = 43) resulted in hospitalization to the intensive care unit (ICU), and 3.2% (n = 27) of patients died during their ED stay (Table 5). In total, 39.3% of the consultations resulted in hospitalization (9.2% to IDCM ward, 25.1% to other wards, and 5% to the ICU). More than half (57.5%) of the patients were discharged from the ED and 39.3% were hospitalized. Between the patients being hospitalized or discharged, the median number of pre-consultations (1 [0–1] compared to 0 [0–1]; p < 0.001; U = 62291.5) and the time interval between

Table 5. The result of the infectious diseases and clinical microbiology (IDCM) consultations

Result	n (%)
Discharged from the ED	491 (57.5)
prescribed oral antibiotics	319 (37.4)
prescribed parenteral antibiotics	14 (1.6)
referred to the outpatient IDCM clinic	37 (4.3)
other*	121 (14.1)
Hospitalization	335 (39.3)
admission to the IDCM ward	78 (9.3)
admission to other wards	214 (25.1)
admission to the ICU	43 (5.0)
Mortality in the ED	27 (3.2)
Total	853 (100.0)

* The patients with no infection were discharged from the ED by an ED physician or left the ED voluntarily. IDCM – infectious diseases and clinical microbiology; ED – emergency department; ICU – intensive care unit.

admission and IDCM consultation (249 min (152–389) compared to 221 min (143–344), $p = 0.017$; $U = 74177.0$) were significantly different.

Discussion

In this study, 2.4% of ED patients required an IDCM consultation, of which 79.6% resulted in the diagnosis of an infectious disease. Time is needed for the initial patient examination in the ED and the results of laboratory tests and radiological imaging. For our hospital, this time is approx. 4 h, and the IDCM consultation concludes within 1.5 h. More than half of ED visits require a multidisciplinary approach, and IDCM consultation is delayed if other departments request a pre-consultation. However, an infectious disease diagnosis in 4 out of 5 patients indicates that consultations were requested with the correct indication. Additionally, the hospitalization of 2 out of 3 patients in other wards supports the importance of a multidisciplinary approach. Of the patients admitted to the other departments, 80.8% had an accompanying infectious disease.

More than half of the patients admitted to the ED of our hospital were older than 65 years. In our country, society is growing older, and the elderly population aged 65 and over has increased by 21.9% in the last 5 years.¹⁰ As the elderly population continues to grow, there will be a gradual increase in the number of such patients seeking access to healthcare. According to studies conducted in Turkey, elderly patients accounted for 10.1–13.8% of all ED visits.^{11–13} In a population-based national study conducted in the USA, more than 3 million of elderly patients attended the ED in 2012, and 18.5% of these admissions were infection-related.¹⁴ In a single-center study conducted at a university hospital in Thailand, 18% of the annual 50,000 admissions to the ED were elderly patients, and 14.5% of the admissions were infection-related.¹⁵ In our study, the population differed from previous research as it exclusively included patients requiring an IDCM consultation. As a result,

the proportion of elderly patients was higher. Younger patients with mild or moderate infections are discharged from the ED to the IDCM outpatient clinic after being examined by the emergency physician. In older patients, infections may be more severe, and hospitalization is often required. This supports the fact that the need for IDCM consultation is higher, especially for people over 65 years of age.

According to the results of our study, a diagnosis of infection was excluded in 20% of the consultations. Diagnosing infections in the ED is challenging because of the heavy workload and diagnostic limitations. Culture results have a limited role in the diagnosis of infections in the ED because significant growth was detected in only 1 patient out of 5 for blood cultures and 2 patients out of 5 for urine cultures. This can result in either failure to recognize an infection in the ED (under-diagnosis) or attributing other diseases to an infection (over-diagnosis). Under-diagnosis may lead to delays in prescribing antibiotics, and over-diagnosis may result in the unnecessary use of antibiotics.^{16,17} In a study by Caterino et al., the diagnoses of bacterial infections by ED physicians were compared with those made by 2 other experts (one board-certified in infectious disease and one board-certified in emergency medicine and internal medicine with expertise in geriatrics), and both under-diagnosis and over-diagnosis were common.¹⁸ Infectious diseases and clinical microbiology consultations are critical for infection diagnosis and management in the ED.

The most common infections in our study were urinary tract infections (32.4%), skin-soft tissue infections (16.9%) and lower respiratory tract infections (10.3%). In the study by Ittisanyakorn et al., the most common infections were pneumonia (32.6%), pyelonephritis (23.1%) and intestinal infections (11.4%).¹⁵ Meanwhile, Goto et al. reported lower respiratory tract infections (26.2%), urinary tract infections (25.3%) and sepsis (18.9%), and Caterino et al. reported gastrointestinal (28.6%), urinary tract (24.7%) and lower respiratory tract (23.4%) infections.^{14,18} In these studies, all patients with bacterial infections admitted to the ED were evaluated. We included only patients who required IDCM consultations. In our center, patients with suspected pneumonia are consulted by the pulmonary medicine consultants working in the ED. For this reason, unlike other studies, the most common diagnosis made by the IDCM consultant was urinary tract infection instead of pneumonia. There are differences in the distribution of infectious diseases in the ED according to the sociodemographic characteristics of the region, structural characteristics of the center and patient profile. More studies should be conducted to understand the characteristics of the patients admitted to the ED and create an action plan.

Limitations

The study was conducted in a single center, and the consultations were retrospectively evaluated. There may have been a selection bias since only patients who consulted

with an IDCM were included in the study. For this reason, patients with mild-to-moderate infectious disease who were examined and discharged by the ED physician were not evaluated. On the other hand, we could not compare the outcomes of patients with and without an IDCM consultation because the study group did not include patients who did not require an IDCM consultation. The impact of IDCM consultations on the timing of antibiotic treatment or patients' outcomes could not be evaluated in the study because patients could not be followed up after they were discharged from the ED or admitted to other services.

The pneumonia rate was low in our study because pulmonary disease consultation was requested for patients with suspected pneumonia. Likewise, patients with mild COVID-19 were not included in the study because they were evaluated in the pandemic outpatient clinic, and patients with moderate-to-severe COVID-19 admitted to the ED were evaluated by a pulmonologist.

Conclusions






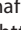


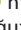

Despite accounting for only 2.4% of total ED visits, IDCM consultations are valuable for the diagnosis and management of infections, especially in older patients requiring a multidisciplinary approach and pre-consultation. Timely and appropriately indicated IDCM consultations have proven to be effective in achieving their intended objectives. The consultations provided by IDCM specialists confirmed infection in 4 out of 5 patients. While $\frac{1}{3}$ of the hospitalized patients were admitted to the IDCM ward, the rest were admitted to other services. Thus, IDCM consultations in the ED play a crucial role not only in the management of IDCM service patients but also in effectively managing infections for patients hospitalized in other departments. Promoting collaborative relationships between IDCM specialists and ED colleagues will be beneficial in diagnosing, managing and preventing infectious diseases in the ED.

Supplementary data

The Supplementary materials are available at <https://doi.org/10.5281/zenodo.8410371>. The package consists of the following file:

Supplementary Table 1. Results of verifying the assumptions for the application of the tests (dataset).

ORCID IDs

Muammer Çelik  <https://orcid.org/0000-0001-6190-5370>
 Adnan Karabacak  <https://orcid.org/0000-0002-7252-3885>
 Tuğçe Açıkgöz  <https://orcid.org/0000-0002-1131-6719>
 Feyzullah Yavuz Atabay  <https://orcid.org/0000-0001-6741-1216>
 Gamze Helvacı  <https://orcid.org/0000-0002-4973-9602>
 Ahmad Nejat Ghaffari  <https://orcid.org/0000-0002-7188-8268>
 Çağlar İrmak  <https://orcid.org/0000-0002-7901-3757>
 Hacer Ceylan Çimendağ  <https://orcid.org/0000-0003-2235-7767>
 Figen Coşkun  <https://orcid.org/0000-0002-7027-8169>
 Vildan Avkan-Oğuz  <https://orcid.org/0000-0001-7648-7730>

References

- Vehreschild JJ, Morgen G, Cornely OA, et al. Evaluation of an infectious disease consultation programme in a German tertiary care hospital. *Infection*. 2013;41(6):1121–1128. doi:10.1007/s15010-013-0512-1
- Fariñas MC, Saravia G, Calvo-Montes J, et al. Adherence to recommendations by infectious disease consultants and its influence on outcomes of intravenous antibiotic-treated hospitalized patients. *BMC Infect Dis*. 2012;12:292. doi:10.1186/1471-2334-12-292
- Kerremans JJ, Verbrugh HA, Vos MC. Frequency of microbiologically correct antibiotic therapy increased by infectious disease consultations and microbiological results. *J Clin Microbiol*. 2012;50(6):2066–2068. doi:10.1128/JCM.06051-11
- Yapar N, Erdenizmenli M, Oğuz VA, et al. Infectious disease consultations and antibiotic usage in a Turkish university hospital. *Int J Infect Dis*. 2006;10(1):61–65. doi:10.1016/j.ijid.2005.03.008
- Çelik M, Nazlı A, Coşkun F, et al. Acil serviste yaşlı hastalarda üriner sistem enfeksiyonu tanı kriterleri nelerdir? Ankara, Turkey: Enfeksiyon Dünyası Çalıştayı; 2022 [In Turkish] https://www.calistay2022.infeksiyondunyasi.org/upload/Calistay_kitabi_2022_web.pdf. Accessed June 1, 2022.
- Eren-Kutsoylu OÖ, Avkan-Oğuz V, Abdullayeva M, et al. Prevalence of multidrug-resistant bacterial colonization and risk factors in geriatric nursing home residents. *Turk J Geriatr*. 2018;21(1):41–48. doi:10.31086/tjgeri.2018137965
- Trick WE, Weinstein RA, DeMarais PL, et al. Colonization of skilled-care facility residents with antimicrobial-resistant pathogens. *J Am Geriatr Soc*. 2001;49(3):270–276. doi:10.1046/j.1532-5415.2001.4930270.x
- Viale P, Tedeschi S, Scudeller L, et al. Infectious diseases team for the early management of severe sepsis and septic shock in the emergency department. *Clin Infect Dis*. 2017;65(8):1253–1259. doi:10.1093/cid/cix548
- Jain SR, Hosseini-Moghaddam SM, Dwek P, et al. Infectious diseases specialist management improves outcomes for outpatients diagnosed with cellulitis in the emergency department: A double cohort study. *Diagn Microbiol Infect Dis*. 2017;87(4):371–375. doi:10.1016/j.diagmicrobio.2016.12.015
- Turkish Statistical Institute (2019) Elderly Statistics. Ankara, Turkey: Turkish Statistical Institute; 2019. <https://data.tuik.gov.tr/Bulten/Index?p=Istatistiklerle-Yasli-lar-2019-33712>. Accessed June 1, 2022.
- Bilgili MA, Öncü MR. Evaluation of geriatric patients applying to the emergency department. *Van Med J*. 2021;28(1):77–83. doi:10.5505/vtd.2021.53179
- Ünsal A, Çevik A, Metintaş S. Emergency department visits by elderly patients [in Turkish]. *Turk J Geriatr*. 2003;6(3):83–88. <https://dergipark.org.tr/tr/download/article-file/225459>. Accessed June 1, 2022.
- Mutlu B. Clinical and demographic characteristics of patients over 65 years admitted to the emergency department [in Turkish]. 2012. <https://tez.yok.gov.tr/UlusalTezMerkezi/giris.jsp> (Search with thesis number 326451) Accessed June 1, 2022.
- Goto T, Yoshida K, Tsugawa Y, Camargo CA, Hasegawa K. Infectious disease-related emergency department visits of elderly adults in the United States, 2011–2012. *J Am Geriatr Soc*. 2016;64(1):31–36. doi:10.1111/jgs.13836
- İttisanyakorn M, Ruchichanantakul S, Vanichkulbodee A, Sri-on J. Prevalence and factors associated with one-year mortality of infectious diseases among elderly emergency department patients in a middle-income country. *BMC Infect Dis*. 2019;19(1):662. doi:10.1186/s12879-019-4301-z
- Gordon LB, Waxman MJ, Ragsdale L, Mermel LA. Overtreatment of presumed urinary tract infection in older women presenting to the emergency department. *J Am Geriatr Soc*. 2013;61(5):788–792. doi:10.1111/jgs.12203
- Chandra A, Nicks B, Maniago E, Nouh A, Limkakeng A. A multicenter analysis of the ED diagnosis of pneumonia. *Am J Emerg Med*. 2010;28(8):862–865. doi:10.1016/j.ajem.2009.04.014
- Caterino JM, Leininger R, Kline DM, et al. Accuracy of current diagnostic criteria for acute bacterial infection in older adults in the emergency department. *J Am Geriatr Soc*. 2017;65(8):1802–1809. doi:10.1111/jgs.14912

Unraveling the role of collateral circulation and serum ELAVL1 in carotid atherosclerosis and ischemic stroke: Insights from clinical observations

Bing Song^{1,C,D}, Xiangyue Chen^{1,A,E,F}, Kun Pan^{2,B,C}, Xiaowei Chen^{1,B}

¹ Department of Ultrasound, Brain Hospital of Hunan Province, the Second People's Hospital of Hunan Province, Changsha, China

² Medical Basic Teaching Experimental Center, Medical College of Hunan University of Chinese Medicine, Changsha, China

A – research concept and design; B – collection and/or assembly of data; C – data analysis and interpretation;

D – writing the article; E – critical revision of the article; F – final approval of the article

Advances in Clinical and Experimental Medicine, ISSN 1899–5276 (print), ISSN 2451–2680 (online)

Adv Clin Exp Med. 2024;33(9):921–928

Address for correspondence

Xiangyue Chen

E-mail: xiang_yc1211@163.com

Funding sources

This study was supported by the University-level scientific research project of Hunan University of Chinese Medicine (natural science; project No. 2022XYLH082).

Conflict of interest

None declared

Received on May 25, 2023

Reviewed on September 2, 2023

Accepted on September 21, 2023

Published online on December 6, 2023

Cite as

Song B, Chen X, Pan K, Chen X. Unraveling the role of collateral circulation and serum ELAVL1 in carotid atherosclerosis and ischemic stroke: Insights from clinical observations. *Adv Clin Exp Med.* 2024;33(9):921–928. doi:10.17219/acem/172700

DOI

10.17219/acem/172700

Copyright

Copyright by Author(s)

This is an article distributed under the terms of the Creative Commons Attribution 3.0 Unported (CC BY 3.0) (<https://creativecommons.org/licenses/by/3.0/>)

Abstract

Background. The (embryonic lethal, abnormal vision, drosophila)-like protein 1 (ELAVL1) is a newly discovered protein associated with cerebral ischemic/reperfusion (I/R) injury. However, little is known of ELAVL1 in ischemic stroke patients.

Objectives. To investigate the clinical significance of collateral circulation and serum ELAVL1 in patients with carotid atherosclerosis (CAS) and ischemic stroke.

Materials and methods. The present prospective cohort investigation included 317 ischemic stroke patients and 300 CAS patients admitted between March 2020 and March 2022. Collateral circulation was measured using digital subtraction angiography (DSA) and graded using the American Society of Interventional and Therapeutic Neuroradiology/Society of Interventional Radiology (ASITN/SIR) grading system. Enzyme-linked immunosorbent assays (ELISAs) were used to measure serum ELAVL1, C-reactive protein (CRP), interleukin-6 (IL-6), and tumor necrosis factor alpha (TNF- α). The serum levels of total cholesterol (TC), triglyceride (TG), high-density lipoprotein cholesterol (HDL-C), and low-density lipoprotein cholesterol (LDL-C) were also measured.

Results. The serum levels of ELAVL1, CRP, IL-6, TNF- α , and LDL-C were all markedly higher, while HDL-C was significantly lower in ischemic stroke patients compared to the CAS patients. Serum ELAVL1 was markedly higher in ASITN/SIR grade 0–1 patients compared to grade 2–4 patients. Also, ELAVL1 correlated positively with serum CRP, IL-6, TNF- α , TC, and LDL-C, and negatively with HDL-C. Receiver operating characteristic (ROC) curves showed that ELAVL1 and collateral circulation have the potential to be used as biomarkers for the diagnosis of ischemic stroke. Meanwhile, CRP, IL-6, TNF- α , HDL-C, ASITN/SIR grading, and ELAVL1 were independent risk factors for ischemic stroke.

Conclusions. We found that serum ELAVL1 was associated with clinical outcomes of ischemic stroke patients, while the combination of ELAVL1 and collateral circulation could be used as a potential biomarker for ischemic stroke diagnosis.

Key words: ischemic stroke, collateral circulation, carotid atherosclerosis, biomarker, observational study

Background

Stroke is the second leading cause of disability and mortality worldwide, with over 13 million new cases annually.^{1–3} In the past 50 years, the overall incidence rate of stroke has shown a downward trend in high-income countries and an upward trend in low- and middle-income countries.^{4,5} According to the 2022 global stroke statistics report, the proportion of people over 65 years old is proportional to the incidence rate of stroke, indicating that age is one of the critical risk factors for stroke.^{6,7} Among stroke patients, over 85% have an ischemic stroke, for which carotid atherosclerosis (CAS) is one of the most common causes.^{8,9} Generally, ischemic stroke is caused by occlusion of the middle cerebral artery, which leads to neuronal death due to insufficient blood and oxygen supply to the brain, resulting in brain tissue damage.^{10,11}

Ischemia/reperfusion (I/R) injury is an unavoidable pathological injury in stroke patients and a major cause of neurological damage.^{12,13} Stroke-induced I/R injury can lead to permanent brain tissue damage and may cause cognitive impairment.^{14,15} Despite the development of treatment strategies, the underlying molecular mechanisms of ischemic stroke are still unclear.^{16,17} In recent years, many molecular biomarkers for ischemic stroke have been identified.^{18,19} However, new potential biomarkers for ischemic stroke diagnosis and prediction of prognosis are still needed.

The (embryonic lethal, abnormal vision, drosophila)-like protein 1 (ELAVL1) is a newly discovered protein associated with the development of many diseases, including brain I/R injury, the main pathological alteration in ischemic stroke.^{20–22} However, no clinical studies have focused on ELAVL1 in stroke patients. It is widely accepted that collateral circulation is changed and is associated with the clinical outcomes of ischemic stroke patients.^{23–25} Nonetheless, measuring collateral circulation alone might not be accurate enough to predict patients' clinical outcomes.²⁶

Objectives

In the present study, we aimed to investigate the clinical significance of collateral circulation and serum ELAVL1 in patients with CAS and ischemic stroke, focusing on their association with patients' severity and prognosis. The study findings might provide a novel biomarker for CAS and ischemic stroke.

Materials and methods

Patients and study design

The present study was designed as a prospective cohort investigation and included 317 ischemic stroke patients admitted to our Department between March 2020 and March

2022. Ischemic stroke diagnosis was based on the guidelines of The Chinese Medical Association (2019 update).^{27,28} The inclusion criteria were: 1. all patients were diagnosed with ischemic stroke using imaging methods, including computed tomography angiography (CTA), digital subtraction angiography (DSA) and magnetic resonance imaging (MRI); 2. patients received no anticoagulant therapy within 3 months before the study. The following patients were excluded: those receiving anticoagulant therapy within 3 months of study commencement, patients with hemorrhagic stroke, and patients with other systematic diseases. Additionally, 300 patients with CAS were enrolled as controls within the same study period. Among CAS patients, the following were excluded: patients with severe systematic infections, patients with cancer, and patients with severe cardiovascular, liver or renal diseases. All patients were consecutively enrolled. We recruited all cases who met the inclusion criteria during the study period. The ethical committee of the Brain Hospital of Hunan Province (Changsha, China) approved the study (Ethics Review Board No. 44; 2021).

Measurement of collateral circulation

The collateral circulation was measured with DSA and graded using the American Society of Interventional and Therapeutic Neuroradiology/Society of Interventional Radiology (ASITN/SIR) grading system, where 0–1 means poor compensatory collateral circulation, grade 2 is moderate compensatory circulation, and grade 3–4 is good compensatory circulation.²⁹

Enzyme-linked immunosorbent assay

Blood samples were collected from all patients within 24 h of admission. Enzyme-linked immunosorbent assay (ELISA) was used to measure serum ELAVL1 (kit purchased from MyBioSource Inc., San Diego, USA), C-reactive protein (CRP), interleukin (IL)-6 and tumor necrosis factor alpha (TNF- α). Kits for CRP, IL-6, and TNF- α were purchased from Nanjing Jiancheng Bioengineering Institute, Nanjing, China, according to the manufacturer's instructions.

Data collection

Demographic data, including age, sex, medical history, and complications, were recorded. The serum levels of total cholesterol (TC), triglyceride (TG), high-density lipoprotein cholesterol (HDL-C), and low-density lipoprotein cholesterol (LDL-C) were measured using an automatic Hitachi 7600 biochemical analyzer (Hitachi Corporation, Tokyo, Japan).

Statistical analyses

The data distribution was analyzed using the Kolmogorov–Smirnov method. All measurement data were non-normally distributed and expressed as median (range). Comparison

between the 2 groups employed a Mann–Whitney U test, while χ^2 tests compared rates (without half adjust). Spearman’s analysis was used for correlation analysis. Receiver operating characteristic (ROC) curves were used to evaluate the diagnostic value. Logistic regression was performed to analyze the risk factor of ischemic stroke. All calculations were made using IBM SPSS v. 22.0 (IBM Corporation, Armonk, USA) and GraphPad v. 6.0 (GraphPad Software, San Diego, USA), and $p < 0.05$ was defined as statistically different.

Results

Basic clinical characteristics

The present study included 317 ischemic stroke patients and 300 CAS patients. As shown in Table 1, no significant differences were found between the 2 groups of patients for age, sex, body mass index (BMI), or complications. However, serum CRP, IL-6, and TNF- α levels were markedly higher

in ischemic stroke patients compared to the CAS patients (all $p < 0.05$). For lipid metabolism, TC and TG showed no significant difference, while LDL-C was remarkably higher and HDL-C was significantly lower in ischemic stroke patients ($p < 0.05$). For ASITN/SIR grading, the frequency of grade 0–1 was significantly higher in ischemic stroke patients compared to the CAS patients ($p < 0.05$).

Serum ELAVL1 was associated with collateral circulation

To further investigate the role of ELAVL1 in CAS and ischemic stroke patients, the levels of ELAVL1 in different patients were determined. Serum ELAVL1 was significantly upregulated in ischemic stroke patients compared to the CAS patients ($p < 0.05$, Fig. 1A). Furthermore, serum ELAVL1 was markedly higher in ASITN/SIR grade 0–1 patients than in grade 2–4 patients ($p < 0.05$, Fig. 1B). These results indicated that serum ELAVL1 might be associated with collateral circulation in CAS and ischemic stroke patients.

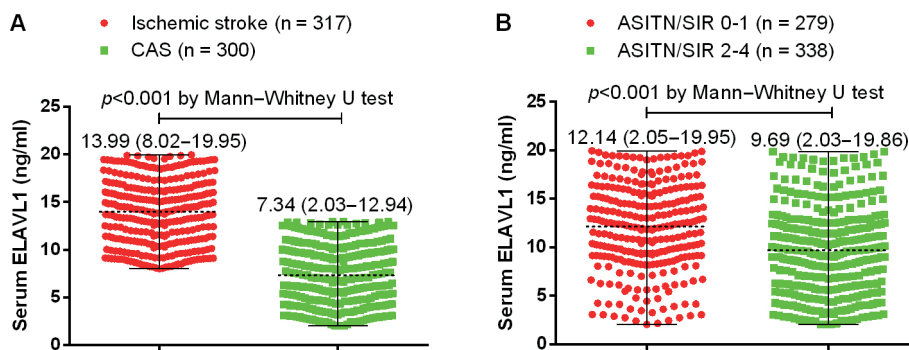


Fig. 1. A. Serum ELAV (embryonic lethal, abnormal vision, drosophila)-like protein 1 (ELAVL1) was evaluated in ischemic stroke patients using an enzyme-linked immunosorbent assay (ELISA) and compared to carotid atherosclerosis (CAS) patients; B. Serum ELAVL1 was evaluated using ELISA in patients with different American Society of Interventional and Therapeutic Neuroradiology/Society of Interventional Radiology (ASITN/SIR) grades. Lines indicate the median (range)

Table 1. Basic characteristics of all patients

Variables		Ischemic stroke (n = 317)	CAS (n = 300)	p-value
Age [years]		52 (35–70)	51 (35–70)	0.891
Sex (male : female, %)		179 (56.47) : 138 (43.53)	165 (55.00) : 135 (45.00)	0.834
BMI [kg/m ²]		25.12 (18.01–31.99)	24.57 (18.03–31.74)	0.714
Complications, n (%)	diabetes	75 (23.66)	70 (23.33)	0.735
	hypertension	69 (21.77)	57 (19.00)	
	current smoker	141 (44.48)	124 (41.33)	
CRP [mg/L]		27.24 (5.32–49.73)	12.67 (3.02–24.95)	<0.001
IL-6 [pg/mL]		32.29 (5.05–59.90)	16.95 (5.04–29.98)	<0.001
TNF- α [pg/mL]		22.98 (5.01–39.85)	12.24 (5.02–19.85)	<0.001
TC [mmol/L]		4.36 (3.25–5.37)	4.22 (3.26–5.38)	0.189
TG [mmol/L]		1.49 (0.93–2.02)	1.44 (0.94–2.01)	0.659
LDL-C [mmol/L]		3.15 (2.21–4.00)	2.88 (2.17–3.79)	<0.001
HDL-C [mmol/L]		1.10 (0.95–1.23)	1.12 (0.97–1.25)	0.002
ASITN/SIR grading, n (%)	0–1	194 (61.20)	85 (28.33)	<0.001
	2–4	123 (38.80)	215 (71.67)	

The p-values were calculated between CAS and ischemic stroke patients using Student’s t-test of Mann–Whitney U test for normally or non-normally distributed data, respectively. χ^2 test was used for comparing rates. CAS – carotid atherosclerosis; BMI – body mass index; CRP – C-reactive protein; IL-6 – interleukin 6; TNF- α – tumor necrosis factor alpha; TC – total cholesterol; TG – triglyceride; LDL-C – low-density-lipoprotein cholesterol; HDL-C – high-density-lipoprotein cholesterol; ASITN/SIR – American Society of Interventional and Therapeutic Neuroradiology/Society of Interventional Radiology.

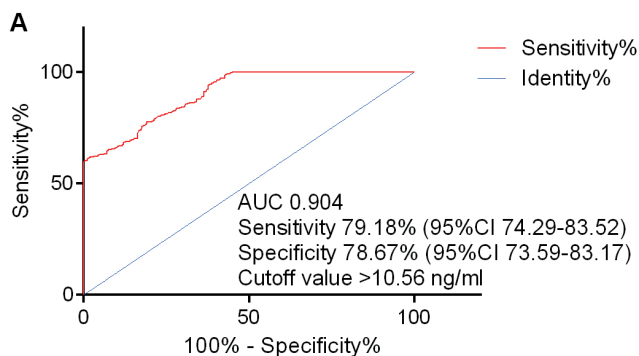
Serum ELAVL1 was associated with inflammatory cytokines and lipid metabolism

We conducted additional correlation analysis for serum ELAVL1, inflammatory cytokines, and lipid metabolism. As shown in Table 2, serum ELAVL1 was positively correlated with serum CRP, IL-6, TNF- α , TC, and LDL-C, and negatively correlated with HDL-C (all $p < 0.05$), suggesting that serum ELAVL1 was associated with the clinical outcomes of CAS in ischemic stroke patients.

Table 2. Spearman's correlation among serum (embryonic lethal, abnormal vision, drosophila)-like protein 1 (ELAVL1), inflammatory cytokines and lipid metabolism in all patients

Variables	Spearman's correlation	p-value
CRP	0.354	<0.001
IL-6	0.334	<0.001
TNF- α	0.335	<0.001
TC	0.098	0.015
TG	-0.019	0.632
LDL-C	0.146	<0.001
HDL-C	-0.076	0.049

BMI – body mass index; CRP – C-reactive protein; IL-6 – interleukin 6; TNF- α – tumor necrosis factor alpha; TC – total cholesterol; TG – triglyceride; LDL-C – low-density-lipoprotein cholesterol; HDL-C – high-density-lipoprotein cholesterol.



Diagnostic value of ELAVL1 and collateral circulation for ischemic stroke

The ROC curves were used to determine the diagnostic value of ELAVL1 and collateral circulation for ischemic stroke. The ELAVL1 showed good diagnostic value for ischemic stroke, with an area under the curve (AUC) = 0.904, sensitivity = 79.18%, specificity = 78.67%, and a cutoff value >10.56 ng/mL (Fig. 2A). Collateral circulation (ASITN/SIR grading) also demonstrated diagnostic value for ischemic stroke, with an AUC = 0.625, sensitivity = 61.88%, specificity = 54.20%, and a cutoff value <2.5 (Fig. 2B).

When practicing the diagnostic mode in the patients using the cutoff value, both ELAVL1 and ASITN/SIR grading could be used as diabetic markers. The combination of ELAVL1 and ASITN/SIR grading showed better sensitivity and accuracy (Table 3). All of these results imply that ELAVL1 and collateral circulation have the potential to be used as biomarkers for the diagnosis of ischemic stroke. Figure 3 shows a typical DSA image of the collateral circulation.

Risk factors for ischemic stroke by logistic regression

Finally, we used univariate and multivariate logistic regression to analyze the risk factors for ischemic stroke. In univariate logistic regression, CRP, IL-6, TNF- α , LDL-C, HDL-C, ASITN/SIR grading, and ELAVL1 were risk factors for ischemic stroke. While in multivariate logistic regression, CRP,

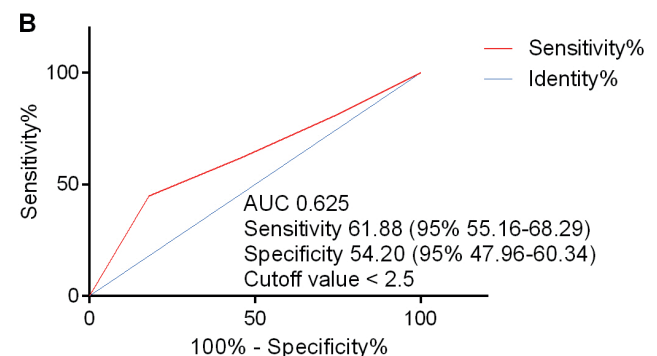


Fig. 2. A. Receiver operating characteristic (ROC) curve of ELAV (embryonic lethal, abnormal vision, drosophila)-like protein 1 (ELAVL1) for the diagnosis of ischemic stroke; B. ROC curve of American Society of Interventional and Therapeutic Neuroradiology/Society of Interventional Radiology (ASITN/SIR) grading for diagnosis of ischemic stroke

Table 3. Diagnostic value of (embryonic lethal, abnormal vision, drosophila)-like protein 1 (ELAVL1) and collateral circulation for ischemic stroke

Methods	True positive	False positive	True negative	False negative	Sensitivity	Specificity	Accuracy
ELAVL1	251	64	236	66	79.18%	78.67%	78.93%
ASITN/SIR grading	232	158	142	85	73.19%	47.33%	60.62%
ELAVL1 + ASITN/SIR grading	300	188	112	17	94.64%	37.33%	66.77%

* Sensitivity = true positive/(true positive + false negative) \times 100%; specificity = true negative/(true negative + false positive) \times 100%; accuracy = (true positive + true negative)/(true positive + false negative + false positive + true negative) \times 100%; ASITN/SIR – American Society of Interventional and Therapeutic Neuroradiology/Society of Interventional Radiology.

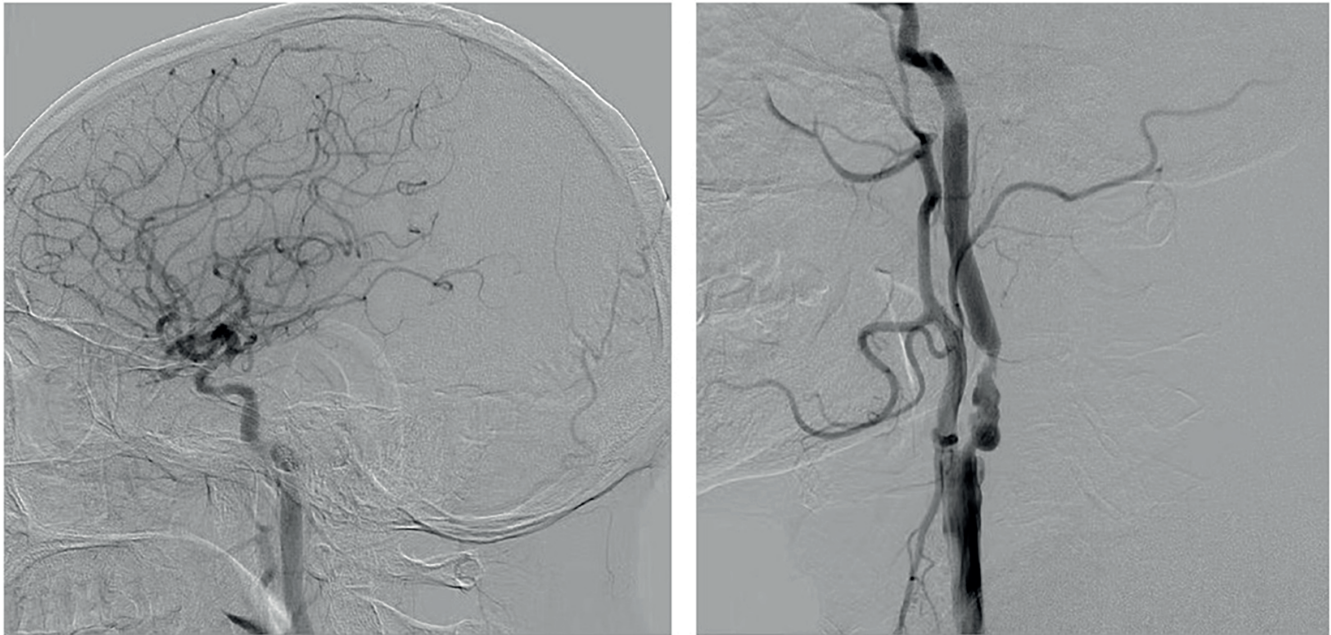


Fig. 3. A typical digital subtraction angiography (DSA) image of collateral circulation from a 52-year-old male patient

Table 4. Logistic regression for risk factors of unstable plaque

Variables	Univariate			Multivariate		
	OR	95% CI	p-value	OR	95% CI	p-value
Age	0.999	0.984–1.014	0.893	0.985	0.944–1.028	0.488
Sex	1.061	0.772–1.458	0.714	1.388	0.546–3.528	0.490
BMI	0.992	0.955–1.032	0.699	1.041	0.931–1.164	0.479
Diabetes	0.982	0.677–1.425	0.924	0.678	0.243–1.890	0.458
Hypertension	0.843	0.569–1.249	0.395	1.058	0.326–3.435	0.925
Current smoker	0.879	0.639–1.210	0.430	0.562	0.217–1.455	0.235
CRP	0.862	0.840–0.883	<0.001	0.818	0.766–0.873	<0.001
IL-6	0.896	0.879–0.914	<0.001	0.868	0.823–0.916	<0.001
TNF-α	0.843	0.818–0.868	<0.001	0.804	0.746–0.867	<0.001
TC	0.840	0.649–1.089	0.189	1.144	0.560–2.336	0.712
TG	0.896	0.547–1.466	0.661	0.910	0.234–3.536	0.892
LDL-C	0.445	0.322–0.616	<0.001	0.613	0.245–1.536	0.296
HDL-C	26.709	3.701–192.777	0.001	8452.881	24.213–2.95×10 ⁶	0.002
ASITN/SIR grading	1.520	1.348–1.714	<0.001	0.433	0.331–0.566	<0.001
ELAVL1	0.561	0.512–0.615	<0.001	1.560	1.122–2.170	0.008

95% CI – 95% confidence interval; OR – odds ratio; BMI – body mass index; CRP – C-reactive protein; IL-6 – interleukin 6; TNF-α – tumor necrosis factor alpha; TC – total cholesterol; TG – triglyceride; LDL-C – low-density-lipoprotein cholesterol; HDL-C – high-density-lipoprotein cholesterol; ELAVL1 – (embryonic lethal, abnormal vision, drosophila)-like protein 1; ASITN/SIR – American Society of Interventional and Therapeutic Neuroradiology/Society of Interventional Radiology.

IL-6, TNF-α, HDL-C, ASITN/SIR grading, and ELAVL1 were independent risk factors for ischemic stroke (Table 4).

Discussion

Stroke is the primary cause of death in China. According to data from China’s National Stroke Epidemiology Survey, the age-standardized incidence rate of stroke in adults

is approx. 1115 cases per 100,000 individuals, with a mortality rate of 115 per 100,000.³⁰ Over the past decade, while the incidence rates have been decreasing in high-income countries, China has seen a gradual increase in stroke incidence, though the mortality rate has remained relatively stable.^{31,32} Ischemic strokes primarily result from occlusion of the cerebral arteries, leading to insufficient blood and oxygen supply to the brain, causing neuronal death and subsequent brain tissue damage.

Currently, ischemic stroke treatment mainly involves thrombolysis, anticoagulation therapy, and surgical interventions.³³ However, the occurrence of I/R injury after treatment often proves difficult to avoid and constitutes a major contributor to neuronal damage. Nonetheless, there are currently no specific drugs or therapies available to effectively address I/R injury and the resulting cognitive impairments following stroke. Thus, timely diagnosis of ischemic stroke is of great significance for patients' treatment and prognosis. In the present study, we demonstrated that serum ELAVL1 was elevated in ischemic stroke patients and correlated with collateral circulation and clinical outcomes. As such, combining collateral circulation and ELAVL1 could be used as a potential biomarker for ischemic stroke diagnosis.

The ELAVL1 is a newly discovered protein associated with the development of many diseases, such as cardiovascular disease (CVD) and cerebral I/R injury. In myocardial I/R injury, ELAVL1 was significantly elevated, and knockdown of ELAVL1 could inhibit ferroptosis and improve I/R injury.³⁴ Du et al. demonstrated that ELAVL1 was upregulated in cerebral I/R injury and facilitated neurobehavioral impairments and brain infarctions after I/R treatment in animal models.²² In an early study, ELAVL1 expression was increased in human hearts and ventricular cardiomyocytes under hyperglycemic conditions and was accompanied by increased inflammation and pyroptosis.³⁵ However, up until now, no study has reported on ELAVL1 in stroke and CAS patients.

In the present research, we demonstrated ELAVL1 upregulation in ischemic stroke patients for the first time, which was associated with inflammation and lipid metabolism, and correlated with collateral circulation. Furthermore, higher levels of ELAVL1 were associated with worse clinical outcomes, consistent with *in vitro* and animal studies using ischemia models. Besides myocardial injury, ELAVL1 also facilitates cellular injury in other diseases. A recent study reported that ELAVL1 knockdown led to the suppression of pyroptosis by inhibiting NLRP3 (NLR family pyrin domain containing 3) in the HK-2 renal tubular cell model of diabetic nephropathy.³⁶ In kidney I/R injury, ELAVL1 promoted ferritinophagy in HK-2 cells and thus aggravated ferroptosis and oxidative stress.³⁷ Similar results are also shown in Parkinson's disease.

Researchers found that elevated ELAVL1 and NLRP3 induced pyroptosis, while downregulation of ELAVL1 inhibited pyroptosis, pyroptosis-induced inflammation and oxidative stress.³⁸ These studies imply a correlation between ELAVL1 and inflammation/oxidative stress, which was also seen in our work, where we demonstrated ELAVL1 was positively correlated with serum CRP, IL-6 and TNF- α . Thus, we speculate that the upregulation of ELAVL1 in ischemic stroke patients is also related to increased inflammatory responses and oxidative stress. However, we did not measure oxidative stress in this study.

Collateral circulation has been widely investigated in stroke patients. It was reported that patients with good

DSA collaterals had markedly smaller hypoperfusion volumes and perfusion mismatch volumes, which was also associated with the hypoperfusion intensity ratio.³⁹ In another study, Sui et al. demonstrated that ASITN/SIR grading was associated with the National Institutes for Health Stroke Scale (NIHSS) and prognosis of wake-up stroke patients.⁴⁰ In a meta-analysis, the authors demonstrated that collateral circulation status and final infarct volume (FIV) are independent outcome predictors for ischemic stroke patients.⁴¹ A more recent study investigated the short-term prognosis of wake-up stroke patients and found that patients with ASITN/SIR grade 2–3 had lower NIHSS and modified Rankin scores (mRS) and higher Barthel index (BI) scores after treatment, indicating collateral circulation is associated with the prognosis of wake-up stroke patients.⁴⁰ However, a recent study demonstrated that inter- and intraobserver agreement of collateral circulation grading using the ASITN/SIR score was poor,²⁶ suggesting that ASITN/SIR grading alone might not be accurate enough for predicting clinical outcomes of ischemic stroke patients.

In addition to ischemic stroke, ASITN/SIR grading is also used to measure collateral circulation in intracranial arterial stenosis and subarachnoid hemorrhage.^{42,43} In our study, we also found that the frequency of 0–1 ASITN/SIR grading was markedly higher in ischemic stroke patients. Besides, we observed that ELAVL1 was negatively associated with ASITN/SIR grades, and when combined, they have the potential for ischemic stroke diagnosis. These findings may provide a potential and novel method for the prediction/diagnosis of ischemic stroke.

Limitations

The study had some limitations. The sample size was small, and the patients were all from a single center. Furthermore, the molecular mechanisms of ELAVL1 in ischemic stroke need to be illustrated in future studies. To further understand the role of ELAVL1 in ischemic stroke, we will conduct studies using both myocardial I/R injury animal models and cellular models. Also, expanding the sample size in clinical investigations is needed in the future.

Conclusions

Serum ELAVL1 was associated with clinical outcomes of ischemic stroke patients. The combination of ELAVL1 and collateral circulation could be used as a potential strategy for the diagnosis of ischemic stroke. All of these results might provide a novel method for the diagnosis of ischemic stroke patients. Since timely treatment is critical, especially in acute ischemic stroke, we think that early diagnosis is of great significance. Thus, novel serum markers may help physicians gather more information on the patients'

condition and better understand the risk for patients susceptible to stroke. However, more clinical and basic studies are still needed to provide deeper insights into the role of ELAVL1 in ischemic stroke.

Data availability


All original data can be obtained from the corresponding author on proper request.


Consent for publication


Not applicable.

ORCID iDs

Bing Song  <https://orcid.org/0009-0001-2538-1861>

Xiangyue Chen  <https://orcid.org/0009-0007-5518-7211>

Kun Pan  <https://orcid.org/0009-0001-1198-1110>

Xiaowei Chen  <https://orcid.org/0009-0004-2162-2527>

References

- Saini V, Guada L, Yavagal DR. Global epidemiology of stroke and access to acute ischemic stroke interventions. *Neurology*. 2021;97(20 Suppl 2): S6–S16. doi:10.1212/WNL.00000000000012781
- Guzik A, Bushnell C. Stroke epidemiology and risk factor management. *Continuum (Minneapolis)*. 2017;23(1):15–39. doi:10.1212/CON.0000000000000416
- Barthels D, Das H. Current advances in ischemic stroke research and therapies. *Biochim Biophys Acta Mol Basis Dis*. 2020;1866(4):165260. doi:10.1016/j.bbadis.2018.09.012
- Béjot Y. Forty years of descriptive epidemiology of stroke. *Neuroepidemiology*. 2022;56(3):157–162. doi:10.1159/000525220
- Chen B, Wei S, Low SW, et al. TRPM4 blocking antibody protects cerebral vasculature in delayed stroke reperfusion. *Biomedicines*. 2023;11(5):1480. doi:10.3390/biomedicines11051480
- Thayabaranathan T, Kim J, Cadilhac DA, et al. Global stroke statistics 2022. *Int J Stroke*. 2022;17(9):946–956. doi:10.1177/17474930221123175
- Li J, Li C, Subedi P, et al. Light alcohol consumption promotes early neurogenesis following ischemic stroke in adult C57BL/6J mice. *Biomedicines*. 2023;11(4):1074. doi:10.3390/biomedicines11041074
- Logroscino G, Beghi E. Stroke epidemiology and COVID-19 pandemic. *Curr Opin Neurol*. 2021;34(1):3–10. doi:10.1097/WCO.0000000000000879
- Bos D, Arshi B, Van Den Bouwhuisen QJA, et al. Atherosclerotic carotid plaque composition and incident stroke and coronary events. *J Am Coll Cardiol*. 2021;77(11):1426–1435. doi:10.1016/j.jacc.2021.01.038
- Feske SK. Ischemic stroke. *Am J Med*. 2021;134(12):1457–1464. doi:10.1016/j.amjmed.2021.07.027
- Tanaka M, Vécsei L. Editorial of Special Issue “Crosstalk between Depression, Anxiety, and Dementia: Comorbidity in Behavioral Neurology and Neuropsychiatry.” *Biomedicines*. 2021;9(5):517. doi:10.3390/biomedicines9050517
- Gomez F, El-Ghanem M, Feldstein E, et al. Cerebral ischemic reperfusion injury: Preventative and therapeutic strategies [published online as ahead of print on September 21, 2022]. *Cardiol Rev*. 2022. doi:10.1097/CRD.0000000000000467
- Tanaka M, Toldi J, Vécsei L. Exploring the etiological links behind neurodegenerative diseases: Inflammatory cytokines and bioactive kynurenines. *Int J Mol Sci*. 2020;21(7):2431. doi:10.3390/ijms21072431
- Amorim S, Felício AC, Aagaard P, Suetta C, Blauenfeldt RA, Andersen G. Effects of remote ischemic conditioning on cognitive performance: A systematic review. *Physiol Behav*. 2022;254:113893. doi:10.1016/j.physbeh.2022.113893
- Di Gregorio F, Battaglia S. Advances in EEG-based functional connectivity approaches to the study of the central nervous system in health and disease. *Adv Clin Exp Med*. 2023;32(6):607–612. doi:10.17219/acem/166476
- Campbell BCV, De Silva DA, Macleod MR, et al. Ischaemic stroke. *Nat Rev Dis Primers*. 2019;5(1):70. doi:10.1038/s41572-019-0118-8
- Iadecola C, Buckwalter MS, Anrather J. Immune responses to stroke: Mechanisms, modulation, and therapeutic potential. *J Clin Invest*. 2020;130(6):2777–2788. doi:10.1172/JCI135530
- Martinez E, Martorell J, Rimbau V. Review of serum biomarkers in carotid atherosclerosis. *J Vasc Surg*. 2020;71(1):329–341. doi:10.1016/j.jvs.2019.04.488
- Kamtchum-Tatuene J, Jickling GC. Blood biomarkers for stroke diagnosis and management. *Neuromol Med*. 2019;21(4):344–368. doi:10.1007/s12017-019-08530-0
- Zhang Z, Yao Z, Wang L, et al. Activation of ferritinophagy is required for the RNA-binding protein ELAVL1/HuR to regulate ferroptosis in hepatic stellate cells. *Autophagy*. 2018;14(12):2083–2103. doi:10.1080/15548627.2018.1503146
- Zhang J, Wang H, Chen H, et al. ATF3-activated accelerating effect of LINC00941/IncIPAF on fibroblast-to-myofibroblast differentiation by blocking autophagy depending on ELAVL1/HuR in pulmonary fibrosis. *Autophagy*. 2022;18(11):2636–2655. doi:10.1080/15548627.2022.2046448
- Du Y, Zhang R, Zhang G, Wu H, Zhan S, Bu N. Downregulation of ELAVL1 attenuates ferroptosis-induced neuronal impairment in rats with cerebral ischemia/reperfusion via reducing DNMT3B-dependent PINK1 methylation. *Metab Brain Dis*. 2022;37(8):2763–2775. doi:10.1007/s11011-022-01080-8
- Ginsberg MD. The cerebral collateral circulation: Relevance to pathophysiology and treatment of stroke. *Neuropharmacology*. 2018;134: 280–292. doi:10.1016/j.neuropharm.2017.08.003
- Desai SM, Jha RM, Linfante I. Collateral circulation augmentation and neuroprotection as adjuvant to mechanical thrombectomy in acute ischemic stroke. *Neurology*. 2021;97(20 Suppl 2):S178–S184. doi:10.1212/WNL.00000000000012809
- Liebeskind DS, Saber H, Xiang B, et al. Collateral circulation in thrombectomy for stroke after 6 to 24 hours in the DAWN trial. *Stroke*. 2022; 53(3):742–748. doi:10.1161/STROKEAHA.121.034471
- Ben Hassen W, Malley C, Boulouis G, et al. Inter- and intraobserver reliability for angiographic leptomeningeal collateral flow assessment by the American Society of Interventional and Therapeutic Neuroradiology/Society of Interventional Radiology (ASITN/SIR) scale. *J NeuroIntervent Surg*. 2019;11(4):338–341. doi:10.1136/neurintsurg-2018-014185
- Liu L, Chen W, Zhou H, et al. Chinese Stroke Association guidelines for clinical management of cerebrovascular disorders: Executive summary and 2019 update of clinical management of ischaemic cerebrovascular diseases. *Stroke Vasc Neurol*. 2020;5(2):159–176. doi:10.1136/svn-2020-000378
- Gu HQ, Yang X, Wang CJ, et al. Clinical characteristics, management, and in-hospital outcomes in patients with stroke or transient ischemic attack in China. *JAMA Netw Open*. 2021;4(8):e2120745. doi:10.1001/jamanetworkopen.2021.20745
- Consoli A, Pizzuto S, Sgreccia A, et al. Angiographic collateral venous phase: A novel landmark for leptomeningeal collaterals evaluation in acute ischemic stroke [published online as ahead of print on December 20, 2022]. *J NeuroIntervent Surg*. 2022. doi:10.1136/jnis-2022-019653
- Wu S, Wu B, Liu M, et al. Stroke in China: Advances and challenges in epidemiology, prevention, and management. *Lancet Neurol*. 2019;18(4):394–405. doi:10.1016/S1474-4422(18)30500-3
- Wang W, Jiang B, Sun H, et al. Prevalence, incidence, and mortality of stroke in China: Results from a nationwide population-based survey of 480 687 adults. *Circulation*. 2017;135(8):759–771. doi:10.1161/CIRCULATIONAHA.116.025250
- Ma Q, Li R, Wang L, et al. Temporal trend and attributable risk factors of stroke burden in China, 1990–2019: An analysis for the Global Burden of Disease Study 2019. *Lancet Public Health*. 2021;6(12):e897–e906. doi:10.1016/S2468-2667(21)00228-0
- Rabinstein AA. Update on treatment of acute ischemic stroke. *Continuum (Minneapolis)*. 2020;26(2):268–286. doi:10.1212/CON.0000000000000840
- Chen HY, Xiao ZZ, Ling X, Xu RN, Zhu P, Zheng SY. ELAVL1 is transcriptionally activated by FOXO1 and promotes ferroptosis in myocardial ischemia/reperfusion injury by regulating autophagy. *Mol Med*. 2021; 27(1):14. doi:10.1186/s10020-021-00271-w
- Jeyabal P, Thandavarayan RA, Joladarashi D, et al. MicroRNA-9 inhibits hyperglycemia-induced pyroptosis in human ventricular cardiomyocytes by targeting ELAVL1. *Biochem Biophys Res Commun*. 2016; 471(4):423–429. doi:10.1016/j.bbrc.2016.02.065

36. Li X, Zeng L, Cao C, et al. Long noncoding RNA MALAT1 regulates renal tubular epithelial pyroptosis by modulated miR-23c targeting of ELAVL1 in diabetic nephropathy. *Exp Cell Res*. 2017;350(2):327–335. doi:10.1016/j.yexcr.2016.12.006
37. Sui M, Xu D, Zhao W, et al. CIRBP promotes ferroptosis by interacting with ELAVL1 and activating ferritinophagy during renal ischaemia–reperfusion injury. *J Cell Mol Med*. 2021;25(13):6203–6216. doi:10.1111/jcmm.16567
38. Zhang Q, Huang XM, Liao JX, et al. LncRNA HOTAIR promotes neuronal damage through facilitating NLRP3 mediated-pyroptosis activation in Parkinson's disease via regulation of miR-326/ELAVL1 axis. *Cell Mol Neurobiol*. 2021;41(8):1773–1786. doi:10.1007/s10571-020-00946-8
39. Guenego A, Fahed R, Albers GW, et al. Hypoperfusion intensity ratio correlates with angiographic collaterals in acute ischaemic stroke with M1 occlusion. *Eur J Neurol*. 2020;27(5):864–870. doi:10.1111/ene.14181
40. Sui H, Yan C, Yang J, Zhao X. Clinical significance of evaluation of collateral circulation in short-term prognosis of wake-up stroke patients. *Adv Clin Exp Med*. 2021;30(2):183–188. doi:10.17219/acem/121927
41. Malhotra K, Safouris A, Goyal N, et al. Association of statin pretreatment with collateral circulation and final infarct volume in acute ischemic stroke patients: A meta-analysis. *Atherosclerosis*. 2019;282:75–79. doi:10.1016/j.atherosclerosis.2019.01.006
42. Hao X, Wang S, Jiang C, et al. The relation between plasma miR-126 levels and cerebral collateral circulation in patients with intracranial arterial stenosis. *Neurol Neurochir Pol*. 2021;55(3):281–288. doi:10.5603/PJNNS.a2021.0019
43. Al-Mufti F, Witsch J, Manning N, et al. Severity of cerebral vasospasm associated with development of collaterals following aneurysmal subarachnoid hemorrhage. *J Neurointervent Surg*. 2018;10(7):638–643. doi:10.1136/neurintsurg-2017-013410

HGFN deficiency exacerbates spinal cord injury by promoting inflammation and cell apoptosis through regulation of the PI3K/AKT signaling pathway

Qinghua Ding^{1,A,D,F}, Hongbin Gao^{1,B,C,F}, Xianghuai Hu^{1,C,E,F}, Weilu Gao^{2,A,B,F}

¹ Department of Spine Surgery, Chaohu Hospital of Anhui Medical University, Hefei, China

² Department of Orthopedics, The First Affiliated Hospital of Anhui Medical University, Hefei, China

A – research concept and design; B – collection and/or assembly of data; C – data analysis and interpretation;

D – writing the article; E – critical revision of the article; F – final approval of the article

Advances in Clinical and Experimental Medicine, ISSN 1899–5276 (print), ISSN 2451–2680 (online)

Adv Clin Exp Med. 2024;33(9):929–940

Address for correspondence

Weilu Gao

E-mail: weiqiang83@163.com

Funding sources

This study was supported by the Anhui Health Commission Scientific Research Project of China (No. AHWJ2021b060), the Scientific Research Fund Project of Anhui Medical University (No. 2020xkj181), and the Basic and Clinical Cooperative Research Promotion Plan of Anhui Medical University (No. 2021xkjT003).

Conflict of interest

None declared

Received on April 10, 2023

Reviewed on June 10, 2023

Accepted on October 10, 2023

Published online on November 28, 2023

Cite as

Ding Q, Gao H, Hu X, Gao W. HGFN deficiency exacerbates spinal cord injury by promoting inflammation and cell apoptosis through regulation of the PI3K/AKT signaling pathway. *Adv Clin Exp Med.* 2024;33(9):929–940. doi:10.17219/acem/174004

DOI

10.17219/acem/174004

Copyright

Copyright by Author(s)

This is an article distributed under the terms of the Creative Commons Attribution 3.0 Unported (CC BY 3.0) (<https://creativecommons.org/licenses/by/3.0/>)

Abstract

Background. Spinal cord injury (SCI) is a devastating neurological disease characterized by neuroinflammation and neuronal apoptosis. The PI3K/AKT signaling pathway is related to the pathological process of SCI. Hematopoietic growth factor inducible neurokinin-1 type (HGFN) is a transmembrane glycoprotein that exerts neuroprotective actions in various neurodegenerative diseases. However, the potential role and mechanism of HGFN in the development of SCI are still unclear.

Objectives. To investigate the effect of HGFN on inflammation and neuronal apoptosis as well as the underlying mechanism in SCI.

Materials and methods. A rat model of SCI was established, and Basso–Beattie–Bresnahan (BBB) motor function assay was performed to detect motor function. Expression of HGFN was measured at 7 days after injury by western blot and immunofluorescence. An HGFN-shRNA-carrying lentivirus was injected into the injury site to block the expression of HGFN. The effects of HGFN on neuronal apoptosis and the PI3K/AKT pathway were analyzed by TUNEL staining and immunofluorescence. The Iba-1 expression and the levels of pro-inflammatory cytokines were measured in spinal cord tissues by immunofluorescence staining and real-time polymerase chain reaction (PCR) analysis.

Results. The SCI rats showed increased expression of HGFN in spinal cord tissues. The HGFN deficiency aggravated SCI lesions, as evidenced by decreased BBB scores. At 7 days post-injury, HGFN knockdown promoted neuronal apoptosis, accompanied by the increased expression level of the apoptosis effector cleaved caspase-3 and cleaved PARP, and decreased anti-apoptotic protein Bcl-2 expression. Moreover, HGFN knockdown aggravated the inflammation process, indicated by increased Iba1-positive cells. The HGFN knockdown increased the production of pro-inflammatory cytokines including IL-1 β , TNF- α and IL-6. Further analysis revealed that HGFN deficiency reduced the activation of the PI3K/AKT pathway in spinal cord tissue after injury.

Conclusions. Lentivirus-mediated downregulation of HGFN exacerbates inflammation and neuronal apoptosis in SCI by regulating the PI3K/AKT pathway, and provides clues for developing novel therapeutic approaches and targets against SCI.

Key words: inflammation, PI3K/AKT pathway, apoptosis, spinal cord injury, HGFN

Background

Spinal cord injury (SCI) is a devastating neurological disease that impairs neurological functions and leads to irreversible motor dysfunction.¹ The initial injury involves mechanical trauma of the spine that provokes a series of cellular and molecular events, including posttraumatic inflammation, edema, motor neuron apoptosis, and death of neurons.^{2,3} Although considerable effort has been devoted to understanding the pathophysiology of SCI, the underlying mechanisms of the pathophysiological cascade of SCI remain elusive. Extensive pathological hallmarks, inflammation responses and neuronal apoptosis represent the major characteristics of SCI.^{4,5} The phosphoinositide 3-kinase (PI3K)/AKT signaling pathway is closely related to the pathological process of SCI, and the activation of the PI3K/AKT pathway delays the inflammatory response and promotes neurological function recovery in the progression of SCI.^{6,7}

Hematopoietic growth factor inducible neurokinin-1 type (HGFIN), an endogenous type I transmembrane glycoprotein, was initially isolated from a cDNA library based on low-metastatic melanoma cells⁸ and has been found to regulate various biological functions.^{9–11} Notably, HGFIN exerts neuroprotective effects by protecting against neuronal apoptosis and enhancing neurogenesis through the regulation of the PI3K/AKT pathways.¹² In addition, HGFIN is upregulated in amyotrophic lateral sclerosis and inhibits neuron cell death.¹³ It has been indicated that HGFIN is significantly associated with inflammatory responses and is considered a negative regulator of inflammation.^{14–16} Hematopoietic growth factor inducible neurokinin-1 type exerts an anti-inflammatory effect in acutely injured kidneys and acute wound healing,^{15,17} and attenuates the inflammatory response of astrocytes and lipopolysaccharide (LPS)-induced inflammation.^{18,19} The inhibition of HGFIN suppresses pro-inflammatory cytokine expression in LPS-induced microglia.²⁰ Importantly, HGFIN expression has been observed to be significantly altered in the progression of SCI and exert a functional role in the regulation of neuronal death and neuroinflammation.²¹ However, the regulatory role and specific mechanism involved in the effect of HGFIN on the pathophysiology of SCI are still unknown.

In the present study, we aimed to investigate the impact of HGFIN on the extent of the SCI model, including neuronal apoptosis and the inflammation process. The expression of HGFIN in spinal cord tissues after SCI was examined. In addition, the impact of HGFIN deficiency on neuronal apoptosis and the inflammatory process was explored following SCI. Moreover, the association between HGFIN and the activation of the PI3K/AKT pathway was examined. We speculated that HGFIN exerted its function through the regulation of PI3K/AKT signaling. Collectively, the target transmembrane glycoprotein,

HGFIN, might be a potential therapeutic strategy for SCI treatment.

Objectives

This study aimed to investigate the effect of HGFIN on rat SCI model. We examined the expression level of HGFIN in the spinal cord tissues following SCI. In addition, we investigated the specific effects of HGFIN on the neuroprotective actions and inflammatory process after SCI. We evaluated the effects of HGFIN on the activation of the PI3K/AKT signaling pathway to further clarify its possible underlying mechanism.

Materials and methods

Animals

All procedures involving the animals were approved by the Animal Care and Use Committee of the Chaohu Hospital at the Anhui Medical University (approval No. KYXM-202207-009). Male Sprague–Dawley (SD) rats (8–12 weeks old) were maintained under standard conditions (22 ± 1°C, 45–55% humidity, and 12-h light/dark cycle). The number of animals subjected to surgical treatment was calculated to be 6 per experimental group. Rats were randomized into 4 groups: 1. Sham group; 2. SCI group; 3. SCI+sh-NC group; 4. SCI+sh-HGFIN group. The assessments were shown as a schematic in Fig. 1A.

Lentivirus construction and animal treatment

Lentiviruses containing HGFIN-shRNA (NM_053110) were constructed and synthesized by Shaanxi YouBio Technology Co., Ltd (Changsha China). The target sequence against HGFIN was as follows: 5'-CGAAGGT-GAAAGATGTGTATG-3'. The virus titer was determined as 1 × 10⁹ TU/mL. For the establishment of the SCI model, SD rats were anesthetized, and a T10 laminectomy was carried out after making a 4-cm longitudinal incision and careful dissection. Vascular clips were placed through the dorsal intervertebral space of T8–T9 to compress the spinal cord for 10 min in order to generate an injury. Rats in the sham group had the surgical procedure without spinal cord contusion. After surgery, the muscles and skin were sutured. After sterile analgesic treatment and ongoing monitoring, rats received bladder massage 3 times a day to prevent urological infection. Following SCI, 10 µL of lentivirus containing HGFIN-shRNA (1 × 10⁹ TU/mL) or NC-shRNA (1 × 10⁹ TU/mL) was locally injected into the injured site immediately using

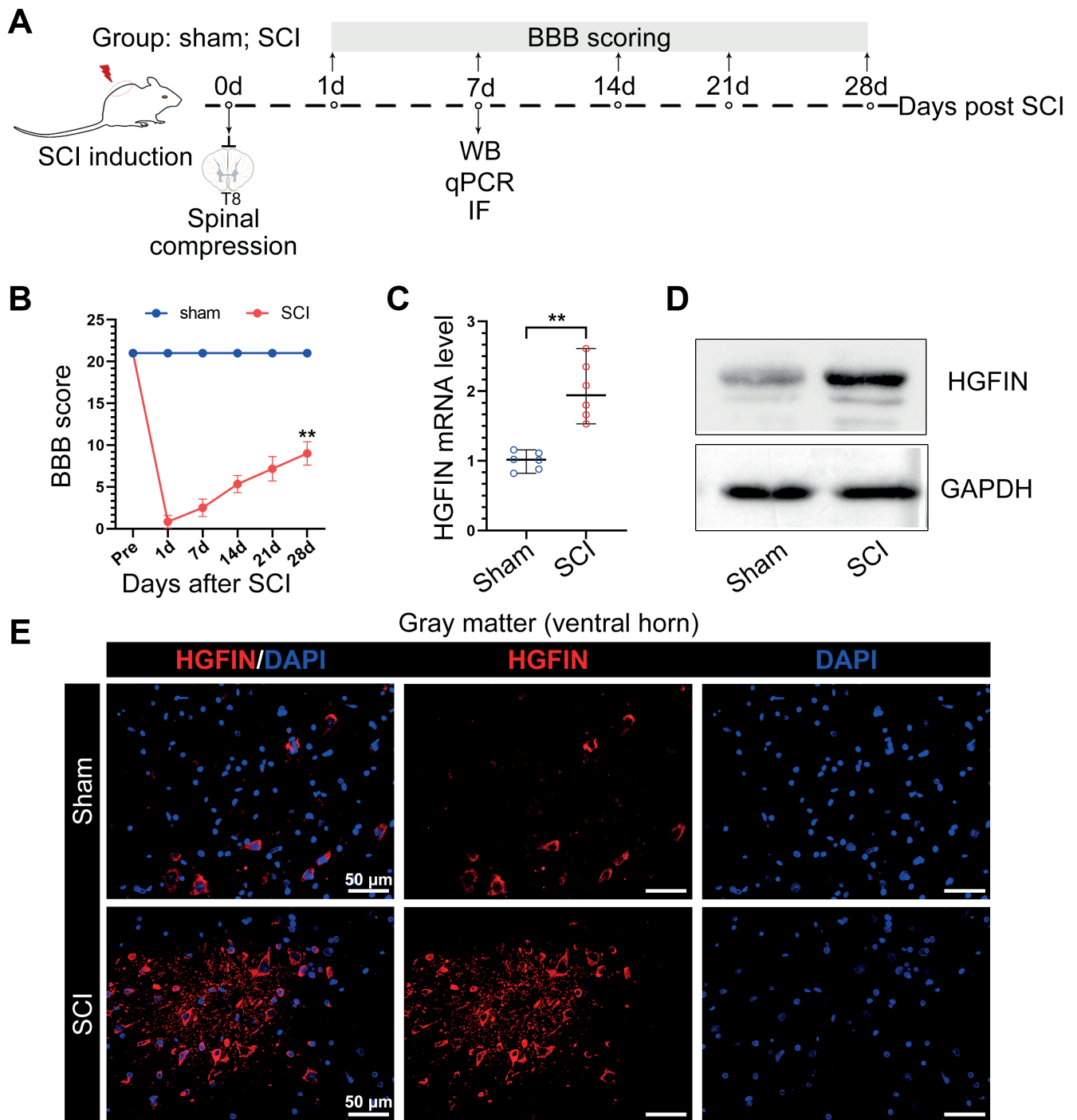


Fig. 1. Expression of hematopoietic growth factor inducible neurokinin-1 type (HGFIN) in the spinal cord after spinal cord injury (SCI). **A.** Experimental protocol for SCI timing and outcome assessment; **B.** Basso–Beattie–Bresnahan (BBB) exercises scored at 1, 7, 14, 21, and 28 days after injury in the sham and SCI groups (n = 6). Differences between group means in BBB scores at 28 days after the injury were identified using the Mann–Whitney U test; **C.** HGFIN mRNA levels in spinal cord tissues after SCI were measured by real-time polymerase chain reaction (PCR). The Mann–Whitney U tests were used to calculate the significant differences; **D.** Western blot results of HGFIN protein levels after SCI; **E.** Immunofluorescence staining for the expression of HGFIN in the grey matter after SCI. Data are presented using medians (range)

**p < 0.01 compared to the sham group; WB – western blot; IF – immunofluorescence.

a microsyringe, while the rats in the sham group received the same volume of normal saline. Behavioral testing was assessed using a well-established Basso–Beattie–Bresnahan (BBB) score assay at 1, 7, 14, 21, and 28 days. The animals were euthanized using 30% volume/min

CO₂. Spinal cord tissues at the lesion sites of the cord were collected from rats on day 7 post-injury. All tissues were quickly placed in paraformaldehyde overnight and embedded in paraffin for further examinations. The assessments are shown as a schematic in Fig. 2A.

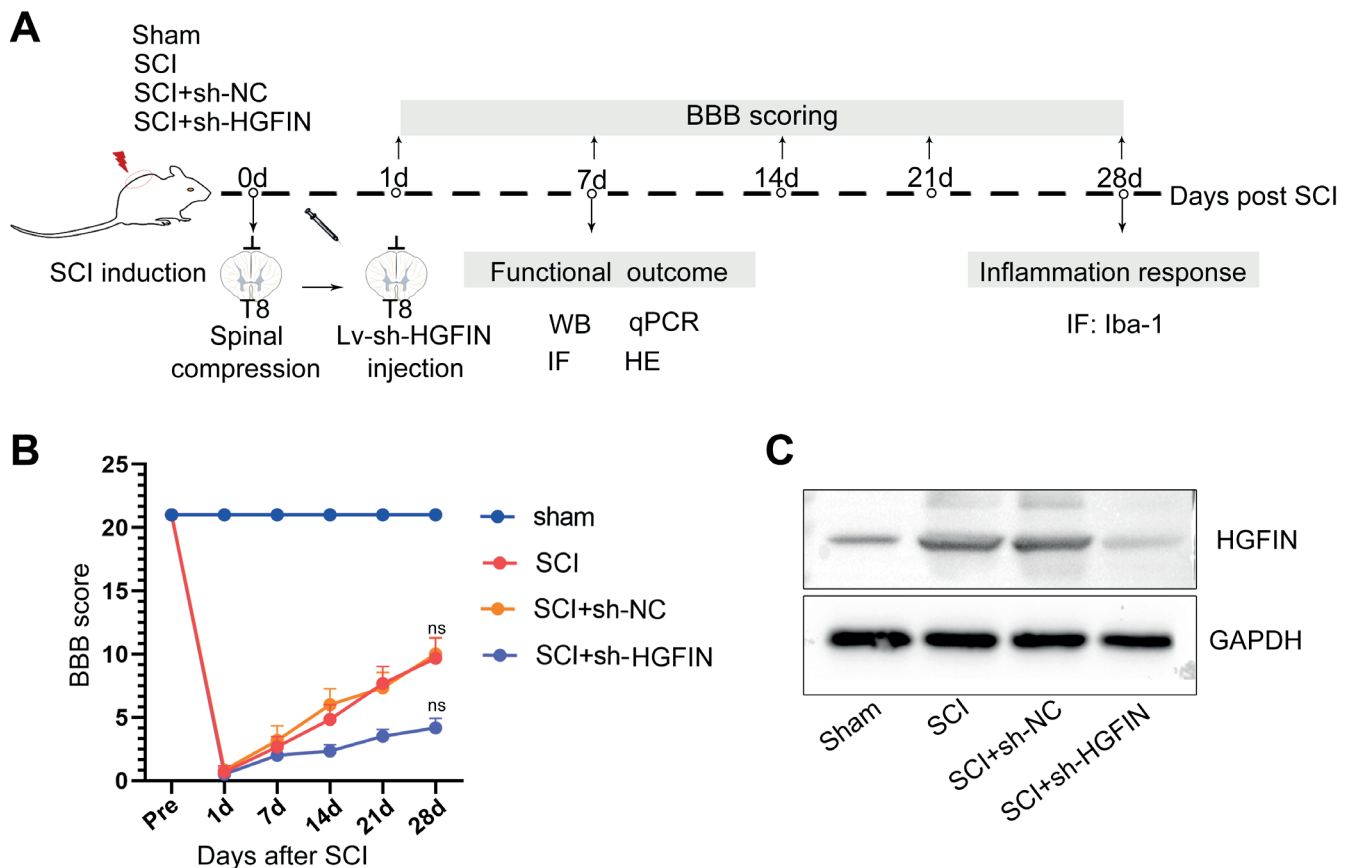


Fig. 2. Hematopoietic growth factor inducible neurokinin-1 type (HGFIN) deficiency aggravates injury to the spinal cord after spinal cord injury (SCI). HGFIN shRNA lentivirus vectors were locally injected into the injured site immediately after SCI. **A.** Timeline of the experimental protocol; **B.** Basso–Beattie–Bresnahan (BBB) exercises were scored at 1, 7, 14, 21, and 28 days after SCI in all groups ($n = 6$). Differences between the group means in BBB scores at 28 days after the injury were identified using the Kruskal–Wallis test with Dunn’s post hoc test; **C.** HGFIN protein levels were detected by western blot assay following injection of sh-HGFIN lentivirus in SCI rats

ns – not significant, compared to the sham or SCI+sh-NC groups; WB – western blot; IF – immunofluorescence; qPCR – quantitative real-time polymerase chain reaction; HE – hematoxylin and eosin.

Real-time polymerase chain reaction

For the real-time polymerase chain reaction (PCR) analysis, total RNA was extracted from spinal cord tissues with TRIpure™ solution (BioTeke, Beijing China). Reverse transcription of the RNA samples was carried out using a PCR system according to the protocol. Data were calculated using the $2^{-\Delta\Delta C_t}$ method and normalized to the housekeeping gene *GAPDH*. Primers were as follows:

rat HGFIN
5'-TAGAAGTCAACATCATCCAGGTA-3' (forward),
5'-ACGGACAGGAGGCACAG-3' (reverse);

rat TNF- α
5'-CGGAAAGCATGATCCGAGAT-3' (forward),
5'-AGACAGAAGAGCGTGGTGGC-3' (reverse);

rat IL-1 β
5'-TTCAAATCTCACAGCAGCAT-3' (forward),
5'-CACGGCAAGACATAGGTAG-3' (reverse);

rat IL-6
5'-CAGCCACTGCCTTCCCTA-3' (forward),
5'-TTGCCATTGCACAACCTCTTT-3' (reverse).

Western blot analysis

For western blot assay, total proteins were extracted from spinal cord tissues and homogenized in RIPA lysates (Solarbio, Beijing, China) supplemented with phenylmethylsulphonyl fluoride (PMSF). The protein concentration was evaluated by the BCA assay kit (Solarbio). Proteins were resolved on sodium dodecyl-sulfate polyacrylamide gel electrophoresis (SDS-PAGE) gels, transferred to the polyvinylidene fluoride membranes (MilliporeSigma, St. Louis, USA), and blocked in the non-fat powdered milk. The membranes were then incubated with primary antibody at 4°C overnight. After incubation with HRP-conjugated secondary antibodies, the blots were developed with enhanced chemiluminescence substrate reagents (Solarbio). Primary antibodies used in the present study included HGFIN (1:5000; Proteintech Genomics, San Diego, USA; 66926-1-Ig), cleaved PARP (1:1000, AF7023; Affinity Biosciences, Cincinnati, USA), cleaved caspase-3 (1:1000, AF7022; Affinity), Bcl-2 (1:1000, AF6139; Affinity), AKT (1:3000, 10176-2-AP; ProteinTech), and p-AKT (1:2000, 66444-1-Ig; ProteinTech).

Immunofluorescent staining

For immunofluorescence staining, spinal cord samples were embedded in paraffin. The sections were deparaffinized and blocked with 1% bovine serum albumin (BSA), followed by incubation at 4°C overnight with primary antibodies against HGFN (66926-1-Ig; ProteinTech), p-AKT (Ser473, 66444-1-Ig; ProteinTech), and ionized calcium-binding adapter molecule-1 (Iba-1, 10904-1-AP; ProteinTech). Then, the tissues were nurtured with Cy3-labeled secondary antibodies (IgG; Invitrogen, Waltham, USA) for 60 min, followed by counterstaining with 4',6-diamidyno-2-fenyloindol (DAPI; Aladdin, Shanghai, China) to stain the cell nucleus. After being mounted, the immunofluorescent images were obtained using a fluorescence microscope (Olympus Corp., Tokyo, Japan).

TUNEL-NeuN staining

Double immunofluorescent staining with a TUNEL-NeuN assay was used to detect neuronal apoptosis. In brief, paraffin-embedded spinal cord samples were deparaffinized and permeabilized in 0.1% Triton X-100 (Beyotime, Shanghai, China). The sections were repaired in citric acid/sodium citrate solution for 10 min. Then, samples were stained with TUNEL reagent using the In Situ Cell Death Detection Kit (No. 12156792910; Roche Diagnostics, Basel, Switzerland) according to protocols. Samples were blocked in 1% BSA and incubated at 4°C overnight with a primary antibody against NeuN (ab104224; Abcam, Cambridge, USA) and visualized with FITC-labeled goat anti-mouse IgG (ab6785; Abcam). The nucleus was counterstained with DAPI and sections were sealed. TUNEL-positive cells (labeled with red fluorescence) and NeuN-positive cells (labeled with green fluorescence) in tissues were captured under a fluorescence microscope. The ratio of NeuN-TUNEL double-stained cells/NeuN-stained cells was calculated for the quantification of neuronal apoptosis.

Hematoxylin and eosin staining

The fixed spinal cord tissues were used for hematoxylin and eosin (H&E) staining according to the routine procedure. In brief, the paraffin-embedded sections were successively deparaffinized, dehydrated and subjected to H&E staining for conventional histopathologic examination in SCI. The sections were incubated with hematoxylin for 5 min, followed by flushing with running water, and counterstained with eosin staining solution for 3 min. After dehydration, clearing and mounting, the sealed slides were captured under a light microscope.

Statistical analyses

All calculations were performed by the GraphPad Prism software (GraphPad Software, San Diego, USA) with a probability value of $p < 0.05$ considered significant; all values were expressed using medians (range). The small sample size limits checking test assumptions reliably. Nonparametric tests were used in the present study. A Mann–Whitney U test was performed to analyze data when comparing 2 groups. The homogeneity of variance was determined via the F-test. In the case of multiple comparisons, a Kruskal–Wallis test with Dunn's post hoc test was performed. The homogeneity of variance was determined via the Brown–Forsythe test.

In the present study, HGFN mRNA levels were analyzed using the Mann–Whitney U test. The quantification of TUNEL/NeuN, p-AKT positive cells, Iba-1 positive cells, and levels of TNF- α , IL-1 β , and IL-6 were analyzed using the Kruskal–Wallis test with a Dunn's post hoc test. Differences between group means in BBB scores were analyzed 28 days after the injury using the Kruskal–Wallis test.

Results

HGFN expression is increased in spinal cord tissues after SCI

An SCI animal model was successfully established. We used BBB scores to assess motor function for 28 days after the SCI. Normal motor function was scored as 21 points. As indicated in Fig. 1B, rats in the SCI groups showed lower BBB scores compared with the sham group. By the time of injury, BBB scores increased progressively and recovered to around 9 at 28 days after SCI. The expression of HGFN in the spinal cord tissues after SCI was determined by western blot and real-time PCR assay. The HGFN mRNA and protein expression levels in spinal cord tissues were significantly increased at 7 days in the SCI group compared with the sham group (Fig. 1C,D). Furthermore, immunofluorescence staining was performed to detect HGFN expression in the spinal cord tissues of SCI rats, and the results indicated that HGFN was highly expressed in the gray matter in the spinal cord tissues of SCI rats (Fig. 1E).

To further explore the regulatory role of HGFN, lentiviruses carrying HGFN shRNA particles were injected into SCI rats to block HGFN expression. Basso–Beattie–Bresnahan motor function scores were performed to assess motor function at indicated time points after SCI. Results of BBB scores indicated that HGFN deficiency aggravated SCI lesions (Fig. 2B). Basso–Beattie–Bresnahan scores in the SCI+sh-HGFN group were lower than those in the SCI+sh-NC group. Animals treated with sh-HGFN accelerated injury and as the observations continued, we noted functional recovery in the SCI+sh-HGFN group, and there were no significant differences in motor

function at the end of observation on day 28 between the SCI+sh-NC and SCI+sh-HGFIN groups. Western blot assay revealed that HGFIN protein expression was up-regulated in SCI rat tissues and when administered with HGFIN shRNA exhibited significantly lower expression of HGFIN (Fig. 2C).

Reduced HGFIN expression promotes SCI-induced neuronal apoptosis

The impact of HGFIN deficiency on neuronal apoptosis was assessed at 7 days after SCI. Double staining of TUNEL and NeuN revealed that SCI caused an elevated number of apoptotic neurons, and treatment with sh-HGFIN further aggravated neuronal apoptosis (Fig. 3A). In addition, the ratio of NeuN-TUNEL double-stained cells/NeuN-stained cells was quantified. A larger percentage of apoptotic neurons was observed in SCI groups ($p < 0.05$), and HGFIN knockdown further promoted neuronal apoptosis by increasing the percentage of apoptotic neurons (Fig. 3B). As indicated in Fig. 3C, the levels of apoptosis effector cleaved caspase-3 and cleaved PARP were found to be significantly upregulated, while the levels of anti-apoptotic protein Bcl-2 were downregulated at 7 days post-SCI. The HGFIN depletion further promoted SCI-induced neuronal apoptosis, as indicated by upregulated cleaved caspase-3, cleaved PARP and downregulated Bcl-2.

Depletion of HGFIN activates the PI3K/AKT signaling pathway

Next, we explored whether HGFIN deficiency was implicated with PI3K/AKT pathway activation. To this end, immunofluorescent staining for p-AKT was performed at 7 days post-injury. As indicated in Fig. 4A, a reduction of p-AKT was observed in the injured spinal cord tissues of SCI rats compared to the sham rats. Knockdown of HGFIN after SCI significantly reduced p-AKT expression in the spinal cord gray and white matter ($p < 0.05$; Fig. 4A,B). Western blot assays further confirmed that HGFIN deficiency decreased the protein expression of p-AKT (Fig. 4C).

Depletion of HGFIN promotes the inflammatory response after SCI

The Iba-1 immunofluorescent assays were performed to assess the reactive inflammatory responses in the injured spinal cord tissues. As shown in Fig. 5A, the number of Iba-1 positive cells in the SCI groups was markedly increased ($p < 0.05$; Fig. 5B). Furthermore, SCI rats administered with HGFIN shRNA showed a larger number of Iba-1 positive cells in the spinal cord tissues at 7 days post-SCI. Hematoxylin and eosin staining was performed to assess the histopathological changes in spinal cord tissues. The results of the staining showed the infiltration

of neutrophils, congestion and structural damage of the SCI, and the injury was notably aggravated following HGFIN knockdown (Fig. 6A). In addition, the effect of HGFIN deficiency on the expression of inflammatory-associated cytokines was measured. The expressions of pro-inflammatory cytokines, including TNF- α , IL-1 β and IL-6, were low in the sham groups and significantly increased in SCI spinal cord rats. The inhibition of HGFIN further promoted the production of pro-inflammatory cytokines ($p < 0.05$; Fig. 6B).

Discussion

Spinal cord injury is a complex and multifaceted disease process, and numerous therapeutic approaches against SCI have generated successful results,^{2,22,23} among which neuroprotection and improving the immune environment are promising strategies.²⁴ Accumulating evidence demonstrates that HGFIN has neuroprotective roles and is implicated in inflammatory responses.^{18,19} Thus, we explored whether HGFIN exerts a regulatory function in SCI progression and can be a potential marker for SCI. In the present study, a rat model of SCI was successfully established, and the expression of HGFIN in the spinal cord tissues of the SCI rats was detected. It has been indicated that HGFIN was aggregated in the grey and white matter of spinal cord tissue in amyotrophic lateral sclerosis patients.²⁵ Consistently, in the present study, immunofluorescent staining for HGFIN revealed that HGFIN was highly expressed in the grey matter of spinal cord tissue after SCI. Hematopoietic growth factor inducible neurokinin-1 type was found to be highly expressed in the spinal cord tissue of SCI rats. Emerging evidence has indicated that HGFIN is recognized as a potential neurodegenerative disease-related marker and is found to be upregulated in numerous neurodegenerative diseases such as Alzheimer's disease, Parkinson's disease and amyotrophic lateral sclerosis.^{26–29} Therefore, lentiviruses carrying HGFIN shRNA were injected into SCI rats to knock down HGFIN, and the effect of HGFIN deficiency on inflammation and neuronal apoptosis was explored.

The destructive effect of neuronal apoptosis in neuronal diseases, including SCI, has been well-documented.^{30,31} It is generally accepted that apoptosis is important in the pathophysiology of SCI, and apoptotic-related signaling and mediators, such as caspase cascades, Bax/Bcl-2, and TNF- α , in apoptosis, are shown to modulate the SCI progression.^{32,33} Previous studies have indicated that the expression of pro-apoptotic proteins was increased after neuronal injury, and anti-apoptotic protein expression was commonly decreased.^{34,35} Following SCI, extensive activation of PARP and activated caspase-3 occurred, and Bcl-2 expression was decreased in spinal cord tissues.³⁶ These findings demonstrated that modifying neuronal apoptosis and improving neuron survival might

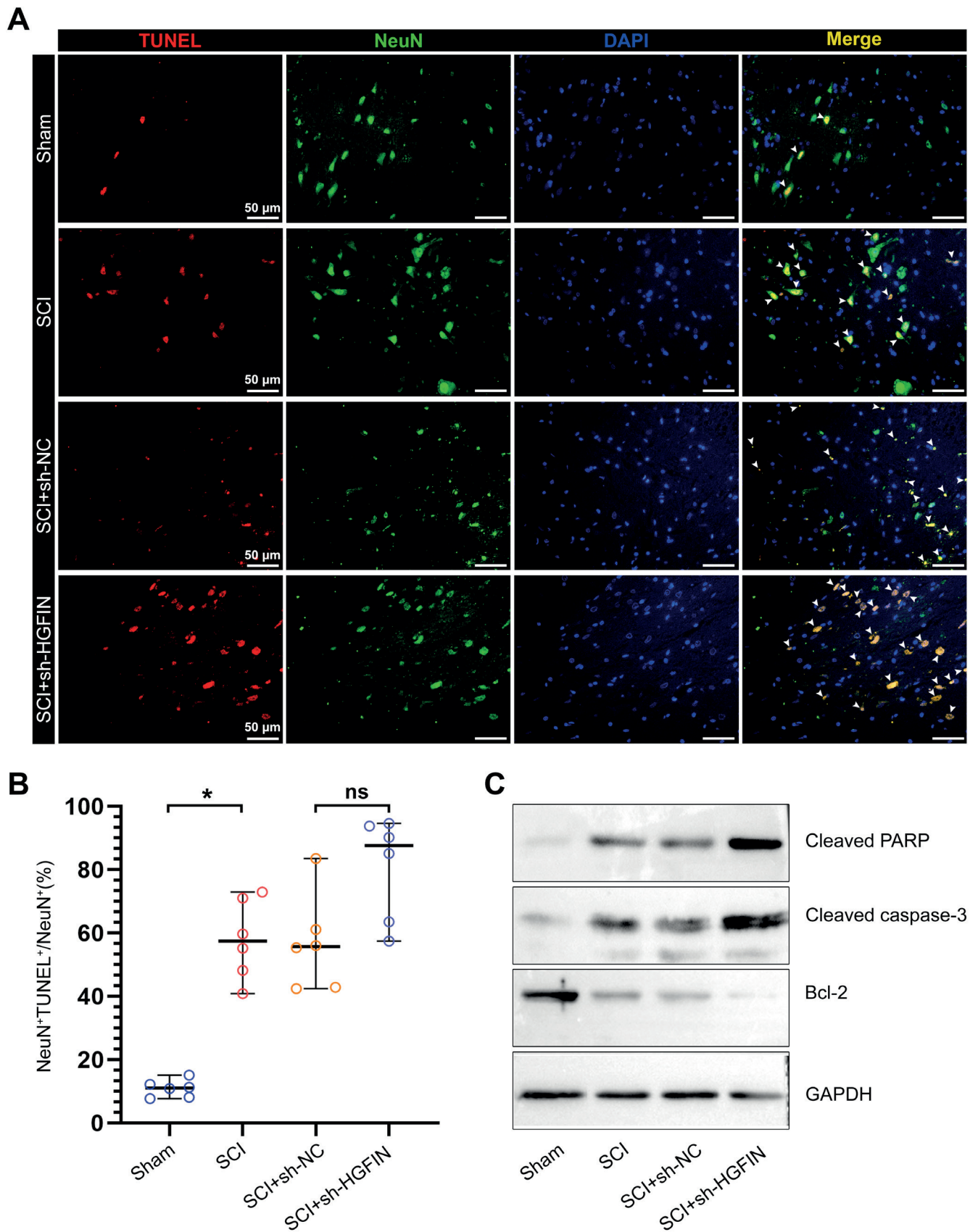


Fig. 3. Effect of hematopoietic growth factor inducible neurokinin-1 type (HGFN)-deficiency on neuronal apoptosis after spinal cord injury (SCI). **A.** Representative images of TUNEL/NeuN double staining after SCI by immunofluorescence in all groups; **B.** Quantitative analysis of the results in panel A ($n = 6$). The Kruskal–Wallis test was used to calculate the significant differences; **C.** Western blot results of apoptosis-related factors, including cleaved caspase-3, cleaved PARP and Bcl-2. Data are presented using the median (range)

* $p < 0.05$ compared to the sham group; ns – not significant, compared to the SCI+sh-NC group.

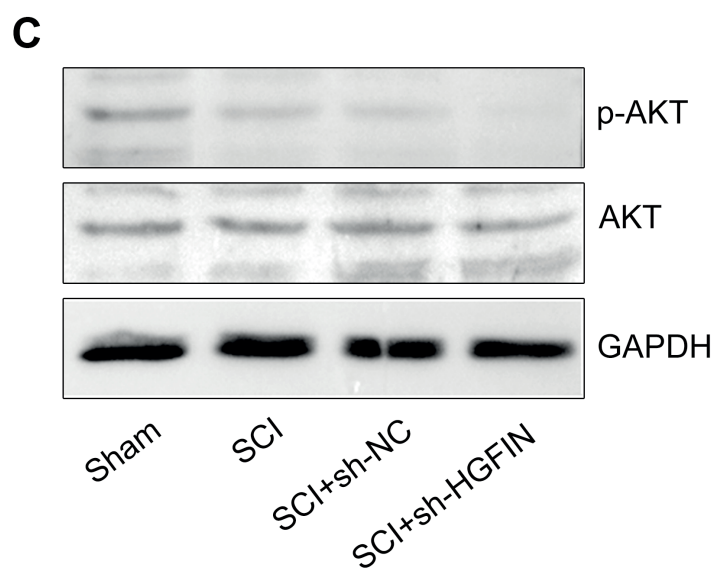
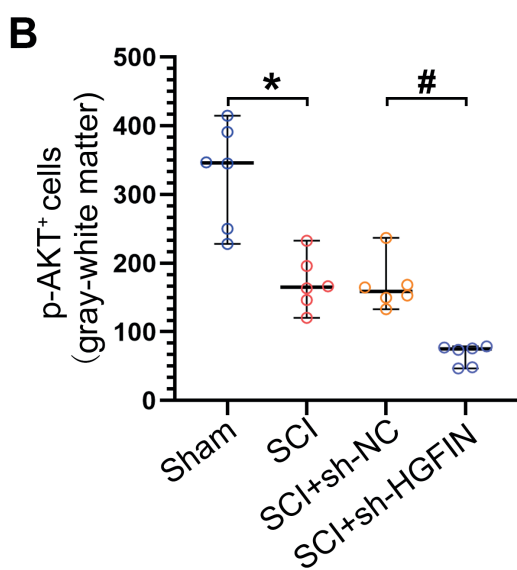
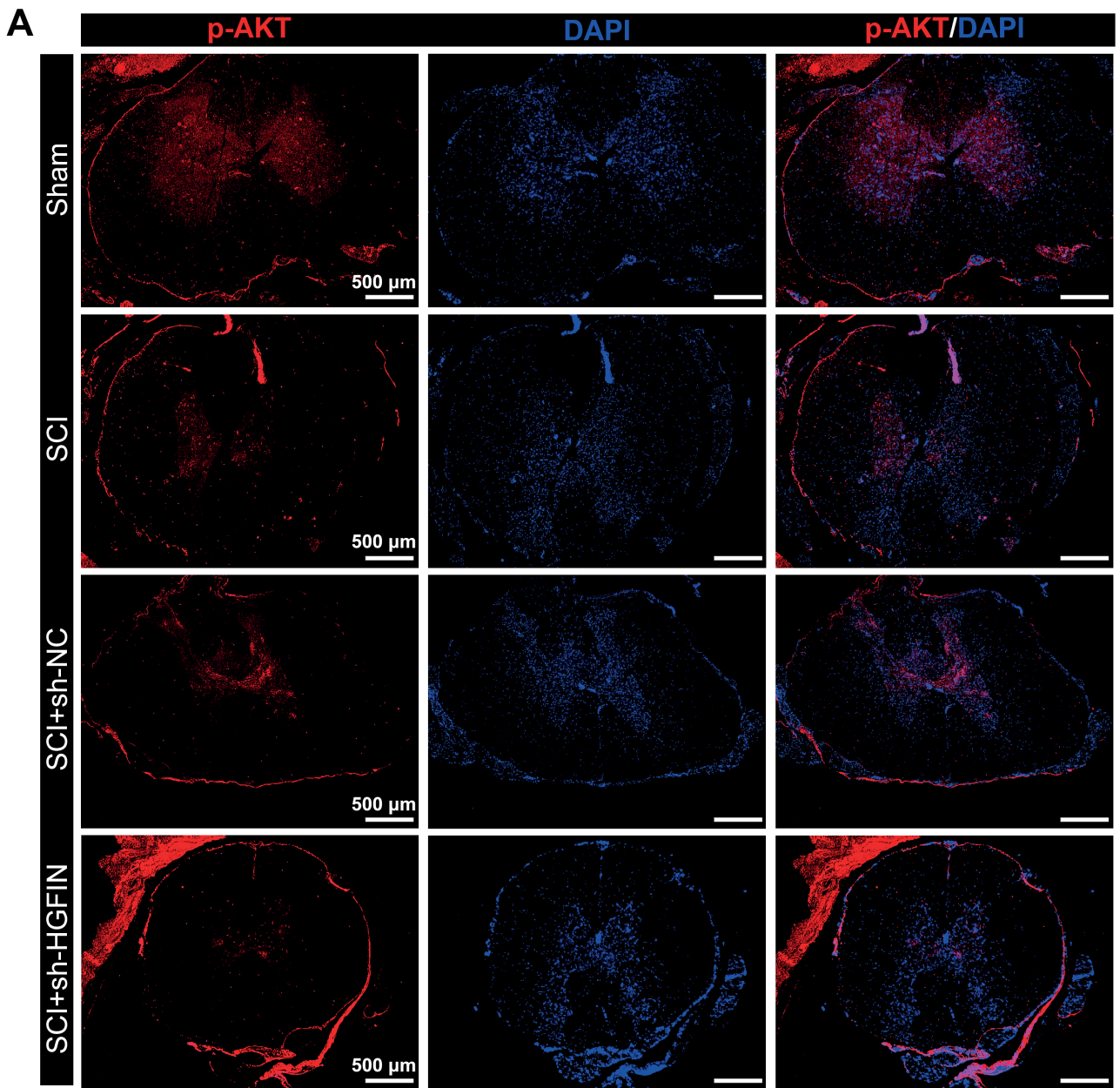


Fig. 4. Downregulation of hematopoietic growth factor inducible neurokinin-1 type (HGFIN) represses activation of the phosphoinositide 3-kinase (PI3K)/AKT pathway after spinal cord injury (SCI). **A.** Immunofluorescence staining for p-AKT in the grey-white matter after injection of sh-HGFIN lentivirus in SCI models; **B.** Quantitative analysis of the number of p-AKT positive cells ($n = 6$). The Kruskal–Wallis test was used to calculate the significant differences; **C.** Western blot results of AKT and p-AKT protein levels. Data are presented using the median (range)

* $p < 0.05$ compared to the sham group; # $p < 0.05$ compared to the SCI+sh-NC group.

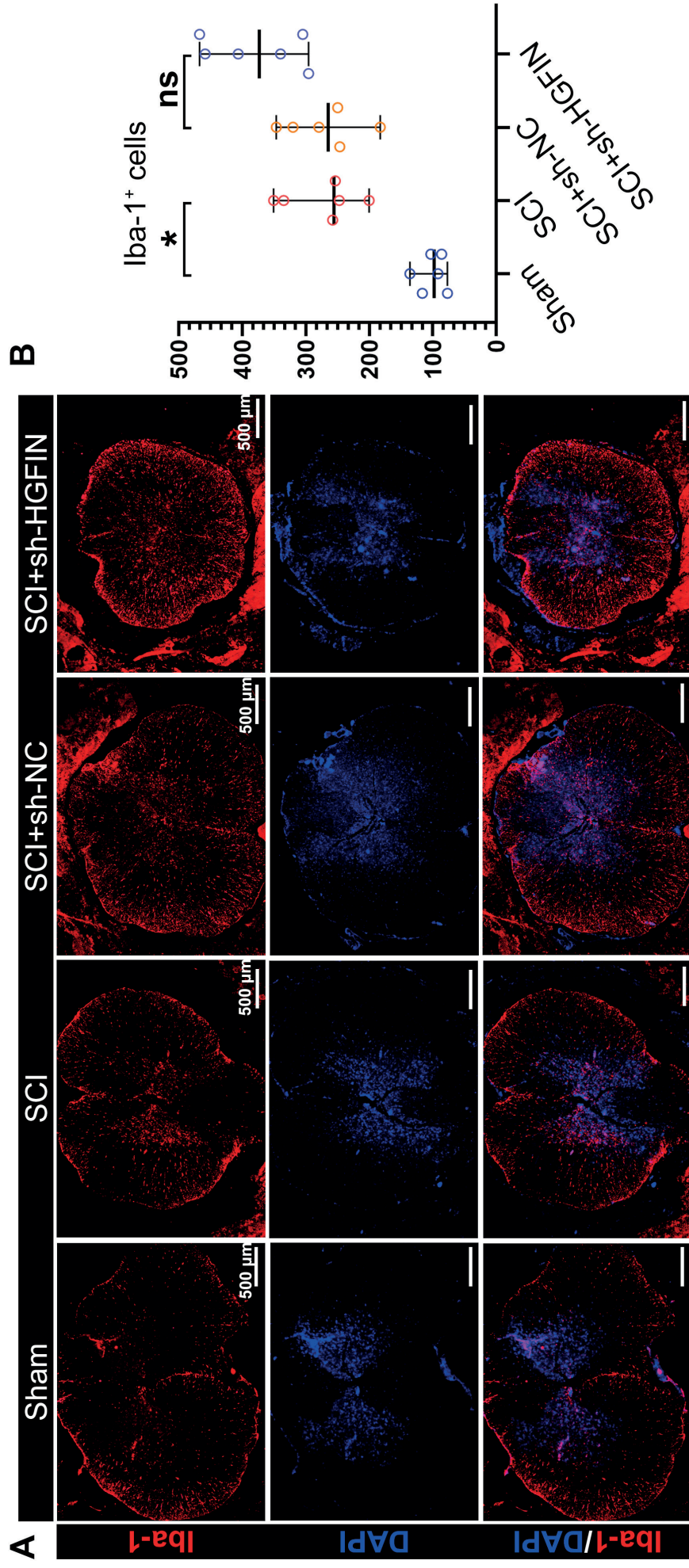


Fig. 5. Effect of hematopoietic growth factor: inducible neurokinin-1 type (HGFN) on Iba-1 expression in the spinal cord after spinal cord injury (SCI). **A.** Representative images of Iba-1 immunofluorescence staining; **B.** Quantitative analysis of the number of Iba-1⁺ positive cells (n = 6). The Kruskal–Wallis test was used to calculate the significant differences; Data are presented using medians (range)

*p < 0.05 compared to the sham group; ns – not significant, compared to the SCI+sh-NC group.

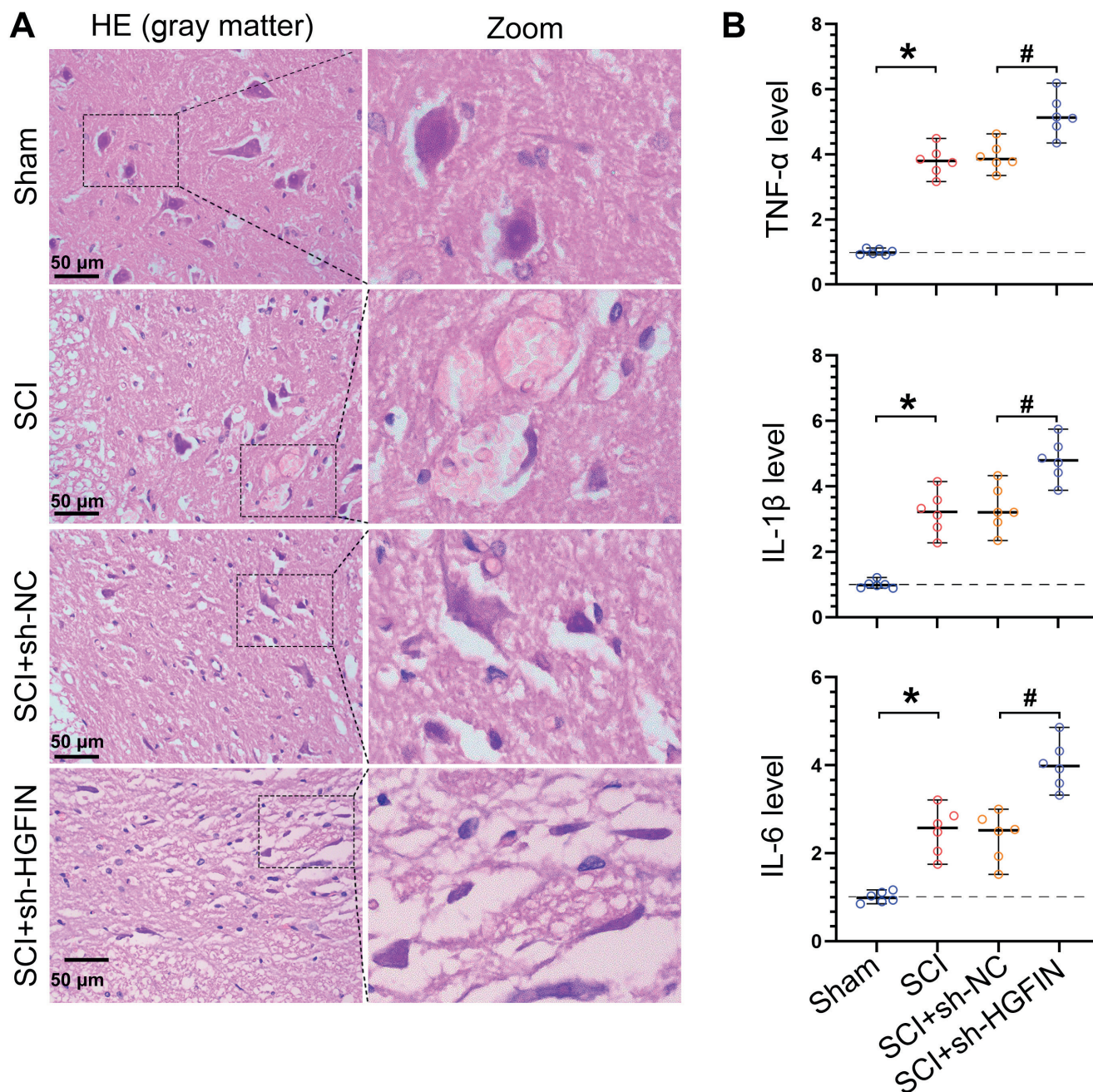


Fig. 6. Downregulation of hematopoietic growth factor inducible neurokinin-1 type (HGFIN) promotes the inflammation response after spinal cord injury (SCI). A. Hematoxylin and eosin staining of spinal cord sections in different groups; B. Relative mRNA expression levels of pro-inflammatory cytokines, including TNF- α , IL-1 β and IL-6, were detected by real-time polymerase chain reaction (PCR). The Kruskal–Wallis test was used to calculate the significant differences. Data are presented using medians (range)

* $p < 0.05$ compared to the sham group; # $p < 0.05$ compared to the SCI+sh-NC group.

be an important strategy for the improvement of SCI. In the present study, the apoptotic mechanism was confirmed by evaluating the extent of apoptosis by TUNEL staining. Consistently, SCI surgery promoted neuronal apoptosis, and the apoptosis-related proteins were significantly changed in the spinal cord tissues of SCI rats. The impact of HGFIN on cell apoptosis was investigated, and SCI rats subjected to LV-shHGFIN aggravated the occurrence of apoptosis, accompanied by increased

pro-apoptotic marker expression and downregulated anti-apoptotic marker Bcl-2. These data suggested that HGFIN might exert an anti-apoptotic effect on SCI progression.

The activation of the PI3K/AKT signaling pathway is crucial for neuron development, which exerts anti-neuroinflammation and anti-apoptotic properties in neurons.^{6,37} Recent studies have focused on the PI3K/AKT pathway in spinal cord neuron progressions, and targeting PI3K/AKT may be an innovative therapeutic approach for

SCI.^{3,38} The PI3K/AKT is a well-known survival signaling pathway that has been shown to suppress neuronal apoptosis, thus improving neural function.^{39,40} In the present research, we have focused on the PI3K/AKT pathway and explored whether HGFIN exerted function through the regulation of PI3K/AKT signaling. It has been proposed that recombinant HGFIN increased the expression of phosphorylated ERK1/2 and AKT in amyotrophic lateral sclerosis patients.²⁵ Consistent with this finding, results of the present study revealed that HGFIN knockdown decreased p-AKT expression after SCI, suggesting that HGFIN exerted its function partly through the regulation of the PI3K/AKT pathway. However, the specific mechanism of HGFIN associated with PI3K/AKT signaling in SCI was not investigated in the current study.

Given the involvement of HGFIN in the inflammatory responses that negatively regulate inflammation,¹⁴ we speculated that HGFIN deficiency promoted the inflammation process in SCI. The Iba-1 is a key glial cell activation marker that is generally used to assess the inflammatory response.^{41,42} Here, we found that HGFIN knockdown increased the number of Iba-1 positive cells following SCI. In addition, research on the progression of SCI found that inflammatory cytokines, such as TNF- α , IL-1 β and IL-6, were significantly increased in spinal cord tissues of the SCI model.⁴ Consistently, the results of the present study demonstrated that SCI rats exhibited inflammatory responses, as indicated by the upregulation of these cytokines in the present study. Moreover, HGFIN expression repressed the production of pro-inflammatory cytokines in macrophages.¹⁶ Here, we demonstrated that HGFIN depletion aggravated inflammatory responses, indicated by the increased expression of pro-inflammatory cytokines and a series of histological alterations.

Spinal cord tissue was collected on days 7, 14 and 28 from SCI rats, which were chosen to represent acute, followed by a subacute phase involving inflammatory processes, and intermediate phases of regeneration, respectively.⁴³ The response to injury starts at 12 h after injury and is peaking on the 7th day. In addition, after 7 days, the spontaneous functional recovery reached a plateau.⁴⁴ Therefore, we investigated the functional role of HGFIN on SCI at 7 days post-SCI. In the present study, the increased apoptosis-related factors and pro-inflammatory cytokines were detected on day 7 post-injury.

Limitations

Our current study was mainly focused on the potential effect of HGFIN on SCI. Nevertheless, there were several limitations. Our data indicated that HGFIN knockdown promoted apoptosis and inflammatory responses, but the role of HGFIN overexpression in these functions is lacking in the present study. This may potentially assist in exploring mechanisms for neuron functional recovery after SCI. Hematopoietic growth

factor inducible neurokinin-1 type plays a dual function in the inflammation process, thus, the underlying mechanisms of the neuroprotective effects of HGFIN against SCI need further research. In addition, we speculated that HGFIN exerted its anti-inflammatory and anti-apoptotic properties by regulating the PI3K/AKT pathway. The specific mechanism associated with the HGFIN-mediated PI3K/AKT pathway should be more deeply evaluated. In addition, the sample size of each group was small and may have limited the generalizability of our results. The nonparametric tests do not indicate significant differences in the quantification of TUNEL/NeuN and Iba-1 positive cells.

Conclusions

Our findings provide evidence that HGFIN might attenuate neuronal apoptosis and inflammation response via regulation of the PI3K/AKT signaling pathway, indicating that targeting HGFIN in the spinal cord tissue might be a promising therapeutic strategy for the treatment of SCI.

Supplementary data

The Supplementary materials are available at <https://doi.org/10.5281/zenodo.8420072>. The package includes the following file: Supplementary Table 1 and information on statistical analysis.

ORCID iDs

Qinghua Ding  <https://orcid.org/0009-0006-3222-7607>
 Hongbin Gao  <https://orcid.org/0009-0004-7784-4006>
 Xianghui Hu  <https://orcid.org/0009-0005-5168-251x>
 Whilu Gao  <https://orcid.org/0000-0002-8824-9382>

References

- McDonald JW, Sadowsky C. Spinal-cord injury. *Lancet*. 2002;359(9304):417–425. doi:10.1016/S0140-6736(02)07603-1
- Ahuja CS, Wilson JR, Nori S, et al. Traumatic spinal cord injury. *Nat Rev Dis Primers*. 2017;3:17018. doi:10.1038/nrdp.2017.18
- Shi Z, Yuan S, Shi L, et al. Programmed cell death in spinal cord injury pathogenesis and therapy. *Cell Prolif*. 2021;54(3):e12992. doi:10.1111/cpr.12992
- Rong Y, Liu W, Wang J, et al. Neural stem cell-derived small extracellular vesicles attenuate apoptosis and neuroinflammation after traumatic spinal cord injury by activating autophagy. *Cell Death Dis*. 2019;10(5):340. doi:10.1038/s41419-019-1571-8
- Orr MB, Gensel JC. Spinal cord injury scarring and inflammation: Therapies targeting glial and inflammatory responses. *Neurotherapeutics*. 2018;15(3):541–553. doi:10.1007/s13311-018-0631-6
- He X, Li Y, Deng B, et al. The PI3K/AKT signaling pathway in inflammation, cell death and glial scar formation after traumatic spinal cord injury: Mechanisms and therapeutic opportunities. *Cell Prolif*. 2022;55(9):e13275. doi:10.1111/cpr.13275
- Zhao R, Wu X, Bi XY, Yang H, Zhang Q. Baicalin attenuates blood-spinal cord barrier disruption and apoptosis through PI3K/Akt signaling pathway after spinal cord injury. *Neural Regen Res*. 2022;17(5):1080–1087. doi:10.4103/1673-5374.324857
- Weterman MAJ, Ajubi N, Van Dinter IMR, et al. *NMB*, a novel gene, is expressed in low-metastatic human melanoma cell lines and xenografts. *Int J Cancer*. 1995;60(1):73–81. doi:10.1002/ijc.291060011

9. Ren F, Zhao Q, Liu B, et al. Transcriptome analysis reveals *GPNMB* as a potential therapeutic target for gastric cancer. *J Cell Physiol.* 2020;235(3):2738–2752. doi:10.1002/jcp.29177
10. Abdelmagid S, Barbe M, Rico M, et al. Osteoactivin, an anabolic factor that regulates osteoblast differentiation and function. *Exp Cell Res.* 2008;314(13):2334–2351. doi:10.1016/j.yexcr.2008.02.006
11. Kuan CT, Wakiya K, Dowell JM, et al. Glycoprotein nonmetastatic melanoma protein B, a potential molecular therapeutic target in patients with glioblastoma multiforme. *Clin Cancer Res.* 2006;12(7 Pt 1):1970–1982. doi:10.1158/1078-0432.CCR-05-2797
12. Ono Y, Tsuruma K, Takata M, Shimazawa M, Hara H. Glycoprotein nonmetastatic melanoma protein B extracellular fragment shows neuroprotective effects and activates the PI3K/Akt and MEK/ERK pathways via the Na⁺/K⁺-ATPase. *Sci Rep.* 2016;6:23241. doi:10.1038/srep23241
13. Tanaka H, Shimazawa M, Kimura M, et al. The potential of *GPNMB* as novel neuroprotective factor in amyotrophic lateral sclerosis. *Sci Rep.* 2012;2:573. doi:10.1038/srep00573
14. Saade M, Araujo De Souza G, Scavone C, Kinoshita PF. The role of *GPNMB* in inflammation. *Front Immunol.* 2021;12:674739. doi:10.3389/fimmu.2021.674739
15. Zhou L, Zhuo H, Ouyang H, et al. Glycoprotein non-metastatic melanoma protein B (*GPNMB*) is highly expressed in macrophages of acute injured kidney and promotes M2 macrophages polarization. *Cell Immunol.* 2017;316:53–60. doi:10.1016/j.cellimm.2017.03.006
16. Ripoll VM, Irvine KM, Ravasi T, Sweet MJ, Hume DA. *GPNMB* is induced in macrophages by IFN-gamma and lipopolysaccharide and acts as a feedback regulator of proinflammatory responses. *J Immunol.* 2007;178(10):6557–6566. doi:10.4049/jimmunol.178.10.6557
17. Yu B, Alboslemy T, Safadi F, Kim MH. Glycoprotein nonmelanoma clone B regulates the crosstalk between macrophages and mesenchymal stem cells toward wound repair. *J Invest Dermatol.* 2018;138(1):219–227. doi:10.1016/j.jid.2017.08.034
18. Neal ML, Boyle AM, Budge KM, Safadi FF, Richardson JR. The glycoprotein *GPNMB* attenuates astrocyte inflammatory responses through the CD44 receptor. *J Neuroinflammation.* 2018;15(1):73. doi:10.1186/s12974-018-1100-1
19. Budge KM, Neal ML, Richardson JR, Safadi FF. Transgenic overexpression of *GPNMB* protects against MPTP-induced neurodegeneration. *Mol Neurobiol.* 2020;57(7):2920–2933. doi:10.1007/s12035-020-01921-6
20. Shi F, Duan S, Cui J, et al. Induction of matrix metalloproteinase-3 (MMP-3) expression in the microglia by lipopolysaccharide (LPS) via upregulation of glycoprotein nonmetastatic melanoma B (*GPNMB*) expression. *J Mol Neurosci.* 2014;54(2):234–242. doi:10.1007/s12031-014-0280-0
21. Yao X, Liu Z, Chen J, et al. Proteomics and bioinformatics reveal insights into neuroinflammation in the acute to subacute phases in rat models of spinal cord contusion injury. *FASEB J.* 2021;35(7):e21735. doi:10.1096/fj.202100081RR
22. Anjum A, Yazid MD, Fauzi Daud M, et al. Spinal cord injury: Pathophysiology, multimolecular interactions, and underlying recovery mechanisms. *Int J Mol Sci.* 2020;21(20):7533. doi:10.3390/ijms21207533
23. Courtine G, Sofroniew MV. Spinal cord repair: Advances in biology and technology. *Nat Med.* 2019;25(6):898–908. doi:10.1038/s41591-019-0475-6
24. Liu X, Zhang Y, Wang Y, Qian T. Inflammatory response to spinal cord injury and its treatment. *World Neurosurg.* 2021;155:19–31. doi:10.1016/j.wneu.2021.07.148
25. Nagahara Y, Shimazawa M, Ohuchi K, et al. *GPNMB* ameliorates mutant TDP-43-induced motor neuron cell death. *J Neurosci Res.* 2016;95(8):1647–1665. doi:10.1002/jnr.23999
26. Hüttenrauch M, Ogorek I, Klafki H, et al. Glycoprotein NMB: A novel Alzheimer's disease associated marker expressed in a subset of activated microglia. *Acta Neuropathol Commun.* 2018;6(1):108. doi:10.1186/s40478-018-0612-3
27. Brekk OR, Honey JR, Lee S, Hallett PJ, Isacson O. Cell type-specific lipid storage changes in Parkinson's disease patient brains are recapitulated by experimental glycolipid disturbance. *Proc Natl Acad Sci USA.* 2020;117(44):27646–27654. doi:10.1073/pnas.2003021117
28. Zigdon H, Savidor A, Levin Y, Meshcheriakova A, Schiffmann R, Futerman AH. Identification of a biomarker in cerebrospinal fluid for neuronopathic forms of Gaucher disease. *PLoS One.* 2015;10(3):e0120194. doi:10.1371/journal.pone.0120194
29. Budge KM, Neal ML, Richardson JR, Safadi FF. Glycoprotein NMB: An emerging role in neurodegenerative disease. *Mol Neurobiol.* 2018;55(6):5167–5176. doi:10.1007/s12035-017-0707-z
30. Abbaszadeh F, Fakhri S, Khan H. Targeting apoptosis and autophagy following spinal cord injury: Therapeutic approaches to polyphenols and candidate phytochemicals. *Pharmacol Res.* 2020;160:105069. doi:10.1016/j.phrs.2020.105069
31. Ding LZ, Xu J, Yuan C, Teng X, Wu QM. MiR-7a ameliorates spinal cord injury by inhibiting neuronal apoptosis and oxidative stress. *Eur Rev Med Pharmacol Sci.* 2020;24(1):11–17. doi:10.26355/eurrev_202001_19890
32. Beattie MS, Farrow AA, Bresnahan JC. Review of current evidence for apoptosis after spinal cord injury. *J Neurotrauma.* 2009;17(10):915–925. doi:10.1089/neu.2000.17.915
33. Mortezaee K, Khanlarkhani N, Beyer C, Zendedel A. Inflammation: Its role in traumatic brain and spinal cord injury. *J Cell Physiol.* 2017;233(7):5160–5169. doi:10.1002/jcp.26287
34. Springer JE, Azbill RD, Knapp PE. Activation of the caspase-3 apoptotic cascade in traumatic spinal cord injury. *Nat Med.* 1999;5(8):943–946. doi:10.1038/11387
35. Liu S, Sarkar C, Dinizo M, et al. Disrupted autophagy after spinal cord injury is associated with ER stress and neuronal cell death. *Cell Death Dis.* 2015;6(1):e1582. doi:10.1038/cddis.2014.527
36. Zhao W, Li H, Hou Y, Jin Y, Zhang L. Combined administration of poly-ADP-ribose polymerase-1 and caspase-3 inhibitors alleviates neuronal apoptosis after spinal cord injury in rats. *World Neurosurg.* 2019;127:e346–e352. doi:10.1016/j.wneu.2019.03.116
37. Chu E, Mychasiuk R, Hibbs ML, Semple BD. Dysregulated phosphoinositide 3-kinase signaling in microglia: Shaping chronic neuroinflammation. *J Neuroinflammation.* 2021;18(1):276. doi:10.1186/s12974-021-02325-6
38. Wang Z, Zhou L, Zheng X, et al. Autophagy protects against PI3K/Akt/mTOR-mediated apoptosis of spinal cord neurons after mechanical injury. *Neurosci Lett.* 2017;656:158–164. doi:10.1016/j.neulet.2017.07.036
39. Sang Q, Sun D, Chen Z, Zhao W. NGF and PI3K/Akt signaling participate in the ventral motor neuronal protection of curcumin in sciatic nerve injury rat models. *Biomed Pharmacother.* 2018;103:1146–1153. doi:10.1016/j.biopha.2018.04.116
40. Felix MS, Bauer S, Darlot F, et al. Activation of Akt/FKHR in the medulla oblongata contributes to spontaneous respiratory recovery after incomplete spinal cord injury in adult rats. *Neurobiol Dis.* 2014;69:93–107. doi:10.1016/j.nbd.2014.05.022
41. Yuan X, Yuan W, Ding L, et al. Cell-adaptable dynamic hydrogel reinforced with stem cells improves the functional repair of spinal cord injury by alleviating neuroinflammation. *Biomaterials.* 2021;279:121190. doi:10.1016/j.biomaterials.2021.121190
42. Takahashi K, Nakamura S, Otsu W, Shimazawa M, Hara H. Progranulin deficiency in Iba-1+ myeloid cells exacerbates choroidal neovascularization by perturbation of lysosomal function and abnormal inflammation. *J Neuroinflammation.* 2021;18(1):164. doi:10.1186/s12974-021-02203-1
43. Margul DJ, Park J, Boehler RM, et al. Reducing neuroinflammation by delivery of IL-10 encoding lentivirus from multiple-channel bridges. *Bioeng Transl Med.* 2016;1(2):136–148. doi:10.1002/btm2.10018
44. Gaviria M, Haton H, Sandillon F, Privat A. A mouse model of acute ischemic spinal cord injury. *J Neurotrauma.* 2002;19(2):205–221. doi:10.1089/08977150252806965

Icariin ameliorates osteoporosis by activating autophagy in ovariectomized rats

Jiaying Zou^{B-D}, Yue Peng^B, Yue Wang^B, Shouzhu Xu^C, Chuandao Shi^A, Qiling Liu^{E,F}

Department of Epidemic and Health Statistics, College of Public Health, Shaanxi University of Chinese Medicine, Xianyang, China

A – research concept and design; B – collection and/or assembly of data; C – data analysis and interpretation; D – writing the article; E – critical revision of the article; F – final approval of the article

Advances in Clinical and Experimental Medicine, ISSN 1899–5276 (print), ISSN 2451–2680 (online)

Adv Clin Exp Med. 2024;33(9):941–952

Address for correspondence

Qiling Liu
E-mail: liuqilingsan@163.com

Funding sources

This study was funded by Qinchuangyuan Traditional Chinese Medicine Innovation Research and Development Transformation Project of Shaanxi Provincial Administration of Traditional Chinese Medicine (grant No. 2022-QCYZH-007), Shaanxi Provincial Administration of Traditional Chinese Medicine Program (grant No. 2021-ZZ-JC005) and the Shaanxi Provincial Key Research and Development Program (grants No. 2021SF-275, 2022SF-357).

Conflict of interest

None declared

Received on April 10, 2023

Reviewed on April 24, 2023

Accepted on October 12, 2023

Published online on January 18, 2024

Cite as

Zou J, Peng Y, Wang Y, Xu S, Shi C, Liu Q. Icariin ameliorates osteoporosis by activating autophagy in ovariectomized rats. *Adv Clin Exp Med*. 2024;33(9):941–952. doi:10.17219/acem/174078

DOI

10.17219/acem/174078

Copyright

Copyright by Author(s)

This is an article distributed under the terms of the Creative Commons Attribution 3.0 Unported (CC BY 3.0) (<https://creativecommons.org/licenses/by/3.0/>)

Abstract

Background. Osteoporosis (OP) is a major problem that increases the mortality and disability rate worldwide. With an increase in the aging population, OP has become a major public threat to human health. Searching for effective and suitable targets for drug treatment in OP has become an urgent need.

Objectives. Osteoporosis is a metabolic bone disease characterized by reduced bone mass and density as well as micro-architectural deterioration. Icariin is a flavonoid extracted from plants of the genus *Epimedium* and has been shown to exert potential anti-OP activity. The present study was designed to observe the effect of icariin on OP and to clarify the underlying mechanisms in ovariectomized (OVX) rats.

Materials and methods. Hematoxylin and eosin (H&E) staining, von Kossa staining and micro-computed tomography (micro-CT) confirmed significant bone loss in the OVX group. Protein expression level was detected with western blot analysis.

Results. Icariin reversed a trend of increased bone turnover by reducing serum alkaline phosphatase (ALP), procollagen type I N-terminal propeptide (PINP), tartrate-resistant acid phosphatase isoform 5b (TRACP-5b), and C-telopeptide of type I collagen (CTX-I). Furthermore, icariin decreased sequestosome 1 (p62) and increased microtubule-associated protein 1 light chain 3II/microtubule-associated protein 1 light chain 3I (LC3II/LC3I), autophagy-related protein 7 (Atg7), and Beclin 1 in the femur of OVX rats, improving the indicators of impaired autophagy in OP.

Conclusions. Icariin reversed the significant upregulation of the serine/threonine protein kinase (Akt), mammalian target of rapamycin (mTOR) and unc-51-like autophagy activating kinase 1 (ULK1) at Ser757, and the downregulation of p-AMP-activated protein kinase (p-AMPK) and ULK1 phosphorylated at Ser555 in the OVX rats, suggesting that the mechanism of icariin action in OP treatment involves the activation and suppression of the AMPK/ULK1 and AKT/mTOR/ULK1 autophagy pathways, respectively.

Key words: autophagy, icariin, osteoporosis, AMP-activated protein kinase/Unc-51-like autophagy activating kinase 1, serine/threonine protein kinase/mammalian target of rapamycin/Unc-51-like autophagy activating kinase 1

Background

Osteoporosis (OP) is a common degenerative bone disease characterized by a reduction in bone mass and the degradation of micro-architectural structures.¹ Epidemiological surveys show that over 200 million women are affected by OP globally, with 8.9 million fractures each year. According to the latest projections, the prevalence of OP will reach 13.6 million by 2030 in women aged ≥ 50 years.² Osteoporosis has become the leading cause of disability and death in the elderly population.

Many phytochemicals are good substitutes for chemically synthesized medications for the treatment of various human diseases.³ Icariin, the main flavonoid isolated from the plant of the genus *Epimedium*, has been identified as a potential drug for treating OP.^{4–6} Icariin mainly affects bone metabolism and promotes bone resorption by regulating estrogen, skeletal accretion, as well as apoptosis and its related signaling pathways. The common signaling pathways include PI3K-Akt, Wnt/ β -catenin, and RANKL/RANK/OPG. They are essential for restoring the balance between bone resorption and formation in the bone remodeling process.⁷

Autophagy is critical for maintaining bone homeostasis through the degradation of abnormal proteins and pathogenic microorganisms. Research links low autophagy to OP.^{8–11} Osteoblasts (OBs) and osteoclasts (OCs) play a crucial role in maintaining bone homeostasis, and the regulation of this process involves autophagy; when autophagy is deficient, it disrupts bone homeostasis and leads to OP.^{12,13} However, the mechanisms mediating OP autophagy remain unclear.

Objectives

In our research, an OP model was established by ovariectomy in rats and icariin was administered by irrigation to study its effects and potential mechanism in autophagy and improvement of OP.

Materials and methods

Animals

The study was approved by the Animal Ethics Committee of the Shaanxi University of Chinese Medicine (approval No. SCXK (Shaanxi) 2019-001). Thirty female adult Sprague–Dawley (SD) rats (200–250 g), 3–4 months of age, purchased from the Experimental Animal Center of the Air Force Medical University (Xi'an, China), had access to clean water and food during the experiment, and were housed at 25°C with 50 \pm 10% humidity and a 12 h/12 h light-dark cycle.

In the present investigation, animal feed was purchased from Chengdu Dashuo Biological Technology Co., Ltd. (Sichuan, China), and its composition was the same in all experimental rats.

Experimental agents

Icariin (20200719) was purchased from Xi'an Yuhui Biotechnology Co. Ltd (Xi'an, China). Alkaline phosphatase (ALP) (JL26470), procollagen type I N-terminal propeptide (PINP) (JL49448), tartrate-resistant acid phosphatase isoform 5b (TRACP-5b) (JL12318), and C-telopeptide of type I collagen (CTX-I) (JL20748) enzyme-linked immunosorbent assay (ELISA) kits were purchased from Jianglai (Shanghai, China). Autophagy-related protein 7 (Atg7) (8558), Akt (9272), p-Akt (4058), Beclin1 (3495), mammalian target of rapamycin (mTOR) (2972), p-unc-51-like autophagy activating kinase 1 (ULK1) (Ser555) (5869), p-mTOR (2971), ULK1 (8054), p-ULK1 (Ser757) (14202), and AMP-activated protein kinase (AMPK) (5832) were purchased from Cell Signaling Technology (Danvers, USA). Microtubule-associated protein 1 light chain 3 (LC3) (GTX127375) was purchased from Genetex (Louis Park, USA), sequestosome 1 (p62) (ab109012) from Abcam (Cambridge, UK), β -actin (bs-0061R) from Bioss (Woburn, USA) and p-AMPK (13S4010) from Bioword (Louis Park, USA). Bicinchoninic acid (BCA) kits were purchased from Thermo Fisher Scientific (Waltham, USA) and dithiothreitol (DTT; 1 mol/L) was obtained from Sigma-Aldrich (St. Louis, USA).

Instruments

Mini-PROTEAN Tetra electrophoresis and blots, a protein semi-dry transfer device, and a gel imaging system were used (Bio-Rad, Hercules, USA). A full wavelength microplate reader (Tecan, Zurich, Switzerland), an automatic high-speed refrigerated centrifuge (Sigma-Aldrich), a SCIENTZ-48 Tissue Grinder (Xinzhì, Hunan, China), an X-Ray Micro-CT SkyScan 1276 (Bruker, Billerica, USA), and a VS200 digital slide scanner (Olympus, Tokyo, Japan) were utilized for tissue analysis.

Groups and animal treatments

Thirty female adult SD rats were randomly divided into control (sham-operated+saline, n = 10), model (ovariectomy+saline, n = 10) and icariin (ovariectomy+icariin, n = 10) groups. The model and icariin groups were subjected to bilateral ovariectomy, and the same amount of fat tissue near the ovary was removed in the control group. One week after the operation, intragastric administration of saline (0.5 mL/100 g) was carried out for 12 consecutive weeks in the model group, to which icariin (120 mg/kg) was added in the icariin group. Body weight of the animals was measured 14 times per week.

Rats were intraperitoneally anesthetized with 10% chloral hydrate (300 mg/kg), and, under anesthesia, blood was collected from the abdominal aorta until the blood flow was exhausted. Death was confirmed by cardiac and respiratory arrest. Bones were frozen to -80°C for testing. None of the rats had peritonitis or its associated symptoms after the administration of 10% chloral hydrate. Rats weighed 340–403 g, and less than 10 mL of blood was collected from each rat at the time of sacrifice.

Measurement of serum metabolism indexes

Serum PINP, ALP, CTX-I, and TRACP-5b are indicators for evaluating bone formation and resorption ability. The levels of ALP (JL26470), PINP (JL49448), TRACP-5b (JL12318), and CTX-I (JL20748) were detected with ELISA. Blood samples were stored at room temperature for 2 h, centrifuged at 4°C for 5 min (3000 rpm), and the serum was separated. The samples were prepared according to the index instruction, a standard curve based on the standard solutions was created, and the sample (50 μL) and horseradish peroxidase (HRP; 100 μL) were added to each well. The well was sealed and placed in a 37°C incubator, and after 60 min, the liquid was poured off, and the sample dried on the absorbent paper. The washing solution (350 μL) was added to each well and maintained for 1 min at room temperature; after repeating 5 times, reaction substrate solutions A (50 μL) and B (50 μL) were added to each well, and they were incubated for 15 min in a 37°C incubator. The termination solution (50 μL) was added to each well for 15 min. A regression equation was formulated according to the standard curve, and the sample optical density (OD) value ($\lambda = 450 \text{ nm}$) was taken into the equation to calculate the sample concentration. The sample size was 7.

Measurement of bone morphology

Hematoxylin and eosin (H&E) staining was used to evaluate the morphological features of the femur. Right distal femurs (1-cm specimens) were fixed for 48 h with 4% paraformaldehyde, decalcified with 10% ethylenediaminetetraacetic acid (EDTA), embedded in paraffin, and sectioned (5- μm thickness). Sections were stained with H&E prior to digital slide scanning. The H&E staining was performed according to the reference literature.¹⁴

Detection of calcium nodules

Calcification nodules can reflect the level of the OB mineralization. Calcium nodules were observed using Von Kossa staining. Right distal femurs (1 cm specimens) were fixed for 48 h with 4% paraformaldehyde, embedded with paraffin, sectioned, and washed subsequently with xylene, gradient alcohol and distilled water. In the next step, 3% silver nitrate was added for 1 h and washed with water

for 5 min, counterstain with toluidine blue for 5 min, then washed with distilled water repeatedly, dried, and sealed with neutral glue. The sample size was 3.

Micro-computed tomography

A micro-computed tomography (micro-CT) system was employed for trabecular bone mass measurement. At the time of execution, the left femur, tibia and vertebrae (L4) were separated and fixed for 24 h in 4% paraformaldehyde before flushing with 70% ethanol. Distal femoral and proximal tibia metaphysis were scanned at a resolution of 8 μm (80-kV voltage, 80- μA current). Micview V2.1.2 software (GE Healthcare, Chicago, USA) was used to analyze the data. Regions of interest segmented with a fixed threshold were reconstructed into 3-dimensional images. Trabecular bone was quantified using bone marrow density (BMD), bone volume over total volume (BV/TV), bone surface over bone volume (Bs/Bv), trabecular thickness (Tb.Th), trabecular number (Tb.N), and trabecular spacing (Tb.Sp). The sample size was 4.

Western blot analysis

Femur (500 mg) at -80°C was cut into fragments with bone shears, ground into powder in liquid nitrogen, and collected in a centrifugal tube. Samples were lysed using 700- μL radioimmunoprecipitation assay (RIPA) buffer and ground with a high-throughput grinder. The homogenized tissues were centrifuged (14,000 rpm, 20 min) at 4°C . The supernatant was transferred to a new EP tube, and 10 μL was separated for quantitative analysis using a BCA protein assay kit. The remaining part was treated with RIPA, $\times 2$ loading buffer, and 1 M DTT by volume, heated for 8 min at 100°C , cooled, mixed and frozen at -80°C . Proteins (80 μg /well) were separated on a 10–15% sodium dodecyl sulfate polyacrylamide gel (SDS-PAGE). Separated proteins were subjected to electroblotting on polyvinylidene fluoride (PVDF) membranes. The membranes were then blocked and incubated with designated primary antibodies (rabbit anti-rat) overnight at 4°C (all antibodies were diluted). Using β -actin (1:5000) as internal control, the autophagy proteins Atg7 (1:2000), p62 (1:2000), LC3 (1:2000), Beclin1 (1:2000), Akt (1:1000), p-Akt (1:1000), mTOR (1:1000), p-mTOR (1:1000), p-AMPK (1:1000), ULK1 (1:1000), p-ULK1 (Ser555) (1:1000), and p-ULK1 (Ser757) (1:1000) were detected. On the following day, samples were washed 3 times (5 min/time) with Tris-buffered saline with Tween (TBST) and were incubated with goat anti-rabbit IgG conjugated to HRP for 2 h, and then the PVDF membranes were washed 4 times (5 min/time) with TBST. Finally, the membranes were exposed using a Molecular Imager[®] ChemiDoc[™] XRS System, and the western blot data were analyzed using ImageJ software (National Institutes of Health (NIH), Bethesda, USA). The sample size was 3 for the western blot.

Statistical analyses

The analysis was carried out using IBM SPSS Statistics for Windows, v. 26.0 (IBM Corp., Armonk, USA). Data are presented as mean \pm standard deviation (M \pm SD). A normality test and homogeneity of variance test were first used for multiple group data; one-way analysis of variance (ANOVA) was used if the data were in accordance with normality and homogeneity of variance; otherwise, the Kruskal–Wallis H test was conducted. A normality test, homogeneity of variance test, sphericity test, and repeated measures analysis of variance test were used for repeated measure data. Fisher's least significant difference (LSD) or Dunn's post hoc test were performed if differences were significant. Differences were considered of statistical significance with $p < 0.05$.

Results

Body weight and condition of the OP rats were ameliorated by icariin

Body weight values increased in all groups after 12 weeks, with a significant uptrend in the model group compared to the control and icariin groups from the 2nd week. Icariin appeared to control body weight but not at a statistically different level when compared to the model group. The fur of the rats in the model group was drier, yellower and duller than that of the control group; reflexes were also slower. Compared to the model group, the icariin group rats exhibited more sleek and white fur, faster reaction times, and reduced body weight (Fig. 1 and Table 1).

Bone metabolism indexes of OP rats were mediated by icariin

The PINP, ALP, CTX-I, and TRACP-5b are indicators of bone metabolism, reflecting bone formation and resorption ability. In the model group, the expression of PINP, ALP, CTX-I, and TRACP-5b was increased. The 4 indexes were reduced in the icariin group compared with the model group (Fig. 2 and Table 2).

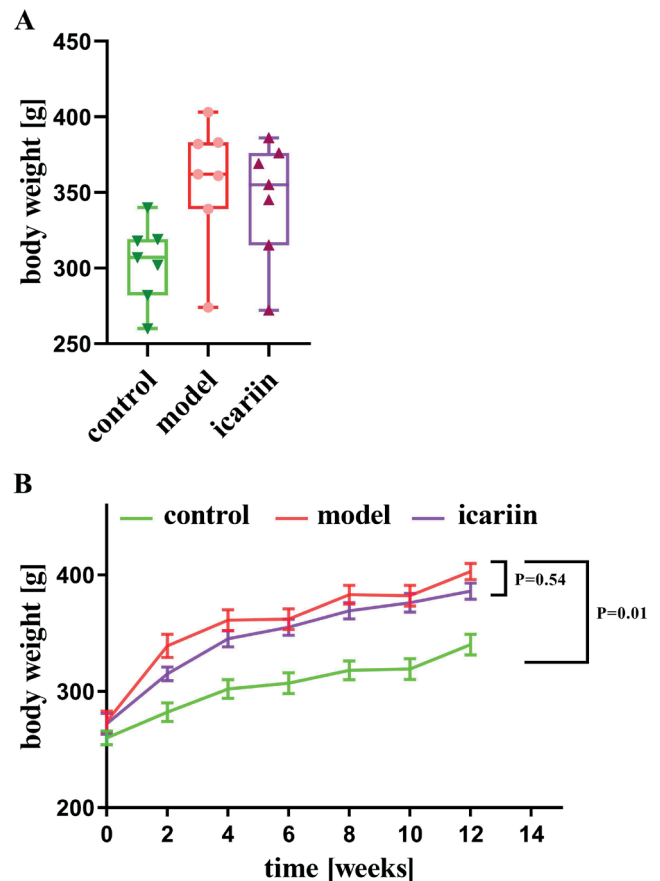


Fig. 1. Icariin ameliorated weight changes in osteoporosis (OP) rats. A. Box plots of 3 body weights at 12th week. Box bodies represent M (p_{25} , p_{75}), and upper bars and lower bars represent maximum and minimum, respectively (n = 7); B. The trend plots of body weight change in the 12 weeks ($F_{2,18} = 4.10$, $p = 0.03$). Repeated measures analysis of variance (ANOVA) and LSD post hoc tests were performed. Body weights in the model group increased from the 2nd week. Icariin could control body weights

Femoral morphological changes and calcium nodules in OP rats were restored by icariin

Morphological features of the femur were evaluated using H&E staining. Compared with the control group, the model group had more pathological changes, such as less femoral trabecular bone, uneven thickness, greater distance, and increased breakpoints. However, compared with the model group, the icariin group displayed multitudinous bone trabecula, and the bone microstructure was generally clear (Fig. 3A).

Table 1. Body weights (X \pm S) of the rats at week 12

Group	Weight [g]	95% CI	F value (repeated measures ANOVA)	p-value
Control	340.00 \pm 9.00	279.68–328.32	4.10	0.03
Model	403.00 \pm 7.00*	318.72–396.71		
Icariin	386.00 \pm 7.00*	308.54–382.32		

* $p < 0.05$ compared to the control group; 95% CI – 95% confidence interval; ANOVA – analysis of variance.

Table 2. Expression of bone formation and resorption indexes in serum (X ± S)

Index	Group	Value [ng/mL]	95% CI	F value (one-way ANOVA)	p-value
PINP	control	1.42 ± 0.59	0.87–1.97	24.84	0.00
	model	3.28 ± 0.44***	2.88–3.69		
	icariin	2.44 ± 0.44*****	2.03–2.85		
ALP	control	3.46 ± 0.33	3.15–3.76	11.32	0.00
	model	5.01 ± 0.66***	4.40–5.62		
	icariin	4.23 ± 0.76**	3.52–4.93		
CTX-I	control	1.16 ± 0.18	0.99–1.32	33.61	0.00
	model	2.41 ± 0.30***	2.13–2.69		
	icariin	1.84 ± 0.35*****	1.51–2.16		
TRACP-5b	control	0.64 ± 0.31	0.35–0.92	33.61	0.00
	model	1.86 ± 0.34***	1.54–2.18		
	icariin	1.56 ± 0.20***	1.38–1.75		

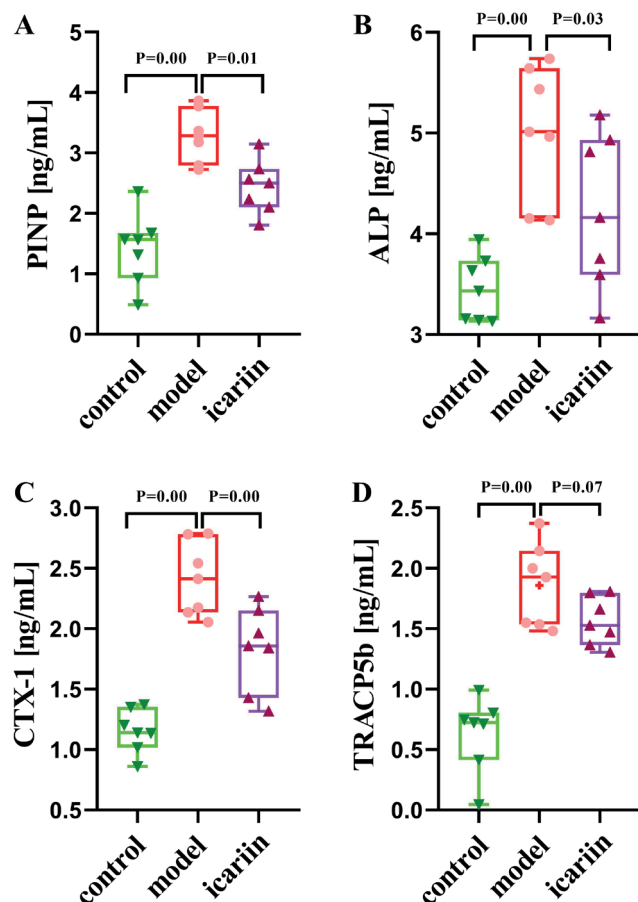
* p < 0.05 compared to the control group; *** p ≤ 0.001 compared to the control group; #p < 0.05 compared to the model group; ##p ≤ 0.01 compared to the model group; ###p ≤ 0.001 compared to the model group; ALP – alkaline phosphatase; PINP – procollagen type I N-terminal propeptide; TRACP-5b – tartrate-resistant acid phosphatase isoform 5b; CTX-I – C-telopeptide of type I collagen; 95% CI – 95% confidence interval; ANOVA – analysis of variance.

The number of femoral calcium nodules was determined with von Kossa staining (Fig. 3B). There was a reduction in the number of calcium nodules in the model group. Compared with the model group, the icariin group displayed an increased trend in calcium nodules, but they were not significantly different (Fig. 3C, Table 3).

Table 3. Levels of calcium nodules in the femur (M (p₂₅, p₇₅))

Group	Gray value	H value	p-value
Control	119.52 (118.50, 120.60)	6.25	0.04
Model	29.39 (25.80, 31.40)*		
Icariin	52.45 (48.00, 53.80)		

*p < 0.05 compared to the control group.



The BMD and trabecula state in OP rats was altered by icariin

The trabecular bone of the femur, tibia and lumbar spine (L4) were scanned with micro-CT (Fig. 4), revealing bone loss and atrophy of the bone trabecula in the model group and an improvement of the trabecular morphology and volume in the icariin group. Bone marrow density in the model group was lower than in the control group, while icariin increased the BMD compared with the model group.

Fig. 2. Icariin improved the bone formation and resorption indexes in serum shown using enzyme-linked immunosorbent assay (ELISA). A. The levels of procollagen type I N-terminal propeptide (PINP) in the serum of 3 groups ($F_{2,18} = 24.84, p = 0.00$); B. The levels of alkaline phosphatase (ALP) in the serum of 3 groups ($F_{2,18} = 11.32, p = 0.00$); C. The levels of C-telopeptide of type I collagen (CTX-I) in the serum of 3 groups ($F_{2,18} = 33.61, p = 0.00$); D. The levels of tartrate-resistant acid phosphatase isoform 5b (TRACP-5b) in the serum of 3 groups ($F_{2,18} = 33.61, p = 0.00$). One-way analysis of variance (ANOVA) and least significant difference (LSD) post hoc tests were performed in the A, B, C, and D plots. Box bodies represent M (p₂₅, p₇₅), and upper bars and lower bars represent maximum and minimum, respectively (n = 7). In the model group, the expression of PINP (A), ALP (B), CTX-I (C), and TRACP-5b (D) were increased, but icariin reduced them

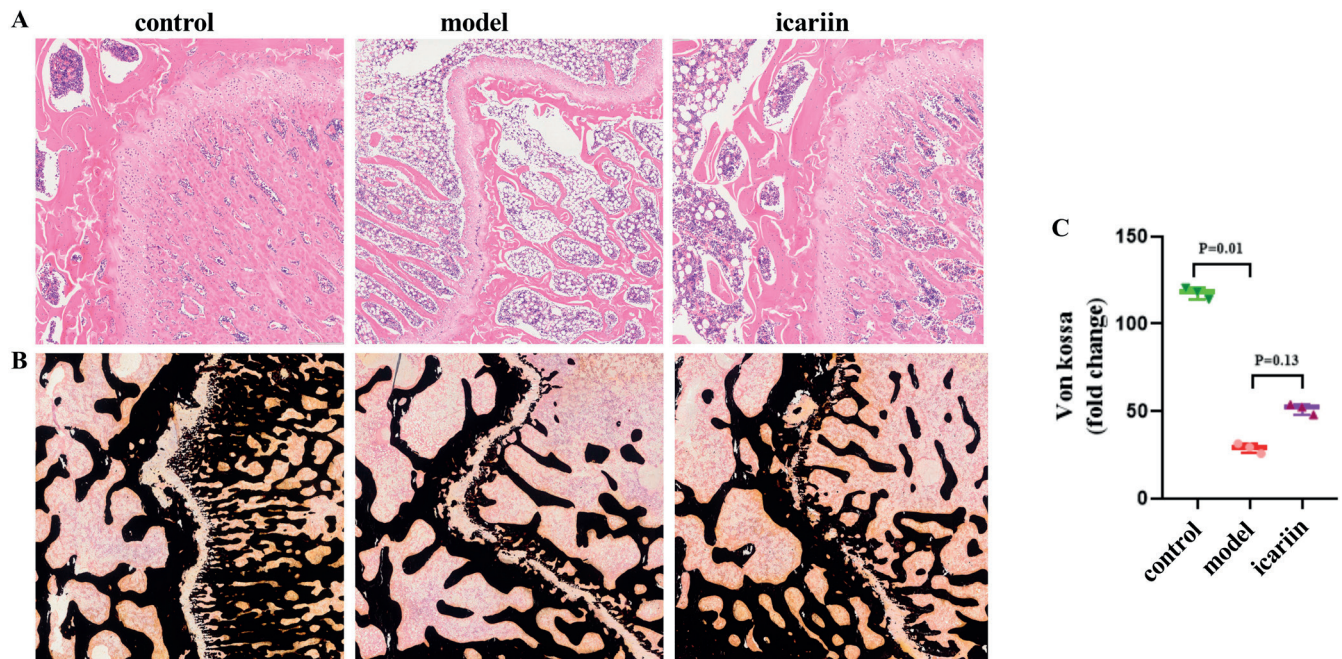


Fig. 3. Icarin restored abnormal morphological structure and calcium levels. A. Hematoxylin and eosin (H&E) staining was used to evaluate the morphological features of the femur (scale bars: 200 μ m); B. Calcium nodules were observed using von Kossa staining (scale bars: 200 μ m); C. The number of the calcium nodules was quantified in the 3 groups. The Kruskal–Wallis H test indicated significant difference ($H = 6.25$, $p = 0.04$). Dunn's post hoc test was performed between group means. Box bodies represent M (p_{25} , p_{75}), upper bars and lower bars represent maximum and minimum, respectively ($n = 3$). The number of the calcium nodules was reduced in the model group and increased in the icariin group

Table 4. Expression of bone mineral density (BMD) and trabecular parameters in the femur

Index	Group	Index value	95% CI	F value (one-way ANOVA)	p-value	H value	p-value
BMD ($X \pm S$) [g/cm^2]	control	1.12 \pm 0.15	(0.88, 1.37)	35.07	0.00	–	–
	model	0.35 \pm 0.17***	(0.08, 0.61)				
	icariin	0.97 \pm 0.08###	(0.84, 1.10)				
Bv/Tv ($X \pm S$) (%)	control	73.98 \pm 6.73	(63.27, 84.68)	56.64	0.00	–	–
	model	9.04 \pm 1.33***	(6.92, 11.16)				
	icariin	41.37 \pm 13.28#####	(20.24, 62.49)				
Bs/Bv ($X \pm S$) [1/mm]	control	19.99 \pm 3.82	(13.91, 26.07)	32.76	0.00	–	–
	model	39.83 \pm 1.32***	(37.73, 41.93)				
	icariin	28.03 \pm 4.49####	(20.89, 35.18)				
Tb.Th ($X \pm S$) [mm]	control	0.18 \pm 0.01	(0.16, 0.19)	33.83	0.00	–	–
	model	0.09 \pm 0.01***	(0.07, 0.11)				
	icariin	0.13 \pm 0.02####	(0.09, 0.16)				
Tb.Sp ($X \pm S$) [mm]	control	0.08 \pm 0.01	(0.07, 0.10)	224.48	0.00	–	–
	model	0.80 \pm 0.04***	(0.74, 0.86)				
	icariin	0.25 \pm 0.08#####	(0.13, 0.38)				
Tb.N, M (p_{25} , p_{75}) [1/mm]	control	4.45 (4.30, 4.80)	–	–	–	8.91	0.01
	model	1.32 (1.00, 1.40)**	–				
	icariin	3.24 (2.90, 3.90)	–				

** $p \leq 0.01$ compared to the control group; * $p \leq 0.001$ compared to the control group; ## $p \leq 0.01$ compared to the model group; ### $p \leq 0.001$ compared to the model group; BMD – bone mineral density; Bv/Tv – bone volume over total volume; Bs/Bv – bone surface over bone volume; Tb.Th – trabecular thickness; Tb.N – trabecular number; Tb.Sp – trabecular spacing.

The Bv/Tv, Tb.Th, Tb.N, Bs/Bv, and Tb.Sp parameters reflect the morphological trabecula structure. The Bv/Tv, Tb.Th and Tb.N in the model group were found to be

lower than in the control group, while Bs/Bv and Tb.Sp were higher. Icarin increased Bv/Tv, Tb.Th and Tb.N and decreased Bs/Bv and Tb.Sp (Table 4).

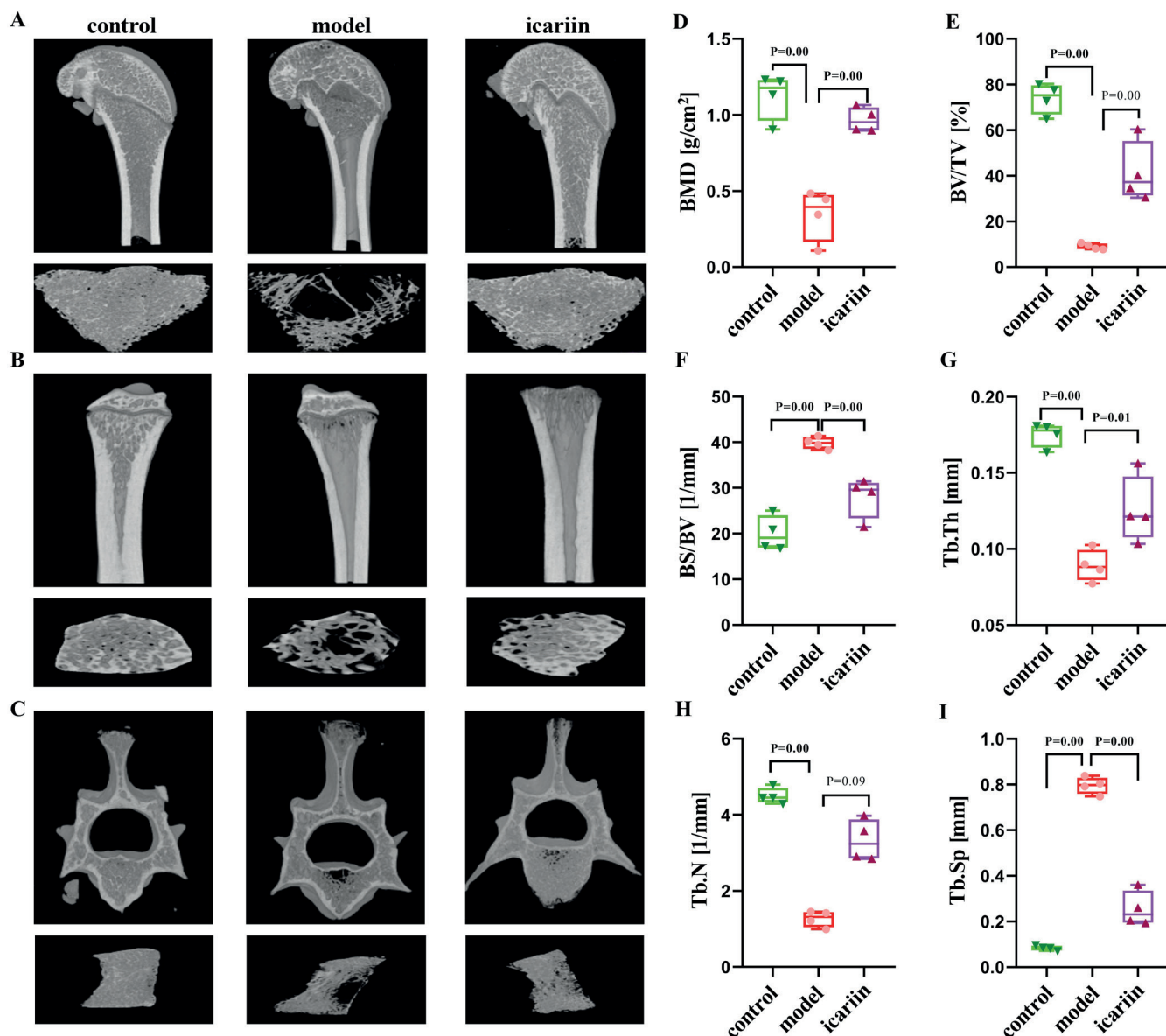


Fig. 4. Icaritin adjusted the trabecular state and parameters. A. Trabecular bones in femur; B. Trabecular bones in tibia; C. Trabecular bones in lumbar (L4). A, B and C were scanned using micro-computed tomography (CT); D. Bone mineral density (BMD): quantification of trabecular bone volume and architecture ($F_{2,9} = 35.07, p = 0.00$); E. Bone volume over total volume (BV/TV) ($F_{2,9} = 56.64, p = 0.00$); F. Bone surface to bone volume (BS/BV) ($F_{2,9} = 32.76, p = 0.00$); G. Trabecular thickness (Tb.Th) ($F_{2,9} = 33.83, p = 0.00$); H. Trabecular number (Tb.N) ($H = 8.91$) ($p = 0.01$); I. Trabecular spacing (Tb.Sp) ($F_{2,9} = 224.48, p = 0.00$). One-way analysis of variance (ANOVA) and least significant difference (LSD) post hoc tests were performed in the D, E, F, G, and I plots. The Kruskal–Wallis H test and Dunn’s post hoc test were performed in H plots. Box bodies represent M (p_{25}, p_{75}), and upper bars and lower bars represent maximum and minimum, respectively ($n = 4$). The BMD, BV/TV, Tb.Th, and Tb.N in the model group were lower than in the control group, while BS/BV and Tb.Sp were higher. Icaritin increased BMD, BV/TV, Tb.Th, Tb.N and decreased BS/BV and Tb.Sp

Autophagy of the OP rats activated by icariin

Autophagy-associated proteins were evaluated using western blotting. As shown in Fig. 5, LC3II/LC3I, Atg7 and Beclin1 were decreased, while p62 was increased in the model group compared to the control group. Icaritin increased the levels of LC3II/LC3I, Atg7 and Beclin 1, and decreased the expression of p62 compared to the model group (Table 5).

A bidirectional switch effect of icariin on autophagy pathways

The ULK1 is a pivotal modulator of autophagy initiation.¹⁵ The Ser555 and Ser757 phosphorylation sites of ULK1 have distinct effects on autophagy. Phosphorylation at the Ser555 site induces autophagy, while phosphorylation at the Ser757 site inhibits autophagy.^{16,17} For the model group, Fig. 6E,F show that ULK1 phosphorylated at Ser555 decreased but ULK1 phosphorylated at Ser757 increased. However, icariin increased Ser555-phosphorylated ULK1 and decreased Ser757-phosphorylated ULK1.

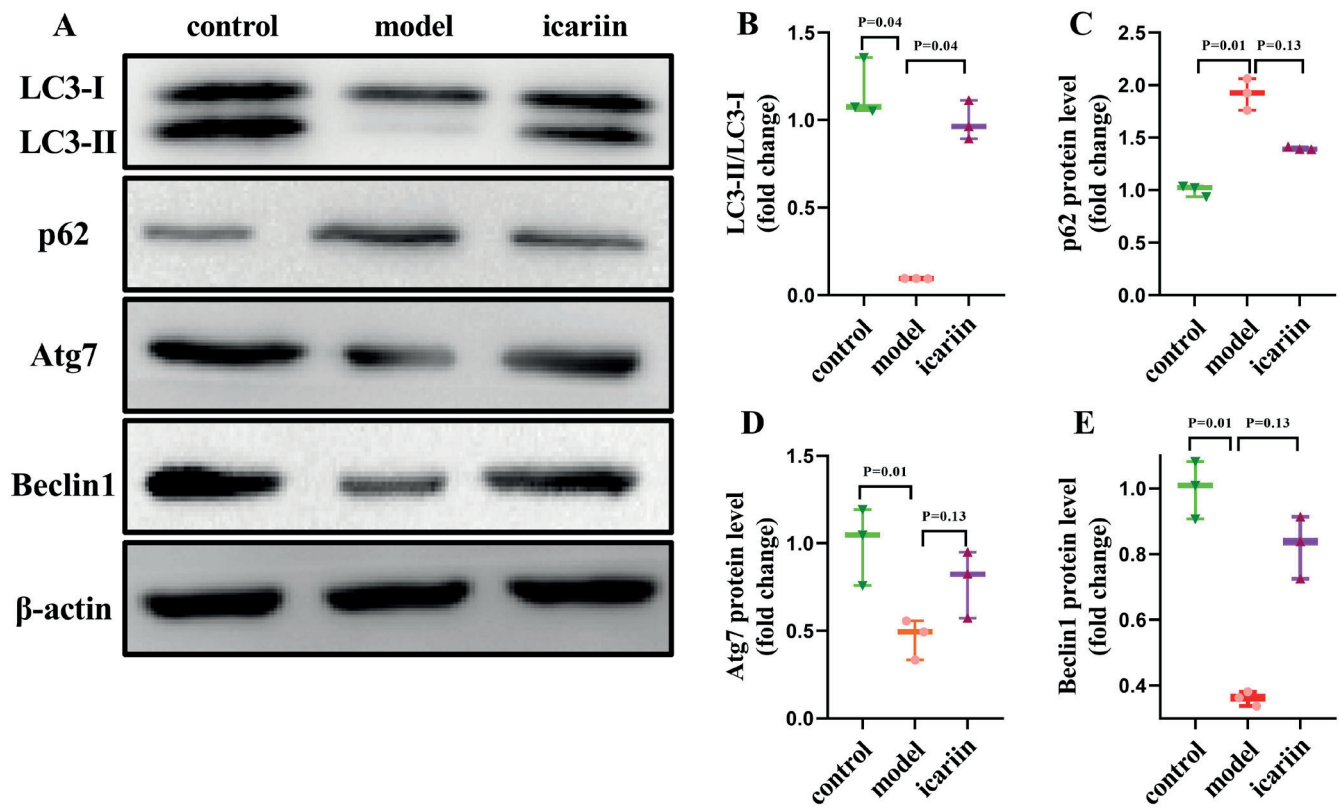


Fig. 5. Icarin activated autophagy levels in osteoporosis (OP) rats. A. Autophagy-associated protein expression of microtubule-associated protein 1 light chain 3 (LC3), sequestosome 1 (p62), autophagy-related protein 7 (Atg7), and Beclin1 in femur by western blotting; B. Quantification of LC3II/LC3I ($H = 6.30$, $p = 0.04$); C. Quantification of p62 ($H = 6.25$, $p = 0.04$); D. Quantification of Atg7 ($H = 6.25$, $p = 0.04$); E. Quantification of Beclin1 ($H = 6.25$, $p = 0.04$). The Kruskal–Wallis H test and Dunn’s post hoc test were performed in B, C, D, and E plots. Box bodies represent M (p_{25} , p_{75}), upper bars and lower bars represent maximum and minimum, respectively ($n = 3$). The LC3II/LC3I, Atg7 and Beclin1 were decreased, while p62 was increased in the model group. Icarin increased the level of LC3II/LC3I, Atg7 and Beclin1 and decreased the expression of p62

Table 5. Levels of autophagy proteins in rats (M (p_{25} , p_{75}))

Protein	Group	Gray value	H value	p-value
LC3II/LC3I	control	1.08 (1.05, 1.36)	6.30	0.04
	model	0.10 (0.09, 0.10)*		
	icariin	0.96 (0.89, 1.11)		
Atg7	control	1.05 (0.76, 1.19)	6.25	0.04
	model	0.49 (0.33, 0.56)*		
	icariin	0.82 (0.57, 0.95)		
Beclin1	control	1.01 (0.91, 1.08)	6.25	0.04
	model	0.36 (0.34, 0.38)*		
	icariin	0.84 (0.73, 0.91)		
p62	control	1.02 (0.94, 1.04)	6.25	0.04
	model	1.93 (1.76, 2.06)*		
	icariin	1.39 (1.39, 1.41)		

* $p < 0.05$ compared to the control group.

The Akt and mTOR, as downstream targets, act on the Ser757 phosphorylation site of ULK1 and are negatively associated with autophagy regulation.¹⁸ As shown in Fig. 6A–C, phosphorylation of Akt and mTOR resulted in significant activation in the model group. However, icariin suppressed the change.

Another upstream kinase, AMPK, acts on the kinase at the Ser555 phosphorylation site of ULK1. As shown in Fig. 6A,D, AMPK levels were significantly suppressed in the model group. Icarin elevated AMPK phosphorylation levels.

The results show that OP modelling in rats suppressed the AMPK/ULK1 pathway and activated the Akt/mTOR/

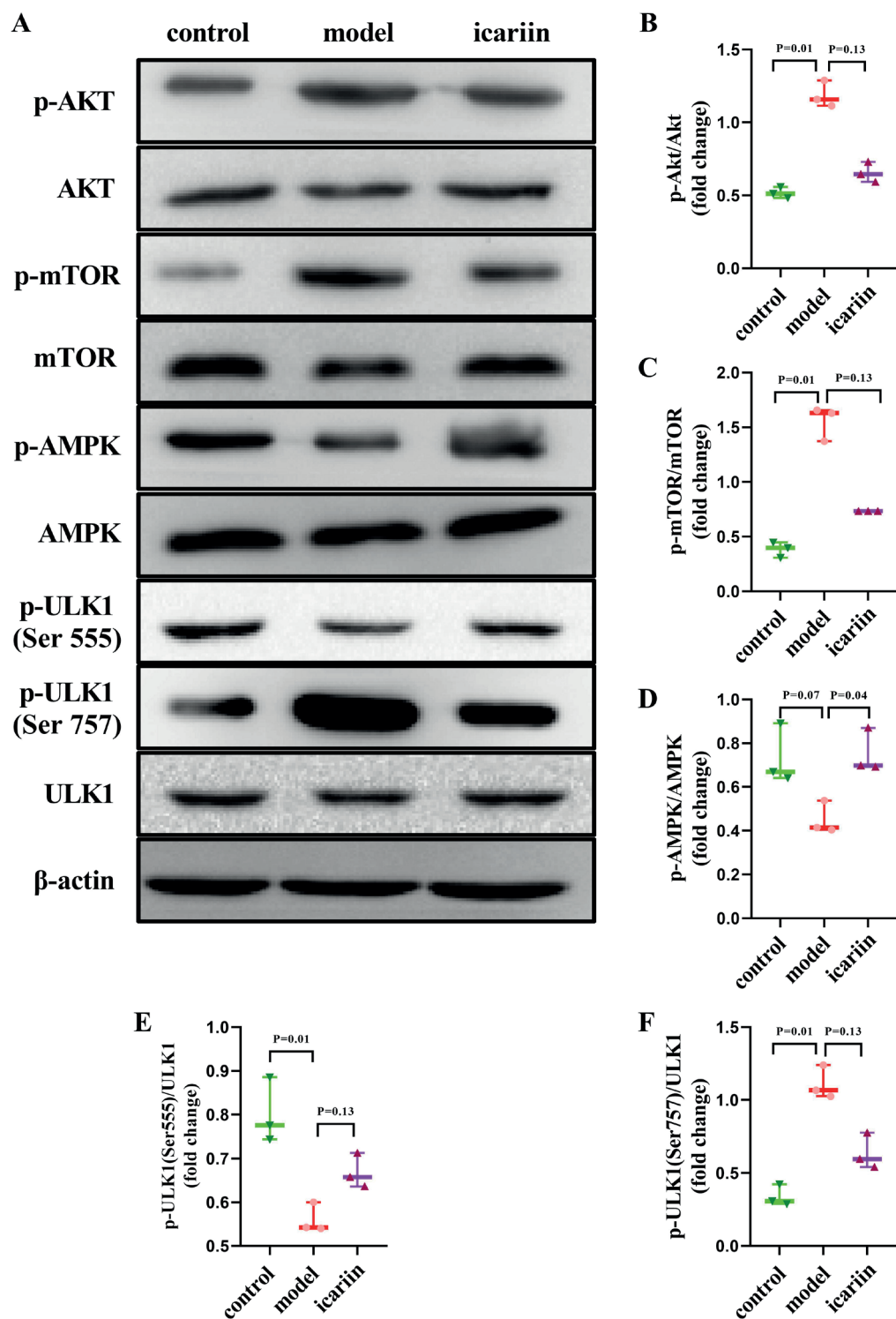


Fig. 6. Icariin mediated autophagy pathways bidirectionally. A. The expression of p-serine/threonine protein kinase (Akt)/Akt total, p-mammalian target of rapamycin (mTOR)/mTOR total, p-AMP-activated protein kinase (AMPK)/AMPK total, p-unc-51-like autophagy activating kinase 1 (ULK1) (Ser555)/ULK1 total, and p-ULK1 (Ser757)/ULK1 total using western blotting; B. Quantification of p-Akt/Akt total (H = 6.25, p = 0.04); C. Quantification of p-mTOR/mTOR total (H = 6.25, p = 0.04); D. Quantification of p-AMPK/AMPK total (H = 6.30, p = 0.04); E. Quantification of p-ULK1 (Ser555)/ULK1 total (H = 6.25, p = 0.04); F. Quantification of p-ULK1 (Ser 757)/ULK1 total (H = 6.25, p = 0.04). The Kruskal–Wallis H test and Dunn’s post hoc test were performed in the B, C, D, E, and F plots. Box bodies represent M (p₂₅, p₇₅), and upper bars and lower bars represent maximum and minimum, respectively (n = 3). The p-AKT/AKT, p-mTOR/mTOR and p-ULK1 (Ser757)/ULK1 were increased, while p-AMPK/AMPK and p-ULK1 (Ser555)/ULK1 were decreased in the model group. Icariin reduced p-AKT/AKT, p-mTOR/mTOR and p-ULK1 (Ser757)/ULK1, and increased p-AMPK/AMPK and p-ULK1 (Ser555)/ULK1

ULK1 pathway, while icariin induced autophagy in a bidirectional switch manner (Table 6).

Discussion

With an aging population, the incidence of OP is a global concern.¹⁹ Serious clinical symptoms such as movement restriction, body deformity, chronic pain, and disability seriously reduce the quality of patients’

life, and therefore, an efficient prevention and treatment strategy is urgently required.²⁰ Osteoporosis is treated clinically with synthetic drugs despite their numerous side effects.²¹ Icariin is a natural herbal extract component that exhibits important pharmacological activities for metabolic bone diseases.²² Autophagy regulates bone balance through bone formation and bone resorption.⁹ The present study investigated the potential of icariin in OP treatment and elucidated its possible mechanism of action in autophagy.

Table 6. Expression of autophagy pathways protein in femur (M (p₂₅, p₇₅))

Protein	Group	Odds of gray value	H value	p-value
Ser555/ULK1	control	0.78 (0.74, 0.89)	6.25	0.04
	model	0.54 (0.54, 0.60)*		
	icariin	0.66 (0.64, 0.71)		
Ser757/ULK1	control	0.31 (0.29, 0.42)	6.25	0.04
	model	1.07 (1.03, 1.24)*		
	icariin	0.60 (0.54, 0.78)		
p-Akt/Akt	control	0.51 (0.48, 0.56)	6.25	0.04
	model	1.16 (1.11, 1.29)*		
	icariin	0.64 (0.59, 0.73)		
p-mTOR/mTOR	control	0.40 (0.31, 0.45)	6.56	0.04
	model	1.63 (1.37, 1.66)*		
	icariin	0.73 (0.73, 0.73)		
p-AMPK/AMPK	control	0.67 (0.64, 0.89)	6.30	0.04
	model	0.41 (0.40, 0.54)		
	icariin	0.70 (0.69, 0.87) [#]		

* p < 0.05 compared to the control group; [#]p < 0.05 compared to the model group; ULK1 – unc-51-like autophagy activating kinase 1; Akt – serine/threonine protein kinase; mTOR – mammalian target of rapamycin; AMPK – AMP-activated protein kinase.

The OP rat model was established by ovariectomy, simulating bone mass loss and structural changes due to estrogen deficiency. Icariin intervention counteracted the increased weight, graying of hair, and slowing of reflexes that were observed in the model group, possibly by restoring the endocrine imbalance and slowing lipid metabolism caused by OP. Bones maintain a dynamic balance through osteoblastic formation and osteoclastic resorption. The ALP and PINP in serum are markers of osteoblastic formation, and CTX-I and TRACP-5b are specific markers of bone resorption, which increases in high turnover bone disease.^{23–26} The blood serum analysis demonstrated that icariin reduced the indicators of bone formation and resorption, and enhanced bone turnover in rats in vivo. Micro-CT is an innovative method for assessing microstructural changes in bone tissue, which is simple, non-invasive and non-destructive to the specimen. Micro-CT scans revealed that icariin increased BMD and improved the trabecula parameters in the OVX rat model. Calcium nodules are mineralized products of the OBs, which can reflect the OB properties. The von Kossa staining revealed an apparent increase in the number of calcium nodules after icariin treatment compared with the OVX group. Therefore, icariin can promote OB formation and differentiation.

At present, the mechanism and targets for OP are unclear, so there are no particularly effective drugs on the market. In this study, autophagy marker proteins, namely Atg7, LC3II/LC3I, p62, and Beclin 1, were measured. The *Atg7*, an autophagy-related gene, is essential for autophagy, and the Atg system can promote LC3II binding and assist autophagosome elongation and closure. Beclin 1 is a protein involved in vesicle trafficking and autophagosome maturation, and increased expression of p62 can

cause protein-specific autophagy degradation.²⁷ Our study showed that the autophagy activation factors LC3II/LC3I, Atg7 and Beclin 1 were reduced while inhibitory factor p62 was increased in OP rats. This situation was reversed after the intervention with icariin. These results confirm other literature precedents indicating that OP is associated with decreased levels of autophagy.²⁸

Our research focused on explaining the bidirectional effects of the autophagy AMPK/ULK1 and AKT/mTOR/ULK1 pathways on OP. The ULK1 is the first initiation complex of autophagy.²⁹ The Ser555 and Ser757 phosphorylation sites of ULK1 have distinct effects on autophagy. The AMPK stimulates the phosphorylation of the ULK1, while AKT and mTOR are inhibitors.^{30,31} This paper reveals that, in OP rats, ULK1 protein phosphorylated at the Ser555 phosphorylation decreased, but ULK1 phosphorylated at Ser757 increased. Therefore, impaired autophagy can induce OP, and appropriate activation of autophagy can have a protective effect against OP. The AMPK acted on the kinase at the ULK1 Ser555 phosphorylating site, and the AMPK/ULK1 (Ser555) pathway was suppressed in OP rats in vivo. The mTOR and AKT acted on the ULK1 Ser757 phosphorylating site and the mTOR/AKT/ULK1 (Ser757) autophagy pathway was promoted. However, the activities of AMPK, AKT, mTOR, ULK1 (Ser757), and ULK1 (Ser555) were modified by the intervention with icariin. The overexpression of AKT, mTOR and ULK1 (Ser757) was suppressed, and low AMPK and ULK1 (Ser555) were improved by icariin. In summary, icariin induced autophagy by activating the AMPK/ULK1 (Ser555) pathway and suppressing the AKT/mTOR/ULK1 pathway.

Icariin affects bone metabolism in various ways. For example, for ULK1, icariin stimulates the osteoblastic differentiation of bone marrow-derived mesenchymal stem cells,

adjusting the bone metabolism balance.³² This is a separate mechanism. In this study, only 2 signaling pathways, AMPK/ULK1 and Akt/mTOR/ULK1 in the autophagy pathway, were selected for study. In our subsequent experiments, we will consider using mesenchymal stem cells from bone marrow to induce osteogenic differentiation and confirm the in vivo experiments.

Limitations

Our research explained the bidirectional effects of the autophagy AMPK/ULK1 and AKT/mTOR/ULK1 pathways on OP. Meanwhile, the mechanisms of the icariin treatment in OP by its mediation of autophagy were explained. However, our study still has some limitations. This research is too basic for further analysis, and deeper investigations are needed. Particularly, this study should be repeated with the addition of another group (ovariectomy+icariin+autophagy inhibitor) to prove the participation of autophagy in the mechanism. Thus, we were not able to fully confirm the in vivo results. We will further examine the mechanism in vitro.

Conclusions

In conclusion, daily oral administration of icariin for 12 weeks restored femur microstructure and increased bone turnover, effectively impeding bone loss caused by OP in rats. The molecular mechanism, at least partially, involves the regulation of the AMPK/ULK1 and AKT/mTOR/ULK1 autophagy pathways. The results provide an experimental basis for the further development of icariin in the field of OP treatment.

Supplementary data

The Supplementary materials are available at <https://doi.org/10.5281/zenodo.8415761>. The package consists of the following files:

Supplementary Table 1. Results of normality and variance homogeneity test of body weights at the 12th week ($X \pm S$).

Supplementary Table 2. Results of normality and variance homogeneity test of indexes of bone formation and resorption in serum ($X \pm S$).

Supplementary Table 3. Results of normality and variance homogeneity test of BMD and trabecular parameters in femur.

ORCID iDs

Jiaying Zou  <https://orcid.org/0009-0005-1486-1121>
 Yue Peng  <https://orcid.org/0000-0001-6036-3880>
 Yue Wang  <https://orcid.org/0009-0008-1241-0767>
 Shouzhu Xu  <https://orcid.org/0000-0003-0596-5939>
 Chuandao Shi  <https://orcid.org/0000-0002-1434-1100>
 Qiling Liu  <https://orcid.org/0000-0002-3479-5601>

References

- Zeng L, Yu G, Yang K, Hao W, Chen H. The improving effect and safety of probiotic supplements on patients with osteoporosis and osteopenia: A systematic review and meta-analysis of 10 randomized controlled trials. *Evid Based Complement Alternat Med*. 2021;2021:9924410. doi:10.1155/2021/9924410
- Damani JJ, De Souza MJ, VanEvery HL, Strock NCA, Rogers CJ. The role of prunes in modulating inflammatory pathways to improve bone health in postmenopausal women. *Adv Nutr*. 2022;13(5):1476–1492. doi:10.1093/advances/nmab162
- Surguchov A, Bernal L, Surguchev AA. Phytochemicals as regulators of genes involved in synucleinopathies. *Biomolecules*. 2021;11(5):624. doi:10.3390/biom11050624
- Mok S, Chen W, Lai W, et al. Icarin protects against bone loss induced by oestrogen deficiency and activates oestrogen receptor-dependent osteoblastic functions in UMR 106 cells. *Br J Pharmacol*. 2010;159(4):939–949. doi:10.1111/j.1476-5381.2009.00593.x
- Zu Y, Mu Y, Li Q, Zhang ST, Yan HJ. Icarin alleviates osteoarthritis by inhibiting NLRP3-mediated pyroptosis. *J Orthop Surg Res*. 2019;14(1):307. doi:10.1186/s13018-019-1307-6
- Yu T, Xiong Y, Luu S, et al. The shared KEGG pathways between icariin-targeted genes and osteoporosis. *Aging*. 2020;12(9):8191–8201. doi:10.18632/aging.103133
- Long Z, Wu J, Xiang W, Zeng Z, Yu G, Li J. Exploring the mechanism of icariin in osteoporosis based on a network pharmacology strategy. *Med Sci Monit*. 2020;26:e924699. doi:10.12659/MSM.924699
- Qi M, Zhang L, Ma Y, et al. Autophagy maintains the function of bone marrow mesenchymal stem cells to prevent estrogen deficiency-induced osteoporosis. *Theranostics*. 2017;7(18):4498–4516. doi:10.7150/thno.17949
- Yin X, Zhou C, Li J, et al. Autophagy in bone homeostasis and the onset of osteoporosis. *Bone Res*. 2019;7(1):28. doi:10.1038/s41413-019-0058-7
- Nollet M, Santucci-Darmanin S, Breuil V, et al. Autophagy in osteoblasts is involved in mineralization and bone homeostasis. *Autophagy*. 2014;10(11):1965–1977. doi:10.4161/auto.36182
- Liu ZZ, Hong CG, Hu WB, et al. Autophagy receptor OPTN (optineurin) regulates mesenchymal stem cell fate and bone-fat balance during aging by clearing FABP3. *Autophagy*. 2021;17(10):2766–2782. doi:10.1080/15548627.2020.1839286
- Wang S, Deng Z, Ma Y, et al. The role of autophagy and mitophagy in bone metabolic disorders. *Int J Biol Sci*. 2020;16(14):2675–2691. doi:10.7150/ijbs.46627
- Yoshida G, Kawabata T, Takamatsu H, et al. Degradation of the NOTCH intracellular domain by elevated autophagy in osteoblasts promotes osteoblast differentiation and alleviates osteoporosis. *Autophagy*. 2022;18(10):2323–2332. doi:10.1080/15548627.2021.2017587
- Liu H, Zhu R, Liu C, et al. Evaluation of decalcification techniques for rat femurs using HE and immunohistochemical staining. *BioMed Res Int*. 2017;2017:9050754. doi:10.1155/2017/9050754
- Grunwald DS, Otto NM, Park JM, Song D, Kim DH. GABARAPs and LC3s have opposite roles in regulating ULK1 for autophagy induction. *Autophagy*. 2020;16(4):600–614. doi:10.1080/15548627.2019.1632620
- Wu X, Liu J, Song H, Yang Q, Ying H, Liu Z. Aurora kinase-B silencing promotes apoptosis of osteosarcoma 143B cells by ULK1 phosphorylation-induced autophagy [in Chinese]. *Nan Fang Yi Ke Da Xue Xue Bao*. 2020;40(9):1273–1279. doi:10.12122/j.issn.1673-4254.2020.09.08
- Liu HT, Pan SS. Late exercise preconditioning promotes autophagy against exhaustive exercise-induced myocardial injury through the activation of the AMPK-mTOR-ULK1 pathway. *BioMed Res Int*. 2019;2019:5697380. doi:10.1155/2019/5697380
- Walker CL, Walker MJ, Liu NK, et al. Systemic bisperoxovanadium activates Akt/mTOR, reduces autophagy, and enhances recovery following cervical spinal cord injury. *PLoS One*. 2012;7(1):e30012. doi:10.1371/journal.pone.0030012
- Tanha K, Fahimfar N, Nematollahi S, et al. Annual incidence of osteoporotic hip fractures in Iran: A systematic review and meta-analysis. *BMC Geriatr*. 2021;21(1):668. doi:10.1186/s12877-021-02603-1
- Yong E, Logan S. Menopausal osteoporosis: Screening, prevention and treatment. *Singapore Med J*. 2021;62(4):159–166. doi:10.11622/smedj.2021036

21. Wang T, Liu Q, Tjhi W, et al. Therapeutic potential and outlook of alternative medicine for osteoporosis. *Curr Drug Targets*. 2017;18(9). doi:10.2174/1389450118666170321105425
22. Zhang X, Chen Y, Zhang C, et al. Effects of icariin on the fracture healing in young and old rats and its mechanism. *Pharm Biol*. 2021; 59(1):1243–1253. doi:10.1080/13880209.2021.1972121
23. Gillet M, Vasikaran S, Inderjeeth C. The role of PINP in diagnosis and management of metabolic bone disease. *Clin Biochem Rev*. 2021; 42(1):3–10. doi:10.33176/AACB-20-0001
24. Sharma U, Pal D, Prasad R. Alkaline phosphatase: An overview. *Indian J Clin Biochem*. 2014;29(3):269–278. doi:10.1007/s12291-013-0408-y
25. Abe S, Yoshihisa A, Ichijo Y, et al. Serum TRACP5b, a marker of bone resorption, is associated with adverse cardiac prognosis in hospitalized patients with heart failure. *CJC Open*. 2021;3(4):470–478. doi:10.1016/j.cjco.2020.12.005
26. Bauer D, Krege J, Lane N, et al. National Bone Health Alliance Bone Turnover Marker Project: Current practices and the need for US harmonization, standardization, and common reference ranges. *Osteoporos Int*. 2012;23(10):2425–2433. doi:10.1007/s00198-012-2049-z
27. Florencio-Silva R, Sasso GRDS, Simões MDJ, et al. Osteoporosis and autophagy: What is the relationship? *Rev Assoc Med Bras*. 2017;63(2): 173–179. doi:10.1590/1806-9282.63.02.173
28. Camuzard O, Santucci-Darmanin S, Breuil V, et al. Sex-specific autophagy modulation in osteoblastic lineage: A critical function to counteract bone loss in female. *Oncotarget*. 2016;7(41):66416–66428. doi:10.18632/oncotarget.12013
29. Zachari M, Ganley IG. The mammalian ULK1 complex and autophagy initiation. *Essays Biochem*. 2017;61(6):585–596. doi:10.1042/EBC20170021
30. Kim J, Kundu M, Viollet B, Guan KL. AMPK and mTOR regulate autophagy through direct phosphorylation of Ulk1. *Nat Cell Biol*. 2011;13(2): 132–141. doi:10.1038/ncb2152
31. Xiang H, Zhang J, Lin C, Zhang L, Liu B, Ouyang L. Targeting autophagy-related protein kinases for potential therapeutic purpose. *Acta Pharm Sin B*. 2020;10(4):569–581. doi:10.1016/j.apsb.2019.10.003
32. Wang Z, Wang D, Yang D, Zhen W, Zhang J, Peng S. The effect of icariin on bone metabolism and its potential clinical application. *Osteoporos Int*. 2018;29(3):535–544. doi:10.1007/s00198-017-4255-1

Endogenous hsa-circ_0007113 binds hsa-miR-515-5p to regulate senescence in human embryonic lung fibroblasts

Hualing Li^{1,2,A–F}, Zhiyi Zhen^{1,B,C}, Junjie Wei^{1,A–C}, Xianxian Fan^{1,B,C}, Pengfei Cao^{1,B,C}, Yitang Zhang^{1,B,C}, Yali Chen^{1,B,C}, Yue Li^{1,E}, Yifan Zhu^{1,C}, Rui Wang^{1,C}, Xingjie Ma^{3,C,E}

¹ Department of Biochemistry, Jiangsu Key Laboratory of Experimental and Translational Non-coding RNA Research, Institute of Translational Medicine, Medical College, Yangzhou University, China

² Department of Pathology, Jiangsu Key Laboratory of Human Zoonosis, Yangzhou University, China

³ Department of Intensive Care, The Affiliated Hospital of Yangzhou University, China

A – research concept and design; B – collection and/or assembly of data; C – data analysis and interpretation;

D – writing the article; E – critical revision of the article; F – final approval of the article

Advances in Clinical and Experimental Medicine, ISSN 1899–5276 (print), ISSN 2451–2680 (online)

Adv Clin Exp Med. 2024;33(9):953–964

Address for correspondence

Hualing Li

E-mail: 2274292599@qq.com

Funding sources

This study was supported by the National Science Foundation of China (grants No. 81671056, No. 81372237 and No. 81100862), the Natural Science Foundation of the Jiangsu Higher Education Institutions of China (grant No. 18KJA320014), CSC (grant No. 2015CXJ070), Student's innovation and entrepreneurship training program of Yangzhou University (grants No. C20221117019Y, No. X20220740, No. X20220765, No. XCX20230826, and No. XCX20230842), and Medical Innovation and Transformation Special Fund of Yangzhou University (grant No. AHYZUZHXM202107).

Conflict of interest

None declared

Received on July 9, 2022

Reviewed on October 7, 2023

Accepted on October 25, 2023

Published online on December 23, 2023

Cite as

Li H, Zhen Z, Wei J, et al. Endogenous hsa-circ_0007113 binds hsa-miR-515-5p to regulate senescence in human embryonic lung fibroblasts. *Adv Clin Exp Med.* 2024;33(9):953–964. doi:10.17219/acem/174494

DOI

10.17219/acem/174494

Copyright

Copyright by Author(s)

This is an article distributed under the terms of the Creative Commons Attribution 3.0 Unported (CC BY 3.0) (<https://creativecommons.org/licenses/by/3.0/>)

Abstract

Background. Cellular senescence can lead to many diseases. However, the roles and regulation of circular RNAs (circRNAs) in senescence are poorly understood.

Objectives. To investigate the altered expression pattern and mechanism of circRNA during cellular senescence and find potential targets to prevent senescence.

Materials and methods. The Arraystar Human circRNA Array and bioinformatics were used to profile the differentially expressed circRNAs in human embryonic lung fibroblasts (IMR-90) between young cells and senescent cells and quantification in the clinical materials. Gene Ontology (GO) and Kyoto Encyclopedia of Genes and Genomes (KEGG) pathway analyses were performed. The miRNA targets were predicted using TargetScan and miRanda.

Results. A total of 113 differentially expressed circRNAs were identified, including 109 upregulated and 4 downregulated circRNAs (fold change >2 and p-value <0.05). Real-time qualitative polymerase chain reaction (qPCR) showed that the expression levels of 4 circRNA were significantly increased in senescent cells, and that of hsa_circ_0007113 was significantly decreased, consistent with the microarray. siRNA against hsa_circ_0007113 increased p21 and p53 expression levels and β -gal staining. The hsa_circ_0007113 has a binding site for miR-515-5p, which is involved in regulating the p53/p21 signaling pathway. The expression level of hsa_circ_0007113 was also decreased in aged people.

Conclusions. The study showed an altered circRNA expression pattern in cellular senescence, which might play important roles in senescence-related physiological processes. These findings provide a new direction for studying the molecular mechanism underlying senescence and a new possibility for the treatment of senescence by modulating circRNAs.

Key words: senescence, human circRNA array, hsa_circ_0007113, hsa-miR-515-5p, P53/P21 pathway

Background

The essence of aging is cellular senescence, in which cellular functions gradually decrease or are lost, leading to a loss of tissue function. Cell senescence can be accelerated or enhanced by external environmental factors such as radiation, oxidizing agents and therapeutic agents.^{1,2} Numerous mechanisms participate in cellular senescence, including DNA damage, telomeres, oncogenes, activated MAPK cascade, and p53 and p16^{Ink4a} pathways.^{3–7}

Non-coding RNAs play a vital role in the regulation of all cellular pathways.⁸ Recently, several studies revealed that non-coding RNAs are linked to the control of cellular senescence.^{9–11} Circular RNA (circRNA) is a special class of non-coding RNA, which has a closed circular structure protecting them from exonuclease R. Circular RNAs are conserved in evolution, stable, abundant, and show specific tissues and developmental stage expression.^{14,15} Moreover, they have been shown to regulate microRNA (miRNA) expression at the transcriptional or post-transcriptional levels.^{12,13} Specific circRNAs play important roles in human diseases such as cancer, stroke, ischemia, neurodegenerative disorders, and heart disease.^{16–22} However, so far, few studies have evaluated circRNA changes in cell senescence.^{21,23,24}

Circular RNA can bind miRNA-induced silencing complexes via the miRNA response element and affect miRNA concentration to regulate the activity of the downstream gene.^{25,26} However, the differential expression of circRNAs during senescence has only rarely been reported. Therefore, this study aimed to use the Arraystar Human circRNA Array to detect the changes in circRNA expression profiles during cellular senescence. Next, the Kyoto Encyclopedia of Genes and Genomes (KEGG) and Gene Ontology (GO) pathway analyses were carried out to anticipate the potential functions of circRNAs during senescence. These findings could provide a better understanding of cellular senescence and eventually slow down senescence associated with pathological conditions.

Objectives

We aimed to find the relationship between senescence and circRNAs with high-throughput quantitative analysis of circRNA. Furthermore, we quantified circRNAs in clinical samples to clarify the potential biomarkers of human aging, which can provide a certain clinical reference value for clinicians.

Materials and methods

Cell culture

The human embryonic lung fibroblast cell line IMR-90 was seeded in a CO₂-incubator containing 5% CO₂ at 37°C

in Dulbecco's modified Eagle's medium (DMEM; Hyclone, Logan, USA) containing 10% fetal bovine serum (FBS; Hyclone) and 1% of penicillin and streptomycin (Gibco, Invitrogen, Waltham, USA). IMR-90 cells were used as young cells in population doublings (PDL) between 15 and 25, and senescent fibroblasts were utilized in PDL 55–65 following additional culture time. Total cellular RNA was isolated using TRIzol reagent (Invitrogen, Waltham, USA).

Labeling and hybridization

Array hybridization and specimen labeling were carried out in accordance with the manufacturer's instructions (Arraystar, Rockville, USA). Total RNA was digested with RNase R (Epicentre, Madison, USA), and the enriched circRNA was amplified and converted into fluorescent cRNA utilizing the random method (Arraystar Super RNA Labeling Kit; Arraystar). The RNeasy Mini Kit was then used to purify the labeled cRNAs (Qiagen, Hilden, Germany). Using a NanoDrop ND-1000, the labeled cRNAs (pmol Cy3/μg) were measured (Thermo Fisher Scientific, Waltham, USA), and 1 μg of cRNA was cleaved by adding 5 μL of a ×10 blocking agent and 1 μL of a ×25 fragmentation buffer. To dilute the labeled cRNA, 25 μL of ×2 hybridization buffer was added to the mixture, and it was incubated for 30 min at 60°C. Finally, space slides containing 50 μL of the hybridization solution were distributed and assembled on the microarray slide for the circRNA expression (Agilent Technologies, Santa Clara, USA). The slides were incubated for 17 h at 65°C in a mixed oven, and then the hybridized arrays were cleaned, fixed, and scanned using the Agilent Scanner G2505C (Agilent Technologies).

Arraystar human circRNA array analysis

The gathered array images were examined using Agilent Feature Extraction software (v. 11.0.1.1; Agilent Technologies). Then, utilizing the R software package (R Foundation for Statistical Computing, Vienna, Austria), quantile normalization and data processing were carried out (Bioconductor, Github, CRAN; <https://www.bioconductor.org/>). Through volcano map screening, the statistically significant differential expression of circRNAs between the 2 groups was determined, which was displayed as hierarchical clustering. Fold changes ≥2 and p-values <0.05 indicated significant differences in the circRNA expression.

Comprehensive analysis of the circRNAs-miRNAs-mRNAs networks

The software StarBase (v. 2.0; <http://starbase.sysu.edu.cn>) was used to anticipate the preferred miRNAs of selected circRNAs. The target miRNAs of the identified circRNAs were anticipated using Mireap, Miranda (v. 3.3a; https://cloud.oebiotech.com/task/detail/array_miranda_plot) and TargetScan (v. 7.0; <http://www.targetscan.org>).

The circRNA-miRNA-mRNA regulation networks were analyzed using miRTarBase (v. 6.1; <https://miRTarBase.cuhk.edu.cn>), and the culminating correlations were clarified with Cytoscape (<https://cytoscape.org/>).

Gene Ontology and KEGG pathway analyses

We used the gene function classification system, GO, to determine the characteristics and functions of our genes of interest.²⁷ In the GO database (<http://www.geneontology.org>), all source genes are mapped to GO terms, and the determination of whether a gene fits a term is calculated using an false discovery rate (FDR) threshold of 0.05. Kyoto Encyclopedia of Genes and Genomes pathway analysis identified the significantly enriched pathways in the source genes, as compared to the whole genome background.²⁸ The calculation equation is identical to that used in GO analysis, and the cascades with FDR ≤ 0.05 were deemed as significant enrichment.

siRNA transfection and SA- β -galactosidase activity

The small interfering RNAs (siRNAs) employed for cell transfection were obtained from RiboBio (Guangzhou, China) with the following sequences: circRNA_0007113 siRNA (5'-CAA GUG UUG CCA ACC CAU CUG AUG GA-3') and Ctrl siRNA (5'-AAU UCU CCG AAC GUG UCA CGU-3'). The siRNA was transfected with Lipofectamine™ 2000 (Invitrogen) at a final concentration of 100 nM. Aging-related senescence-associated (SA) β -galactosidase activity was validated using a kit purchased from Cell Signaling Technology (CST; Danvers, USA).

Human blood sample collection and real-time quantitative polymerase chain reaction analysis

Total blood specimens were obtained from 40 healthy individuals, aged 30–39 or 60–69 years (male, body mass index (BMI) = 20–26 kg/m²) who visited the hospital for routine health examinations. All participants gave their informed consent for inclusion in the study prior to participation. The study was conducted in accordance with the Declaration of Helsinki, and the protocol was approved by the Ethics Committee of the Hospital and Medical College of Yangzhou University (approval No. YXYLL-2020-02).

TRIzol reagent was used to extract the total cellular RNA, which was then transcribed into cDNA with a Reverse Transcription Kit (Takara, Shiga, Japan). Real-time qualitative polymerase chain reaction (qPCR) was conducted using a kit following the manufacturer's instructions (Takara Bio SYBR Green; Takara). The reaction parameters were as follows: 95°C for 30 s, then 35 amplification cycles

(5 s at 95°C, 30 s at 60°C). All specimens were normalized to glyceraldehyde-3-phosphate dehydrogenase (GAPDH), and the experiment was repeated 3 times. Finally, SDS v. 1.4 software (Applied Biosystems, Foster City, USA) was used to analyze the data based on the $2^{-\Delta\Delta C_t}$ method. Origin v. 9.0 software (OriginLab, Northampton, USA) was utilized to analyze the histogram.

Protein extraction and western blotting

Radioimmunoprecipitation assay (RIPA) buffer (Beyotime Biotechnology, Shanghai, China) was used to lyse IMR90 cells, and protein was measured using a Bicinchoninic (BCA) protein assay kit (Bio-Rad, Hercules, USA). Total protein (35 μ g) was isolated using 10% sodium dodecyl sulfate–polyacrylamide gel electrophoresis (SDS-PAGE) and transferred to polyvinylidene difluoride (PVDF) membranes (MilliporeSigma, St. Louis, USA). The membranes were blocked with 5% skimmed milk in Tris-buffered saline with Tween (TBST) buffer, and then the primary anti-p53 and anti-p21 antibodies were introduced and incubated overnight at 4°C (Santa Cruz Biotechnology, Santa Cruz, USA). Membranes were washed thrice in TBST, and incubated with the secondary horseradish peroxidase (HRP)-conjugated antibodies (1:5,000 in TBST; Beijing Zhong-Shan Biotechnology, Beijing, China) for 1 h at room temperature. The protein was exposed using an improved chemiluminescence reagent (Millipore Sigma), and the reactive bands were analyzed for relative intensity using ImageJ software v. 1.46 (National Institutes of Health, Bethesda, USA).

Statistical analyses

All observations in this study were made in triplicate, and the results were analyzed using GraphPad Prism v. 8 software (GraphPad Software Inc., San Diego, USA). The one-sample nonparametric test was used to compare the difference between candidate circRNA and its corresponding control. The Shapiro–Wilk test and Bartlett test were used to determine the variables' normality, whereas homogeneity and a t-test (if not specifically indicated) or Wilcoxon Mann–Whitney test were used to compare the differences to control samples. A value of $p < 0.05$ was considered statistically significant.

Results

Differential expression profile analysis of circRNA between young and senescent human embryonic lung fibroblasts

A total of 3,936 circRNAs were identified using the circRNA microarray and displayed as hierarchical clustering (Fig. 1A) and box plot analysis (Fig. 1B). Scatter (Fig. 1C) and volcano plots (Fig. 1D) were used to identify differences

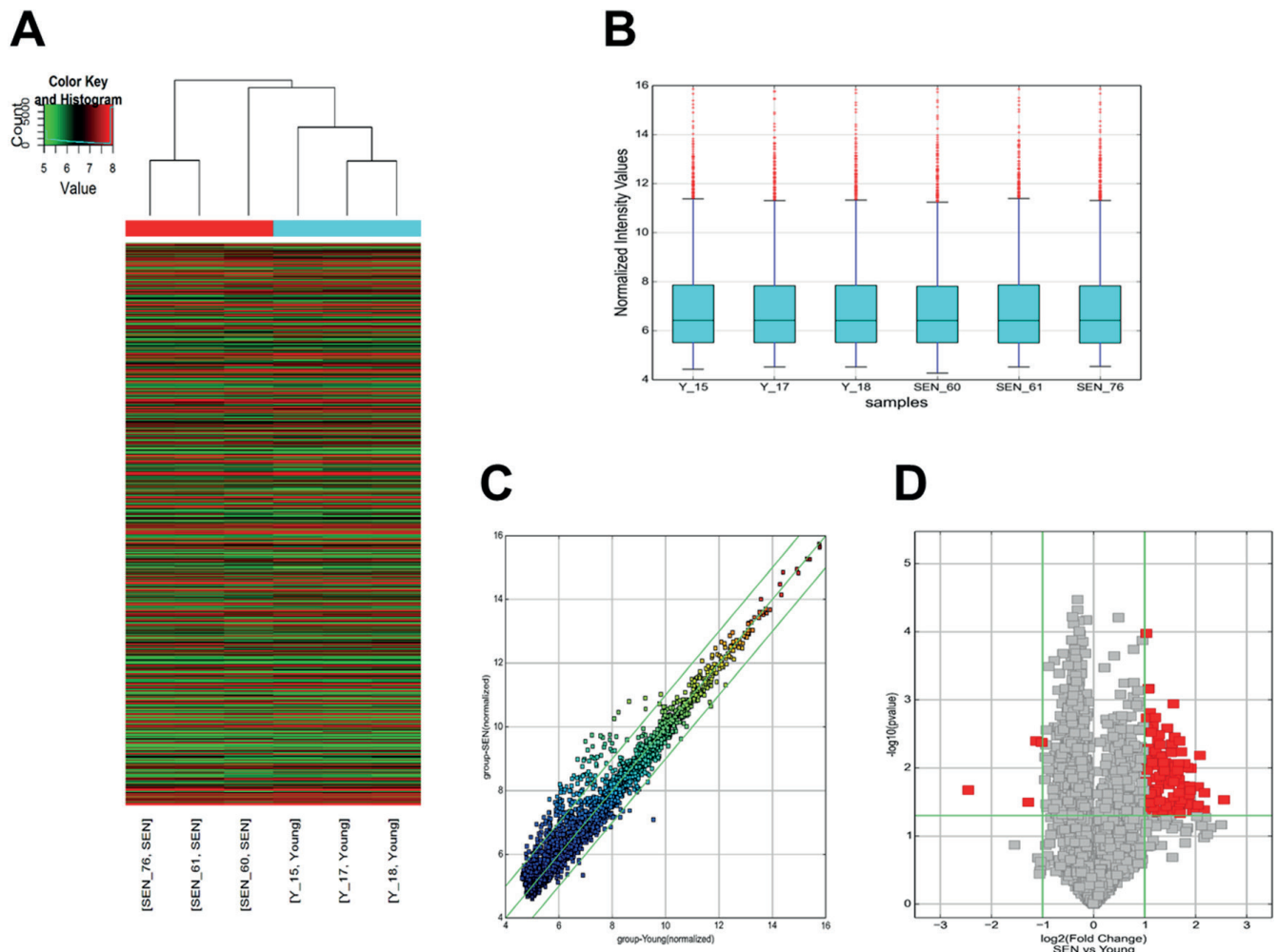


Fig. 1. Chip analysis of the circular RNAs in proliferating (Y_15, Y_17, Y_18) and senescent (SEN_60, SEN_61, SEN_76) IMR-90 cells. A. Hierarchical clustering result analysis; B. Box plot result analysis. The boxplot was generated using R. The outliers are represented as red dots beyond the upper and lower whisker boundaries. They are defined as values $> (Q3 + 1.5 * IQR)$ or $< (Q1 - 1.5 * IQR)$ ($IQR = \text{interquartile range}$); C. Scatter plot result analysis; D. Volcano plot analysis. Total 113 differentially expressed circRNAs (difference > 2.0 times, $*p < 0.05$), including 109 upregulated and 4 downregulated. More than 80% were of the exon type

Table 1. The upregulated circRNAs in this study

circRNA	Alias	circRNA type	Gene symbol	Fold change	p-value
hsa_circRNA_102602	hsa_circ_0052318	exonic	ZNF418	5.87	0.029
hsa_circRNA_100748	hsa_circ_0020926	exonic	STIM1	4.49	0.023
hsa_circRNA_001405	hsa_circ_0001167	intronic	PREX1	4.48	0.042
hsa_circRNA_103517	hsa_circ_0067997	exonic	FNDC3B	4.23	0.007
hsa_circRNA_001350	hsa_circ_0000253	intronic	BLNK	4.13	0.019
hsa_circRNA_100358	hsa_circ_0000139	exonic	GON4L	4.12	0.035
hsa_circRNA_000942	hsa_circ_0001303	antisense	UBA7	4.03	0.041
hsa_circRNA_000454	hsa_circ_0001703	intronic	SEPT7P2	3.85	0.043
hsa_circRNA_000618	hsa_circ_0000708	intronic	FAM65A	3.74	0.010
hsa_circRNA_104600	hsa_circ_0005927	exonic	VDAC3	3.70	0.021
hsa_circRNA_100057	hsa_circ_0008275	exonic	VPS13D	3.69	0.034
hsa_circRNA_103542	hsa_circ_0068464	exonic	EIF4A2	3.68	0.019
hsa_circRNA_103178	hsa_circ_0062577	exonic	CABIN1	3.67	0.025
hsa_circRNA_100018	hsa_circ_0009361	exonic	GNB1	3.60	0.031
hsa_circRNA_100063	hsa_circ_0010039	exonic	CASP9	3.58	0.010

Table 1. The upregulated circRNAs in this study – cont.

circRNA	Alias	circRNA type	Gene symbol	Fold change	p-value
hsa_circRNA_101295	hsa_circ_0030777	exonic	PCCA	3.44	0.009
hsa_circRNA_001747	hsa_circ_0000246	exonic	MCU	3.41	0.033
hsa_circRNA_100147	hsa_circ_0004240	exonic	EIF3I	3.41	0.018
hsa_circRNA_101643	hsa_circ_0036750	exonic	C15orf38-AP3S2	3.34	0.019
hsa_circRNA_102978	hsa_circ_0004525	exonic	RBCK1	3.29	0.029
hsa_circRNA_103665	hsa_circ_0070033	exonic	NUP54	3.29	0.005
hsa_circRNA_001547	hsa_circ_0001874	intronic	BICD2	3.28	0.030
hsa_circRNA_103410	hsa_circ_0003266	exonic	LRIG1	3.23	0.046
hsa_circRNA_102333	hsa_circ_0047303	exonic	ZNF521	3.22	0.032
hsa_circRNA_104693	hsa_circ_0003691	exonic	ASAP1	3.21	0.004
hsa_circRNA_104126	hsa_circ_0076798	exonic	GCLC	3.19	0.023
hsa_circRNA_101491	hsa_circ_0034762	exonic	MAPKBP1	3.19	0.028
hsa_circRNA_000593	hsa_circ_0000550	antisense	SLC10A1	3.18	0.014
hsa_circRNA_100395	hsa_circ_0015278	exonic	KLHL20	3.17	0.037
hsa_circRNA_104323	hsa_circ_0079534	exonic	MACC1	3.17	0.009
hsa_circRNA_104551	hsa_circ_0083294	exonic	TNKS	3.14	0.010
hsa_circRNA_101524	hsa_circ_0035360	exonic	UNC13C	3.13	0.040
hsa_circRNA_100802	hsa_circ_0009018	exonic	EXT2	3.13	0.030
hsa_circRNA_001026	hsa_circ_0000141	intronic	SMG5	3.09	0.009
hsa_circRNA_104044	hsa_circ_0075447	exonic	GMDS	3.04	0.010
hsa_circRNA_101037	hsa_circ_0025767	exonic	TMTC1	3.04	0.013
hsa_circRNA_104553	hsa_circ_0083335	exonic	MTMR9	3.00	0.004
hsa_circRNA_001255	hsa_circ_0000630	intronic	BBS4	2.98	0.010
hsa_circRNA_102979	hsa_circ_0059151	exonic	RBCK1	2.97	0.027
hsa_circRNA_103863	hsa_circ_0001495	exonic	CCNB1	2.96	0.016
hsa_circRNA_102728	hsa_circ_0006110	exonic	USP34	2.96	0.001
hsa_circRNA_100244	hsa_circ_0000075	exonic	FGGY	2.95	0.045
hsa_circRNA_101591	hsa_circ_0036282	exonic	ARID3B	2.95	0.009
hsa_circRNA_000578	hsa_circ_0000487	intronic	DLEU2	2.95	0.009
hsa_circRNA_100749	hsa_circ_0020927	exonic	STIM1	2.92	0.010
hsa_circRNA_000250	hsa_circ_0000848	intronic	SMAD7	2.89	0.004
hsa_circRNA_100921	hsa_circ_0023920	exonic	PICALM	2.89	0.011
hsa_circRNA_100850	hsa_circ_0006857	exonic	PACS1	2.88	0.015
hsa_circRNA_104803	hsa_circ_0087354	exonic	UBQLN1	2.87	0.006
hsa_circRNA_101956	hsa_circ_0041551	exonic	ANKFY1	2.85	0.032
hsa_circRNA_101742	hsa_circ_0004683	exonic	C16orf62	2.85	0.011
hsa_circRNA_001653	hsa_circ_0001568	intronic	DUSP22	2.79	0.034
hsa_circRNA_001503	hsa_circ_0001191	intronic	DYRK1A	2.79	0.018
hsa_circRNA_100384	hsa_circ_0002093	exonic	SFT2D2	2.78	0.011
hsa_circRNA_000921	hsa_circ_0001120	intronic	SNED1	2.77	0.045
hsa_circRNA_100752	hsa_circ_0020976	exonic	OR51B5	2.74	0.009
hsa_circRNA_101958	hsa_circ_0041555	exonic	UBE2G1	2.72	0.003
hsa_circRNA_104426	hsa_circ_0081188	exonic	SLC25A13	2.68	0.037
hsa_circRNA_103278	hsa_circ_0001265	exonic	MTMR14	2.65	0.008
hsa_circRNA_102247	hsa_circ_0046462	exonic	TBCD	2.62	0.011
hsa_circRNA_104780	hsa_circ_0001861	exonic	GRHRP	2.58	0.008
hsa_circRNA_101401	hsa_circ_0032641	exonic	MLH3	2.56	0.010

Table 1. The upregulated circRNAs in this study – cont.

circRNA	Alias	circRNA type	Gene symbol	Fold change	p-value
hsa_circRNA_102246	hsa_circ_0046449	exonic	TBCD	2.54	0.042
hsa_circRNA_104401	hsa_circ_0005513	exonic	GTF2I	2.53	0.007
hsa_circRNA_000644	hsa_circ_0000861	antisense	XLOC_012735	2.50	0.015
hsa_circRNA_000274	hsa_circ_0000919	intronic	ATP13A1	2.49	0.015
hsa_circRNA_102851	hsa_circ_0008032	exonic	HAT1	2.46	0.005
hsa_circRNA_001587	hsa_circ_0000979	intronic	XLOC_001374	2.45	0.007
hsa_circRNA_101759	hsa_circ_0038608	exonic	EARS2	2.45	0.013
hsa_circRNA_104948	hsa_circ_0001897	exonic	POMT1	2.45	0.031
hsa_circRNA_103140	hsa_circ_0061891	exonic	PDXK	2.43	0.003
hsa_circRNA_101746	hsa_circ_0038349	exonic	C16orf62	2.40	0.009
hsa_circRNA_000042	hsa_circ_0000036	intronic	THEMIS2	2.40	0.004
hsa_circRNA_100442	hsa_circ_0002274	exonic	LPGAT1	2.39	0.004
hsa_circRNA_000422	hsa_circ_0001545	intragenic	TCOF1	2.39	0.020
hsa_circRNA_000679	hsa_circ_0001248	intronic	TTC38	2.38	0.045
hsa_circRNA_100100	hsa_circ_0010931	exonic	TMEM50A	2.34	0.028
hsa_circRNA_100588	hsa_circ_0018293	exonic	ANXA8L2	2.34	0.014
hsa_circRNA_101635	hsa_circ_0036666	exonic	NTRK3	2.32	0.006
hsa_circRNA_104135	hsa_circ_0007874	exonic	MTO1	2.31	0.002
hsa_circRNA_102251	hsa_circ_0002225	exonic	TBCD	2.30	0.022
hsa_circRNA_104367	hsa_circ_0080170	exonic	TNS3	2.25	0.038
hsa_circRNA_001800	hsa_circ_0001033	intronic	TTC31	2.23	0.002
hsa_circRNA_104694	hsa_circ_0007934	exonic	ZFAT	2.22	0.008
hsa_circRNA_104816	hsa_circ_0087493	exonic	IARS	2.19	0.003
hsa_circRNA_102476	hsa_circ_0007396	exonic	MYO9B	2.18	0.024
hsa_circRNA_000926	hsa_circ_0001022	intragenic	ACTR2	2.16	0.006
hsa_circRNA_104744	hsa_circ_0002606	exonic	MLLT3	2.16	0.033
hsa_circRNA_001380	hsa_circ_0000540	intragenic	FBXO34	2.15	0.002
hsa_circRNA_000082	hsa_circ_0000189	intragenic	NVL	2.15	0.020
hsa_circRNA_101070	hsa_circ_0026512	exonic	EIF4B	2.15	0.033
hsa_circRNA_100699	hsa_circ_0020250	exonic	ATE1	2.14	0.006
hsa_circRNA_100604	hsa_circ_0009172	exonic	DNA2	2.14	0.006
hsa_circRNA_101248	hsa_circ_0029976	exonic	NBEA	2.12	0.022
hsa_circRNA_100981	hsa_circ_0024737	exonic	VWA5A	2.11	0.001
hsa_circRNA_100999	hsa_circ_0025006	exonic	ADIPOR2	2.11	0.005
hsa_circRNA_000046	hsa_circ_0000059	intronic	CAP1	2.10	0.002
hsa_circRNA_102575	hsa_circ_0051527	exonic	EML2	2.10	0.001
hsa_circRNA_102509	hsa_circ_0006446	exonic	LSM14A	2.07	0.003
hsa_circRNA_102551	hsa_circ_0003859	exonic	LTBP4	2.07	0.011
hsa_circRNA_103009	hsa_circ_0003853	exonic	NAPB	2.06	0.008
hsa_circRNA_101743	hsa_circ_0006797	exonic	C16orf62	2.05	0.002
hsa_circRNA_103232	hsa_circ_0002877	exonic	MKL1	2.05	0.000
hsa_circRNA_102074	hsa_circ_0043815	exonic	STAT3	2.04	0.016
hsa_circRNA_000526	hsa_circ_0000248	intronic	ADK	2.03	0.022
hsa_circRNA_103593	hsa_circ_0069031	exonic	TMEM128	2.03	0.007
hsa_circRNA_001104	hsa_circ_0001157	antisense	DHX35	2.01	0.041
hsa_circRNA_102813	hsa_circ_0007052	exonic	CLASP1	2.00	0.008

Table 2. The downregulated circular RNAs (circRNAs) in this study

circRNA	Alias	circRNA type	Gene symbol	Fold change	p-value
hsa_circRNA_104700	hsa_circ_0005273	exonic	PTK2	5.48	0.021
hsa_circRNA_104147	hsa_circ_0004905	exonic	IBTK	2.43	0.032
hsa_circRNA_100601	hsa_circ_0007113	exonic	HERC4	2.18	0.004
hsa_circRNA_400011	hsa_circ_0092374	intronic	GADD45A	2.03	0.004

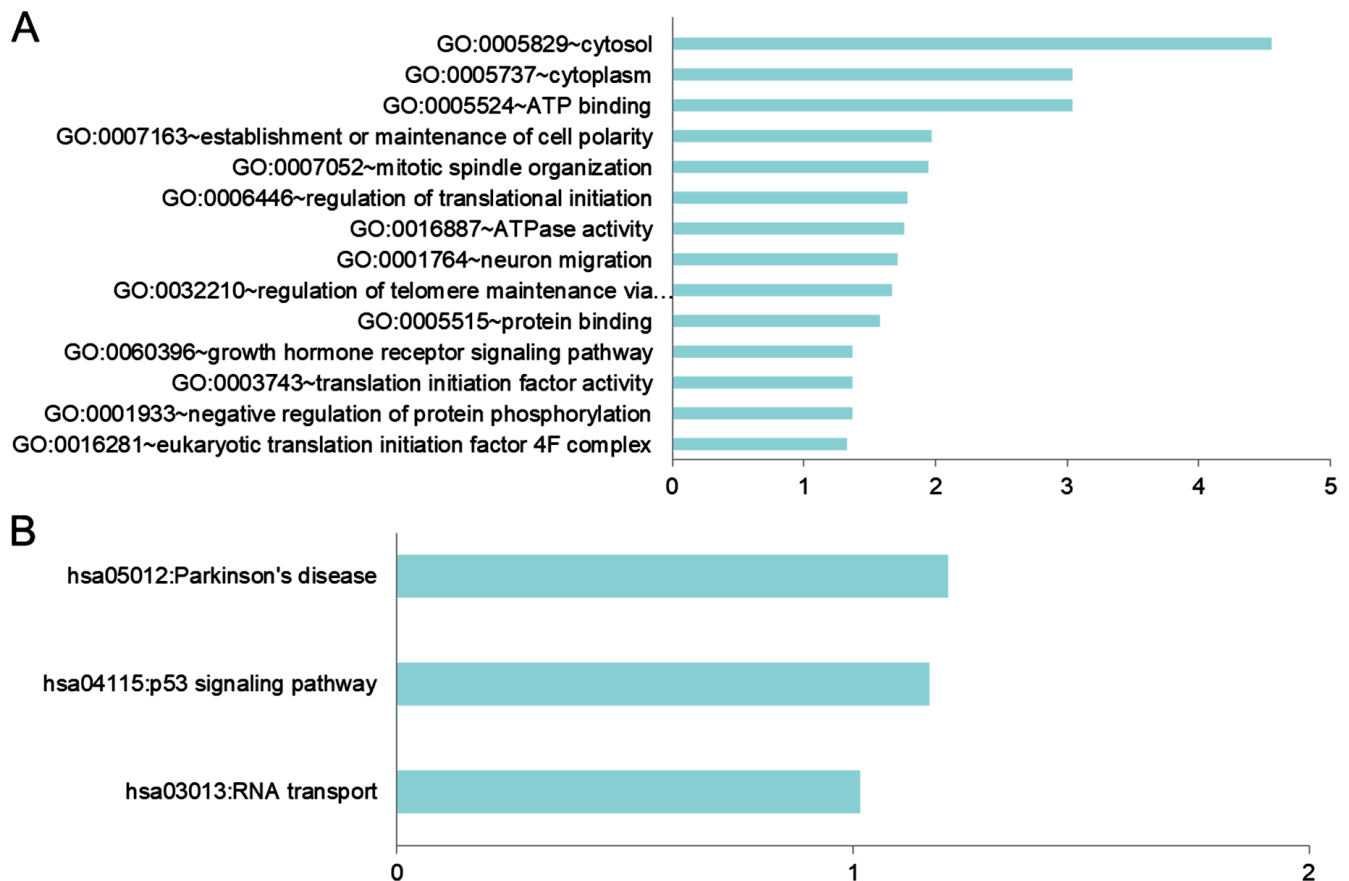


Fig. 2. Bioinformatics analyses of 113 differentially expressed circular RNAs (circRNAs). A. Gene Ontology (GO); B. Kyoto Encyclopedia of Genes and Genomes (KEGG)

in circRNAs between young and senescent cells. Among them, as shown in Table 1,2, 113 differentially expressed circular RNAs (circRNAs) were analyzed; 109 circRNAs were upregulated, and 4 circRNAs were downregulated, with $p < 0.05$ and $|\log_2(\text{fold change})| > 1$. More than 80% of the differentially expressed circRNAs belong to exonic circRNA, which is exclusively composed of exons.

Gene Ontology and Kyoto Encyclopedia of Genes and Genomes pathway analyses

The mRNAs produced from the parent genes of 113 changed circRNAs were examined using GO and KEGG pathway analysis to hypothesize the pathological and physiological significance of circRNAs throughout cellular senescence. The main supplemented and meaningful GO terminologies and biological process (BP) were “establishment

or maintenance of cell polarity”, “regulation of translational initiation” and “ATPase activity”. In terms of molecular function (MF), it was found that most of the circRNA-associated mRNAs were in “ATP binding” and “protein binding” states. As for cellular components (CC), the most enriched CC terms were “cytosol” and “cytoplasm” (Fig. 2A). Gene-enriched KEGG cascade analysis demonstrated that these pathways may be linked with the progression of aging. Most of these circRNAs are target genes linked with Parkinson’s disease, p53 signaling pathway and RNA transport (Fig. 2B).

Differentially expressed circRNAs’ evaluation with qPCR

Nine significantly upregulated and 4 significantly downregulated circRNAs were chosen for qPCR confirmation. Primers are shown in Table 3. We found that

Table 3. Primers used in this study

Name	Forward (5'-3')	Reverse (5'-3')
hsa_circ_0007113	TGGGAAGCATTGTCACTGAG	CAAGCATACACCTGGCCTTT
hsa_circ_0009361	GCCGAGCAACTTAAGAACCA	AGTGCTCTCAATGCCACCT
hsa_circ_0092374	AGCTCCCACGGACTGAAAG	TTAGCTTCTCCCTGCAA
hsa_circ_0004905	GTTTTGACCTGTCCGTTTC	AAGAGACGGGTCTCGCTAT
hsa_circ_0006110	ATGGTTCCTGTTACTCTTGAGG	TGCTGCCATTGGAGTCCTTA
hsa_circ_0083335	TTTGTGTGATGGTGGCTTG	GACGGATGAACCTCTGTCTT
hsa_circ_0001303	AAAATAACTGGCAAATATATCATTGAG	AGAAGCCCTGCCCTTCTC
hsa_circ_0003691	GCTGCTTAGACGCTGGATTT	AGAAGCCCTGCCCTTCTC
hsa_circ_0005927	TCCTCTCCAAAATGCCAGAG	ACTCTGTCTGCTGCTGCTAC
hsa_circ_0068464	TCATGTTTCATGCCCTGATTT	ACCAGAGTCTCCCGAATG
hsa_circ_0001703	GCTGGGGTCTTGCTATCTGA	TGCCACTTGTTTACCTTGG
hsa_circ_0005273	TGAGAGAAGTACCATAGAAATTTAGCA	AGTCGCTGTGCCATTGTTT
hsa_circ_0004905	CACAACCTCAAACCCGTCT	TCAAGAGGTTGTTGCACAGG
P53	CCCCAGCCAAAGAAGAAAC	AACATCTCGAAGCGCTCAC
P21	GGGATGTCGCTCAGAACCCA	AAGTTCATCGCTCACGGG
18SRNA	CGAACGCTGCGCCTATCAACTT	ACCCGTGGTCACCATGGTA
GAPDH	GAGTCCACTGGCGTCTTAC	ATCTTGAGGCTGTTGCATACTTCT

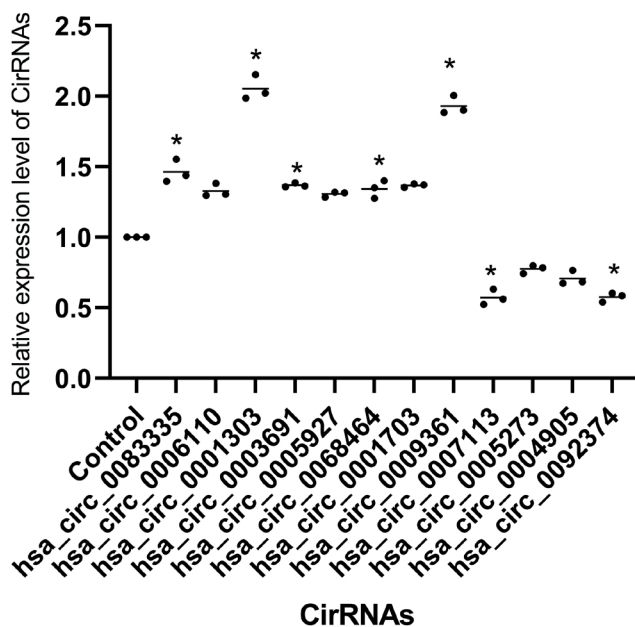


Fig. 3. Validation of 9 upregulated and 4 downregulated circular RNAs (circRNAs) using real-time qualitative polymerase chain reaction (qPCR). The Wilcoxon Mann–Whitney test was employed to analyze the differences between each circRNA group and the control group. The *hsa_circ_0083335*, *hsa_circ_0006110*, *hsa_circ_0001303*, *hsa_circ_0003691*, *hsa_circ_0005927*, *hsa_circ_0068464*, *hsa_circ_0001703*, *hsa_circ_0009361*, *hsa_circ_0001703*, *hsa_circ_0009361*, *hsa_circ_0007113*, *hsa_circ_0005273*, *hsa_circ_0004905*, and *hsa_circ_0092374* vs control: $Z = -2.087$, $p = 0.037$. The test assumptions are as follows: H_0 : The relative expression levels of circRNA X exhibit a similar overall distribution to that of the control group; H_1 : The relative expression levels of circRNA X differ from those of the control group, $\alpha = 0.05$.

hsa_circRNA_0083335, *hsa_circRNA_0068464*, *hsa_circRNA_0009361* and *hsa_circ_0001303* expression levels were significantly elevated in senescent cells, while the *hsa_circ_0007113* and *hsa_circ_0092374* expression

levels were significantly decreased, which was in line with the microarray results (Fig. 3).

Cellular senescence was exacerbated after siRNA treatment of *hsa_circ_0007113*

Following the administration of siRNA to silence *hsa_circ_0007113*, the expression levels of p21 and p53 were significantly elevated (Fig. 4AB). Moreover, the signal was significantly increased after β -gal staining, indicating that cell senescence was exacerbated after siRNA treatment against *hsa_circ_0007113* (Fig. 5A–C).

hsa_circ_0007113 could alleviate cellular senescence via miR-515-5p

CircRNAs can serve as “sponges” for miRNAs to control target gene expression. Therefore, we established a regulation network of circRNAs-microRNAs-mRNAs. The *hsa_circ_0007113* is anticipated to bind with 275 miRNAs, thereby controlling a wide array of genes. It was found that *hsa_circ_0007113* has a binding site for miR-515-5p, which is involved in the regulation of p53/p21 signaling pathway (Fig. 6). Five miRNAs, including *hsa-miR-515-5p*, *hsa_miR-1301-3p*, *hsa-miR-181c-5p*, *hsa-miR-22-5p*, and *hsa-miR-141-5p*, were selected and were shown to target cellular processes including inflammation (IL17A, IL11RA, IL17AC), energy metabolism (ATP2B1, ATP7B, ATP12A), cell apoptosis (BCL2, BCL2L13, CASP9, CASP7, CASP10), cell senescence (SIRT2, GPR17, GPR135), cell cycle and division (CDK11A, CDK6), and zinc finger protein (ZNF784, ZNF655, ZNF589).

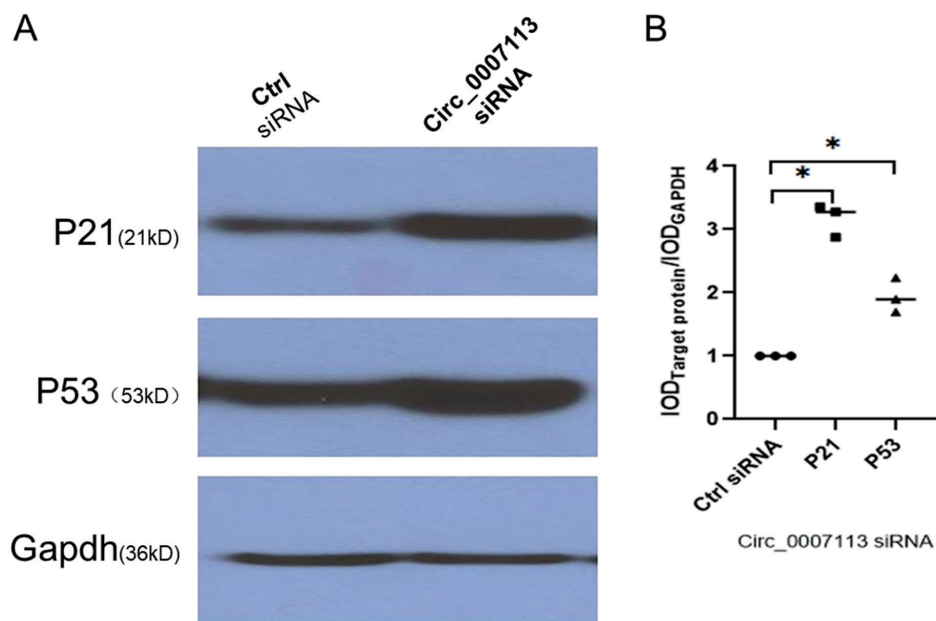


Fig. 4. Silencing of hsa_circ_0007113 increases the expression of p53 and p21. A. Protein expression of p53 and p21 was identified with western blotting. Glyceraldehyde-3-phosphate dehydrogenase (GAPDH) was used as a reference; B. Quantification of the western blot bands. The data were expressed with median (3 distinct repetitions, t-test, p21: p = 0.013; p53:p = 0.037, df = 4,* denotes p < 0.05)

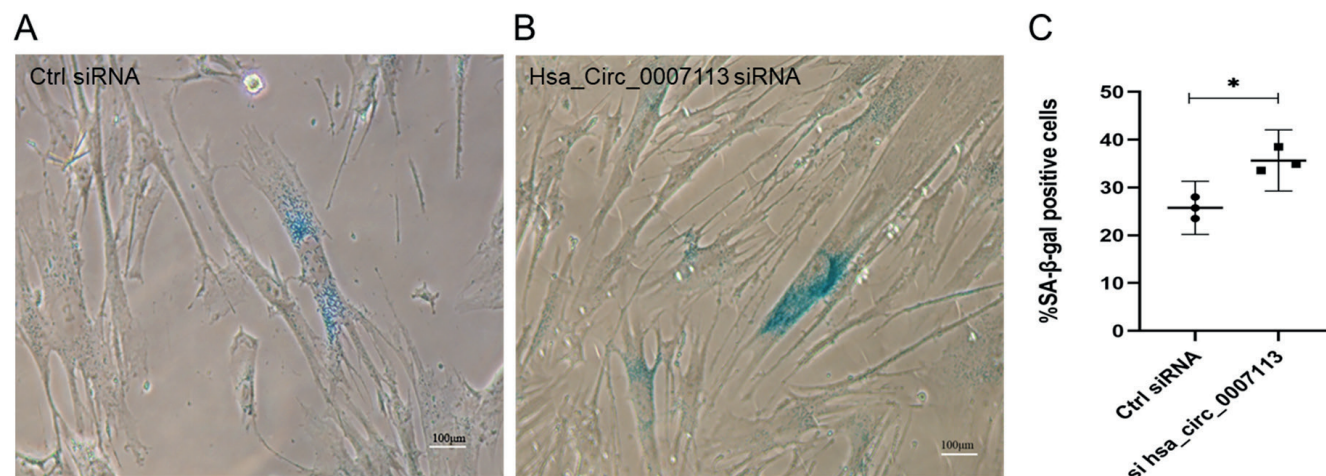


Fig. 5. After silencing of hsa_circ_0007113, SA-β-gal staining showed that the SA-β-gal expression of senescent cells was increased (×100). A. Control siRNA; B. has_circ_0007113 siRNA; C. Quantification of the positive cells. The data were expressed as mean with 95% confidence interval (95% CI) (3 distinct repetitions, t-test, p = 0.029, df = 4, *denotes p < 0.05)

The expression of hsa_circ_0007113 decreases with aging

The relative expression of hsa_circ_0007113 was measured in 40 healthy individuals, 30–39 and 60–69 years old, and was shown to be higher in the 30–39-year-old group compared to the 60–69-year-old group (Fig. 7).

Discussion

Age-linked diseases like osteoarthritis, atherosclerosis, cancer, Parkinson’s disease, Alzheimer’s disease, and type 2 diabetes are all impacted by cellular senescence.^{16–22,29,30} Therefore, understanding the regulatory mechanism of cellular senescence may enable interventions in these aging-related

diseases. The main signaling pathways controlling cellular senescence from a mechanical perspective are P53-P21^{CIP1} and P16^{INK4A}-Rb. Thus, it is thought that P53 and P16^{INK4A} are crucial elements in the induction of cellular senescence.³¹

Circular RNAs are important molecules involved in many biological processes, play important roles in regulating many cellular functions, and are expected to be biomarkers or treatment targets for diseases. However, their role in cellular senescence and the mechanisms of how circRNAs regulate it have not been previously described.

Therefore, the present study focused on the examination of alterations in circRNA expression profiles in senescence using the Arraystar Human circRNA Array, showing they are altered during cellular senescence. There were 109 up-regulated and 4 downregulated circRNAs, possibly playing important roles in senescence-related physiological

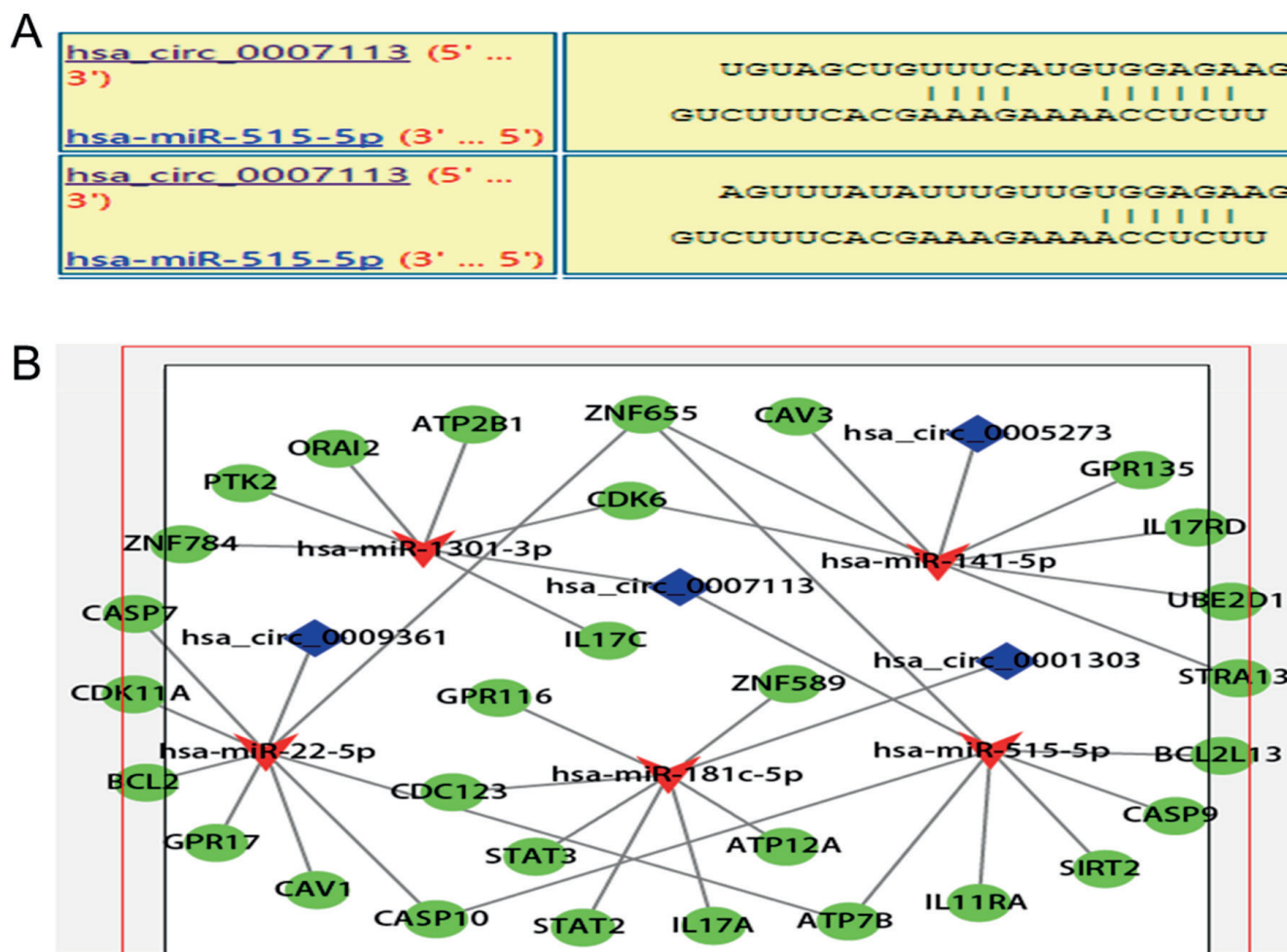


Fig. 6. hsa_circ_0007113 alleviates cellular senescence state via the regulation of hsa_miR-515-5p. **A.** hsa_circ_0007113 has a binding site for miR-515-5p; **B.** The network of selected target genes of hsa-miR-515-5p, hsa_miR-1301-3p, hsa-miR-181c-5p, hsa-miR-22-5p, and hsa-miR141-5p

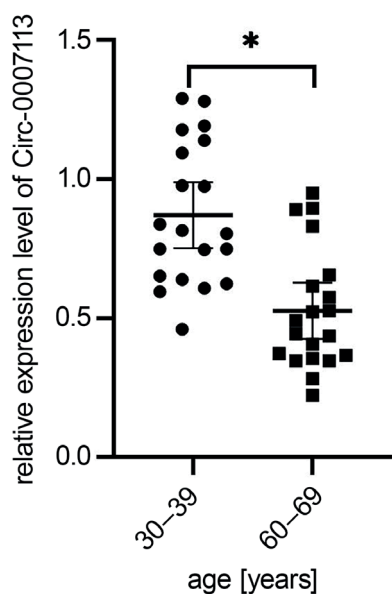


Fig. 7. Comparison of whole blood hsa_circ_0007113 levels in healthy individuals of 30–39 compared to 60–69 years. The hsa_circ_0007113 levels were determined using real-time qualitative polymerase chain reaction (qPCR). The data were expressed as mean with 95% confidence interval (95% CI) (40 distinct repetitions, t-test, p = 0.036, df = 38, *denotes p < 0.05)

processes. Most circRNAs related to aging showed a trend towards increased expression, and we speculate that this may be due to the tendency of circRNA to accumulate in aging tissues, which in turn leads to their upregulation. In the microarray results, the most upregulated and down-regulated circRNA were hsa_circ_0052318 (fold = 5.78) and hsa_circ_00052730 (fold = -5.48), respectively. However, the differential expression of circRNA detected was not as obvious as it is in cancer. This may be because cancer is a pathological process and is affected by drug stimulation, while aging is an overall slower, chronic and progressive physiological process. As this study revealed differentially expressed circRNA in human embryonic lung fibroblasts, our results may offer a new avenue for studying the molecular mechanism underlying senescence, and novel opportunities for senescence medication through the modulation of circRNAs.

Among the differentially expressed circRNA, circRNA_0007113, a downregulated circRNA, was selected, and the pathological phenotype associated with cellular senescence was investigated. The parent gene of circRNA_0007113 is ubiquitin ligase E3 (HERC4). hsa_circ_0007113 was obtained from exons 19 to 23 of the HERC4 gene. E3 ubiquitin

ligase, a novel protein only discovered in recent years, plays a vital role in the ubiquitin-protease system due to its substrate recognition specificity and is also inextricably linked to cellular aging.³² Currently, there are limited data on its related functions, such as participating in lung, cervical, breast and liver cancer, and participating in the incidence and development of other tumors as well,³³ but its role in the aging process has not been reported. To begin preliminary investigations on the potential effect of circRNA_0007113 in cellular senescence, loss-of-function experiments were conducted using siRNA silencing. The results demonstrated that reducing circRNA_0007113 expression significantly increased the p53 and p21 protein expression levels, which are well known to trigger cell senescence.³⁴ These results were also confirmed with β -gal staining.³⁵ The role of circRNA_0007113 in cellular senescence has not been reported yet, and no other studies are available for comparison. Still, circRNAs have been shown to be involved in all cellular processes, including senescence.^{23–26} The present study also suggests that hsa_circRNA_0007113 is involved in total body senescence, as hsa_circRNA_0007113 levels were lower in older individuals than in younger participants. Therefore, additional studies are necessary to confirm and refine the potential mechanisms.

Competing endogenous RNAs analyses showed that circRNAs modulate miRNA target gene expression. Therefore, a bioinformatics analysis was performed, which suggested that hsa_circ_0007113 has a binding site for miR-515-5p. The miR-515-5p was also reported to be involved in the p53/p21 pathway,^{36,37} supporting the association of hsa_circ_0007113 with cell senescence. Indeed, the levels of p53 and p21 were increased in senescent cells, and studies showed that p53 expression is necessary for the maintenance of senescence.^{38–42} However, it is noteworthy that decreasing p53 and p21 expression in senescent cells leads to the restoration of the cell cycle and immortalization.^{38–42} Therefore, silencing hsa_circ_0007113 would increase miR-515-5p levels, leading to higher levels of p53 and p21, supporting the hypothesis that a reduction in hsa_circ_0007113 is a hallmark of cellular senescence. Notably, KEGG pathway analysis showed p53 signaling to be enriched under these circumstances. Thus, hsa_circ_0007113 could bind miR-515-5p, modulating the p53/p21 pathway and regulating cell senescence. However, hsa_circ_0007113 is only 1 of many factors that regulate cellular senescence. In this study, the new function of one circRNA derived from the *HERC4* gene was elaborated, the function was verified in human lung fibroblasts, and its relationship with aging was confirmed.

Limitations

The specific molecular mechanism requires further clarification. For example, over-expression of hsa_circ_0007113 both in vitro and in vivo would also show the function.

Conclusions

This study showed that altered circRNA expression patterns are present in cellular senescence, which may play important roles in senescence-related physiological processes. These findings offer a fresh approach to understanding the molecular mechanism underlying senescence, as well as a new way to potentially cure senescence by altering circRNAs. Additional investigations are necessary to recognize circRNA roles in cellular senescence.

ORCID iDs

Hualing Li  <https://orcid.org/0000-0002-4668-8977>
 Zhiyi Zhen  <https://orcid.org/0009-0003-9429-1186>
 Junjie Wei  <https://orcid.org/0009-0005-9549-2726>
 Xianxian Fan  <https://orcid.org/0009-0005-7487-3351>
 Pengfei Cao  <https://orcid.org/0009-0007-7818-4646>
 Yitang Zhang  <https://orcid.org/0009-0005-6203-1501>
 Yali Chen  <https://orcid.org/0009-0006-5290-0512>
 Yue Li  <https://orcid.org/0009-0001-9396-9464>
 Yifan Zhu  <https://orcid.org/0009-0005-1485-3738>
 Rui Wang  <https://orcid.org/0009-0001-4023-9230>
 Xingjie Ma  <https://orcid.org/0000-0003-3528-5854>

References

- Chinta SJ, Lieu CA, Demaria M, Laberge RM, Campisi J, Andersen JK. Environmental stress, ageing and glial cell senescence: A novel mechanistic link to Parkinson's disease? *J Intern Med*. 2013;273(5):429–436. doi:10.1111/joim.12029
- Campisi J, Robert L. Cell senescence: Role in aging and age-related diseases. *Interdiscip Top Gerontol Geriatr*. 2014;39:45–61. doi:10.1159/000358899
- Childs BG, Durik M, Baker DJ, van Deursen JM. Cellular senescence in aging and age-related disease: From mechanisms to therapy. *Nat Med*. 2015;21(12):1424–1435. doi:10.1038/nm.4000
- Galbiati A, Beauséjour C, d'Adda di Fagagna F. A novel single-cell method provides direct evidence of persistent DNA damage in senescent cells and aged mammalian tissues. *Aging Cell*. 2017;16(2):422–427. doi:10.1111/ace1.12573
- Victorelli S, Passos JF. Telomeres and cell senescence: Size matters not. *EBioMedicine*. 2017;21:14–20. doi:10.1016/j.ebiom.2017.03.027
- Childs BG, Baker DJ, Kirkland JL, Campisi J, van Deursen JM. Senescence and apoptosis: Dueling or complementary cell fates? *EMBO Rep*. 2014;15(11):1139–1153. doi:10.15252/embr.201439245
- Ben-Porath I, Weinberg RA. The signals and pathways activating cellular senescence. *Int J Biochem Cell Biol*. 2005;37(5):961–976. doi:10.1016/j.biocel.2004.10.013
- Hombach S, Kretz M. Non-coding RNAs: Classification, biology and functioning. *Adv Exp Med Biol*. 2016;937:3–17. doi:10.1007/978-3-319-42059-2_1
- Abdelmohsen K, Gorospe M. Noncoding RNA control of cellular senescence. *Wiley Interdiscip Rev RNA*. 2015;6(6):615–629. doi:10.1002/wrna.1297
- Munk R, Panda AC, Grammatikakis I, Gorospe M, Abdelmohsen K. Senescence-associated microRNAs. *Int Rev Cell Mol Biol*. 2017;334:177–205. doi:10.1016/bs.ircmb.2017.03.008
- Maoz R, Garfinkel BP, Soreq H. Alzheimer's disease and ncRNAs. *Adv Exp Med Biol*. 2017;978:337–361. doi:10.1007/978-3-319-53889-1_18
- Memczak S, Jens M, Elefsinioti A, et al. Circular RNAs are a large class of animal RNAs with regulatory potency. *Nature*. 2013;495(7441):333–338. doi:10.1038/nature11928
- Chen S, Huang V, Xu X, et al. Widespread and functional RNA circularization in localized prostate cancer. *Cell*. 2019;176(4):831–843. doi:10.1016/j.cell.2019.01.025
- Chen LL. The biogenesis and emerging roles of circular RNAs. *Nat Rev Mol Cell Biol*. 2016;17(4):205–211. doi:10.1038/nrm.2015.32
- Meng X, Li X, Zhang P, Wang J, Zhou Y, Chen M. Circular RNA: An emerging key player in RNA world. *Brief Bioinformatics*. 2016;18(4):547–557. doi:10.1093/bib/bbw045

16. Panda AC, Grammatikakis I, Munk R, Gorospe M, Abdelmohsen K. Emerging roles and context of circular RNAs. *Wiley Interdiscip Rev RNA*. 2017;8(2). doi:10.1002/wrna.1386
17. Meng S, Zhou H, Feng Z, et al. CircRNA: Functions and properties of a novel potential biomarker for cancer. *Mol Cancer*. 2017;16(1):94. doi:10.1186/s12943-017-0663-2
18. Su M, Xiao Y, Ma J, et al. Circular RNAs in cancer: Emerging functions in hallmarks, stemness, resistance and roles as potential biomarkers. *Mol Cancer*. 2019;18(1):90. doi:10.1186/s12943-019-1002-6
19. Du WW, Yang W, Chen Y, et al. Foxo3 circular RNA promotes cardiac senescence by modulating multiple factors associated with stress and senescence responses. *Eur Heart J*. 2017;38(18):1402–1412. doi:10.1093/eurheartj/ehw001
20. Li J, Song Y, Wang J, Huang J. Plasma circular RNA panel acts as a novel diagnostic biomarker for colorectal cancer detection. *Am J Transl Res*. 2020;12(11):7395–7403. PMID:33312376. PMCID:PMC7724351.
21. Li S, Hu W, Deng F, et al. Identification of circular RNA hsa_circ_0001599 as a novel biomarker for large-artery atherosclerotic stroke. *DNA Cell Biol*. 2021;40(3):457–468. doi:10.1089/dna.2020.5662
22. Wen G, Zhou T, Gu W. The potential of using blood circular RNA as liquid biopsy biomarker for human diseases. *Protein Cell*. 2021;12(12):911–946. doi:10.1007/s13238-020-00799-3
23. Cai H, Li Y, Niringiyumukiza JD, Su P, Xiang W. Circular RNA involvement in aging: An emerging player with great potential. *Mech Ageing Dev*. 2019;178:16–24. doi:10.1016/j.mad.2018.11.002
24. Panda AC, Grammatikakis I, Kim KM, et al. Identification of senescence-associated circular RNAs (SAC-RNAs) reveals senescence suppressor CircPVT1. *Nucleic Acids Res*. 2017;45(7):4021–4035. doi:10.1093/nar/gkw1201
25. Yu AQ, Wang ZX, Wu W, Chen KY, Yan SR, Mao ZB. Circular RNA CircCCNB1 sponges micro RNA-449a to inhibit cellular senescence by targeting CCNE2. *Ageing (Albany NY)*. 2019;11(22):10220–10241. doi:10.18632/ageing.102449
26. Si C, Wang J, Ma W, et al. Circular RNA expression profile in human fibroblast premature senescence after repeated ultraviolet B irradiations revealed by microarray. *J Cell Physiol*. 2019;234(10):18156–18168. doi:10.1002/jcp.28449
27. Ashburner M, Ball CA, Blake JA, et al. Gene Ontology: Tool for the unification of biology. *Nat Genet*. 2000;25(1):25–29. doi:10.1038/75556
28. Kanehisa M, Goto S. KEGG: Kyoto Encyclopedia of Genes and Genomes. *Nucleic Acids Res*. 2000;28(1):27–30. doi:10.1093/nar/28.1.27
29. McCulloch K, Litherland GJ, Rai TS. Cellular senescence in osteoarthritis pathology. *Ageing Cell*. 2017;16(2):210–218. doi:10.1111/accel.12562
30. Chinta SJ, Woods G, Demaria M, et al. Cellular senescence is induced by the environmental neurotoxin paraquat and contributes to neuropathology linked to Parkinson's disease. *Cell Rep*. 2018;22(4):930–940. doi:10.1016/j.celrep.2017.12.092
31. Aravinthan A. Cellular senescence: A hitchhiker's guide. *Hum Cell*. 2015;28(2):51–64. doi:10.1007/s13577-015-0110-x
32. George AJ, Hoffiz YC, Charles AJ, Zhu Y, Mabb AM. A comprehensive atlas of E3 ubiquitin ligase mutations in neurological disorders. *Front Genet*. 2018;9:29. doi:10.3389/fgene.2018.00029
33. Humphreys LM, Smith P, Chen Z, Fouad S, D'Angiolella V. The role of E3 ubiquitin ligases in the development and progression of glioblastoma. *Cell Death Differ*. 2021;28(2):522–537. doi:10.1038/s41418-020-00696-6
34. Mijit M, Caracciolo V, Melillo A, Amicarelli F, Giordano A. Role of p53 in the regulation of cellular senescence. *Biomolecules*. 2020;10(3):420. doi:10.3390/biom10030420
35. Debacq-Chainiaux F, Erusalimsky JD, Campisi J, Toussaint O. Protocols to detect senescence-associated beta-galactosidase (SA- β gal) activity, a biomarker of senescent cells in culture and in vivo. *Nat Protoc*. 2009;4(12):1798–1806. doi:10.1038/nprot.2009.191
36. Pardo OE, Castellano L, Munro CE, et al. miR-515-5p controls cancer cell migration through MARK4 regulation. *EMBO Rep*. 2016;17(4):570–584. doi:10.15252/embr.201540970
37. Zhang M, Muralimanoharan S, Wortman AC, Mendelson CR. Primate-specific miR-515 family members inhibit key genes in human trophoblast differentiation and are upregulated in preeclampsia. *Proc Natl Acad Sci U S A*. 2016;113(45):E7069–E7076. doi:10.1073/pnas.1607849113
38. Assmus B, Urbich C, Aicher A, et al. HMG-CoA reductase inhibitors reduce senescence and increase proliferation of endothelial progenitor cells via regulation of cell cycle regulatory genes. *Circ Res*. 2003;92(9):1049–1055. doi:10.1161/01.RES.0000070067.64040.7C
39. Beausejour CM, Krtolica A, Galimi F, et al. Reversal of human cellular senescence: Roles of the p53 and p16 pathways. *EMBO J*. 2003;22(16):4212–4222. doi:10.1093/emboj/cdg417
40. Demidenko ZN, Korotchkina LG, Gudkov AV, Blagosklonny MV. Paradoxical suppression of cellular senescence by p53. *Proc Natl Acad Sci U S A*. 2010;107(21):9660–9664. doi:10.1073/pnas.1002298107
41. Kumar M, Lu Z, Takwi AAL, et al. Negative regulation of the tumor suppressor p53 gene by microRNAs. *Oncogene*. 2011;30(7):843–853. doi:10.1038/onc.2010.457
42. Rufini A, Tucci P, Celardo I, Melino G. Senescence and aging: The critical roles of p53. *Oncogene*. 2013;32(43):5129–5143. doi:10.1038/onc.2012.640

Sinapine thiocyanate alleviates intervertebral disc degeneration by not regulating JAK1/STAT3/NLRP3 signal pathway

Pengfei Yu^{A,B,D,F}, Zhijia Ma^{A,B,F}, Hong Jiang^{B,C,F}, Jintao Liu^{A,D–F}, Hongwei Li^{C–F}

Department of Orthopedic Surgery, Suzhou Hospital of Traditional Chinese Medicine, Jiangsu, China

A – research concept and design; B – collection and/or assembly of data; C – data analysis and interpretation; D – writing the article; E – critical revision of the article; F – final approval of the article

Advances in Clinical and Experimental Medicine, ISSN 1899–5276 (print), ISSN 2451–2680 (online)

Adv Clin Exp Med. 2024;33(9):965–977

Address for correspondence

Hongwei Li
E-mail: hongwei_li151@126.com

Funding sources

This work was supported by Suzhou Gusu Health Talent Plan talent research project (grant No. GSWS2021049), Traditional Chinese Medicine (TCM) technology development plan of Jiangsu Province (grant No. QN202222) and Science and Technology Development Program of Suzhou (grants No. SKY2023066, No. SKYD2022139 and No. SKYXD2022051).

Conflict of interest

None declared

Received on November 8, 2022

Reviewed on February 1, 2023

Accepted on October 25, 2023

Published online on February 13, 2024

Cite as

Pengfei Y, Zhijia M, Hong J, Jintao L, Li H. Sinapine thiocyanate alleviates intervertebral disc degeneration not by regulating JAK1/STAT3/NLRP3 signal pathway. *Adv Clin Exp Med.* 2024;33(9):965–977. doi:10.17219/acem/174508

DOI

10.17219/acem/174508

Copyright

Copyright by Author(s)

This is an article distributed under the terms of the Creative Commons Attribution 3.0 Unported (CC BY 3.0) (<https://creativecommons.org/licenses/by/3.0/>)

Abstract

Background. Intervertebral disc degeneration (IDD) is a major cause of low back pain. Sinapine thiocyanate (ST) has been reported to have a wide range of biological activities. However, the treatment of IDD with ST has not been studied.

Objectives. To explore the role and mechanism of ST treatment in IDD.

Materials and methods. Nucleus pulposus cells (NPCs) were induced using lipopolysaccharide (LPS), which was used as an in vitro model of IDD. Cell activity, oxidative stress-related indicators and protein expression were detected using MTT (3-(4,5-dimethylthiazol-2-yl)-2,5-diphenyltetrazolium bromide) assay, enzyme-linked immunosorbent assay (ELISA) and western blot. Pyroptosis was evaluated with propidium iodide (PI)/Hoechst double staining and immunofluorescence for NOD-like receptor protein 3 (NLRP3), and pyroptosis-related proteins and inflammatory factors were measured with western blot and ELISA. The pathological changes of IDD were assessed with hematoxylin & eosin (H&E) and safranin-O staining.

Results. Our results showed that ST alleviated LPS-induced degeneration of NPCs, as evidenced by reducing reactive oxygen species (ROS), malondialdehyde (MDA), matrix metalloproteinase-13 (MMP-13), a disintegrin and metalloproteinase with thrombospondin motifs-5 (ADAMTS-5), and increasing collagen II and aggrecan expression. Moreover, ST repressed LPS-induced pyroptosis by inhibiting NLRP3, caspase-1 p20, interleukin (IL)-1 β and IL-18. Further studies showed that ST did not restrain the activation of the JAK1/STAT3 signaling pathway induced by colivelin, or of the enhanced pyroptosis induced by polyphyllin VI. Sinapine thiocyanate alleviated IDD in vivo and suppressed NLRP3-mediated pyroptosis and the JAK1/STAT3 signaling pathway.

Conclusions. Sinapine thiocyanate could alleviate IDD, although this did not include a reduction in NLRP3-mediated pyroptosis and inactivation of the JAK1/STAT3 signaling pathway, thus potentially being a candidate drug for IDD treatment.

Key words: intervertebral disc degeneration, pyroptosis, sinapine thiocyanate, JAK1/STAT3 signaling pathway

Background

Low back pain (LBP) is the main cause of adult disability and labor loss.¹ Intervertebral disc degeneration (IDD) is a common cause of LBP, which causes a huge mental and economic burden to patients and society.² During IDD, the degenerative nucleus pulposus breaks through the fibrous ring and compresses the nerve root, which leads to LBP and affects both work and private life.³ At present, the treatment methods for LBP caused by IDD are relatively limited, mainly including conservative treatment (such as bed rest, traction, physiotherapy, and anti-inflammatory analgesia) and surgical treatments (such as open nucleus pulposus extraction, vertebral fusion, and endoscopic nucleus pulposus extraction). Generally, after 3 months of conservative treatment, if the treatment for patients with IDD is ineffective, surgical treatment is recommended.⁴ Unfortunately, the 2 treatment methods are mainly symptomatic treatment for pain relief, which cannot delay or reverse the pathological process of IDD.^{5,6} The biological mechanism of IDD is complicated, involving mechanical and oxidative stress, DNA damage, inflammatory responses, abnormal signal pathway activation, and abnormal expression of miRNA.^{7–9} Currently, the pathological changes of IDD are mainly characterized by the decrease of nucleus pulposus cells (NPCs) and extracellular matrix (ECM).^{10,11} Hence, exploring the pathological mechanism of NPC death under different stress states is conducive to finding new targets and drugs for the treatment of IDD.

Oxidative inflammatory responses are one of the main causes of abnormal cell function in multiple diseases.^{12–15} So far, researchers found that reactive oxygen species (ROS) were increased in degenerative nucleus pulposus (NP) tissue.¹⁶ Abnormally elevated ROS could downregulate the expression of COL2A1 in human and rat NPCs.¹⁷ Pro-inflammatory cytokines could also repress the synthesis of ECM protein deposition in human and rat NPCs by increasing the expression of matrix-degrading enzymes, namely matrix metalloproteinase (MMP)-3 and MMP-13.¹⁸ Pyroptosis is a form of cell death,¹⁹ the predominant feature of which depends on the activation of caspase-1 mediated by the NLRP3 inflammasome, and which is accompanied by the increase of active inflammatory factors interleukin (IL)-1 β and IL-18.^{20,21} Studies have shown that IDD was accompanied by pyroptosis of NPCs, which mainly presented as the upregulation of NLRP3 and caspase-1 expression.²² Therefore, inhibiting the activation of ROS and NLRP3 is of great significance in delaying the progression of IDD.

The JAK/STAT signaling pathway is involved in many important biological processes, such as immune regulation, inflammatory responses and apoptosis.²³ In pathological conditions, JAK phosphorylation is activated and combined with phosphorylated STAT, which affects the transcription of a series of cytokines and participates in the regulation of the inflammatory response and

oxidative stress.²⁴ Interleukin 21 could stimulate the up-regulation of ADAMTS-7 and MMP-13 by enhancing STAT3 in NPCs.²⁵

Sinapine thiocyanate (ST), whose molecular formula is C₁₇H₂₄N₂O₅S, is the main active component of sinapine in semen raphanin.²⁶ Sinapine thiocyanate has a variety of biological activities, including anti-oxidant, anti-inflammatory, anti-radiation, anti-aging, anti-hypertensive, and anti-androgen activity, while also inhibiting angiogenesis.^{27–30} It is reported that ST could also reduce cholesterol and low-density lipoprotein (LDL), significantly improve hypertension symptoms, prevent thrombosis, and attenuate thrombosis caused by inflammatory injury of vascular endothelial cells (VECs).³¹ Sinapine thiocyanate improved vascular endothelial injury in hypertensive rats by inhibiting the activation of NLRP3 and the expression of related inflammatory factors (IL-1 β and IL-18), and also alleviated human umbilical vein endothelial cells (HUVEC) injury induced by the administration of angiotensin II.³² Moreover, ST could inhibit the proliferation and migration of pancreatic cancer cells by upregulating GADD45A.³³ However, the effects and mechanisms of ST in IDD are still unclear. In addition, as a strong inflammatory stimulating factor, lipopolysaccharide (LPS) could lead to gene upregulation and the secretion of diverse pro-inflammatory cytokines and matrix-degrading enzymes, including disintegrin and metalloproteinase with thrombospondin motifs-5 (ADAMTS-5) and MMPs in NP cells, thereby causing a decrease in proteoglycan content and IDD.^{34,35} The current study aimed to explore whether ST could affect ECM degradation and oxidative stress in IDD by regulating NLRP3-mediated pyroptosis via the JAK1/STAT3 signaling pathway. Our study provides new ideas for the research and development of novel methods for IDD treatment.

Objectives

Our study aimed to explore whether ST could alleviate IDD *in vitro* and *in vivo*.

Materials and methods

Isolated and culture of NPCs

Nucleus pulposus cells were extracted according to a previous study.³⁶ Rats (6–8 weeks, 260–280 g) were euthanized by intraperitoneal injection of sodium pentobarbital (120 mg/kg), sterilized with alcohol, and then the intervertebral disc (L2–L6) tissue was obtained under sterile conditions. After washing, the outer layer of the intervertebral disc annulus fibrosus was cut, and then the nucleus pulposus tissues were stripped and placed in a sterile Petri dish. Nucleus pulposus tissues were disaggregated into

small pieces (~1 mm³), transferred to a 15 mL centrifuge tube, and digested for 20 min with 0.25% trypsin ethylenediaminetetraacetic acid (EDTA) at 30°C. The digestion was terminated using Dulbecco's modified Eagle's medium (DMEM)/F12 medium (Gibco, Waltham, USA) containing 10% fetal bovine serum (FBS; Invitrogen, Waltham, USA). The precipitates were collected by centrifugation (1,000 rpm, 5 min), and treated with 0.2% type II collagenase for 2 h; then, the cells were collected and resuspended in DMEM/F12 medium containing 10% FBS. Cells were cultured in an incubator at 37°C and 5% CO₂, and used in subsequent experiments at passages 2 and 3.

MTT assay

Nucleus pulposus cells (5×10³ cells per well) were inoculated in 96-well plates and cultured at 37°C and 5% CO₂ for 24 h. Then, MTT solution (Beyotime Biotechnology, Shanghai, China) was added and cells were cultured for 4 h. Then the culture medium was discarded, and 150 µL dimethyl sulfoxide (DMSO) (100%) was added. The absorbance value at 570 nm was detected using a microplate reader (BioTek, Winooski, USA); 3 independent experiments were performed.

DCFH-DA detection

Dichloro-dihydro-fluorescein diacetate (DCFH-DA) assay (Beyotime Biotechnology) was made into a working solution with a final concentration of 10 µM using phosphate-buffered saline (PBS). Nucleus pulposus cells (5×10³) were placed into 96-well plates and underwent the indicated treatment. After 24 h, DCFH-DA staining solution was added to each well for 20 min. Next, cells were washed 3 times with serum-free medium, and then the distribution of ROS in cells was observed under fluorescence microscopy (model IX71; Olympus Corp., Tokyo, Japan). Then, the excitation/emission wavelength of 488/525 nm was examined using a microplate reader (Gen5; BioTek, Winooski, USA). At least 3 images were taken per treatment, and relative ROS levels were analyzed by normalizing to the control group. The investigator was blinded to the experimental conditions when taking the images, and 3 independent experiments were performed.

Enzyme-linked immunosorbent assay

Nucleus pulposus cells (4×10⁵ cells per well) were inoculated in 6-well plates containing slides. After 24 h culture, the supernatant was collected by centrifugation (2000 rpm, 20 min), and the expression of IL-1β, IL-18, malondialdehyde (MDA), and superoxide dismutase (SOD) were detected using enzyme-linked immunosorbent assay (ELISA) kit according to the manufacturer's instructions (Nanjing Jiancheng Bioengineering Institute, Nanjing, China). Three independent experiments were performed.

Western blot

Nucleus pulposus cells (4×10⁵ cells per well) were inoculated in 6-well plates and cultured at 37°C and 5% CO₂. After 24 h, 200 µL radioimmunoprecipitation assay buffer (RIPA) lysate was added to each well, and cells were lysed on ice for 30 min. The supernatant was collected by centrifugation (12,000 rpm, 5 min, 4°C), and the protein content was detected using a bicinchoninic acid (BCA) assay. For each group, 30 µg of protein samples was subjected to 10% sodium dodecyl sulfate–polyacrylamide gel electrophoresis (SDS-PAGE), and then electrically transferred to a polyvinylidene difluoride (PVDF) membrane. The membranes were blocked for 1 h with 5% skimmed milk powder solution prepared in Tris-buffered saline + 0.1% Tween-20 (TBST), and then incubated overnight in diluted primary antibody (collagen II (ab34712, 1:1000; Abcam, Cambridge, UK), aggrecan (ab3778, 1:1000; Abcam), MMP-13 (ab39012, 1:1000; Abcam), ADAMTS-5 (ab231595, 1:1000; Abcam), NLRP3 (ab263899, 1:1000; Abcam), ASC (ab151700, 1:1000; Abcam), caspase-1 (ab138483, 1:1000; Abcam), caspase-1 p20 (sc-398715, 1:1000; Santa Cruz Biotechnology, Santa Cruz, USA), JAK1 (ab133666, 1:1000; Abcam), p-JAK1 (ab138005, 1:1000; Abcam), STAT3 (ab68153, 1:1000; Abcam), p-STAT3 (ab109085, 1:1000; Abcam), and GAPDH (ab8245, 1:2000; Abcam)) at 4°C. After washing, the membranes were incubated for 1 h with the diluted second antibody (Goat Anti-Rabbit IgG H&L (1:5000, ab96899; Abcam) or Goat Anti-Mouse IgG H&L (1:5000, ab96879; Abcam)), and then the protein was visualized using an electrochemiluminescence reagent (ECL; Beyotime Biotechnology) in a gel imaging system (Bio-Rad, Hercules, USA). Three independent experiments were performed.

Propidium iodide/Hoechst 33342 double staining

Nucleus pulposus cells (2×10⁴ cells per well) were inoculated in 24-well plates containing slides. After incubating for 24 h, the NPCs were administered Hoechst 33342 and propidium iodide (PI), and stained for 30 min at 4°C. After washing, the cells were observed under a fluorescence microscope (Olympus Corp.). At least 3 images were taken per treatment. The investigator was blinded to the experimental conditions when taking the images. Three independent experiments were performed.

Immunofluorescence

Nucleus pulposus cells (2×10⁴ cells per well) were inoculated in 24-well plates containing slides and cultured at 37°C and 5% CO₂ for 24 h. Next, cells were fixed in 4% paraformaldehyde for 15 min, treated with 0.5% TritonX-100 for 20 min, and then blocked with goat serum for 30 min. The cells were incubated overnight in a wet

box with anti-NLRP3 (ab4207, 1:200; Abcam) at 4°C, and then incubated for 1 h with Alexa 488-conjugated antibody (ab150129, 1:200; Abcam) at room temperature. The nuclei were counterstained for 5 min with DAPI (4',6-diamidino-2-phenylindole) reagent (cat. No. H-1200-10; Vector Laboratories, Burlingame, USA), samples were mounted using an anti-fluorescence quenching agent, and then images were collected using a fluorescent microscope (Olympus Corp.). At least 3 images were taken per treatment. The investigator was blinded to the experimental conditions when taking the images. Three independent experiments were performed.

Intervertebral disc degeneration rat model

Sprague Dawley (SD) rats (female, $n = 24$) were randomly divided into 4 groups: sham operation group (sham, $n = 6$), intervertebral disc degeneration group (IDD, $n = 6$), intervertebral disc degeneration + 4 mg/kg ST group (IDD + 4 mg/kg ST, $n = 6$), and intervertebral disc degeneration + 8 mg/kg ST group (IDD + 8 mg/kg ST, $n = 6$). The concentrations of ST were used based on previous investigations.³² Rats were anesthetized by intraperitoneal injection of 10% chloral hydrate (3.6 mL/kg), the C5/6 intervertebral disc was marked, and the local skin was disinfected with alcohol. The C5/6 intervertebral discs in the IDD group and ST treatment group were punctured with a 30 G sterile needle from the dorsal side along the horizontal direction of the cone end plate with a penetration depth of 5 mm, and the needle was rotated 360° and retained for 30 s. The sham group was sutured after skin incision only without the needle penetration. Following the operation, 100,000 units of penicillin were injected intraperitoneally for 3 days to prevent infection. After the operation, the ST treatment group was administrated 4 mg/kg and 8 mg/kg per day by gavage, and the sham group and IDD group were given the same amount of normal saline by gavage. The treatment continued for 4 weeks, at which time rats were euthanized by intraperitoneal injection of sodium pentobarbital (120 mg/kg). All animal experiments were approved by the animal ethics committee of the Suzhou Hospital of Traditional Chinese Medicine, affiliated with Nanjing University of Chinese Medicine. Three independent experiments were performed.

Hematoxylin & eosin and safranin-O staining

Nucleus pulposus tissues from rat discs were fixed in 40 g/L paraformaldehyde and then decalcified in 10% EDTA for 15 days. After preparation and dehydration, IDD tissues were embedded in paraffin and cut into 5 µm continuous sections. According to previous studies, we detected IDD by safranin-O staining and hematoxylin & eosin (H&E) staining. The slices were placed in the oven (70°C) for 1 h, soaked in xylene for 30 min, rehydrated with a gradient concentration of absolute ethanol (100%,

95%, 85%, 75%), stained with hematoxylin for 3 min, and then treated with 2% acetic acid for 1 min and ammonia for 1 min. For H&E staining, the sections were treated for 5 s with 95% absolute ethanol and then stained for 2 min with an eosin staining solution. For safranin-O staining, the sections were stained with fast green for 6 min, differentiated with 1% acetic acid for 15 s, and then stained with safranin-O for 6 min. Subsequently, the slices were dehydrated using gradient concentrations of absolute ethanol (75%, 85%, 95%, 100%), treated for 6 min with xylene solution, and then sealed with neutral resin. The results of 6 random fields were observed and photographed in an optical microscope (model IX-71; Olympus Corp.). At least 3 images were taken per treatment. The investigator was blinded to the experimental conditions when taking the images. Three independent experiments were performed.

Statistical analyses

IBM SPSS v. 22.0 software (IBM Corp., Armonk, USA) was used to analyze the experimental data, and data were expressed as mean ± standard deviation ($M \pm SD$) for all data points. Multiple comparisons were performed using non-parametric analysis of variance (ANOVA) (Kruskal–Wallis test) followed by Dunn's post hoc test without any correction. A p -value of <0.05 was considered statistically significant.

Results

Sinapine thiocyanate attenuated LPS-induced decrease in the activity of NPCs

First, we evaluated the effect of ST on the activity of NPCs. The chemical structure of ST is shown in Fig. 1A. Sinapine thiocyanate at concentrations of 0, 10, 25, 50, 75, and 100 mg/L was added into NP cells for 24 h, and MTT assay showed that ST (0–75 mg/L) had no toxicity to NPCs, but ST at 100 mg/L significantly weakened their activity to 83.76% (Fig. 1B). In addition, LPS (10 µg/mL) was used to maintain the degenerative status of NP cells. Nucleus pulposus cells were stimulated with 10 µg/mL LPS, 10 µg/mL LPS + 25 mg/L ST, 10 µg/mL LPS + 50 mg/L ST, or 10 µg/mL LPS + 75 mg/L ST for 24 h. The results showed that LPS could reduce the activity of NPCs, which is reversed by ST (75 mg/L) treatment in a concentration-dependent manner (Fig. 1C).

Sinapine thiocyanate restrained LPS-induced degeneration of NPCs

Next, the effect of ST on LPS-induced degeneration of NPCs was explored. Lipopolysaccharide facilitated increased ROS in NPCs, which was inhibited by ST

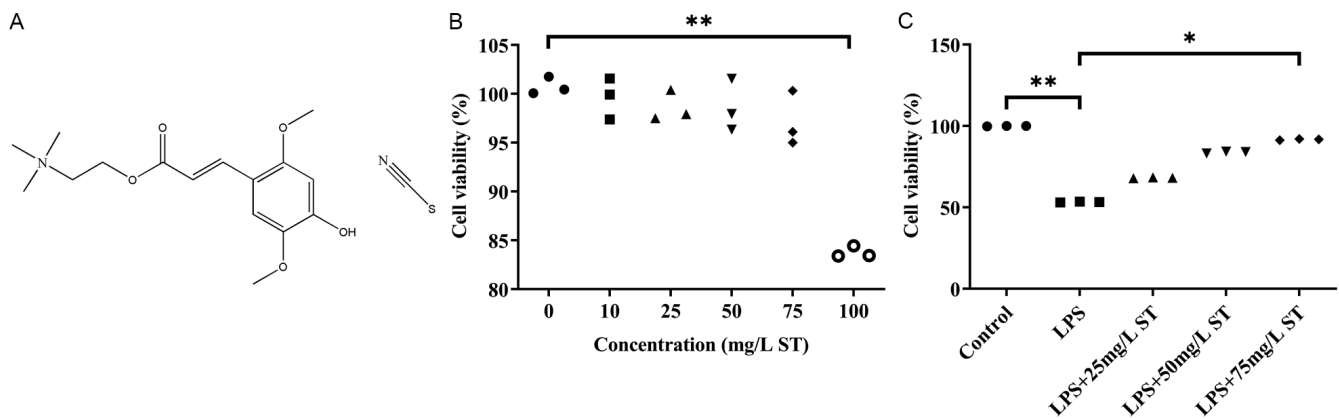


Fig. 1. Effect of sinapine thiocyanate on the activity of nucleus pulposus cells. A. The chemical structural formula of sinapine thiocyanate; B,C. The viability of nucleus pulposus cells was measured using MTT assay

** $p < 0.01$; * $p < 0.05$.

in a concentration-dependent manner (Fig. 2A,B). Oxidative stress-related indexes MDA and SOD were also measured, showing that ST could block the increase of MDA and decrease of SOD induced by LPS in NPCs (Fig. 2C,D). Moreover, LPS significantly reduced the expression of collagen II and aggrecan, and increased the expression of MMP13 and ADAMTS-5. However, ST inhibited the loss of collagen II and aggrecan and repressed the expression of MMP13 and ADAMTS-5 in LPS-induced NPCs (Fig. 2E–I). These results suggested that ST effectively alleviated the degeneration of NPCs induced by LPS.

Sinapine thiocyanate suppressed LPS-induced pyroptosis of NPCs

The death of NPCs is key to IDD,³⁷ and we assessed whether ST could induce NPCs pyroptosis. Hoechst and PI double staining were performed, highlighting that LPS boosted nuclear PI and increased the red fluorescence compared with the control group, while this was attenuated by the addition of ST (Fig. 3A). Moreover, the expression of NLRP3 was detected using immunofluorescence. The results showed that the fluorescence signal of NLRP3 was increased in LPS-treated NPCs, and this could be gradually weakened by the addition of ST (Fig. 3B). Furthermore, pyroptosis-associated proteins were assessed with western blot, which showed that LPS-induced facilitation of NLRP3, ASC and caspase-1 p20 was inhibited by ST (Fig. 4A–D). Expression of IL-1 β and IL-18 downstream of NLRP3 was significantly diminished by ST in LPS-induced NPCs (Fig. 4E,F). In addition, the effect of ST on the JAK1/STAT3 signaling pathway was analyzed. The results showed that ST could decrease the activation of the JAK1/STAT3 signaling pathway induced by LPS in NPCs (Fig. 4G–I). These results indicated that ST restrained NLRP3-mediated pyroptosis and JAK1/STAT3 signaling pathway in LPS-induced NPCs.

Sinapine thiocyanate alleviated NPCs degeneration, but not through JAK1/STAT3/NLRP3 signaling

The role of NLRP3-mediated pyroptosis and JAK1/STAT3 signaling in the protective effect of ST on NPCs were then explored. Polyphyllin VI has been reported to activate pyroptosis by increasing NLRP3.³⁸ Our findings showed that polyphyllin VI enhanced LPS-induced upregulation of NLRP3 (Fig. 5A,B). Moreover, ST reversed the effect of polyphyllin VI on collagen II and aggrecan in LPS-induced NPCs (Fig. 5C,D). In addition, the increase of IL-1 β and IL-18 induced by polyphyllin VI was not significantly attenuated by ST in LPS-induced NPCs (Fig. 5E,F). We used colivelin as an activator of STAT3,³⁹ which further induced ROS production in LPS-treated NPCs, which was not prevented by the addition of ST (Fig. 6A,B). Colivelin significantly increased the ratio of p-STAT3/STAT3, further increased NLRP3, and did not significantly reduce the expression of collagen II and aggrecan in LPS-induced NPCs, which were not significantly restored by ST (Fig. 6C–G). Finally, ST treatment did not significantly block colivelin-induced increases in IL-1 β and IL-18 (Fig. 6H,I). These results suggest that ST may resist LPS-induced degeneration of NPCs, but not by regulating the JAK/STAT3/NLRP3 signaling pathway.

Sinapine thiocyanate repressed IDD in vivo

The improvement of ST on IDD was then verified in vivo. The IDD model was constructed through annulus fibrosus puncture, which caused a reduction of NPCs and the loss of ECM. The results of H&E and safranin-O staining confirmed the successful construction of the model. Compared to the control group, the LPS group showed various degenerative changes, including a reduction in NP size and dense ECM, and the addition of ST effectively

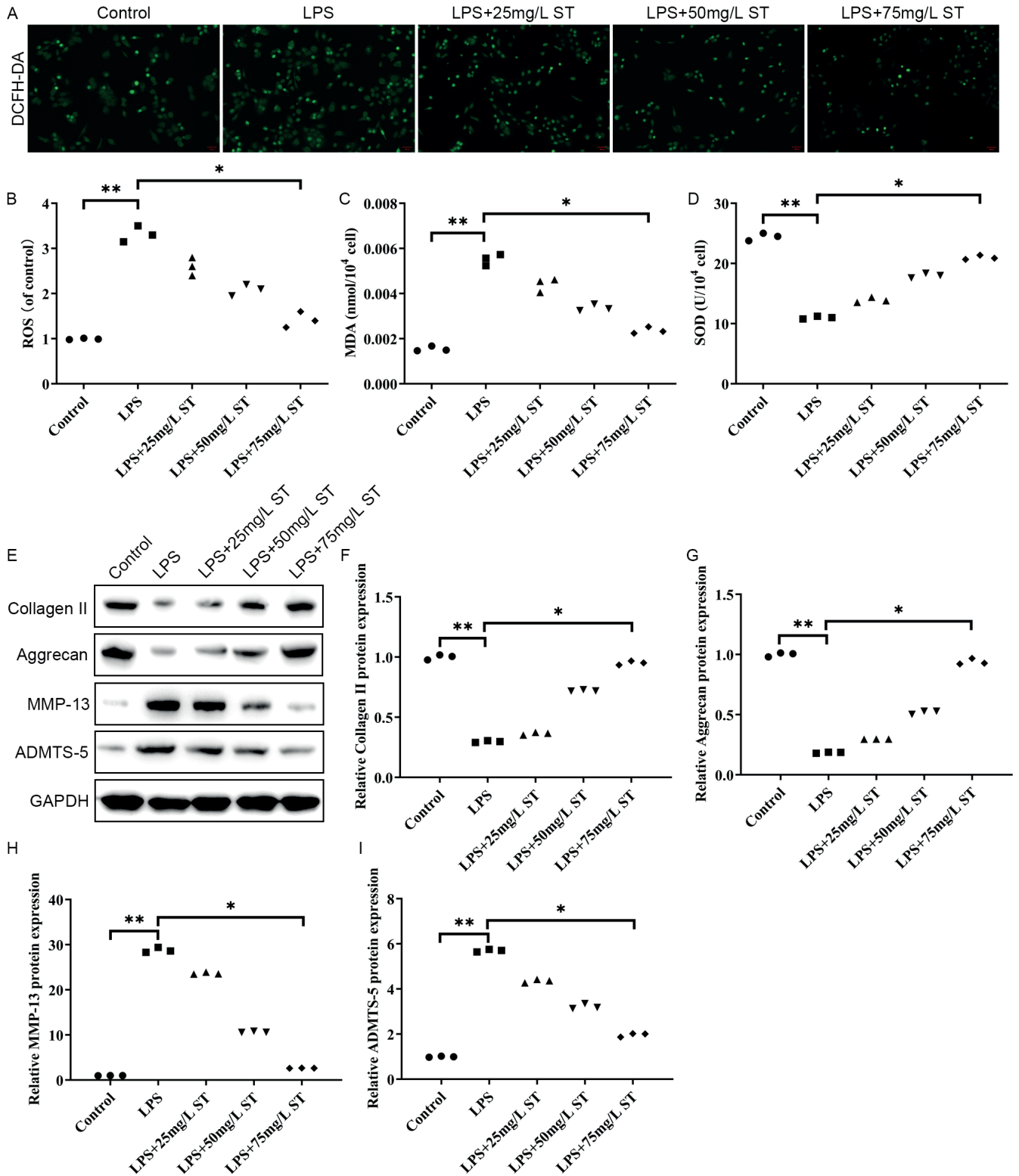


Fig. 2. Effect of sinapine thiocyanate on the degeneration of nucleus pulposus cells. A,B. Reactive oxygen species (ROS) levels were assessed using the dichloro-dihydro-fluorescein diacetate (DCFH-DA) assay method; C,D. The content of malondialdehyde (MDA) and superoxide dismutase (SOD) was evaluated with enzyme-linked immunosorbent assay (ELISA); E-I. The expression of collagen II, aggrecan, matrix metalloproteinase (MMP)-13, and ADMTS-5 was detected with western blot

**p < 0.01; *p < 0.05.

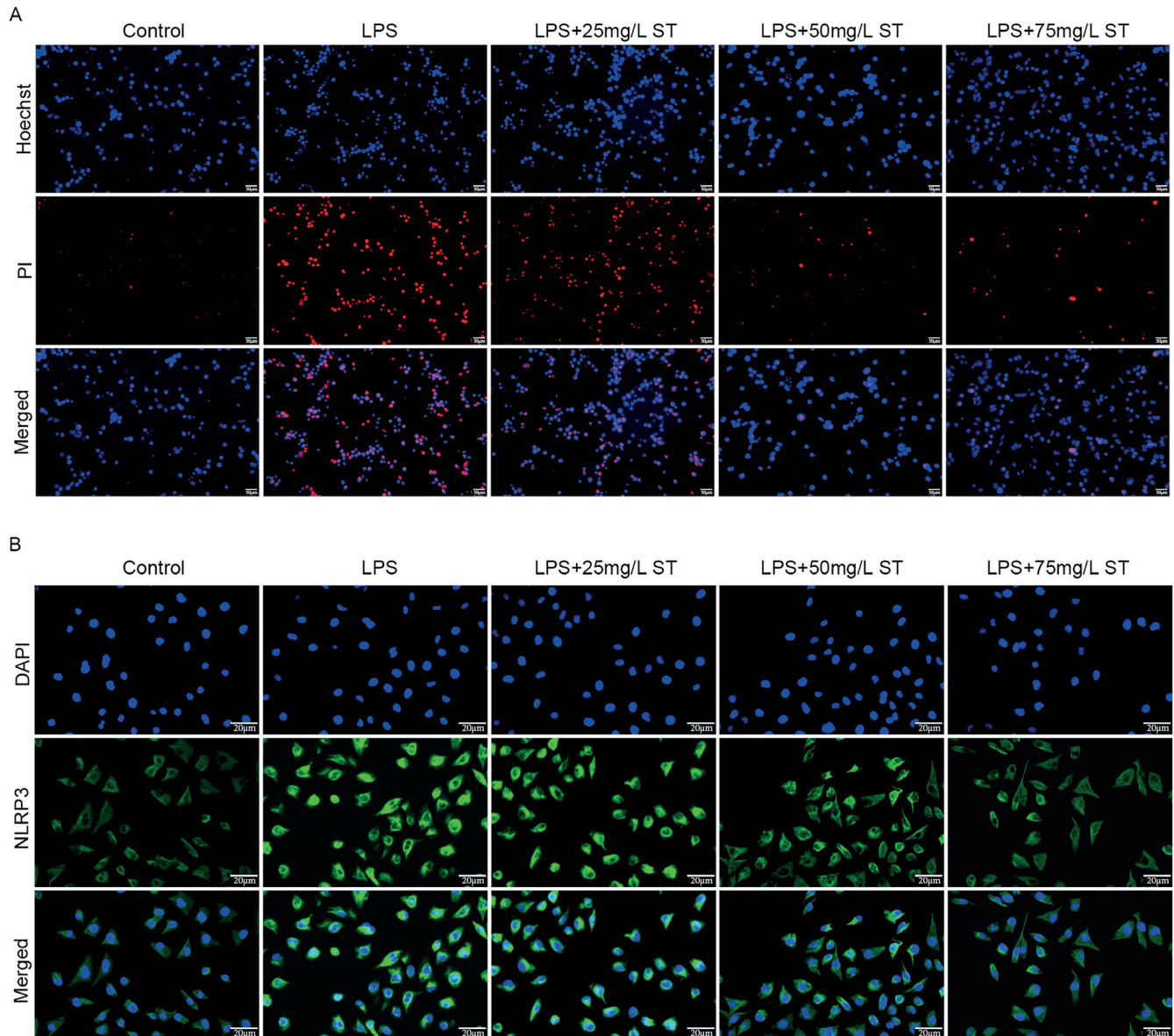


Fig. 3. Effect of sinapine thiocyanate on pyroptosis. A. Cell death of nucleus pulposus cells was measured with propidium iodide/Hoechst double staining; B. NLRP3 expression was assessed with immunofluorescence

alleviated these symptoms in IDD (Fig. 7A, 7B). Moreover, ST significantly inhibited the activation of JAK1/STAT3, reduced the expression of NLRP3, and promoted the expression of collagen II and aggrecan in IDD tissue (Fig. 7C–H). Finally, the high levels of IL-1 β and IL-18 in our IDD model were reduced following treatment with ST (Fig. 7I, J). These results demonstrated that ST-attenuated IDD reduced the activation of JAK1/STAT3 and restrained NLRP3-mediated pyroptosis *in vivo*.

Discussion

In this study, LPS was used to maintain the degenerative status of NPCs *in vitro* because LPS stimulates the decrease of ECM and increase of NLRP3 inflammasome

in NPCs.^{40–42} Our study is the first to report the effect of ST on IDD, and we demonstrated that ST improved the activity of NPCs, reduced ROS and MDA, increased SOD, expedited collagen and aggrecan expression, and reduced MMP-13 and ADAMTS-5 expression in LPS-treated NPCs. These results indicate that ST alleviated the degeneration of NPCs.

Pyroptosis is an “inflammatory death”, which is mainly characterized by the activation of caspase-1 or caspase-11 with the activity of inflammatory factors IL-1 β and IL-18.⁴³ NOD-like receptor protein 3 has also been shown to recruit and activate caspase-1 to induce pyroptosis.⁴³ At present, studies have confirmed that NLRP3 and IL-1 β play key roles in the pathogenesis of IDD.^{44,45} Comparing 45 degenerative intervertebral discs with 7 normal intervertebral discs, Chen et al. found that NLRP3 and

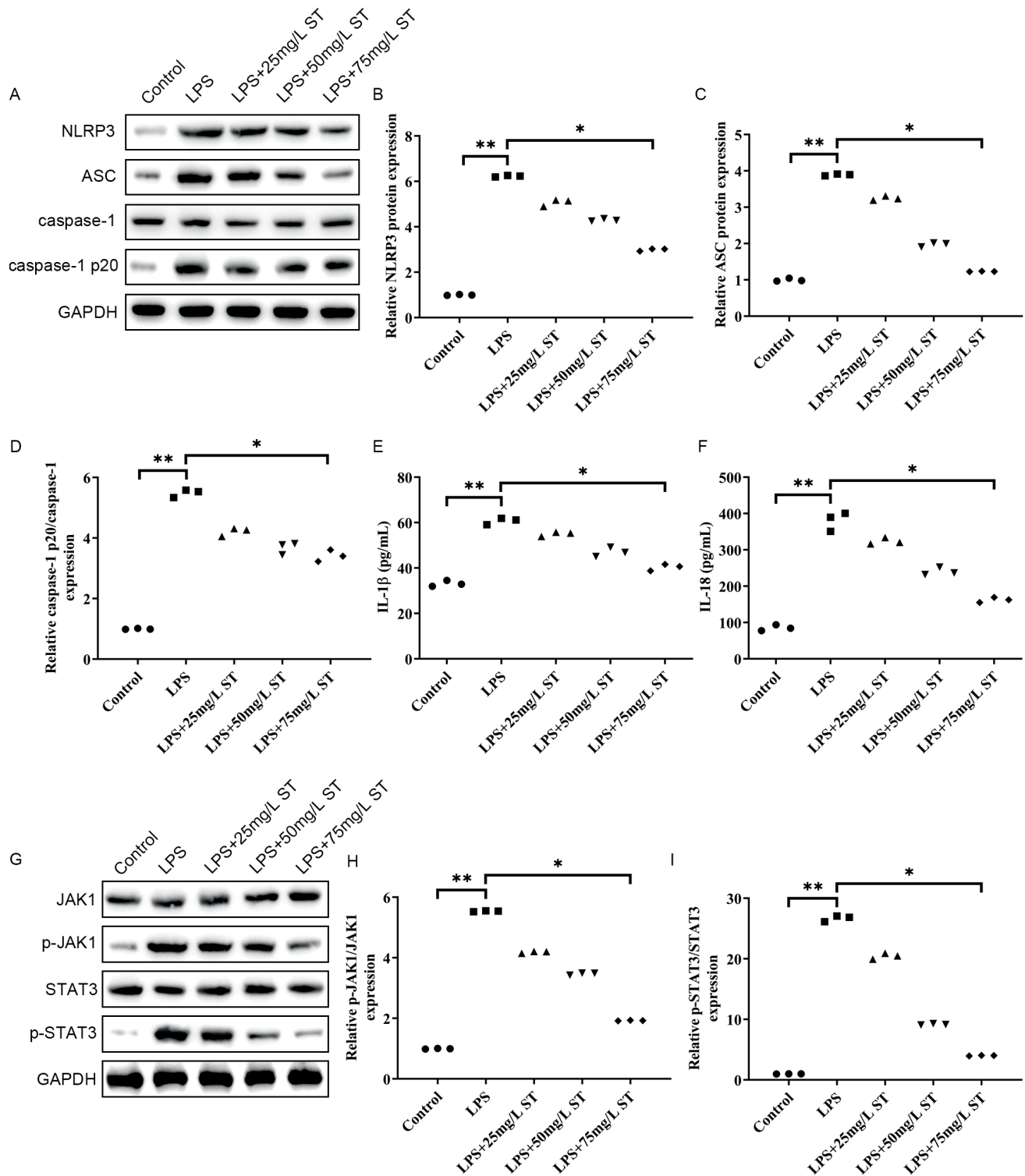


Fig. 4. Sinapine thiocyanate repressed NLRP3-mediated pyroptosis and JAK1/STAT3 signaling pathway. A–D. The expression of NLRP3, ASC, caspase-1, and caspase-1 p20 was detected with western blot; E, F. The content of interleukin (IL)-1 β and IL-18 was evaluated using enzyme-linked immunosorbent assay (ELISA); G–I. The expression of JAK, p-JAK, STAT3, and p-STAT3 was measured with western blot

** $p < 0.01$; * $p < 0.05$.

its downstream targets, caspase-1 and IL-1 β , were significantly upregulated in the degenerative group.⁴⁶ Zhang et al. established a mouse IDD model using the annulus fibrosus puncture method, and compared with the sham operation group, the expression levels of NLRP3, caspase-1,

p20 and gasdermin D (GSDMD) in the IDD model group were significantly increased.⁴⁷ Studies have shown that knocking down NLRP3 or inhibiting caspase-1 expression could weaken the inflammatory response and degeneration of NPCs.⁴⁸ Sinapine thiocyanate has been reported

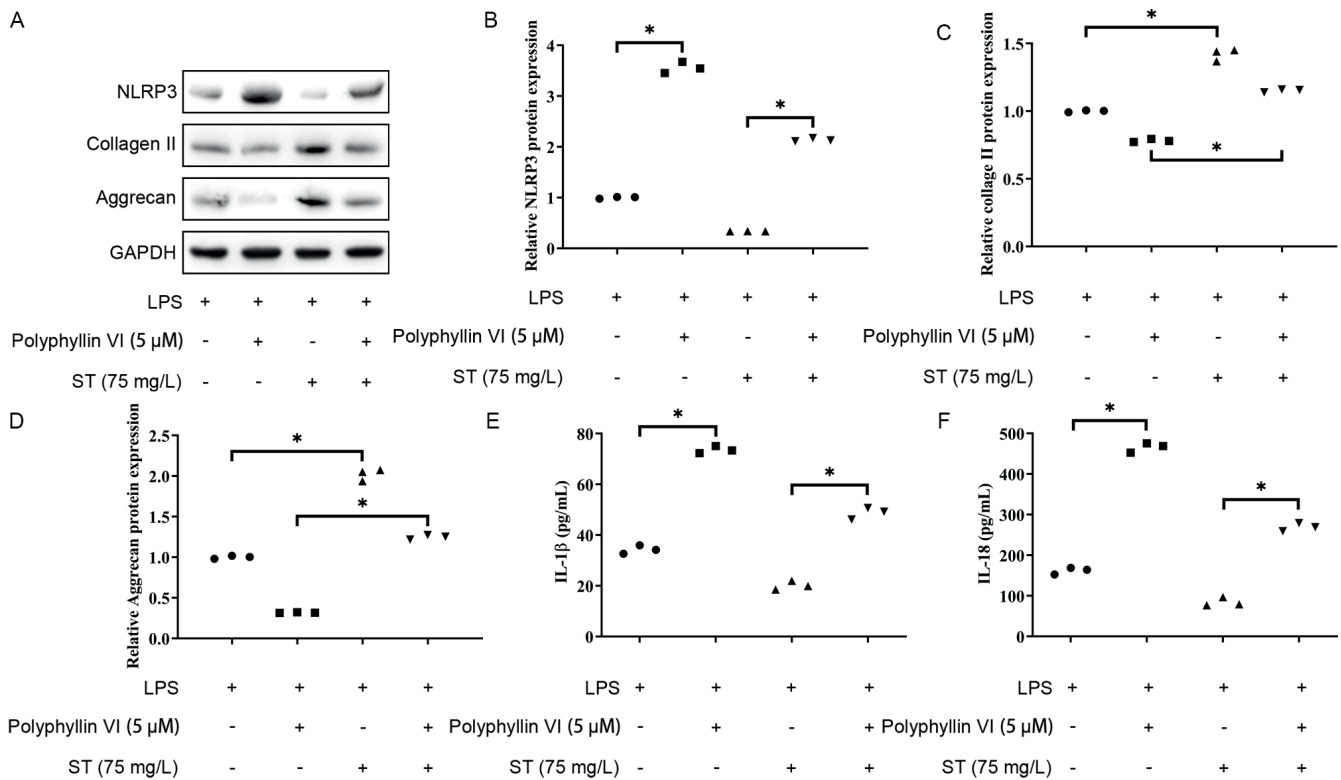


Fig. 5. Sinapine thiocyanate restrained degeneration of nucleus pulposus cells by reducing NLRP3-mediated pyroptosis. A–D. The expression of NLRP3, collagen II and aggrecan was measured with western blot; E, F. The content of interleukin (IL)-1β and IL-18 was evaluated with enzyme-linked immunosorbent assay (ELISA)

*p < 0.05.

to reduce the dysfunction of VECs caused by hypertension by inhibiting NLRP3-mediated pyroptosis.³² Similarly, our study found that ST could reduce pyroptosis of LPS-treated NPCs by inhibiting NLRP3, caspase-1, p20, IL-1β, and IL-18. The activation of pyroptosis was also induced by polyphyllin VI, which was confirmed by the change of NLRP3, IL-1β and IL-18. However, ST treatment did not significantly reverse the activation of pyroptosis induced by polyphyllin VI. These results suggest that ST might protect NPCs, but not by regulating NLRP3-mediated pyroptosis. Moreover, polyphyllin VI might modulate the effect of ST on IDD.

Our study found that ST could also inhibit the activation of the JAK1/STAT3 signaling pathway. JAK/STAT signaling is a common pathway for a variety of cytokines and growth factors to transmit signals into target cells, which mediates a variety of biological reactions, including cell proliferation, differentiation, migration, apoptosis, and inflammation.⁴⁹ The activation of JAK/STAT signaling promotes the occurrence and development of various diseases, including IDD.^{23,50} Resveratrol reversed the degeneration of NPCs by increasing ECM production (collagen II and aggrecan), and repressing the activation of JAK1/STAT3 and the secretion of IL-6.⁵¹ Meanwhile, STAT3 could combine with NLRP3 to promote cell death.⁵² In our study, colivelin, the activator of STAT3, could upregulate ROS and NLRP3-mediated pyroptosis and not significantly enhance the degeneration of NPCs, while the addition of ST did not

significantly restore these effects. In addition, ST could only partially restore NPC function following colivelin treatment. Our rat IDD model was used to further verify the role of ST in IDD. Sinapine thiocyanate effectively alleviated IDD, reduced NLRP3-mediated pyroptosis and restrained the activation of the JAK1/STAT3 signaling pathway.

Limitations

The question whether ST alleviated IDD in vivo by regulating JAK1/STAT3/NLRP3 needs further verification. In addition, ST might regulate pyroptosis in IDD through a variety of signaling pathways, and our study lacked the required exploration. Furthermore, our experimental sample size seriously affects the conclusions we can draw. Increased sample sizes are required to further verify our conclusion.

Conclusions

These findings provide a new perspective on the treatment of IDD. Our data demonstrated that ST suppressed LPS-induced degeneration of NPCs, but not through regulating JAK1/STAT3/NLRP3 signaling. Sinapine thiocyanate may, therefore, become a candidate drug for IDD treatment.

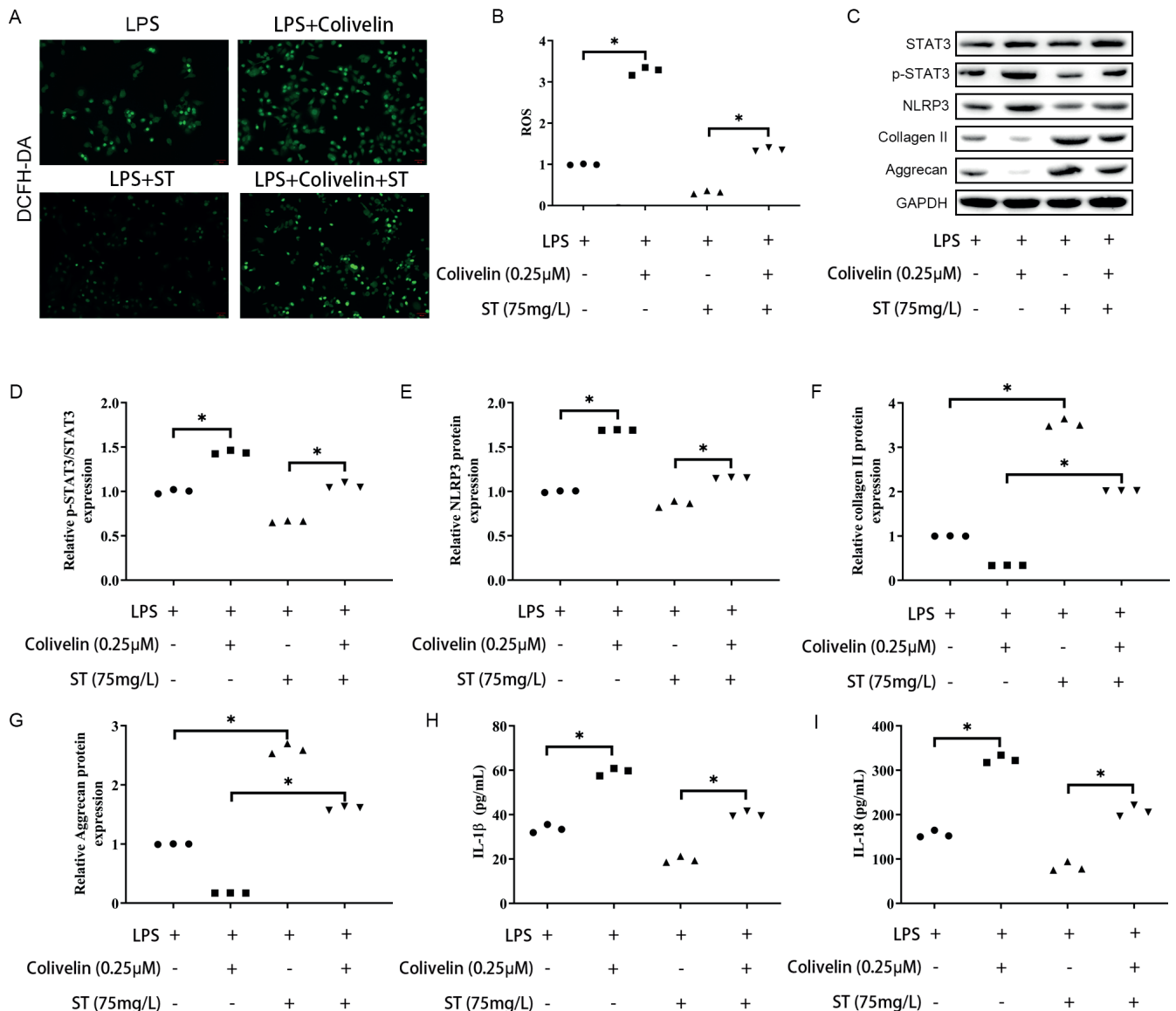


Fig. 6. Sinapine thiocyanate restrained degeneration of nucleus pulposus cells by JAK1/STAT3/NLRP3 signaling pathway. A–B. Reactive oxygen species (ROS) levels were assessed using the dichloro-dihydro-fluorescein diacetate (DCFH-DA) assay method; C–G. The expression of STAT3, p-STAT3, NLRP3, collagen II, and aggrecan was measured with western blot. H–I. The content of interleukin (IL)-1β and IL-18 was evaluated using enzyme-linked immunosorbent assay (ELISA)

* $p < 0.05$.

Supplementary data

The Supplementary materials are available at <https://doi.org/10.5281/zenodo.10222233>. The package includes the following files:

Supplementary Table 1. The analysis results of data from Fig. 1 through non-parametric ANOVA (Kruskal–Wallis test) followed by Dunn’s post hoc test without any correction.

Supplementary Table 2. The analysis results of data from Fig. 2 through non-parametric ANOVA (Kruskal–Wallis test) followed by Dunn’s post hoc test without any correction.

Supplementary Table 3. The analysis results of data from Fig. 3 through non-parametric ANOVA (Kruskal–Wallis test) followed by Dunn’s post hoc test without any correction.

Supplementary Table 4. The analysis results of data from Fig. 4 through non-parametric ANOVA (Kruskal–Wallis test) followed by Dunn’s post hoc test without any correction.

Supplementary Table 5. The analysis results of data from Fig. 5 through non-parametric ANOVA (Kruskal–Wallis test) followed by Dunn’s post hoc test without any correction.

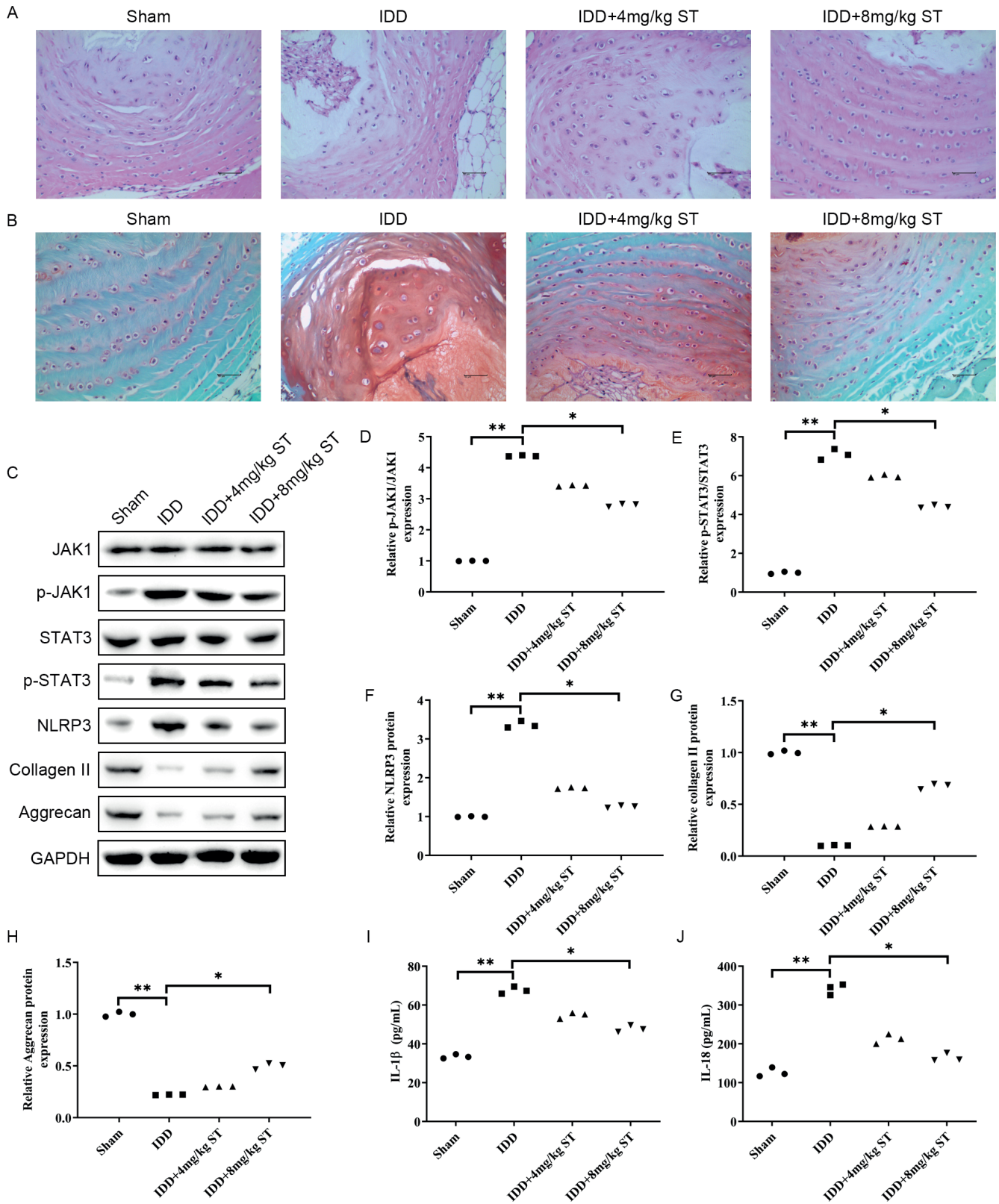


Fig. 7. Sinapine thiocyanate improved intervertebral disc degeneration (IDD) in vivo. A, B. Pathological change of the intervertebral disc was assessed with hematoxylin & eosin (H&E) and safranin-O staining; C–H. The expression of JAK, p-JAK, STAT3, p-STAT3, NLRP3, collagen II, and aggrecan was detected using western blot; I–J. The content of interleukin (IL)-1β and IL-18 was evaluated with enzyme-linked immunosorbent assay (ELISA)

**p < 0.01; *p < 0.05.

Supplementary Table 6. The analysis results of data from Fig. 6 through non-parametric ANOVA (Kruskal–Wallis test) followed by Dunn’s post hoc test without any correction.

Supplementary Table 7. The analysis results of data from Fig. 7 through non-parametric ANOVA (Kruskal–Wallis test) followed by Dunn’s post hoc test without any correction.

Data availability

The datasets generated and/or analyzed during the current study are available from the corresponding author on reasonable request.

Consent for publication

Not applicable.

ORCID iDs

Pengfei Yu  <https://orcid.org/0000-0003-4702-2648>
 Zhijia Ma  <https://orcid.org/0000-0001-5542-2591>
 Hong Jiang  <https://orcid.org/0000-0001-5192-5933>
 Jintao Liu  <https://orcid.org/0000-0002-7965-4837>
 Hongwei Li  <https://orcid.org/0009-0007-2306-4110>

References

- Urits I, Burshstein A, Sharma M, et al. Low back pain, a comprehensive review: Pathophysiology, diagnosis, and treatment. *Curr Pain Headache Rep.* 2019;23(3):23. doi:10.1007/s11916-019-0757-1
- Wang Y, Che M, Xin J, Zheng Z, Li J, Zhang S. The role of IL-1 β and TNF- α in intervertebral disc degeneration. *Biomed Pharmacother.* 2020;131:110660. doi:10.1016/j.biopha.2020.110660
- Molladavoodi S, McMorran J, Gregory D. Mechanobiology of annulus fibrosus and nucleus pulposus cells in intervertebral discs. *Cell Tissue Res.* 2020;379(3):429–444. doi:10.1007/s00441-019-03136-1
- Mitchell UH, Helgeson K, Mintken P. Physiological effects of physical therapy interventions on lumbar intervertebral discs: A systematic review. *Physiother Theory Pract.* 2017;33(9):695–705. doi:10.1080/09593985.2017.1345026
- Kos N, Gradisnik L, Velnar T. A brief review of the degenerative intervertebral disc disease. *Med Arch.* 2019;73(6):421–424. doi:10.5455/medarh.2019.73.421-424
- Eisenstein SM, Balain B, Roberts S. Current treatment options for intervertebral disc pathologies. *Cartilage.* 2020;11(2):143–151. doi:10.1177/1947603520907665
- Shao Z, Wang B, Shi Y, et al. Senolytic agent Quercetin ameliorates intervertebral disc degeneration via the Nrf2/NF- κ B axis. *Osteoarthritis Cartilage.* 2021;29(3):413–422. doi:10.1016/j.joca.2020.11.006
- Wang Z, Zhang S, Zhao Y, et al. MicroRNA-140-3p alleviates intervertebral disc degeneration KLF5/N-cadherin/MDM2/Slug axis. *RNA Biol.* 2021;18(12):2247–2260. doi:10.1080/15476286.2021.1898176
- Yan Q, Xiao Q, Ge J, et al. Bioinformatics-based research on key genes and pathways of intervertebral disc degeneration. *Cartilage.* 2021;13(2 Suppl):582S–591S. doi:10.1177/1947603520973247
- Zhang Y, He F, Chen Z, et al. Melatonin modulates IL-1 β -induced extracellular matrix remodeling in human nucleus pulposus cells and attenuates rat intervertebral disc degeneration and inflammation. *Aging (Albany NY).* 2019;11(22):10499–10512. doi:10.18632/aging.102472
- Zhang XB, Hu YC, Cheng P, et al. Targeted therapy for intervertebral disc degeneration: Inhibiting apoptosis is a promising treatment strategy. *Int J Med Sci.* 2021;18(13):2799–2813. doi:10.7150/ijms.59171
- Pan X, Shao Y, Wang F, et al. Protective effect of apigenin magnesium complex on H₂O₂-induced oxidative stress and inflammatory responses in rat hepatic stellate cells. *Pharm Biol.* 2020;58(1):553–560. doi:10.1080/13880209.2020.1772840
- Deeb RS, Hajjar DP. Repair mechanisms in oxidant-driven chronic inflammatory disease. *Am J Pathol.* 2016;186(7):1736–1749. doi:10.1016/j.ajpath.2016.03.001
- Isik A, Wysocki AP, Memiş U, Sezgin E, Yezhikova A, Islambekov Y. Factors associated with the occurrence and healing of umbilical pilonidal sinus: A rare clinical entity. *Adv Skin Wound Care.* 2022;35(8):1–4. doi:10.1097/01.ASW.0000833608.27136.d1
- Isik A, Soran A, Grasi A, Barry N, Sezgin E. Lymphedema after sentinel lymph node biopsy: Who is at risk? *Lymphat Res Biol.* 2022;20(2):160–163. doi:10.1089/lrb.2020.0093
- Zhu X, Liu S, Cao Z, et al. Higenamine mitigates interleukin-1 β -induced human nucleus pulposus cell apoptosis by ROS-mediated PI3K/Akt signaling. *Mol Cell Biochem.* 2021;476(11):3889–3897. doi:10.1007/s11010-021-04197-z
- Chen J, Liu GZ, Sun Q, et al. Protective effects of ginsenoside Rg3 on TNF- α -induced human nucleus pulposus cells through inhibiting NF- κ B signaling pathway. *Life Sci.* 2019;216:1–9. doi:10.1016/j.lfs.2018.11.022
- Feng C, He J, Zhang Y, et al. Collagen-derived N-acetylated proline-glycine-proline upregulates the expression of pro-inflammatory cytokines and extracellular matrix proteases in nucleus pulposus cells via the NF- κ B and MAPK signaling pathways. *Int J Mol Med.* 2017;40(1):164–174. doi:10.3892/ijmm.2017.3005
- Bergsbaken T, Fink SL, Cookson BT. Pyroptosis: Host cell death and inflammation. *Nat Rev Microbiol.* 2009;7(2):99–109. doi:10.1038/nrmicro2070
- McKenzie BA, Mamik MK, Saito LB, et al. Caspase-1 inhibition prevents glial inflammasome activation and pyroptosis in models of multiple sclerosis. *Proc Natl Acad Sci U S A.* 2018;115(26):E6065–E6074. doi:10.1073/pnas.1722041115
- Wang S, Yuan YH, Chen NH, Wang HB. The mechanisms of NLRP3 inflammasome/pyroptosis activation and their role in Parkinson’s disease. *Int Immunopharmacol.* 2019;67:458–464. doi:10.1016/j.intimp.2018.12.019
- Zhou Y, Chen Z, Yang X, et al. Morin attenuates pyroptosis of nucleus pulposus cells and ameliorates intervertebral disc degeneration via inhibition of the TXNIP/NLRP3/caspase-1/IL-1 β signaling pathway. *Biochem Biophys Res Commun.* 2021;559:106–112. doi:10.1016/j.bbrc.2021.04.090
- Xin P, Xu X, Deng C, et al. The role of JAK/STAT signaling pathway and its inhibitors in diseases. *Int Immunopharmacol.* 2020;80:106210. doi:10.1016/j.intimp.2020.106210
- Morris R, Kershaw NJ, Babon JJ. The molecular details of cytokine signaling via the JAK/STAT pathway. *Protein Sci.* 2018;27(12):1984–2009. doi:10.1002/pro.3519
- Chen B, Liu Y, Zhang Y, Li J, Cheng K, Cheng L. IL-21 is positively associated with intervertebral disc degeneration by interaction with TNF- α through the JAK-STAT signaling pathway. *Inflammation.* 2017;40(2):612–622. doi:10.1007/s10753-017-0508-6
- Guan H, Lin Q, Ma C, Ju Z, Wang C. Metabolic profiling and pharmacokinetic studies of sinapine thiocyanate by UHPLC-Q/TOF-MS and UHPLC-MS/MS. *J Pharm Biomed Anal.* 2022;207:114431. doi:10.1016/j.jpba.2021.114431
- Chen S, Jin YT, Zhu ZY, et al. In vivo study on site of action of sinapine thiocyanate following acupoint herbal patching. *Evid Based Complement Alternat Med.* 2018;2018:9502902. doi:10.1155/2018/9502902
- Fan W, Huang Y, Wang L, et al. Effect of stimulating the acupoints Feishu (BL 13) and Dazhui (GV 14) on transdermal uptake of sinapine thiocyanate in asthma gel. *J Tradit Chin Med.* 2017;37(4):503–509. PMID:32188209.
- Guo X, Lu H, Lin Y, et al. Skin penetration of topically applied white mustard extract and its effects on epidermal Langerhans cells and cytokines. *Int J Pharm.* 2013;457(1):136–142. doi:10.1016/j.ijpharm.2013.09.015
- Yun WJ, Yao ZH, Fan CL, et al. Systematic screening and characterization of Qi-Li-Qiang-Xin capsule-related xenobiotics in rats by ultra-performance liquid chromatography coupled with quadrupole time-of-flight tandem mass spectrometry. *J Chromatogr B Analyt Technol Biomed Life Sci.* 2018;1090:56–64. doi:10.1016/j.jchromb.2018.05.014
- Li Y, Zhang X, Yang W, et al. Mechanism of the protective effects of the combined treatment with rhynchophylla total alkaloids and sinapine thiocyanate against a prothrombotic state caused by vascular endothelial cell inflammatory damage. *Exp Ther Med.* 2017;13(6):3081–3088. doi:10.3892/etm.2017.4357

32. Liu Y, Yin H lin, Li C, et al. Sinapine thiocyanate ameliorates vascular endothelial dysfunction in hypertension by inhibiting activation of the NLRP3 inflammasome. *Front Pharmacol*. 2021;11:620159. doi:10.3389/fphar.2020.620159
33. Wang J, Zeng Z, Lei S, et al. Sinapine thiocyanate inhibits the proliferation and mobility of pancreatic cancer cells by up-regulating GADD45A. *J Cancer*. 2022;13(4):1229–1240. doi:10.7150/jca.65212
34. Liu MC, Chen WH, Wu LC, et al. Establishment of a promising human nucleus pulposus cell line for intervertebral disc tissue engineering. *Tissue Eng Part C Methods*. 2014;20(1):1–10. doi:10.1089/ten.tec.2013.0048
35. Kim JS, Ellman MB, Yan D, et al. Lactoferricin mediates anti-inflammatory and anti-catabolic effects via inhibition of IL-1 and LPS activity in the intervertebral disc. *J Cell Physiol*. 2013;228(9):1884–1896. doi:10.1002/jcp.24350
36. Zhang C, Tong T, Miao DC, Wang LF. Vitamin D inhibits TNF- α induced apoptosis of human nucleus pulposus cells through regulation of NF- κ B signaling pathway. *J Orthop Surg Res*. 2021;16(1):411. doi:10.1186/s13018-021-02545-9
37. Bai Z, Liu W, He D, et al. Protective effects of autophagy and NFE2L2 on reactive oxygen species-induced pyroptosis of human nucleus pulposus cells. *Aging (Albany NY)*. 2020;12(8):7534–7548. doi:10.18632/aging.103109
38. Teng JF, Mei QB, Zhou XG, et al. Polyphyllin VI induces caspase-1-mediated pyroptosis via the induction of ROS/NF- κ B/NLRP3/GSDMD signal axis in non-small cell lung cancer. *Cancers (Basel)*. 2020;12(1):193. doi:10.3390/cancers12010193
39. Gao H, Wang W, Li Q. GANT61 suppresses cell survival, invasion and epithelial-mesenchymal transition through inactivating AKT/mTOR and JAK/STAT3 pathways in anaplastic thyroid carcinoma. *Cancer Biol Ther*. 2022;23(1):369–377. doi:10.1080/15384047.2022.2051158
40. Gu R, Huang Z, Liu H, et al. Moracin attenuates LPS-induced inflammation in nucleus pulposus cells via Nrf2/HO-1 and NF- κ B/TGF- β pathway. *Biosci Rep*. 2019;39(12):BSR20191673. doi:10.1042/BSR20191673
41. Liu J, Jiang T, He M, et al. Andrographolide prevents human nucleus pulposus cells against degeneration by inhibiting the NF- κ B pathway. *J Cell Physiol*. 2019;234(6):9631–9639. doi:10.1002/jcp.27650
42. Chen J, Bian M, Pan L, Yang H. α -Mangostin protects lipopolysaccharide-stimulated nucleus pulposus cells against NLRP3 inflammasome-mediated apoptosis via the NF- κ B pathway. *J Appl Toxicol*. 2022;42(9):1467–1476. doi:10.1002/jat.4306
43. Yu P, Zhang X, Liu N, Tang L, Peng C, Chen X. Pyroptosis: Mechanisms and diseases. *Signal Transduct Target Ther*. 2021;6(1):128. doi:10.1038/s41392-021-00507-5
44. Huang Y, Peng Y, Sun J, et al. Nicotinamide phosphoribosyl transferase controls NLRP3 inflammasome activity through MAPK and NF- κ B signaling in nucleus pulposus cells, as suppressed by melatonin. *Inflammation*. 2020;43(3):796–809. doi:10.1007/s10753-019-01166-z
45. Sun Z, Zheng X, Li S, et al. Single impact injury of vertebral endplates without structural disruption, initiates disc degeneration through Piezo1 mediated inflammation and metabolism dysfunction. *Spine (Phila Pa 1976)*. 2022;47(5):E203–E213. doi:10.1097/BRS.00000000000004203
46. Chen Z, Jin S, Wang M, et al. Enhanced NLRP3, caspase-1, and IL-1 β levels in degenerate human intervertebral disc and their association with the grades of disc degeneration. *Anat Rec (Hoboken)*. 2015;298(4):720–726. doi:10.1002/ar.23059
47. Zhang J, Zhang J, Zhang Y, et al. Mesenchymal stem cells-derived exosomes ameliorate intervertebral disc degeneration through inhibiting pyroptosis. *J Cell Mol Med*. 2020;24(20):11742–11754. doi:10.1111/jcmm.15784
48. Song Y, Wang Y, Zhang Y, et al. Advanced glycation end products regulate anabolic and catabolic activities via NLRP3-inflammasome activation in human nucleus pulposus cells. *J Cell Mol Med*. 2017;21(7):1373–1387. doi:10.1111/jcmm.13067
49. Murray PJ. The JAK-STAT signaling pathway: Input and output integration. *J Immunol*. 2007;178(5):2623–2629. doi:10.4049/jimmunol.178.5.2623
50. Wang Z, Zhang J, Zheng W, He Y. Long non-coding RNAs H19 and HOTAIR implicated in intervertebral disc degeneration. *Front Genet*. 2022;13:843599. doi:10.3389/fgene.2022.843599
51. Wu C, Ge J, Yang M, et al. Resveratrol protects human nucleus pulposus cells from degeneration by blocking IL-6/JAK/STAT3 pathway. *Eur J Med Res*. 2021;26(1):81. doi:10.1186/s40001-021-00555-1
52. Jiang Q, Tang G, Zhong X, Ding D, Wang H, Li J. Role of Stat3 in NLRP3/caspase-1-mediated hippocampal neuronal pyroptosis in epileptic mice. *Synapse*. 2021;75(12):e22221. doi:10.1002/syn.22221

Is the facial bone wall critical to achieving esthetic outcomes in immediate implant placement with immediate restoration? A systematic review

Sergio Charifker Ribeiro Martins^{1,A–F}, Marcio da Costa Marques^{1,A–C}, Michael Gomes Vidal^{1,A–D}, Pedro Henrique Moreira Paulo Tolentino^{1,A–D}, Roberto Galvão Dinelli^{1,A–D}, Gustavo Vicentis de Oliveira Fernandes^{2,3,C–F}, Jamil Awad Shibli^{1,A–F}

¹ Department of Periodontology, Dental Research Division, Guarulhos University, Brazil

² Department of Periodontics and Oral Medicine, University of Michigan School of Dentistry, Ann Arbor, USA

³ A.T. Still University-Missouri School of Dentistry & Oral Health, St. Louis, USA

A – research concept and design; B – collection and/or assembly of data; C – data analysis and interpretation; D – writing the article; E – critical revision of the article; F – final approval of the article

Advances in Clinical and Experimental Medicine, ISSN 1899–5276 (print), ISSN 2451–2680 (online)

Adv Clin Exp Med. 2024;33(9):979–997

Address for correspondence

Gustavo Vicentis de Oliveira Fernandes
E-mail: gustfernandes@gmail.com

Funding sources

None declared

Conflict of interest

None declared

Received on July 31, 2023

Reviewed on August 28, 2023

Accepted on October 10, 2023

Published online on January 5, 2024

Cite as

Martins SCR, da Costa Marques M, Gomes Vidal M, et al. Is the facial bone wall critical to achieving esthetic outcomes in immediate implant placement with immediate restoration? A systematic review. *Adv Clin Exp Med.* 2024;33(9):979–997. doi:10.17219/acem/173573

DOI

10.17219/acem/173573

Copyright

Copyright by Author(s)

This is an article distributed under the terms of the Creative Commons Attribution 3.0 Unported (CC BY 3.0) (<https://creativecommons.org/licenses/by/3.0/>)

Abstract

Background. Rehabilitation in the anterior region requires specific conditions for success, such as the presence of papilla, emergence profile, and balance between pink and white esthetic.

Objectives. This systematic review aimed to evaluate the esthetic risk associated with immediate implant placement with immediate restoration in the anterior superior area, where the facial bone plate may be absent or deficient.

Materials and methods. The search was done in PubMed, Embase, Cochrane, Lilacs, Scopus, Scielo, and Google Scholar databases. The investigation involved clinical studies and observational studies published between January 2012 and July 2023. Studies were excluded if there was less than 12-month follow-up, no immediate restoration or facial defect, heavy smokers, or systemic disease. The risk of bias was assessed using the ROBINS-I and Modified-Cochrane RoB tools.

Results. Twelve studies were included in this systematic review. The thinner the facial plate, the higher the alveolus's risk of gingival recession or shrinkage. There was an increased interproximal recession when the thin phenotype was associated with flap surgery. An increase in pink esthetic score (PES) was reached when immediate implant placement (IIP) and immediate restoration were done. Soft tissue augmentation achieved more gingival-level stability. Regardless of the initial phenotype, an esthetic outcome was delivered. The risk of bias was high in 1 study and moderate in 3 studies.

Conclusions. It is possible to conclude that esthetic results and increased final PES or patient satisfaction index in IIP treatments associated with immediate restoration could be obtained even in buccal bone wall defects or gingival recession, regardless of their extension.

Key words: esthetic region, facial bone plate deficiency, immediate implant placement, immediate restoration, peri-implant recession

Background

Several clinical situations can predispose patients to tooth loss,^{1–3} which can cause functional impairment and esthetic challenges for clinicians. Rehabilitation in the anterior zone requires specific conditions for success, such as the presence of papilla, an emergence profile, and a balance between pink and white esthetics.⁴ Previous studies^{5–8} suggest that buccal-plate bone loss results in esthetic sequelae, mainly influenced by the reduction/absence of papillae and the position of the gingival and/or peri-implant mucosa. Currently, several procedures are proposed to increase the predictability of results.^{9–11}

Among the available therapies, implant placement following correct three-dimensional (3D) positioning, filling the socket with a bone substitute, using connective tissue graft, and immediate restoration are procedures that can minimize peri-implant tissue loss over time.^{4,12–15} Otherwise, in light of current knowledge, the clinician's concern in achieving successful rehabilitation is no longer only the success of the osseointegration,^{16–20} but also peri-implant esthetics.^{4,21}

Some factors may interfere with the peri-implant tissue framework in anterior rehabilitation, such as periodontal phenotype, 3D implant position, and prosthetic management with an adequate emergence profile. Then, immediate restoration can be considered an essential variable in the treatment plan,^{4,22–24} especially in areas with a compromised buccal bone plate and high esthetic demand. Therefore, the anterior area of the maxilla present several anatomic and esthetic characteristics that must be considered during dental implant treatment: 1. Thin facial bone that is more prone to resorption due to decreased vascular supply²⁵ after tooth loss^{26,27}; 2. Reduced buccolingual dimensions and facial bone concavity^{28–30}; 3. The type of implant connection used due to the risk of bone loss³¹; 4. Risk of fenestration and exposure of the apical implant's threads^{28,32}; and 5. Peri-implant mucosal recession.^{31,33,34}

Evaluation of the buccal bone plate demonstrated that most cases were <1 mm thick, with 50% presenting <0.5 mm thickness.³⁵ Moreover, <10% of sites showed buccal plate thickness \geq 2 mm.³⁶ Another study reported that the mean width of the facial alveolar bone wall in anterior teeth was around 0.9 mm.³⁷ It is clear that thinner buccal bone will probably result in a greater and considerable amount of vertical bone loss.³¹ The literature showed that initial buccal bone thickness and subsequent vertical height bone loss (after implantation) were 1.2 mm with a loss of 0.7 mm,³³ 1.25 mm with a loss of 0.49 mm³⁸ and 0.5 mm with a loss of 1 mm.³⁴ Consequently, the thinner the bone, the greater the vertical loss.

Objectives

Despite the clinical relevance of the topic, well-delineated clinical studies are scarce regarding immediate

implant placement (IIP) in anterior sites with buccal bone defects already present. Also, there is a gap in the literature on whether such a condition incurs esthetic problems after the healing period of the peri-implant tissue. As such, the goal of this systematic review was to evaluate the esthetic risk caused by IIP with immediate restoration in the anterior area, where the facial bone plate may be absent or deficient.

This systematic review followed the Preferred Reporting Items for Systematic Reviews and Meta-Analyses (PRISMA) guidelines and was registered on the International Prospective Register of Systematic Reviews (PROSPERO) platform (CRD42022341534). The focus question was developed based on the Patient (P), Intervention (I), Comparison (C), and Outcomes (O) (PICOS) strategy, in addition to the design of the studies (S) conducted.³⁹ The focus question was: “For IIP immediately restored, does the absence of a buccal bone plate mean an increased risk for the esthetic and peri-implant mucosa recession?” P. Patients undergoing at least 1 immediate implant in an esthetic region; I. IIP and immediate restoration in sockets with buccal bone defects; C. Buccal bone defects at the IIP with immediate restoration; O. Recession of the peri-implant mucosa and esthetic risk, and if there are procedures in the literature permitting higher predictability in circumventing this bone defect, allowing a better esthetic result; S. Clinical studies and observational studies (cohort studies, case-control studies and cross-sectional studies).

Eligibility criteria

The criteria for inclusion included: 1. Clinical studies and observational studies (cohort studies, case-control studies and cross-sectional studies); 2. Minimum follow-up of 12 months; 3. IIP with immediate restoration in the anterior superior esthetic region; 4. Evaluation of esthetic clinical parameters; 5. Treated sockets (or study group) with buccal wall defects. The exclusion criteria were: 1. Follow-up time of less than 12 months; 2. Without immediate restoration; 3. Diabetic patients; 4. Smokers consuming more than 10 cigarettes per day; 5. Patients systemically compromised.

Information sources and search strategy

Two independent examiners (PHMPT and RGD) performed a broad search for articles in 7 databases: PubMed/Medline, Embase, Cochrane, Lilacs, Scopus, Scielo, and Google Scholar. The investigation included clinical and observational studies (cohort, case-control and cross-sectional studies) published between January 2012 and July 2023 in any language. It used the following descriptors and combination strategies: “peri-implant soft tissue” OR “gingival recession” OR “gingival deficiency” OR “buccal plate deficiency” OR “facial bone defect” OR “facial bone

deficiency” OR “buccal bone defect” AND “immediate implant” OR “single implant” OR “maxillae anterior implant” OR “immediate” OR “immediately” OR “extraction” OR “socket” OR “dental implantation” OR “endosseous implant” OR “dental implants” OR “single tooth” AND “esthetic area” OR “esthetic zone” OR “esthetic region” OR “aesthetic.”

Data collection and selection process and data items

A thorough analysis of the data was performed by 2 independent researchers (PHMPT and RGD) for sequential comparison in Microsoft Excel v. 16.50 (Microsoft Corp., Redmond, USA). Information about the authors, year of publication, type of study, follow-up, number of patients, number of implants, eligibility criteria applied, pre-operative patient evaluation, buccal plate defect size, bone graft used, soft tissue graft, number of teeth extracted, extraction technique, implants’ settings, implant position, postoperative care, provisional restoration and definitive prosthesis delivered, implant success/survival rate, esthetic outcome parameters measured in the study, and conclusions were registered when available.

Risk of bias assessment

The risk of bias was assessed using the Risk of Bias In Non-Randomized Studies – of Interventions (ROBINS-I), which is a tool for the prospective and retrospective case-control

papers, and using the Modified Cochrane Risk of Bias tool for the randomized controlled trials (RCTs) included in this research.⁴⁰ When up to 1 “Y” (Yes) or 1 “high risk” were found, the judgment was “low risk of bias”; if 2 “Y” (Yes) or 1 “high risk” and 1 “unclear” were found, the judgment was “moderate risk”; if 3 “yes” or 2 “high risk,” the judgment was “high risk of bias.”

Results

Screening and study selection

An initial search found 32,904 articles, of which, after filtering for the date (last 11 years and 6 months) and study design – randomized clinical trials, 2,485 works were selected ($k = 0.93$). After reading the titles, the reviewers excluded 2,081 studies and another 429 due to duplicity. A total of 186 articles were separated for reading of the abstracts, of which 161 were excluded. Of the 25 remaining articles, 13 did not meet the selection criteria because they did not deal with alveoli with vestibular wall defects (Table 1; $k = 0.98$). Finally, 12 studies were selected for this systematic review (Fig. 1).

Study characteristics

Table 2 describes the types of studies analyzed, the mean follow-up time, and the number of implants and patients evaluated. Among the evaluated studies, there were

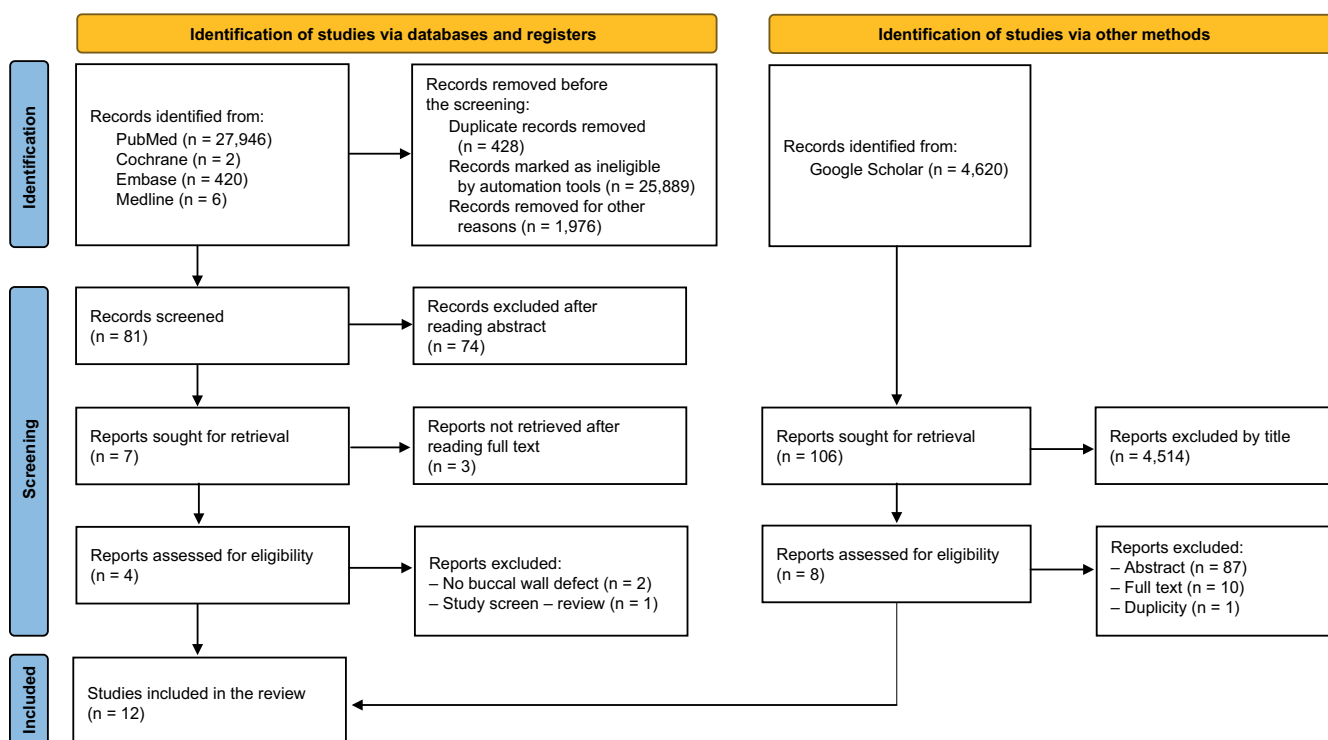


Fig. 1. Research flow and the number of articles included in this systematic review

Table 1. Articles excluded with justification after full-text reading

Author/year	Title	Exclusion criteria
Kirsten et al., 2021	Immediate single-tooth implant placement with simultaneous bone augmentation versus delayed implant placement after alveolar ridge preservation in bony defect sites in the esthetic region: A 5-year randomized controlled trial	There was no immediate provisional.
Happe et al., 2021	Peri-implant soft-tissue esthetic outcome after immediate implant placement in conjunction with xenogeneic acellular dermal matrix or connective tissue graft: A randomized controlled clinical study	intact buccal wall after extraction
Sanz et al., 2016	The effect of placing a bone replacement graft in the gap at immediately placed implants: A randomized clinical trial	intact extraction socket following
Ferrantino et al., 2021	Esthetic outcomes of non-functional immediately restored single post-extraction implants with and without connective tissue graft: A multicenter randomized controlled trial	duplicity
Lemes et al., 2014	Behavior of the buccal crestal bone levels after immediate placement of implants subjected to immediate loading	6-month follow up
Chu et al., 2015	Subclassification and clinical management of extraction sockets with labial dentoalveolar dehiscence defects	case report
Kan et al., 2018	Immediate implant placement and provisionalization of maxillary anterior single implants	guideline
Sun et al., 2019	Comparing conventional flap-less immediate implantation and socket-shield technique for esthetic and clinical outcomes: A randomized clinical study	intact facial alveolar bone wall, without bone or soft-tissue defects.
Rosa et al., 2014	Immediate implant placement, reconstruction of compromised sockets, and repair of gingival recession with a triple graft from the maxillary tuberosity: A variation of the immediate dentoalveolar restoration technique	case report
Arora et al., 2017	Immediate implant placement and restoration in the anterior maxilla: Tissue dimensional changes after 2–5 year follow up	any fenestration or dehiscence in the socket wall of the failing tooth
Arora et al., 2018	Immediate and early implant placement in single-tooth gaps in the anterior maxilla: A prospective study on ridge dimensional, clinical, and esthetic changes	There was a group where provisioning was not performed immediately.
Kuchler et al., 2015	Immediate implant placement with simultaneous guided bone regeneration in the esthetic zone: 10-year clinical and radiographic outcomes	The work did not describe provisioning and did not specify whether the transmucosal was customized.
Ma et al., 2019	Immediately restored single implants in the esthetic zone of the maxilla using a novel design: 5-year results from a prospective single-arm clinical trial	In 2 patients, provisionalization was not immediately performed and the presence of bone defects was not described.

3 RCTs,^{41–43} 7 prospective studies^{44–50} and 2 retrospective studies.^{13,51} The follow-up was from 12 months^{41–45,47,50} to 7 years,⁵¹ and the number of patients included in the studies varied from 100 to 1,245.^{45,50} All studies included patients with at least 1 hopeless tooth in the esthetic maxillary area with an indication of extraction and the possibility of IIP, with the maintenance of the adjacent teeth. The eligibility criteria implemented by the studies are summarized in Supplementary Table 1. The preoperative evaluation, size of the vestibular defect, and the presence of bone graft and/or soft tissue are detailed in Table 3.

The extraction technique and postoperative control are summarized in Table 4. The implants were loaded with immediate restoration, lacking occlusal contacts, and the minimum torque reported ranged from 15 N•cm⁴⁸ to 35 N•cm.^{43,44,49} The presence of an initial esthetic defect had at least 1 mm⁵¹ of gingival recession until the total absence of a facial plate.⁴⁴ Although most of the studies used a minimally invasive technique to remove the target tooth,^{13,42–51} Lee et al.⁴¹ compared 2 groups in which 1 used a flapless procedure and the other used a raised flap.

The conclusion of each article is summarized in Supplementary Table 2.

Patients' assessment

For the initial assessment of the patient, a cone beam computed tomography (CBCT) was used, as well as the clinical parameters including the pink esthetic score (PES).⁵⁰ Photographs, periodontal phenotype, preoperative soft tissue level, and CBCT scans were also used as initial references,^{42,48,49,51} which permitted comparison with the final restoration. Ferrantino et al.⁴³ treated alveoli with up to 1 mm of bony defect, whereas most authors limited the maximal crestal bone defect to 5 mm.^{41,42,45,50} Other studies considered different parameters, including 10 mm of vertical bone defect⁴⁴ and dehiscence of more than 2/3 of the buccal plate.⁵¹ Although most treatments involved reconstruction of the buccal plate with different types of graft, some authors did not reconstruct the wall.^{41,44} Instead, they intended to compare the local bone and soft tissue changes without the interference of socket

Table 2. Types of study, follow-up, and number of patients and implants evaluated in the articles included

Author/year	Title	Type of study	Follow-up	N (patients); n (implants)
Noelken et al., 2018 ¹³	Clinical and esthetic outcome with immediate insertion and provisionalization with or without connective tissue grafting in presence of mucogingival recessions: A retrospective analysis with follow-up between 1 and 8 years.	retrospective study	1–8 years	N = 26; n = 26
Lee et al., 2020 ⁴¹	Predicting bone and soft tissue alterations of immediate implant sites in the esthetic zone using clinical parameters.	randomized controlled trial	12 months	N = 39; n = 39
Zuiderveld et al. 2017 ⁴²	Effect of connective tissue grafting on peri-implant tissue in single immediate implant sites: An RCT.	randomized controlled trial	12 months	N = 60; n = 60
Ferrantino et al., 2021 ⁴³	Esthetic outcomes of non-functional immediately restored single post-extraction implants with and without connective tissue graft: A multicenter randomized controlled trial.	randomized controlled trial	12 months	N = 59; n = 59
Pohl et al., 2020 ⁴⁴	Gingival recession behavior with immediate implant placement in the anterior maxilla with buccal dehiscence without additional augmentation – a pilot study.	prospective case series (observational)	12 months	N = 24; n = 24
Staas et al., 2021 ⁴⁵	Does initial buccal crest thickness affect final buccal crest thickness after flapless immediate implant placement and provisionalization: A prospective cone beam computed tomogram cohort study.	prospective cohort study (observational)	12 months	N = 100; n = 100
Elaskary et al., 2020 ⁴⁶	A novel method for immediate implant placement in defective fresh extraction sites.	prospective case series (observational)	13 months	N = 12; n = 12
Frizzera et al., 2018 ⁴⁷	Impact of soft tissue grafts to reduce peri-implant alterations after immediate implant placement and provisionalization in compromised sockets.	randomized controlled trial	12 months	N = 24; n = 24
Noelken et al., 2013 ⁴⁸	Maintenance of marginal bone support and soft tissue esthetics at immediately provisionalized OsseoSpeed™ implants placed into extraction sites: 2-year results.	prospective case series (observational)	2 years	N = 20; n = 37
Da Rosa et al., 2014 ⁴⁹	Esthetic outcomes and tissue stability of implant placement in compromised sockets following immediate dentoalveolar restoration: Results of a prospective case series at 58 months follow-up.	prospective case series (observational)	58.56 months (mean)	N = 18; n = 18
Groenendijk et al., 2021 ⁵⁰	Does the pre-operative buccal soft tissue level at teeth or gingival phenotype dictate the aesthetic outcome after flapless immediate implant placement and provisionalization? Analysis of a prospective clinical case series.	prospective case series (observational)	12 months	N = 97; n = 97
Sicilia-Felechosa et al., 2019 ⁵¹	Flapless immediate implant placement and provisionalization in periodontal patients: A retrospective consecutive case series study of single-tooth sites with dehiscence-type osseous defects	retrospective consecutive case	1 year min. to 7 years max.	N = 40; n = 40

Table 3. Preoperative analysis, buccal defect size, and bone graft and/or soft tissue presence

Author/year	Patient analysis pre-op	Buccal plate defect size	Bone graft	Soft tissue grafts
Noelken et al., 2018 ¹³	CBCT, position of the lip-line, overall gingival biotype.	Seven (27%) extraction sockets showed a pristine facial bone wall (between 0-mm and 1-mm facial bone loss), 13 (50%) sites had partial bony defects (between 1-mm and 7.5-mm facial bone loss), and 6 (23%) sites presented a total loss of the facial bone wall (between 7.5-mm and 13-mm facial bone loss).	Autogenous bone grafts harvested at the mandibular ramus by a bone block and particulated in a bone mill or by collecting bone chips by a bone scraper.	Autogenous bone graft + connective tissue graft group: subepithelial connective tissue graft was harvested at the palate in the premolar region. Autogenous bone graft group: no soft tissue graft.
Lee et al., 2020 ⁴¹	Measurements of the implant site were performed at the time of the surgery: vertical distance between the buccal gingival margin and the buccal crest; thickness of the mid-buccal gingiva at the level of gingival margin and 3 mm apically from the gingival margin. Phenotype categorized into “thick” gingiva or “thin” gingiva; thickness of the mid-buccal bone crest at the level of crestal margin and 3 mm apically to the crestal margin.	Fenestration with a diameter <5 mm affecting less than half of the socket wall.	no graft	no graft

Table 3. Preoperative analysis, buccal defect size, and bone graft and/or soft tissue presence – cont.

Author/year	Patient analysis pre-op	Buccal plate defect size	Bone graft	Soft tissue grafts
Zuiderveld et al., 2017 ⁴²	The height of the bone defect was measured after the failing tooth was extracted, using a periodontal probe at the mid-buccal, mesial and distal aspect of the failing tooth and the adjacent teeth.	less than 5 mm	1/1 autologous harvested from the maxillary tuberosity region/anorganic bovine bone (Bio-Oss®).	Control group: no soft tissue graft; test group: connective tissue graft harvested from the maxillary tuberosity region.
Ferrantino et al., 2021 ⁴³	Clinical examination and CBCT.	less than 1 mm	Bovine bone mineral (DBBM) (Bio-Oss®, Geistlich Biomaterials, Wolhusen, Switzerland).	Test group: patients received a sub-epithelial CTG harvested from palate or tuberosity. Control group: no soft tissue graft.
Pohl et al., 2020 ⁴⁴	Test group: presence of a partial defect of the buccal bony alveolar lamella (at least 25% of the length of the corresponding tooth) up to a completely missing buccal plate. Control group: intact buccal bone wall.	Buccal plate vertical defect – 4.96 mm (min. 2.26 mm; max. 9.68 mm horizontal defect – 4.25 mm (min. 3.2 mm; max. 5.91 mm).	no graft	no graft
Staas et al., 2021 ⁴⁵	CBCT	Bone crest defect ≤5 mm.	Bovine bone (Bio Oss™ S 0.25–1 mm, Geistlich Biomaterials).	no graft
Elaskary et al., 2020 ⁴⁶	A CBCT scan was used for diagnosis and treatment planning. Impressions were also taken and cast in dental stone to fabricate computer-guided surgical templates.	Group 1: no bone defect but thin buccal plate and intact soft tissue; Group 2: deficient buccal bone but intact soft tissue.	Mixture of autogenous bone chips and DBBM in a ratio of approx. 3:1, covered by a slowly resorption xenograft cortical membrane. Autogenous chips harvested from the area of vestibular access with scrapers.	Subepithelial connective tissue graft harvested from the palate.
Frizzera et al., 2018 ⁴⁷	CBCT and clinical evaluation.	Probing depth and clinical attachment level >3 mm.	Xenograft – bovine bone + 10% porcine collagen (Bio-Oss Collagen; Geistlich Biomaterials).	Autogenous – connective tissue; Xenograft-collagen matrix (Mucograft; Geistlich Biomaterials).
Noelken et al., 2013 ⁴⁸	CBCT was performed to evaluate the dimensions of the facial bony lamella prior to surgery. Especially, the thickness of the facial lamella was measured in relation to a defined reference point. The thickness of the facial lamella was measured in distances of 1, 3, and 6 mm apically to this reference level.	Eight extraction sockets showed no recession and a pristine facial bone wall, 11 sites showed a combination of a pristine soft tissue condition and defects of the facial bone walls of various dimension, 18 sites showed a combination of facial recession and bone deficiencies.	Autogenous bone grafts harvested at the mandibular ramus by particulating a bone block in a bone mill or by collecting bone particles by a disposable filter.	Connective tissue graft harvested from the maxillary tuberosity region (test group).
da Rosa et al. 2014 ⁴⁹	CBCT; photograph; gingival biotype	Bony dehiscence in which the defect involves the coronal and medium third of the root without affecting the apical third.	IDR – published by Rosa et al.; autologous removed from tuberosity.	no graft
Groenendijk et al., 2021 ⁵⁰	Light photographs perpendicular to the tooth arch placed into a digital format. Reference lines drawn through gingival margin of the contra-lateral incisor, incisal edge of contra-lateral incisor, and distal from the central and lateral incisors. The gingival margin of the failing tooth at T0 was drawn in blue as a reference at different time points	Crestal bone defect not exceeding 5 mm.	DBBM (Bio-Oss®; Geistlich Biomaterials).	no graft
Sicilia-Felechosa et al., 2019 ⁵¹	Virtual surgery study using a programming software based on the CBCT examination.	Ranging from ≤1/3 or pocket depth 5–6 mm from gingival margin until bone dehiscence ≥2/3 or pocket depth ≥10 mm from gingival margin.	Combination of autogenous bone from drilling and DBBM, or only DBBM (Bio-Oss®; Geistlich Pharma AG).	Autogenous (connective tissue –85%); allogeneic dermis (15%; AlloDerm RTM, BioHorizons).

CBCT – cone beam computed tomography; DBBM – deproteinized bovine bone mineral; IDR – immediate dentoalveolar restoration.

Table 4. Extraction technique, diameter and type of implants used, implant position, postoperative control, and implant survival rate

Author/year	Tooth extraction technique	Implant used	Implant dimensions and platform	Implant position	Post-op control	Implant survival rate
Noelken et al., 2018 ¹³	Atraumatically extraction to maintain alveolar bone and gingival architecture.	Osseo-Speed™ (Astra Tech AB)	Conical connection; diameters: between 3.5 mm and 5.0 mm; length: 15 mm and 17 mm.	Aligned to the oral lamella of the socket. Placement depth determined by the interproximal and facial soft tissue and bone height.	The patients were examined preoperatively, at implant placement, at prosthetic delivery, and at annual follow-up visits up to 9 years following implant insertion.	100%
Lee et al., 2020 ⁴¹	The surgical procedure involved extraction of the tooth with or without elevation of a flap (flapless group, n = 18; flap-involving group, n = 21).	Full OS-SEOTITE Certain Tapered Implant (Biomet 3i, Palm Beach Gardens, USA).	Internal parallel connection. The size of the implant was selected based on the restorative plan and bone dimensions.	The implants were placed at the level of the buccal crest. The horizontal distance between the implant platform and buccal plate should be more than 1 mm.	All patients were seen at 1, 2, 3, 6, and 12 months, and received oral hygiene instructions and a prophylaxis.	One out of 39 implants failed and was removed 4 weeks after its placement. 36 implants had radiographs available and 34 implants had gingival and ridge measurements available for clinical and radiographic analysis.
Zuiderveld et al., 2017 ⁴²	As atraumatically as possible by detaching the periodontal ligament from the failing tooth without raising a flap.	Nobel Active (Nobel Biocare AB, Gothenburg, Sweden).	Conical connection. The implant dimension was not described in the paper.	Palatal side of the alveolus according to the manufacturer's manual by using a template representing the ideal position of the prospective implant crown; 3 mm apically to the most apical prospective clinical crown.	Patients were instructed to follow a soft diet and to avoid exerting force on the provisional restoration.	One implant in each group was lost due to failing osseointegration (96.7% implant survival in both groups).
Ferrantino et al., 2021 ⁴³	Extraction performed as gently and atraumatically as possible, followed by careful cleaning of the socket for any residue of granulation tissue. The status of a chronic infection in the alveolar socket was recorded.	Imax, iRES SAGL	Internal parallel walls; diameters: 3.85 mm or 4.2 mm; lengths: 11.5 mm, 13 mm and 16 mm.	Not detailed in the paper.	<ul style="list-style-type: none"> • Ibuprofen 400 mg twice a day for 2 days. • Chlorhexidine mouthwash 0.2% for 1 min twice a day for 2 weeks. • Amoxicillin 1 g twice a day for 6 days. Patients allergic to penicillin were prescribed clindamycin 300 mg twice a day for 6 days. 	One implant failure was recorded in each group. Test group: 96.8%; control group: 96.4%.
Pohl et al., 2020 ⁴⁴	Cautious and utterly careful tooth extraction, the alveola was carefully excochleated without elevating the flap and under careful preservation of the papilla.	Nobel-Replace Tapered; Nobel® Biocare, Kloten, Switzerland.	Conical connection; diameter: 4.3 mm; length: 13 mm and 16 mm.	The buccal crestal margin of the implant had to be at least 3 mm below the deepest indentation of the gingival margin and 3 mm palatally of the same. The implant had no direct contact with the buccal portions of the facial bone or soft tissue. Thus, the orientation of the implant position was soft-tissue- but not hard-tissue-related.	For assessing the mesial and distal bone level, intraoral radiographs (Sidedix®; Sirona, Bensheim, Germany) were taken on the day of surgery and 4, 6, and 12 months postoperatively.	100%
Staas et al., 2021 ⁴⁵	Atraumatic tooth removal technique.	NobelActive Conical Connection™ (Nobel-Biocare, Washington, DC, USA).	Conical connection; diameter: 3.0 mm (x6), 3.5 mm (x47), 4.3 diameter (x45). length: between 11.5 mm and 18 mm.	The seat of the implant was placed 3 mm apically from the buccal gingival margin and at least 2 mm palatal of the buccal bone plate.	Amoxicillin 500 mg x3 day for 5 days (clindamycin 600 mg/x4 day 5 days if allergic to penicillin) and chlorhexidine 0.12% twice a day for 14 days.	100% (2 patients excluded due to trauma and relocation).

Table 4. Extraction technique, diameter and type of implants used, implant position, postoperative control, and implant survival rate – cont.

Author/year	Tooth extraction technique	Implant used	Implant dimensions and platform	Implant position	Post-op control	Implant survival rate
Elaskary et al., 2020 ⁴⁶	Atraumatically using periosteum. Vestibular access horizontal incision made at the socket site 3–4 mm apically to the mucogingival junction and extending 5–10 mm horizontally, submucoperiosteal tunnel created from the facial aspect of the socket orifice until the vestibular access incision.	Megagen implant	Conical connection; diameter and length not described in the text.	Optimum prosthetically guided position with the implant shoulder placed 3–4 mm apically to the labial gingival margin.	Antibiotics (Ciprofloxacin) and non-steroidal anti-inflammatory (Catafast) for 5 days, mouth washing with chlorhexidine 0.12% during 10 days; 6 and 13 months to measure facial bone thickness and height. Pink esthetic score was recorded at 6 and 13 months.	100%
Frizzera et al., 2018 ⁴⁷	Flapless, with a facial pouch creation for the soft tissue augmentations groups.	Flash (Conexão Sistemas de Prótese)	Diameter: 3.5 mm; Length: according to the amount of apical bone; Platform: conical morse-taper.	Implant platform was placed 4 mm below the facial gingival margin (ideal implant position).	Antibiotic (amoxicillin for 7 days) and analgesic for pain relief (paracetamol 750 mg). Chlorhexidine 0.12% for mouth washing. Measurements of soft tissue at 6 and 12 months after the surgery.	100%
Noelken et al., 2013 ⁴⁸	Atraumatically extracted using the periosteum technique maintaining the alveolar socket walls and gingival architecture. All procedures were performed without raising a flap even when a facial bone defect was observed.	Osseo-Speed™ implants (Astra Tech AB).	Conical connection; Diameters: 3.5–5.0 mm Length: 11–17 mm.	In contact with the oral lamella of the socket. Depth was determined by the interproximal and facial soft tissue and bone height.	Antibiotic prophylaxis (starting the day before surgery until 7 days postoperatively; clindamycin 300 mg 3–4 times/day) and a prescription for post-surgical chlorhexidine rinse 0.2%, for 10 days. After implant placement, the subjects returned for a follow-up visit after 7–10 days for control of the implants, the temporary restoration, and the healing process.	100%
da Rosa et al., 2014 ⁴⁹	As atraumatically as possible using periosteum and mini lifters after minimal incision made around the tooth with microblade. Maintain the integrity of remaining bone wall and papillae.	Nobel replace Tapered TiUnite – (Nobel Biocare).	Conical connection; diameter and length: according to socket dimensions.	Ideal 3D position. Cingulum axis of the alveolus.	500 mg of amoxicillin x3 day (azithromycin 500 mg x2 day if allergic) for 10 days/4mg dexamethasone x2 day for 3 days. Mouth washing with chlorhexidine solution x2 day for 14 days.	100%
Groenendijk et al., 2021 ⁵⁰	After atraumatic extraction, the socket was cleaned extensively using a bone excavator to remove remnants of the periodontal ligament and/or inflammation tissue and to promote bleeding. The keratinized gingiva remained intact as no flaps were raised.	NobelActive Internal implants (Nobel Biocare, Washington DC, USA).	Conical connection. The implant dimension was not described in the paper.	Implant seat positioned 3 mm deeper than the buccal gingival margin.	Amoxicillin every 8 h during 5 days postoperatively and to rinse with 0.12% chlorhexidine solution twice a day during 14 days post-surgery.	100% (3 patients excluded due to trauma, relocation or missing photographs).

Table 4. Extraction technique, diameter and type of implants used, implant position, postoperative control, and implant survival rate – cont.

Author/year	Tooth extraction technique	Implant used	Implant dimensions and platform	Implant position	Post-op control	Implant survival rate
Sicilia-Felechosa et al., 2019 ⁵¹	All surgeries were carried out by an experienced periodontist with the aid of a surgical microscope. Dental extractions were atraumatically performed to the maximum possible extent. Use of sclerotome, forceps and root elevators, avoiding bucco-lingual luxation movements.	Conical: Zimmer Biomet hybrid micro-surface topography (machined surface at the most coronal aspect and dual acid-etched surface on the remainder of the implant body; OSSEOTITE®, Zimmer Biomet). Parallel-walled: Nobel Biocare Speedy®, anodized surface (Ti-Unite®, Nobel Biocare)	Implant length [mm]: 11.5 (n = 1), 13 (n = 13) and 15 (n = 26). Implant diameter [mm]: 3.4 (n = 2), 4.1 (n = 33) and 5.1 (n = 5). External hexagon.	The implants were placed according to the CBCT setting following a computer-oriented surgery procedure with multiple screens.	Not described in the paper.	One implant placed failed at 5.6 years. The remaining implants (39) were monitored, achieving a success percentage of 98.3% (95% CI: 91–99%) in a follow-up period that ranged from 1 to 7 years.

CBCT – cone beam computed tomography.

grafting after IIP and immediate restoration in the presence of a partial or completely missing buccal bone.

The PES was used to compare initial and final photographs of the patient using the contralateral tooth as a reference.^{13,42,44,46–48,50,51} Some points were evaluated, such as the medial and distal papillae, soft tissue contour, gingival margin level, soft tissue color, and texture. On the other hand, Ferrantino et al.⁴³ applied the Implant Crown Aesthetic Index (ICAI) to clinical digital photographs taken during the follow-up. In contrast, da Rosa et al.⁴⁹ chose the gingiva morphometry method. Staas et al.⁴⁵ and Lee et al.⁴¹ assessed the relationship between the bone margin and thickness as well as the interproximal bone peek to measure the esthetic risk of IIP and immediate restoration and gingival/bone changes during the healing time. Some authors also evaluated patient satisfaction.⁵¹

Bone graft and soft tissue

In paper by Sicilia-Felechosa et al.,⁵⁰ the authors did not describe the bone substitute used, while most of the others chose xenografts.^{43,45,47,51} Two studies had grafted the buccal alveolar space in front of the implant surface with autologous bone chips,^{13,48} while 1 decided to use a specific graft technique using thin lamina of bone from tuberosities.⁴⁹ The association between xenograft and autologous chips was also considered to fill the buccal gap.^{42,46,51}

Regarding soft tissue grafts, there was no preference regarding their use or not. While some authors proceeded with gingival volume augmentation,^{42,43,46–48,51} others did not consider this option.^{13,41,44,45,49,50} Subepithelial connective tissue grafts removed from the palate^{42,46–48} or tuberosity⁴² were used to increase gingival volume. Allogenic dermis (AlloDerm RTM, Biohorizons, Allergan Corp., Dublin, Ireland)⁵¹ and a collagen matrix (Mucograft, Geistlich, Wolhusen, Switzerland)⁴⁷ were also considered.

Implant settings

Tapered implants were used in several studies (Table 4).^{13,41–49,51} Nevertheless, 1 author used a parallel implant,⁵¹ and another did not describe the type of implant used.⁵⁰ The diameter of the implants varied from 3.0 mm⁴⁵ to 5.1 mm,⁵¹ and was chosen based on the socket dimensions. The position of the implant was more palatal, following the best 3D position, creating a gap between the implant surface and the buccal bone wall, which could be filled with graft or not, as described above. This gap ranged from 1 mm⁴¹ to 3 mm long⁴⁴ and was filled as mentioned above. The abutment connection dictates the distance from the perspective of the clinical crown margin to the implant seat. The most commonly described distance was 3–4 mm,^{42,45–47} although implant seats coinciding with the facial bone crest level were found.⁴¹

Implant success/survival rate

The implant success rate (Table 4) was measured based on the absence of pain complaints, discomfort, infection, no implant mobility, and no bone loss (less than 1 mm in the 1st year). A high success rate was found in all of the selected papers. Some authors showed a 100% success rate,^{13,44,46–49} while others described 1 implant loss out of 39%,⁴¹ or 96.80% implant survival.⁴³ Others had a success rate of 98.3%,⁵¹ 96.7%,⁴² while some had a success rate of around 100% after excluding patients who lost the implant due to trauma or did not undergo the follow-up maintenance.^{45,50}

Immediate/provisional restoration

The immediate restoration procedure was mandatory to be included in this review (Table 5). Although different

restorative protocols were found, all authors used temporary restorative crowns during implant healing. Elaskary et al.⁴⁶ chose to maintain the gingival architecture with personalized provisional healing at the gingival margin level instead of installing a complete restorative crown. Some authors^{43,47,49} described a subgingival concave contour of the immediate restoration to maintain the gingival margin position and create space for the soft tissue ingrown. Nevertheless, Groenendijk et al.⁵⁰ differed in 3 clinical situations that could be found during the extraction procedures and 3 restorative approaches: 1. Gingival recession, which should lead to a more concave contour in the subgingival area of the prosthesis, allowing the growth of soft tissue; 2. Gingival margin in the right position, in which the restoration should support the tissue without compression; and 3. When there was a more coronal position of the gingival margin, the restorative crown should compress the soft tissue to promote a controlled recession.

Table 5. Immediate restoration, period for rehabilitation, esthetic outcomes, and measured parameters

Author/year	Provisionalisation	Definitive prosthesis deliver	Esthetics outcomes	Measure parameters
Noelken et al., 2018 ¹³	The temporary restorations were either manufactured from acrylic denture teeth to be cemented on top of titanium abutments using a temporary cement or individual temporary screw-retained restorations fabricated by a laboratory technician using temporary abutments.	Final restoration fabricated after a minimum of 3 months of healing. Zirconia crowns were cemented on top of zirconia abutments.	The primary outcome parameter of this retrospective study was the facial soft tissue level. The secondary outcome parameters were the width of the keratinized mucosa, the interproximal and facial marginal bone levels, the soft tissue esthetics, and overall implant success.	Evaluation of primary and secondary outcome parameter was measured by a periodontal probe with 1 mm calibration. The Pink Esthetic Score (PES) assessed the configuration of the mesial/distal papillae, the vertical level, the contour and symmetry of the soft tissue margin, and the texture and color of the soft tissue on a rating scale (0–2). The status of the interproximal marginal bone level was determined using digital periapical radiographs with paralleling technique.
Lee et al., 2020 ⁴¹	A provisional abutment with a screw-retained custom provisional crown placed immediately. Provisional crowns were free of any occlusal contact. Details about restoration contours not described.	The patients were referred for definitive restorations 6 months after placement. More details are not described in the paper.	Alterations of bone and soft tissue were measured. Linear regression analysis was performed to analyze the association between different clinical parameters and outcomes of interest.	Measurements of tissue alterations obtained at the follow-up visits included: vertical gingival margin (GM) change: mid-buccal gingival level changes calculated through the measurement obtained from the baseline visit compared with the measurement obtained at the 12-month follow-up visit; horizontal buccal ridge dimensional change: longitudinal remodeling of the buccal ridge in the horizontal plane assessed on casts using a stent to measure changes from presurgical baseline to the 12-month cast, with the reference plane of the measurement located 3 mm apically to the preoperative gingival margin; interproximal marginal bone level change: distance between the most coronal bone to implant contact (BI) and the implant platform level (IP) measured both at the mesial and distal sites on digital periapical radiographs

Table 5. Immediate restoration, period for rehabilitation, esthetic outcomes, and measured parameters – cont.

Author/year	Provisionalisation	Definitive prosthesis deliver	Esthetics outcomes	Measure parameters
Zuiderveld et al., 2017 ⁴²	Immediate implant-level impression taken to fabricate a screw-retained lab-made provisional crown using engaging temporary abutment and composite. Then, a corresponding healing abutment was connected to the implant. The same day as implant placement, the healing abutment was removed and the screw-retained provisional crown was fitted directly onto the implant with 20 N·cm and adjusted to free it from centric contacts with antagonist teeth.	After a 3-month provisional phase, a final open tray impression was taken at implant level using polyether impression material. Next, an individualized zirconia abutment was made. Abutment screws were torqued with 35 N·cm. Depending on the location of the screw access hole, the final crown was screw-retained or cement-retained with glass ionomer cement.	Esthetics of the peri-implant mucosa and implant crown were assessed from photographs taken using the pink esthetic score-white esthetic score (PES/WES).	Change in mid-buccal mucosal level (MBML) compared to the preoperative situation. In addition, gingival biotype, esthetics (using the Pink Esthetic Score – White Esthetic Score), marginal bone level, soft tissue peri-implant parameters and patient satisfaction were assessed.
Ferrantino, et al., 2021 ⁴³	A customized screw-retained resin crown was positioned on an anti-rotational titanium temporary abutment over the implant without any occlusal contact. Special attention was paid to the trans-mucosal shape of the provisional restoration to support the soft-tissue margin of the post-extraction site without any compression and to provide space for a stable blood clot formation.	After 6 months – screw-retained or cemented restoration was fabricated and delivered to the patient after the pick-up impression was treated with a polyether material. For screw-retained restorations, a prefabricated anti-rotational titanium abutment was used, while a customized anti-rotational titanium abutment was manufactured for cemented restorations. Final crowns were either made with monolithic zirconia; porcelain fused to metal or porcelain fused to zirconia.	An esthetic assessment was carried out on digital clinical photos taken during a 1-year follow-up visit on a computer screen by an independent blinded investigator. The pictures of the buccal and occlusal aspects included the 2 adjacent teeth and the contralateral dentition. Further analysis of the primary outcome variable considered the 4 items regarding the esthetic of the mucosa and the 5 items regarding the esthetic appearance of the crown separately.	Implant Crown Aesthetic Index (ICAL) at the 1-year follow-up.
Pohl et al., 2020 ⁴⁴	Provisional rehabilitation in both groups was done using a copy abutment initially in synthetic material exactly imitating the gingival emergence profile of the original tooth. Special care was taken not to give any pressure due to the abutment design to the soft tissues as seen by a change of the color from pink to white as this might influence the soft tissue margin. On the 3 rd to 5 th postoperative day, this abutment was replaced by a copy of zirconium oxide and fixed with a torque of 20 N·cm. Both abutments were provided with the same provisional crown having no interproximal contact with neighboring teeth or eccentric contact with opposing teeth.	After a healing phase of 3–4 months, the abutment screws were fixed using a torque of 25 N·cm, and the provisional crowns were replaced by ceramic crowns by the use of conventional impression technique. In case of a possible visibility of abutment margins due to mucosal retraction, the abutment was ground using diamond drills taking special attention not to touch the soft tissue. The definitive abutments were neither removed at that time nor at any later point of time.	For assessing the buccal soft tissue profile, intra-oral photographs were taken preoperatively and postoperatively after 1 year. The images each comprised the region to be assessed as well as the contralateral tooth. The parameters assessed included: the mesial and distal papilla, the level, contour, color, structure and texture of the soft tissue, and the alveolar ridge of both the test and the control tooth. All measurements of the Pink Esthetic Score (PES) were taken in blinded manner by 2 students in training for dentist, an experienced implantologist and an experienced implant prosthodontist. In addition, a straight line was placed through the most apical point of the gingiva of the neighboring teeth of the implant, and a vertical to this line to the most apical point of the mucosa of the implant crown was determined. Measurements were done in mm based on the actual crown length of one of the neighboring teeth.	The buccal defect was determined with sagittal reconstruction according to the longitudinal axis of the implant in the postoperative cone beam computed tomography (CBCT) scan. The distance between 2 verticals on the implant axis from the most crestal bone margin to the upper implant edge yielded the vertical defect of the buccal lamella. In addition, the maximum size of the defect was evaluated at the transverse section and vertical to the implant axis. For assessing the mesial and distal bone level, intraoral radiographs were taken on the day of surgery and 4, 6, and 12 months postoperatively. The distance between the upper edge of the implant and the first contact of the bone with the implant body was determined both mesially and distally following calibration with the known implant length.

Table 5. Immediate restoration, period for rehabilitation, esthetic outcomes, and measured parameters – cont.

Author/year	Provisionalisation	Definitive prosthesis deliver	Esthetics outcomes	Measure parameters
Staas et al., 2021 ⁴⁵	A titanium temporary customized platform-switch Procera™ abutment was placed allowing fabrication of a composite screw-retained provisional restoration.	After implant placement (3–9 months), the final impression was taken to fabricate either an individualized, screw-retained, zirconium-oxide porcelain veneered crown, or an individualized zirconium-oxide abutment with a resin cemented porcelain.	Correlation between buccal bone thickness and radiographs analyses.	Radiographic procedure measurements. Thickness of the buccal crest was measured at the level of the implant-shoulder, ensuring that thickness of the buccal crest was measured at the same position and angulation at all time points.
Elaskary et al., 2020 ⁴⁶	Customized healing abutment screwed to the implant, adequately finished, and polished to ensure a proper soft tissue emergence profile.	The definitive restoration was delivered 3 months postoperatively.	Two examiners were trained and calibrated to access the esthetic appearance at 6 and 13 months using pink esthetic score (PES). The comparison was made with the contralateral natural tooth. Mesial papilla, distal papilla, soft tissue level, soft tissue contour, deficient alveolar process, soft tissue color, and texture were evaluated.	Cone beam computed tomography (CBCT): superimposing the images at baseline and 6 or 13 months. The facial bone thickness measured on the 6/13 months images from the implant surface to the outer surface of bone at 3 points. Same was done with the contralateral tooth. Facial bone high measured from the facial bone crest and implant platform.
Frizzera et al., 2018 ⁴⁷	20 N·cm screw retained interim restoration or cemented provisional over 20 N·cm torque abutments.	After 6-month final restoration with emergence profile copied from interim restoration. Abutments customized in zirconia and subgingival concave contour to deliver cemented porcelain restoration. Cementation line 0.5 mm bellow gingival margin.	Clinical photographs at baseline and at 6 and 12 months after the surgery, where marginal peri-implant recession (MPR), mesial papilla (MP), and distal papilla (DP) migration were measured based on the adjacent teeth. Pink esthetic score (PES) and modified PES (mPES) were assessed to evaluate soft tissue esthetic outcomes.	Photographic evaluation of peri-implant soft tissue margin and interproximal papillae based on the adjacent teeth. Measurement of the facial bone thickness (FBT) in contact with the implant at different levels, the soft tissue thickness (STT) 2 mm below the gingival margin, and the distance between the implant platform and the 1 st bone-to-implant contact (DIPBIC). Line connecting the mesial and distal bone crest was created and the distance to the palatal bone was recorded to assess the size of the format of the ridge defect (FRD).
Noelken et al., 2013 ⁴⁸	Healing abutments (Healing Abutment Uni 4.5/5.0; Astra Tech AB) were used during the short time of fabrication of the temporary restoration. Manufactured acrylic denture teeth were adjusted to the implant site and cemented on top of titanium abutments (n = 12) using a temporary cement or individual temporary screw-retained restorations fabricated by a laboratory technician using temporary abutments (n = 25). All temporary restorations were inserted at the day of implant placement and adjusted to clear all contacts.	A minimum of 3 months. The final zirconia crowns or bridges were cemented on top of zirconia abutments using a temporary cement or a glass ionomer cement.	–	status of the interproximal marginal bone level was determined using digital periapical radiographs. To ensure reproducibility between the examinations, radiographs were taken with paralleling technique using commercially available film holders. status of the facial bone level was determined with cone beam computed tomography (CBCT) data, specifically by the reconstruction according to the long axis of the teeth/implants at pre-treatment examination, at 1-year and/ or 2-year follow-up. The thickness of the facial bone wall was measured 1, 3, and 6 mm apically to this reference level at the facial aspect of the implant.
da Rosa et al. 2014 ⁴⁹	Provisional crown applied using veneers previously prepared with light curing composite resin. Ideal emergency profile with concave contour allowing free space to accommodate the soft tissue.	After 6 months – cemented metal-ceramic or ceramic zirconia restoration over customized abutment with subgingival contours. Cement line established between 0.5 mm and 1 mm below the gingival margin.	Gingivomorphometry method. Two clinically photographs: 1 week after definitive crown deliver/last follow up visit (1 photograph for rehabilitation planning).	Crown high baseline/follow up; mesial papilla high baseline/follow up; distal papilla high baseline/follow up.

Table 5. Immediate restoration, period for rehabilitation, esthetic outcomes, and measured parameters – cont.

Author/year	Provisionalisation	Definitive prosthesis deliver	Esthetics outcomes	Measure parameters
Groenendijk et al., 2021 ⁵⁰	Titanium temporary abutment positioned onto the implant that allowed the fabrication of a screw-retained temporary crown.	Six months later, either an individualized, screw-retained, zirconium-porcelain crown, or an individualized zirconium abutment with a cemented porcelain facing.	Pink esthetic outcome.	Both the implant and contralateral site were photographed in a standardized way at different timepoints; preoperatively, 7–14 days postoperatively, direct after placement of the permanent crown, and 1 year post-operation. On each time point, 2 light photographs were taken: 1 perpendicular to the mid-buccal of the tooth arch, and 1 perpendicular to the implant site. Before examination, the light photographs were placed in a digital format. Evaluation of the pink esthetic outcome was executed by 2 blinded examiners, who were not involved in the patient treatments.
Sicilia-Felechosa et al., 2019 ⁵¹	Immediately produced in the laboratory a direct-to-implant screw-retained resin provisional prosthesis which completely sealed the gingival alveolus and offered support for soft tissues, without creating additional pressure on the tissues at the critical and subcritical contour levels. The restorations were designed in such a way that no direct occlusal contact was allowed during the 1 st 3 months.	Not described in the paper.	Soft-tissue esthetics were achieved analyzing the intraoral pictures taken in the last follow-up visit according to the Pink Esthetic Score and using the contralateral tooth as a reference. At last, patient subjective satisfaction was secondarily assessed through a clinical questionnaire consisting of 6 questions with 4 options (bad, average, good and excellent) to analyze esthetics, comfort, chewing function, and global evaluation.	The stability of interproximal bone levels was achieved assessing the distance from the implant's platform to the 1 st implant/bone contact point by means of calibrated digital periapical X-rays and using a dedicated software.

One point of convergence between all authors was the necessity of leaving the immediate restoration with a lack of occlusal contacts. Meanwhile, a healing time of 3^{13,42,44–46,48} or 6 months^{41,43,47,49} was allowed before delivering the final restoration (Table 5). Various materials were used for the final crown and the cemented or screw-retained prosthesis. The definitive restorative crowns were made from multiple materials, including metal-ceramic,^{43,49} monolithic zirconia, zirconium oxide^{45,48} or ceramic.⁴⁴ Those prosthetic crowns could be 1 piece screwed to the implant^{43,45} or 2 pieces using a zirconia abutment to receive the cemented crown.^{13,45,48}

Phenotypes and esthetics

Regardless of the importance of the initial phenotype, the thinner the buccal plate thickness, the higher the risk of gingival recession or shrinkage of the alveoli. The final result showed (in most cases across all studies) that the esthetic result can be delivered. The thin phenotype could promote great changes in the mid-buccal gingival margin and the mid-buccal ridge dimension. Also, when combined with flap release, there was an increase in the interproximal gingival recession⁴¹ (Table 6).

Even when IIP and immediate restoration involved compromised sockets presenting with buccal bone deficiency or gingival recession, an increase in the PES could be achieved.⁵⁰ Many different approaches could overcome bone deficiency, as shown by da Rosa et al.,⁴⁹ and achieved stable peri-implant soft tissue levels after 58 months, even in compromised fresh sockets. Another study²⁴ did not proceed with any kind of buccal plate reconstruction or soft tissue augmentation, and, at the end of the follow-up, still demonstrated an increase in PES for patients treated with IIP and immediate restoration in the presence of bone deficiency, even though minimal adjustment of the restoration had to be performed in every patient due to slight alterations of the gingival margin.

Although the association between buccal gap filling and soft tissue augmentation is not mandatory for satisfactory esthetic results,⁴³ its application adjunctive to immediate restoration in IIP seemed to deliver the most predictable treatment, guaranteeing marginal gingival level stability.^{42,46,47} In addition, using subepithelial connective tissue grafts improved the results compared to other soft tissue substitutes.⁴⁷ Even though an expected increase in PES was noticed, reaching the maximal score in 73–89% of cases, there was still a risk of a gingival recession of 1–2 mm in around 20% of the treatments.⁵¹

Table 6. Average bone loss found in the studies included

Authors/year	Average bone loss
Noelken et al., 2018 ¹³	0.1 ±0.5 (range: 1.4–1.1 mm) in the ABG group and 0.0 ±0.5 (range: –1.0–0.9 mm) in the ABG/CTG.
Lee et al., 2020 ⁴¹	The mean buccal ridge dimensional reduction at 12 months was 1.01 ±0.87 mm. The mean interproximal crestal bone loss was 0.81 ±0.90 mm. Mean interproximal marginal bone gain was 1.28 ±2.22 mm.
Zuiderveld et al., 2017 ⁴²	The average loss of marginal bone was 0.06 ±0.42 mm and 0.04 ±0.46 mm on the mesial side in the control and test group, respectively. Distal sides of the control and test groups gained, on average, 0.03 ±0.38 mm and 0.02 ±0.37 mm, respectively. The intergroup results were comparable.
Ferrantino et al., 2021 ⁴³	Not evaluated in the paper.
Pohl et al., 2020 ⁴⁴	The average postoperative bone level for the TG was 2.60 ±2.67 mm (mesial, 2.46 ±3.45 mm; distal 2.97 ±2.40 mm) and for the CG was 1.72 ±1.09 mm (mesial 1.55 ±1.43 mm; distal 1.88 ±0.96 mm), and the bone level at 12 months was 1.58 ±2.33 mm (mesial 1.42 ±2.32 mm; distal 1.75 ±2.34 mm) for TG and 1.42 ±0.71 mm (mesial 1.24 ±0.76 mm; distal 1.59 ±0.82 mm) for CG.
Staas et al., 2021 ⁴⁵	Directly postoperatively (T1), mean BCT increased from 0.6 mm at baseline (SD = 0.5) to 3.3 mm (SD = 1.2). After 1 year (T3) mean BCT reduced to 2.4 mm (SD = 1.1). Mean BCH at T0 was 0.7 mm (SD = 0.5), which enlarged to 3.1 mm (SD = 1.2) directly postoperatively (T1). Over a period of 1 year (T3) BCH condensed to 1.7 mm (SD = 2.4).
Elaskary et al., 2020 ⁴⁶	Initial bone thickness (mean): intact wall – 0.76 ±0.42 mm/bone deficiency – 0 mm. 6 months: intact wall – 1.88 ±0.73 mm/bone deficiency – 2.34 ±0.78 mm. 13 months: intact wall – 1.84 ±0.74 mm/bone deficiency – 2.18 ±0.73 mm. At 13 months, the mean distance from the implant platform to the bone crest in socket with intact bone wall was significant less than in sockets with deficient facial bone. The soft tissue level score was 2 for all cases in both groups, though.
Frizzera et al., 2018 ⁴⁷	No bone loss >1.5 mm detected in periapical radiographs after 1 year follow up.
Noelken et al., 2013 ⁴⁸	Three implants showed a decrease of the marginal bone level of more than 1 mm apically to the reference level. Marginal bone height at the level of the implant shoulder averaged 0.1 ±0.55 mm (range: 1.25–1.47 mm) at the final follow-up. The mean interproximal bone level (as measured against the implant shoulder) changed from 0.82 ±0.96 mm at implant insertion to 0.24 ±0.58 mm at prosthesis delivery, and further to 0.14 ±0.57 mm at the 1-year follow-up. Finally, at the 2-year follow-up, 0.07 ±0.58 mm was recorded. The thickness of the facial bony lamellae at the condemned teeth as well as at the implants measured increased thickness of the facial bone dimension.
da Rosa et al., 2014 ⁴⁹	Not evaluated in the paper.
Groenendijk et al., 2021 ⁵⁰	Not evaluated in the paper.
Sicilia-Felechosa et al., 2019 ⁵¹	Average bone loss ranged from 0.47 mm at 8 weeks of follow-up to 1.45 mm for the case that has been monitored for 7 years. From 8 weeks to 1 year (initial adaptation period), the data from 36 patients showed an apical displacement of the interproximal bone level of 0.25 mm.

ABG – autogenous bone grafting; CTG – connective tissue graft; TG – test group; CG – control group; BCT – buccal crest thickness; SD – standard deviation; BCH – buccal crest height.

Quality assessment

Quality assessment was performed using 2 different risk assessment tools according to the study design. Three RCTs included in this review were assessed using the modified Cochrane risk-of-bias tool,⁴⁰ while all other papers were judged according to the ROBIN-I risk of bias tool. One paper was classified as high risk of bias, 3 had a moderate risk and 8 had a low risk of bias (Fig. 2).

Discussion

This study intended to guide clinicians and clarify the understanding of IIP procedures in esthetic areas, which can involve soft and/or bone tissue grafts to maintain and stabilize the position of the gingival margin. Then, this systematic study aimed to assess whether there is increased esthetic risk in oral rehabilitation with a partial or total absence of the buccal bone plate in esthetic areas when associated with IIP and immediate restoration.

Alveolar bone wall and IIP

Tooth loss leads to alveolar ridge changes in the apical-coronal and buccolingual directions, affecting and compromising the esthetic result of implant-supported rehabilitation. The presence of the marginal bone crest determines the final position of the gingival margin, and the extension of this bone defect can be an esthetic risk factor in IIP. Depending on the bone involvement level, such as in cases of large defects or those involving interproximal areas, alveolar preservation and delayed implant placement have been recommended.⁵² These types of defects can be classified as: 1. Involving the buccal bone wall, with greater or lesser extension restricted to the medial surface; 2. “V” or “U”-shaped defects; and 3. Defects affecting adjacent teeth, such as “UU” defects. In larger defects or those involving papillae, there is a recommendation to perform alveolar preservation and subsequent placement due to the accentuated risk of marginal recession and compromised final esthetic. However, all studies included in this review presented buccal-wall defects at the time of IIP, with various

Articles	Pre intervention	At intervention			Post intervention		
	Bias due confounding	Bias in selection of participant	Bias in classification of intervention	Deviation from intended intervention	Missing data	Measurements of outcomes	Reported results
da Rosa et al.	N	N	N	N	N	N	N
Staas et al.	Y	N	N	N	N	N	N
Groenendijk et al.	Y	N	Y	N	N	N	N
Noelker et al.	N	N	N	N	N	N	N
Pohl et al.	N	N	N	N	N	N	N
Elaskary et al.	N	N	N	N	N	N	N
Neolken et al.	N	Y	Y	N	N	N	N
Sicilia-Felochosa et al.	Y	Y	N	N	N	N	N
Frizzera et al.	N	N	N	N	N	N	N

N = no; Y = yes.

Articles	Blinding participants and personnel	Blinding outcome assessment	Incomplete outcome data	Random sequence generation	Allocation concealment	Selective reporting	Other source of bias
Ferrantino et al.	High	Low	Low	Low	Low	Low	Low
Zuidervelt et al.	High	Low	Low	Low	Low	Low	Low
Lee et al.	High	High	Low	Low	Unclear	High	Low

Articles	Judgement
da Rosa et al.	Low risk of bias
Staas et al.	Low risk of bias
Groenendijk et al.	Moderate risk of bias
Ferrantino et al.	Low risk of bias
Zuidervelt et al.	Low risk of bias
Lee et al.	High risk of bias
Noelker et al.	Low risk of bias
Pohl et al.	Low risk of bias
Elaskary et al.	Low risk of bias
Neolken et al.	Moderate risk of bias
Sicilia-Felochosa et al.	Moderate risk of bias
Frizzera et al.	Low risk of bias

Fig. 2. Risk of bias assessment of non-randomized studies (above) (ROBIN-I), randomized studies (below) (modified Cochrane risk-of-bias tool), and result (judgment)

extensions, with analysis of this paradigm being the goal. Defects ranging from approx. 0.1 mm up to the absence of bone on the entire buccal surface were found, though there was no involvement of the interproximal bone crest.

Elevation of the vestibular flap and exposure of the bone defect can lead to greater procedure-related morbidity, more significant postoperative discomfort, decreased facial blood supply, and compromise the vitality of adjacent

tissues.⁴¹ Otherwise, flapless surgeries allow greater preservation of the buccal bone. Within these facts, most studies reported^{13,24–33,44,51,53} this approach for tooth removal, whereas Lee et al.⁴¹ used a minimally traumatic approach and flap elevation, randomizing the cases. The authors found a greater interproximal gingival recession in the group where the elevation flap was applied.

The need for an intact buccal wall with an unaltered gingival margin and a considerable buccal bone plate volume for IIP, as described by Buser et al.,⁵⁴ or the contraindication of IIP due to large and deep bone defects, as recommended by Kan et al.,⁵² were refuted by Sicilia-Felechosa et al.⁵¹ The latter approached IIP with immediate restoration in defects with more than 2/3 of the buccal bone wall compromised or a probing depth of more than 10 mm. Similarly, Pohl et al.⁴⁴ rehabilitated alveolar sockets with vertical defects ranging from 2.26 mm to 9.68 mm and horizontal defects between 3.2 mm and 5.91 mm, and showed that IIP without additional augmentation, but with immediate provisionalization, was a viable alternative even with the buccal wall missing in the esthetic maxillary zone.

Buccal space and bone grafts

The literature suggests that spaces of at least 2 mm between the implant surface and the buccal wall region, either from the remnant buccal-bone plate or from the buccal mucosa in patients with buccal-wall defects, must be filled by bone grafts to promote a thicker buccal bone wall when >2 mm-wide buccal gaps followed by IIP is done.⁵⁵ In addition, it can favor an adequate emergence profile of less than 30°.⁴⁵ The ideal, or more palatal, implant position could be achieved in a guided manner^{46,51} or by using the palatal wall as a reference. The correct 3D position of the implant consisted of an apical-coronal position 3–4 mm below the ideal gingival margin^{27,42,44–47} in the rehabilitations using conical connections. Meanwhile, in the rehabilitations using internal parallel connections, the implants were positioned at the bone crest level.⁴¹

The correct choice of grafting material to fill the gap allows the maintenance of ridge volume to minimize the losses arising from the facial wall remodeling.⁴⁵ The filling of this space was conducted in some studies^{43,45,47,51} using xenograft, while autogenous bone was the material of choice in other studies.^{42,46,51} Other authors^{13,47,48} chose only autogenous bone differing in particulates or bone lamina removed from the tuberosity; the final esthetic result was not negatively affected even though some decrease of marginal bone level occurred. The research with tuberosity bone did not evaluate the bone response through time, only the soft tissue aspect.

Immediate restoration and esthetic score

Recent studies reported results without augmentation to fill the gap or using a connective tissue graft. They

compared intact and defective alveoli walls in which IIP and immediate restorations were performed with a flap or flapless procedure; moreover, they verified the influence of the subgingival contour in the tissue response.^{41,44} There was an association between flap release and increased interproximal gingival recession,⁴¹ and, despite reporting that the esthetic result could be achieved in all cases regardless of the group, adjustments in the prosthetic margins of less than 0.2 mm had to be performed to make the definitive implant-supported restoration.⁴⁴

In general, preparation of the immediate restoration must respect the contours of the gingival architecture to promote soft tissue support without causing pressure on the gingival margin. In contrast, this contour must be concave below this margin in a subcritical space, allowing soft tissue growth. However, Groenendijk et al.⁵⁰ observed that in the presence of a more coronal position of the gingiva, the provisional restoration should compress the gingival margin and promote apical migration of the soft tissues. The temporary restoration must have no occlusal contact during the wound healing period. Noelken et al.¹³ considered splinting it with the adjacent teeth to prevent micromovements. The permanence of the provisional restoration can range from 3 to 6 months.

Although the recommendation for connective tissue grafts combined with IIP is found in the literature,⁴ increasing the predictability of results, some authors showed no difference in esthetics evaluation and patient satisfaction when comparing those with soft tissue grafts to a group without tissue augmentation.^{42,43} Ferrantino et al.⁴³ described that the complexity of the treatment might explain the different conclusions; the final result of the treatment can also be influenced by the correct development of the provisional restoration, which would help not only in assuring esthetic satisfaction of the patient but also in better healing of the post-extraction socket and the stability of the peri-implant soft tissue. Moreover, the more palatal positioning of the implant, the more influence it has on the maintenance of the gingival margin, allowing space for the creation of a thicker bone crest (after filling the gap) and soft tissue volume gain, even without the need for grafting,⁴⁴ leading to similar results when treating patients with or without gingival margin defects.⁵⁰

Elaskary et al.⁴⁶ demonstrated that the obtention of a buccal bone plate approx. 2 mm thick was possible, even with large bone defects at the time of tooth extraction; however, this was not associated with soft tissue defects. In that study, compensation for the lack of facial wall was provided by a mix of autogenous and xenograft biomaterials covered by a collagen membrane and subepithelial connective tissue graft. Also, both groups (without buccal-wall defects and partially lacking them) had a good score for the peri-implant soft tissue level. Pohl et al.⁴⁴ did not perform any soft or hard tissue graft augmentation to compare alveoli that had IIP with or without defects; therefore, they verified improvement or maintenance of the PES in most

cases. In addition, in all cases, regardless of the group, adjustments in the prosthetic margins were made to obtain the definitive prostheses.

The technique chosen by Sicilia-Felochosa et al.⁵¹ was autogenous or allogeneic connective tissue grafts combined with bone filling of the facial defect (autogenous bone grafts and/or deproteinized bovine bone mineral) without a collagen membrane. The authors obtained a 98% success rate over a 7-year follow-up. High success rates were associated with good esthetic results, with more than 70% of patients having a PES equal to or greater than 12 (PES index between 0 and 14). However, 8 out of 39 patients followed up (21.6%) had a 1–2 mm recession, compromising the final score.

Frizzera et al.⁴⁷ compared the results of 3 groups that received IIP, analyzing the different responses for connective tissue graft, collagen matrix and non-soft tissue augmentation. In all procedures, the gaps were filled with bone grafts covered by collagen membranes to isolate the buccal defect. The best result was found when utilizing an autogenous connective tissue graft, maintaining the volume obtained after 12 months. In addition, even though no recession was detected in the groups, the palatal position of the implant associated with a subcritical prosthetic contour allowed tissue growth. Therefore, soft tissue depression or color change was observed when the autogenous soft tissue was not used.

Limitations

The present systematic review had some limitations: 1. A low number of clinical studies were included ($n = 12$), which suggests that more well-standardized trials with long-term analysis are required to better verify tissue stability; 2. No other biomaterial was used to fill the gap between the implant and buccal wall or combined with the implant,¹⁷ such as bone graft with platelet-rich fibrin (PRF) or PRF alone. This fact can be considered in future investigations due to the potential of healing presented by PRF^{56,57}; 3. 33.3% of the studies ($n = 4$) had a moderate or high risk of bias; 4. Only 1 study showed long-term results (around 58 months); 5. Hexagon implants were sometimes used, which typically cause more marginal bone loss than morse-taper implants⁵⁸; and 6. There was some divergence in the type of tools used among the studies, which can cause impairment or confusion; 7. The effect of abutment disconnection, which is important for the maintenance of soft tissue height, was not evaluated in the included studies.

Conclusions

Considering the limitations of this systematic review, the consensus was that an esthetic result and increased final PES or patient satisfaction index in IIP treatments

associated with immediate restoration could be obtained even in the presence of buccal bone wall defects or gingival recession, regardless of their extension. Thus, there is no absolute contraindication for this type of treatment, but extreme attention to the treatment plan is recommended.

Supplementary data

The Supplementary materials are available at <https://doi.org/10.5281/zenodo.8410418>. The package includes the following files:

Supplementary Table 1. Inclusion and exclusion criteria used in the studies selected in this study.

Supplementary Table 2. Conclusions of the evaluated studies.

ORCID iDs

Sergio Charifker Ribeiro Martins

<https://orcid.org/0000-0003-2848-7677>

Marcio da Costa Marques <https://orcid.org/0000-0003-0810-312X>

Pedro Henrique Moreira Paulo Tolentino

<https://orcid.org/0000-0001-9631-3885>

Roberto Galvão Dinelli <https://orcid.org/0000-0003-4217-8678>

Gustavo Vicentis de Oliveira Fernandes

<https://orcid.org/0000-0003-3022-4390>

Jamil Awad Shibli <https://orcid.org/0000-0003-1971-0195>

References

- Helal O, Göstemeyer G, Krois J, Fawzy El Sayed K, Graetz C, Schwenck F. Predictors for tooth loss in periodontitis patients: Systematic review and meta-analysis. *J Clin Periodontol*. 2019;46(7):699–712. doi:10.1111/jcpe.13118
- Monteiro R, Moura-Netto C, Veiga N, Amaral S, Fernandes G. Periodontal regeneration after third molar extraction causing attachment loss in distal and furcation sites of the second molar: A case report with 12 months follow-up. *J Clin Rev Case Rep*. 2022;7(11):128–132. <https://www.opastpublishers.com/open-access-articles/periodontal-regeneration-after-third-molar-extraction-causing-attachment-loss-in-distal-and-furcation-sites-of-the-second-molar.pdf>. Accessed November 2, 2023.
- Heboyan A, Avetisyan A, Karobari MI, et al. Tooth root resorption: A review. *Sci Prog*. 2022;105(3):003685042211092. doi:10.1177/00368504221109217
- De Siqueira GRC, Tavares JR, Pedrosa RF, De Siqueira RAC, Fernandes GVDO. Immediate implant with provisionalization and soft tissue grafting after 4-year follow-up. *Clin Adv Periodontics*. 2022;12(1):32–38. doi:10.1002/cap.10162
- Araujo MG, Lindhe J. Dimensional ridge alterations following tooth extraction. An experimental study in the dog. *J Clin Periodontol*. 2005;32(2):212–218. doi:10.1111/j.1600-051X.2005.00642.x
- Van Der Weijden F, Dell'Acqua F, Slot DE. Alveolar bone dimensional changes of post-extraction sockets in humans: A systematic review. *J Clin Periodontol*. 2009;36(12):1048–1058. doi:10.1111/j.1600-051X.2009.01482.x
- Tan WL, Wong TLT, Wong MCM, Lang NP. A systematic review of post-extraction alveolar hard and soft tissue dimensional changes in humans. *Clin Oral Implants Res*. 2012;23(Suppl 5):1–21. doi:10.1111/j.1600-0501.2011.02375.x
- Scala A, Lang NP, Schweikert MT, De Oliveira JA, Rangel-Garcia I, Botticelli D. Sequential healing of open extraction sockets: An experimental study in monkeys. *Clin Oral Implants Res*. 2014;25(3):288–295. doi:10.1111/clr.12148
- Isella JM, Greenwell H, Miller RL, et al. Ridge preservation with freeze-dried bone allograft and a collagen membrane compared to extraction alone for implant site development: A clinical and histologic study in humans. *J Periodontol*. 2003;74(7):990–999. doi:10.1902/jop.2003.74.7.990

10. Wang RE, Lang NP. Ridge preservation after tooth extraction. *Clin Oral Implants Res.* 2012;23(Suppl 6):147–156. doi:10.1111/j.1600-0501.2012.02560.x
11. Barone A, Ricci M, Tonelli P, Santini S, Covani U. Tissue changes of extraction sockets in humans: A comparison of spontaneous healing vs ridge preservation with secondary soft tissue healing. *Clin Oral Implants Res.* 2013;24(11):1231–1237. doi:10.1111/j.1600-0501.2012.02535.x
12. Kan JYK, Rungcharassaeng K, Deflorian M, Weinstein T, Wang H, Tesitori T. Immediate implant placement and provisionalization of maxillary anterior single implants. *Periodontol 2000.* 2018;77(1):197–212. doi:10.1111/prd.12212
13. Noelken R, Moergel M, Pausch T, Kunkel M, Wagner W. Clinical and esthetic outcome with immediate insertion and provisionalization with or without connective tissue grafting in presence of mucogingival recessions: A retrospective analysis with follow-up between 1 and 8 years. *Clin Implant Dent Rel Res.* 2018;20(3):285–293. doi:10.1111/cid.12595
14. Bittner N, Schulze-Späte U, Silva C, et al. Changes of the alveolar ridge dimension and gingival recession associated with implant position and tissue phenotype with immediate implant placement: A randomised controlled clinical trial. *Int J Oral Maxillofac Implants (Berl).* 2019;12(4):469–480. PMID:31781700.
15. Baskaran P, Prakash PSG, Appukkuttan D, et al. Clinical and radiological outcomes for guided implant placement in sites preserved with bioactive glass bone graft after tooth extraction: A controlled clinical trial. *Biomimetics.* 2022;7(2):43. doi:10.3390/biomimetics7020043
16. Borges H, Correia A, Castilho R, Fernandes G. Zirconia implants and marginal bone loss: A systematic review and meta-analysis of clinical studies. *Int J Oral Maxillofac Implants.* 2020;35(4):707–720. doi:10.11607/jomi.8097
17. De Oliveira Fernandes G, Santos N, De Sousa M, Fernandes J. Liquid platelet-rich fibrin coating implant surface to enhance osseointegration: A double-blinded, randomized split-mouth trial with 1-year follow-up. *Int J Oral Maxillofac Implants.* 2022;37(1):159–170. doi:10.11607/jomi.9107
18. Couto BADA, Fernandes JCH, Saavedra-Silva M, Roca H, Castilho RM, Fernandes GVD. Antisclerostin effect on osseointegration and bone remodeling. *J Clin Med.* 2023;12(4):1294. doi:10.3390/jcm12041294
19. Orvalho JM, Fernandes JCH, Moraes Castilho R, Fernandes GVO. The macrophage's role on bone remodeling and osteogenesis: A systematic review [published online as ahead of print on February 20, 2023]. *Clin Rev Bone Miner Metab.* 2023. doi:10.1007/s12018-023-09286-9
20. Fernandes PRE, Otero AIP, Fernandes JCH, Nassani LM, Castilho RM, De Oliveira Fernandes GV. Clinical performance comparing titanium and titanium–zirconium or zirconia dental implants: A systematic review of randomized controlled trials. *Dent J.* 2022;10(5):83. doi:10.3390/dj10050083
21. Kucera O, Lotková H, Kand'ár R, Hézová R, Muzáková V, Cervinková Z. The model of D-galactosamine-induced injury of rat hepatocytes in primary culture. *Acta Medica (Hradec Kralove).* 2006;49(1):59–65. PMID:16696445.
22. Cho YB, Moon SJ, Chung CH, Kim HJ. Resorption of labial bone in maxillary anterior implant. *J Adv Prosthodont.* 2011;3(2):85–89. doi:10.4047/jap.2011.3.2.85
23. Tarnow D, Chu S, Salama M, et al. Flapless postextraction socket implant placement in the esthetic zone: Part 1. The effect of bone grafting and/or provisional restoration on facial-palatal ridge dimensional change: A retrospective cohort study. *Int J Periodontics Restorative Dent.* 2014;34(3):323–331. doi:10.11607/prd.1821
24. Groenendijk E, Staas TA, Bronkhorst E, Raghoobar GM, Meijer GJ. Immediate implant placement and provisionalization: Aesthetic outcome 1 year after implant placement. A prospective clinical multicenter study. *Clin Implant Dent Relat Res.* 2020;22(2):193–200. doi:10.1111/cid.12883
25. Lee C, Chiu T, Chuang S, Tarnow D, Stoupe J. Alterations of the bone dimension following immediate implant placement into extraction socket: Systematic review and meta-analysis. *J Clin Periodontol.* 2014;41(9):914–926. doi:10.1111/jcpe.12276
26. Cardaropoli G, Araújo M, Lindhe J. Dynamics of bone tissue formation in tooth extraction sites: An experimental study in dogs. *J Clin Periodontol.* 2003;30(9):809–818. doi:10.1034/j.1600-051X.2003.00366.x
27. Buckwalter JA, Glimcher MJ, Cooper RR, Recker R. Bone biology. I: Structure, blood supply, cells, matrix, and mineralization. *Instr Course Lect.* 1996;45:371–386. PMID:8727757.
28. Lin CY, Wang HL. Facial fenestration and dehiscence defects associated with immediate implant placement without flap elevation in anterior maxillary ridge: A preliminary cone beam computed tomography study. *Int J Oral Maxillofac Implants.* 2018;33(5):1112–1118. doi:10.11607/jomi.6575
29. Zhang W, Skrypczak A, Weltman R. Anterior maxilla alveolar ridge dimension and morphology measurement by cone beam computerized tomography (CBCT) for immediate implant treatment planning. *BMC Oral Health.* 2015;15(1):65. doi:10.1186/s12903-015-0055-1
30. Elian N, Cho SC, Froum S, Smith RB, Tarnow DP. A simplified socket classification and repair technique. *Pract Proced Aesthet Dent.* 2007;19(2):99–104; quiz 106. PMID:17491484.
31. Kaminaka A, Nakano T, Ono S, Kato T, Yatani H. Cone-beam computed tomography evaluation of horizontal and vertical dimensional changes in buccal peri-implant alveolar bone and soft tissue: A 1-year prospective clinical study. *Clin Implant Dent Rel Res.* 2015;17(Suppl 2):e576–e585. doi:10.1111/cid.12286
32. Chan HL, Garaicoa-Pazmino C, Suarez F, et al. Incidence of implant buccal plate fenestration in the esthetic zone: A cone beam computed tomography study. *Int J Oral Maxillofac Implants.* 2014;29(1):171–177. doi:10.11607/jomi.3397
33. Cardaropoli G, Lekholm U, Wennstrom JL. Tissue alterations at implant-supported single-tooth replacements: A 1-year prospective clinical study. *Clin Oral Implants Res.* 2006;17(2):165–171. doi:10.1111/j.1600-0501.2005.01210.x
34. Takuma T, Oishi K, Manabe T, Yoneda S, Nagata T. Buccal bone resorption around posterior implants after surgery: A 1-year prospective study. *Int J Oral Maxillofac Implants.* 2014;29(3):634–641. doi:10.11607/jomi.3018
35. Januário AL, Duarte WR, Barriviera M, Mesti JC, Araújo MG, Lindhe J. Dimension of the facial bone wall in the anterior maxilla: A cone-beam computed tomography study. *Clin Oral Implants Res.* 2011;22(10):1168–1171. doi:10.1111/j.1600-0501.2010.02086.x
36. Fuentes R, Flores T, Navarro P, Salamanca C, Beltrán V, Borie E. Assessment of buccal bone thickness of aesthetic maxillary region: A cone-beam computed tomography study. *J Periodontol Implant Sci.* 2015;45(5):162–168. doi:10.5051/jpis.2015.45.5.162
37. Zekry A, Wang R, Chau ACM, Lang NP. Facial alveolar bone wall width: A cone-beam computed tomography study in Asians. *Clin Oral Implants Res.* 2013;25(2):194–206. doi:10.1111/clr.12096
38. Vera C, De Kok IJ, Chen W, Reside G, Tyndall D, Cooper LF. Evaluation of post-implant buccal bone resorption using cone beam computed tomography: A clinical pilot study. *Int J Oral Maxillofac Implants.* 2012;27(5):1249–1257. PMID:23057042.
39. Ortega-Martinez J, Perez-Pascual T, Mareque-Bueno S, Hernandez-Alfaro F, Ferrer-Padro E. Immediate implants following tooth extraction: A systematic review. *Med Oral Patol Oral Cir Bucal.* 2012;17(2):e251–e261. doi:10.4317/medoral.17469
40. Higgins JPT, Altman DG, Gotzsche PC, et al. The Cochrane Collaboration's tool for assessing risk of bias in randomised trials. *BMJ.* 2011;343:d5928. doi:10.1136/bmj.d5928
41. Lee C, Sanz-Miralles E, Zhu L, Glick J, Heath A, Stoupe J. Predicting bone and soft tissue alterations of immediate implant sites in the esthetic zone using clinical parameters. *Clin Implant Dent Relat Res.* 2020;22(3):325–332. doi:10.1111/cid.12910
42. Zuiderveld EG, Meijer HJA, Den Hartog L, Vissink A, Raghoobar GM. Effect of connective tissue grafting on peri-implant tissue in single immediate implant sites: A RCT. *J Clin Periodontol.* 2017;45(2):253–264. doi:10.1111/jcpe.12820
43. Ferrantino L, Camurati A, Gambino P, et al. Aesthetic outcomes of non-functional immediately restored single post-extraction implants with and without connective tissue graft: A multicentre randomized controlled trial. *Clin Oral Implants Res.* 2021;32(6):684–694. doi:10.1111/clr.13733
44. Pohl V, Fürhauser L, Haas R, Pohl S. Gingival recession behavior with immediate implant placement in the anterior maxilla with buccal dehiscence without additional augmentation: A pilot study. *Clin Oral Invest.* 2020;24(4):1455–1464. doi:10.1007/s00784-019-03176-5
45. Staas TA, Groenendijk E, Bronkhorst E, Verhamme L, Raghoobar GM, Meijer GJ. Does initial buccal crest thickness affect final buccal crest thickness after flapless immediate implant placement and provisionalization: A prospective cone beam computed tomogram cohort study. *Clin Implant Dent Relat Res.* 2022;24(1):24–33. doi:10.1111/cid.13060

46. Th Elaskary A, Gaweesh YY, Maebed M, Cho SC, El Tantawi M. A novel method for immediate implant placement in defective fresh extraction sites. *Int J Oral Maxillofac Implants*. 2020;35(4):799–807. doi:10.11607/jomi.8052
47. Frizzera F, De Freitas R, Muñoz-Chávez O, Cabral G, Shibli J, Marcantonio E. Impact of soft tissue grafts to reduce peri-implant alterations after immediate implant placement and provisionalization in compromised sockets. *Int J Periodontics Restorative Dent*. 2018;39(3):381–389. doi:10.11607/prd.3224
48. Noelken R, Neffe BA, Kunkel M, Wagner W. Maintenance of marginal bone support and soft tissue esthetics at immediately provisionalized OsseoSpeed™ implants placed into extraction sites: 2-year results. *Clin Oral Implants Res*. 2013;25(2):214–220. doi:10.1111/clr.12069
49. Martins Da Rosa JC, Pértile De Oliveira Rosa AC, Francischone CE, Salles Sotto-Maior B. Esthetic outcomes and tissue stability of implant placement in compromised sockets following immediate dentoalveolar restoration: Results of a prospective case series at 58 months follow-up. *Int J Periodontics Restorative Dent*. 2014;34(2):199–208. doi:10.11607/prd.1858
50. Groenendijk E, Bronkhorst EM, Meijer GJ. Does the pre-operative buccal soft tissue level at teeth or gingival phenotype dictate the aesthetic outcome after flapless immediate implant placement and provisionalization? Analysis of a prospective clinical case series. *Int J Implant Dent*. 2021;7(1):84. doi:10.1186/s40729-021-00366-3
51. Sicilia-Felechosa A, Pereira-Fernández A, García-Lareu J, Bernardo-González J, Sicilia-Blanco P, Cuesta-Fernández I. Flapless immediate implant placement and provisionalization in periodontal patients: A retrospective consecutive case-series study of single-tooth sites with dehiscence-type osseous defects. *Clin Oral Implants Res*. 2019;31(3):229–238. doi:10.1111/clr.13559
52. Kan JYK, Rungcharassaeng K, Sclar A, Lozada JL. Effects of the facial osseous defect morphology on gingival dynamics after immediate tooth replacement and guided bone regeneration: 1-year results. *J Oral Maxillofac Surg*. 2007;65(7 Suppl 1):13–19. doi:10.1016/j.joms.2007.04.006
53. Zuiderveld EG, Meijer HJA, Vissink A, Raghoobar GM. The influence of different soft-tissue grafting procedures at single implant placement on esthetics: A randomized controlled trial. *J Periodontol*. 2018;89(8):903–914. doi:10.1002/JPER.18-0061
54. Buser D, Chappuis V, Belser UC, Chen S. Implant placement post extraction in esthetic single tooth sites: When immediate, when early, when late? *Periodontol 2000*. 2017;73(1):84–102. doi:10.1111/prd.12170
55. Levine RA, Dias DR, Wang P, Araújo MG. Effect of the buccal gap width following immediate implant placement on the buccal bone wall: A retrospective cone-beam computed tomography analysis. *Clin Implant Dent Relat Res*. 2022;24(4):403–413. doi:10.1111/cid.13095
56. Simões-Pedro M, Tróia PMBPS, Dos Santos NBM, Completo AMG, Castilho RM, De Oliveira Fernandes GV. Tensile strength essay comparing three different platelet-rich fibrin membranes (L-PRF, A-PRF, and A-PRF+): A mechanical and structural in vitro evaluation. *Polymers (Basel)*. 2022;14(7):1392. doi:10.3390/polym14071392
57. Pascoal MDANC, Dos Santos NBM, Completo AMG, Fernandes GV. Tensile strength assay comparing the resistance between two different autologous platelet concentrates (leucocyte-platelet rich fibrin versus advanced-platelet rich fibrin): A pilot study. *Int J Implant Dent*. 2021;7(1):1. doi:10.1186/s40729-020-00284-w
58. Fuda S, Martins BGDS, Castro FCD, et al. Marginal bone level and clinical parameter analysis comparing external hexagon and Morse taper implants: A systematic review and meta-analysis. *Diagnostics (Basel)*. 2023;13(9):1587. doi:10.3390/diagnostics13091587

Prebiotics and sepsis in infants: An updated systematic review and meta-analysis

Yuejia Qin^{1,2,3,4,A–D}, Linhui Pan^{1,3,4,E,F}

¹ Anesthesiology Department, Tumor Hospital Affiliated to Guangxi Medical University, Nanning, China

² Intensive Care Unit, Liuzhou People's Hospital Affiliated to Guangxi Medical University, China

³ Guangxi Clinical Research Center for Anesthesiology (GK AD22035214), Nanning, China

⁴ Guangxi Health Commission Key Laboratory of Basic Science and Prevention of Perioperative Organ Dysfunction, Nanning, China

A – research concept and design; B – collection and/or assembly of data; C – data analysis and interpretation;

D – writing the article; E – critical revision of the article; F – final approval of the article

Advances in Clinical and Experimental Medicine, ISSN 1899–5276 (print), ISSN 2451–2680 (online)

Adv Clin Exp Med. 2024;33(9):999–1005

Address for correspondence

Linhui Pan

E-mail: dr_pan2@sina.com

Funding sources

Funding for self-funded project (chief investigator: Yuejia Qin) from Guangxi Health Commission (grant No. Z20200089, 2020–2023).

Conflict of interest

None declared

Received on March 28, 2023

Reviewed on August 31, 2023

Accepted on October 19, 2023

Published online on January 5, 2024

Abstract

Background. Sepsis is a critical situation, and its treatment and reduction are important clinical issues. Antibiotics are a routine treatment option, but their adverse effects are a concern in pediatric patients, especially infants. Prebiotics might be an alternative option.

Objectives. The aim of this study was to provide an updated systemic review and meta-analysis of randomized controlled trials (RCTs) on the use of prebiotics for sepsis in infants, which could assist clinicians in deciding whether to use this treatment.

Methods. The study included RCTs related to prebiotics and sepsis in infants. A random effects model and the odds ratio (OR) were applied to estimate the effect of prebiotic use and the incidence of sepsis in infants. The analysis included 16 studies with a total of 6,438 infants. The primary outcome was the OR of sepsis for infants who received prebiotics.

Results. The results of the meta-analysis demonstrated that the pooled OR of sepsis was significantly lower for infants who used prebiotics. However, the results indicated a medium level of heterogeneity.

Conclusions. The results showed that the use of prebiotics might be associated with a reduction of sepsis in infants. The standardized application of this treatment might be an intriguing topic for future clinical research.

Key words: sepsis, meta-analysis, odds ratio, infant, prebiotic

Cite as

Qin Y, Linhui Pan L. Prebiotics and sepsis in infants: An updated systematic review and meta-analysis. *Adv Clin Exp Med.* 2024;33(9):999–1005. doi:10.17219/acem/174307

DOI

10.17219/acem/174307

Copyright

Copyright by Author(s)

This is an article distributed under the terms of the Creative Commons Attribution 3.0 Unported (CC BY 3.0) (<https://creativecommons.org/licenses/by/3.0/>)

Introduction

Infants are prone to sepsis, especially those with lower birth weight, lower gestational age, asphyxia, and those administered antibiotics.^{1–3} In addition, infants can easily contract infections, such as necrotizing enterocolitis, which can lead to sepsis and alterations in laboratory parameters.⁴ Changes in non-cytotoxic T lymphocytes could also occur after the onset of sepsis due to the suppression of immune function in infants.⁵ Furthermore, sepsis in infants may result in warm shock physiology accompanied by vasodilation, which could contribute to septic shock and increase the mortality rate.⁶ Therefore, understanding the relationship between infants and sepsis is critical.

The therapeutic options for treating sepsis in infants are limited. Mechanical ventilation and empirical antibiotics have been reported to be associated with higher sepsis frequency in infants.^{1–3} Thus, clinicians may need to establish other therapeutic options for such patients, and one possible alternative is prebiotics. The current evidence on the mechanisms of prebiotics in immune function mostly comes from animal studies, which provide clues about how to relieve sepsis in infants through immunomodulatory actions.

Prebiotics could promote the growth of beneficial bacteria, enhance immune-stimulatory processes, and increase the expression of immunomodulatory functions with antioxidant characteristics.^{7–9} Furthermore, they may enhance intestinal trophic effects and immune system maturation.¹⁰

Oligosaccharides from human breast milk are prebiotics that have been shown to modulate immune responses,¹¹ which is consistent with the latest studies on the mechanisms of prebiotic effects on immunomodulatory function. In addition, prebiotics seem to have no significant side effects,¹² and may help to avoid mechanical ventilation use in infants. Therefore, they have the potential to decrease sepsis risk in such patients.¹³

Objectives

Sepsis is a critical situation in clinical practice for which antibiotic therapy is a routine option. However, adverse effects of antibiotics have to be considered in pediatric patients. This meta-analysis aimed to provide an update on the effects of prebiotic use in sepsis events in infants. Based on the literature, we hypothesized that prebiotics would decrease the risk of sepsis. We included randomized controlled trials (RCTs) with placebo controls (no administration of prebiotics) due to the lower risk of bias in such studies. The results could provide valuable information on how to manage infants.

Methods

Literature database and enrollment criteria

We searched the literature using the following keywords: “prebiotic,” “versus,” “placebo,” “comparison,” “short-chain galacto-oligosaccharides,” “long-chain fructo-oligosaccharides,” “pectin-derived acidic oligosaccharides,” “acidic oligosaccharides,” “sepsis,” “neonate,” “infant,” “septic,” “oligosaccharides,” “fructans,” “oligofructose,” “inulin,” “randomized,” “clinical,” “controlled,” “trials,” “treatment,” “therapy,” “efficacy,” and “outcome.” We searched the ScienceDirect, PubMed, Web of Science, Embase, and the Cochrane Central Register of Controlled Trials databases for relevant prospective RCT studies published before October 2022. The inclusion criteria were: 1. Studies comparing prebiotics with placebo in infants; 2. Those with information on the sepsis characteristics, including the occurrence and rates; 3. Reports published in journals in the Science Citation Index Database written in English; and 4. RCTs with a placebo-controlled design.

Assessment of study quality and data collection

We conducted the meta-analysis in accordance with the Cochrane Handbook for Systematic Reviews and Interventions¹⁴ and the Preferred Reporting Items for Systematic Reviews and Meta-Analyses (PRISMA) guidelines.¹⁵ Data collected from the studies included sepsis events, the number of infants who experienced such events after receiving prebiotics or a placebo, the odds ratio (OR), and the standard error (SE).

Data collection and assessment

Two reviewers screened abstracts and collections of articles and extracted data on sepsis outcomes from the texts, tables and figures. The risk of bias was then assessed according to the following criteria: 1. Bias arising from the randomization process; 2. Bias due to deviations from intended interventions; 3. Bias due to missing outcome data; 4. Bias in the measurement of the outcomes, and 5. Bias in the selection of the reported results. The reviewers showed strong agreement in their assessments ($\kappa = 0.9$). Ultimately, the final results were reviewed by all authors.

Meta-analysis and statistical analysis

We generated pooled estimates of the relative risks (RRs) and ORs for sepsis events and prebiotic treatments and used the Cochrane Collaboration Review Manager Software Package RevMan v. 5.4 (Cochrane Collaboration, Copenhagen, Denmark) to perform the meta-analyses.

The Mantel–Haenszel method was used to calculate RR, with DerSimonian and Laird’s random effects models and summary statistics also produced. The risk estimates of individual studies were combined using the variance-weighted averages in the random effects model.

The group that received prebiotic treatments and the control group were compared to determine whether prebiotics decreased the rate of sepsis events. The χ^2 tests were performed, and the I^2 statistic was used to examine the heterogeneity between studies.¹⁵ According to the Cochrane Handbook for Systematic Reviews and Interventions,¹⁴ the choice between a fixed-effect and a random-effects meta-analysis should not solely be made according to the statistical test for heterogeneity. Methodological or conceptual heterogeneity is unavoidable in a meta-analysis, so a random effects model may be more reasonable. Therefore, a random effects model was applied in this study. Two-sided p-values were obtained from the statistical analyses, and a funnel plot was used to assess publication bias.

Results

Study screening and enrollment

After the initial search, 112 articles were selected, with no additional records found from other sources. These articles included 59 duplicates, which were removed. After evaluating the relevance of the abstracts and titles of the remaining

53 articles, 19 were excluded. The full texts of the remaining 34 articles were screened, and 18 more were discarded.

Ultimately, 16 articles were included in the meta-analysis.^{16–31} The PRISMA flow diagram of this study is shown in Fig. 1. The prebiotics group included 3,211 infants, with 3,227 infants in the control group (the total population size was 6,438). Table 1 summarizes the demographic data and characteristics of the 16 studies. Figure 2 shows the assessment of risk bias of the included 16 studies.

Risk ratio and odds ratio of sepsis events between groups

The prebiotics group had a significantly lower RR of sepsis events according to the random effects model ($Z = 3.70$ and $p = 0.001$ for overall effect). Low heterogeneity was obtained, with an I^2 value of 32% (Fig. 3). The prebiotics group also had a significantly lower OR of sepsis events according to the model ($Z = 3.31$ and $p = 0.001$ for overall effect), and the heterogeneity was low, with an I^2 value of 38% (Fig. 4).

Discussion

The results suggest that prebiotic treatment could be beneficial for reducing the rate of sepsis events in this large sample of infants, which was supported by the RR, OR and 95% confidence intervals (95% CIs). One strength of this

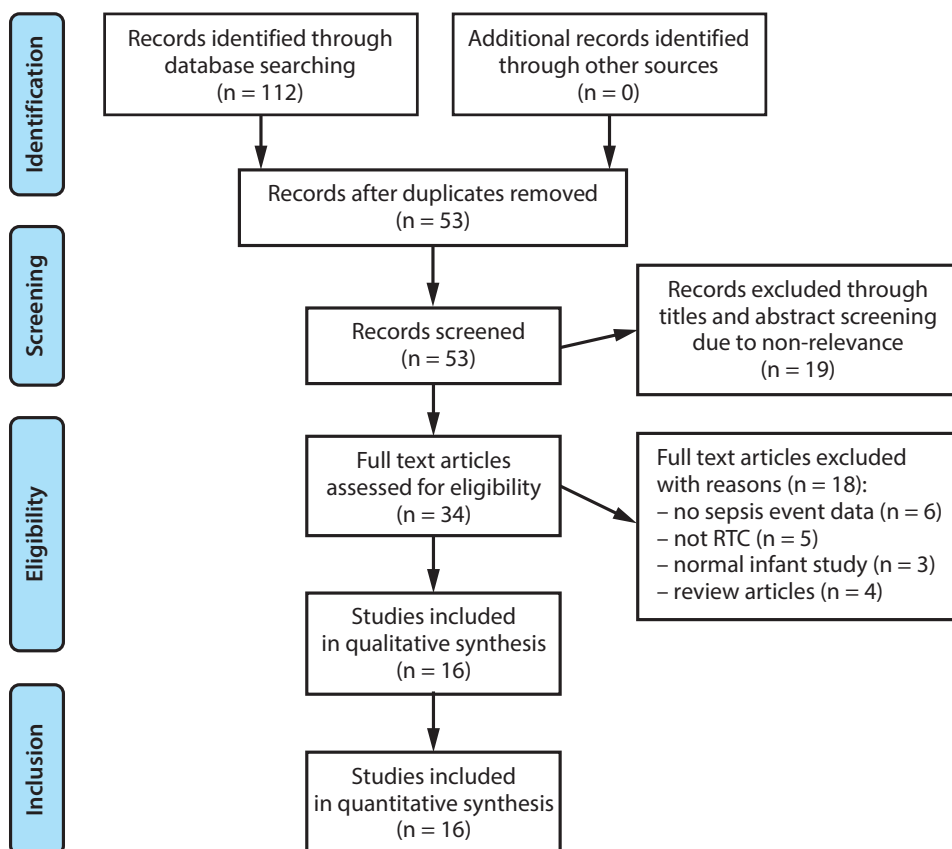


Fig. 1. Preferred Reporting Items for Systematic Reviews and Meta-Analyses (PRISMA) flowchart. The identification and selection of potentially relevant literature, through abstract and title screening, adhered to the PRISMA guidelines. The full texts of eligible studies were screened, and suitable articles were enrolled into the final meta-analysis

Table 1. Summary of enrolled studies

Studies	Subjects (prebiotic compared to control)	Prebiotic content compared to control	Blinded and treatment duration	Outcome of interest
Armanian et al., 2016 (Iran) ¹⁶	25 (30.48 ±2.31 weeks old) compared to 50 (29.80 ±2.16 weeks old)	short chain galactooligosaccharides/ long chain fructooligosaccharides 1.5 g/kg/day compared to distilled water	double-blinded 21 days	growth of beneficial <i>Lactobacillus</i> colonies, sepsis, fecal microbiota pattern, duration of dependency to oxygen, hospitalization, and death
Campeotto et al., 2011 (France) ¹⁷	24 (15 M, 9 F, 33.5 ±1.3 weeks old) compared to 34 (16 M, 18 F, 33.4 ±1.4 weeks old)	fermentation-induced non-digestible oligosaccharides compared to formula	double-blinded 30 days	benefits on inflammatory and immune markers, sepsis, inflammatory and immune markers
Dasopoulou et al., 2015 (Greece) ¹⁸	85 (34 ±0.33 weeks old) compared to 82 (34 ±0.33 weeks old)	short chain galactooligosaccharides/ long chain fructooligosaccharides 1.2 g/kg/day compared to formula	double-blinded 16 days	increase motilin, reduce gastric residue, motilin, necrotizing enterocolitis, mortality, sepsis, and feeding intolerance
Dilli et al., 2015 (Turkey) ¹⁹	100 (52 M, 48 F, 29 ±1.7 weeks old) compared to 100 (58 M, 42 F, 28.2 ±2.2 weeks old)	inulin 1.35 g/kg/day compared to maltodextrin	double-blinded 56 days	inulin could not decrease necrotizing enterocolitis sepsis, mortality, duration of hospital stay
Guney-Varal et al., 2017 (Turkey) ²⁰	70 (29.7 ± 1.9 weeks old compared to 40 (29.3 ± 1.7 weeks old)	383 mg of fructooligosaccharides and 100 mg of galactooligosaccharides compared to formula	double-blinded 36.5 ±12.6 days	≥stage 2 necrotizing enterocolitis and mortality, culture-proven sepsis and days to reach full enteral feeding
LeCouffe et al., 2014 (the Netherlands) ²¹	48 (26 M, 22 F, 30.2 ±1.6 weeks old) compared to 45 (26 M, 19 F, 29.5 ±2.0 weeks old)	short chain galactooligosaccharides/ long chain fructooligosaccharides, pectin-derived acidic oligosaccharides 1.5 g/kg/day compared to maltodextrin	single-blinded 28 days	neurodevelopmental outcome, sepsis
Luoto et al., 2014 (Finland) ²²	23 (11 M, 12 F) compared to 24 (19 M, 5 F) 32–35 weeks old	short chain galactooligosaccharides/ polydextrose 1.2 g/kg/day compared to microcrystalline cellulose and dextrose anhydrate	double-blinded 57 days	respiratory tract infections and its duration, sepsis
Modi et al., 2010 (UK) ²³	73 (48 M, 25 F, 30 ±0.5 weeks old) compared to 81 (50 M, 31 F, 31 ±0.5 weeks old)	short chain galactooligosaccharides/ long chain fructooligosaccharides 1.2 g/kg/day compared to formula	double-blinded 28 days	necrotizing enterocolitis, mortality, sepsis, feeding intolerance
Nandhini et al., 2016 (India) ²⁴	108 compared to 110	100 mg of fructooligosaccharide compared to no intervention	open-label 7 days	necrotizing enterocolitis, mortality, sepsis, hospitalization duration, number of days to reach full enteral feeding and colony counts in stool culture
Niele et al., 2013 (the Netherlands) ²⁵	48 (30.1 ±1.6 weeks old) compared to 46 (29.5 ±2 weeks old)	short chain galactooligosaccharides/ long chain fructooligosaccharides, pectin-derived acidic oligosaccharides 1.5 g/kg/day compared to maltodextrin	double-blinded 28 days	allergic and infectious diseases, sepsis
Panigrahi et al., 2017 (India) ²⁶	2278 compared to 2278 (2314 M, 2242 F)	150 mg of fructooligosaccharide with 100 mg maltodextrin as excipient compared to 250 mg of maltodextrin	double-blinded	a composite of sepsis or death, the former composed of septicemia, meningitis, culture-negative sepsis other infections (including diarrhea, omphalitis, local infections, abscess, and otitis media) and weight gain
Riskin et al., 2010 (Israel) ²⁷	15 (10 M, 5 F, 30.3 ±2.8 weeks old) compared to 13 (5 M, 8 F, 128.7 ±2.9 weeks old)	digestible oligosaccharides lactulose 1.5 g/kg/day compared to dextrose	double-blinded 35 days	necrotizing enterocolitis, mortality, sepsis, feeding intolerance, and days to reach full enteral feeding
Serce et al., 2020 (Turkey) ²⁸	104 (61 M, 43 F 29 ±1.9 weeks old) compared to 104 (52 M, 52 F 28 ±2.2 weeks old)	383 mg of fructooligosaccharide, 100 mg of galactooligosaccharide, 2 mg of bovine lactoferrin compared to distilled water	double-blinded 21 days	necrotizing enterocolitis severity, mortality, sepsis, hospitalization duration, time to reach 100 mL/kg/day of oral feeding
Torres et al., 2020 (Peru) ²⁹	99 compared to 100	oligosaccharides compared to mature breast milk	single-blinded	late-onset sepsis, neonatal sepsis
van den Berg et al., 2013 (the Netherlands) ³⁰	38 (21 M, 17 F, 29.9 ±1.7 weeks old) compared to 39 (24 M, 15 F, 29.6 ±2.1 weeks old)	short chain galactooligosaccharides/ long chain fructooligosaccharides, pectin-derived acidic oligosaccharides 1.5 g/kg/day compared to maltodextrin	single-blinded 28 days	neurodevelopment, cytokines, infections, sepsis
Westerbeek et al., 2011 (the Netherlands) ³¹	73 (29.9 ±1.9 weeks old) compared to 81 (29.3 ±2.1 weeks old)	short chain galactooligosaccharides/ long chain fructooligosaccharides, pectin-derived acidic oligosaccharides 1.5 g/kg/day compared to maltodextrin	double-blinded 28 days	stool viscosity, stool frequency, stool pH, sepsis

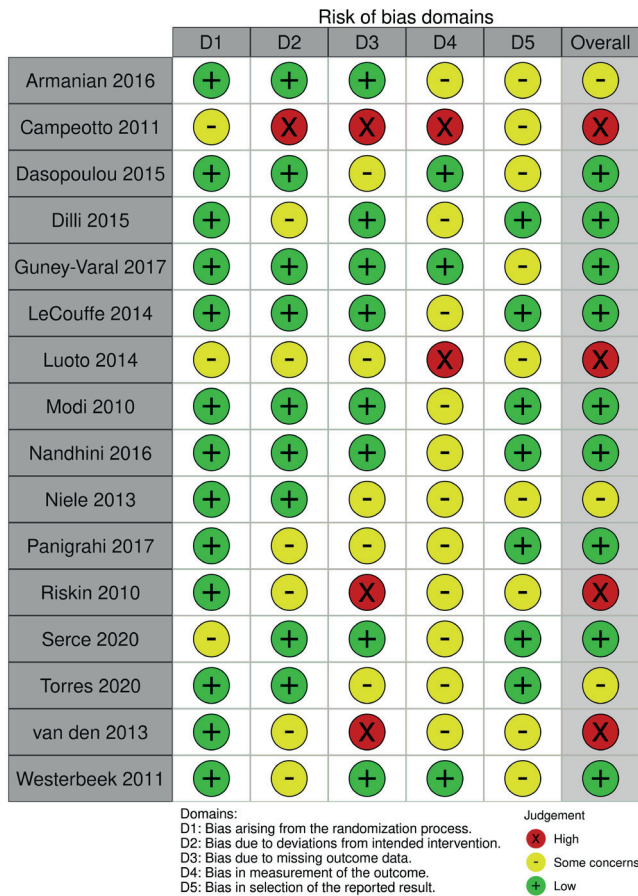


Fig. 2. Risk of bias assessment visualization. The risk of bias assessment updated version (ROB v2) was used to assess the risk of bias for the randomized controlled trials (RCTs)

meta-analysis is that the studies were RCTs, and most only used prebiotics for the treatment groups. The results indicate that this treatment could be an option for infant patients.

Prebiotics may decrease the colonization and growth of pathogenic bacteria and other pathogens, which could help decrease the risk of sepsis and mortality.³² In the intestines, they may also reduce pathogen cytotoxicity and adhesion,³³ improve motility and permeability, and improve the integrity of the epithelial surface.³⁴ Furthermore, strengthening of the intestinal barrier by prebiotics may prevent sepsis and infection by inhibiting the migration of pathogens and toxins across the intestinal mucosa and promoting their removal. In addition, prebiotics could enhance immune responses and modulate the responses to pathogens or toxins.^{35–38}

Oligosaccharides are prebiotics reported to significantly enhance the growth of probiotic bacteria, such as *Bifidobacteria* and *Lactobacilli*. In addition, oligosaccharides may reduce pathogen adhesion.³⁹ A study on the long-term safety and effects of prebiotics in pediatric patients found that they can decrease the amount of antibiotics required, which suggests that this treatment is associated with a lower rate of infection.⁴⁰ Another study also supports the protective role of prebiotics in suppressing the germination of spores, inhibiting growth into toxin-producing cells, and reducing the colonization of pathogens in the gut.⁴¹ These mechanisms could explain the decreased rate of sepsis events among infants that received prebiotics.

The effects of prebiotics are comparable to those of breast milk in several ways, such as increased body weight, lower fever rates, modulatory effects on diarrhea, decreased constipation,

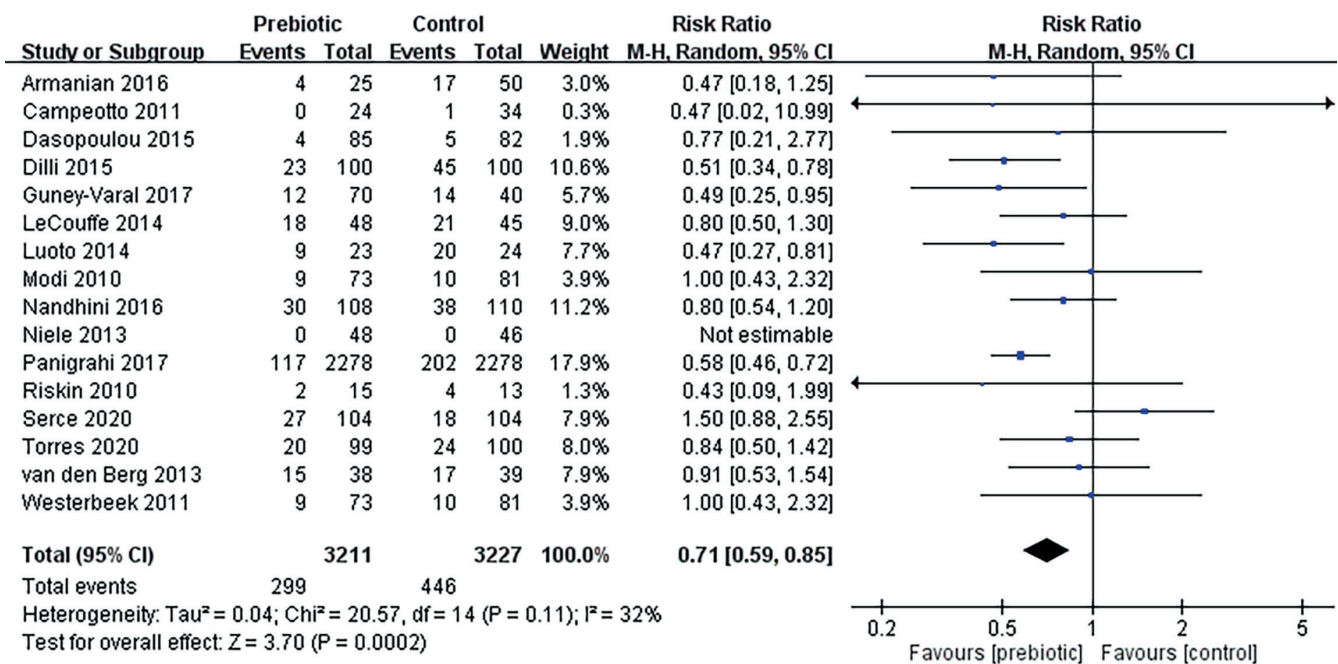


Fig. 3. Forest plot of risk ratio (RR) for sepsis events in infants (prebiotic compared to control). The prebiotic group of preterm infants had a significantly lower RR of sepsis events than the control group

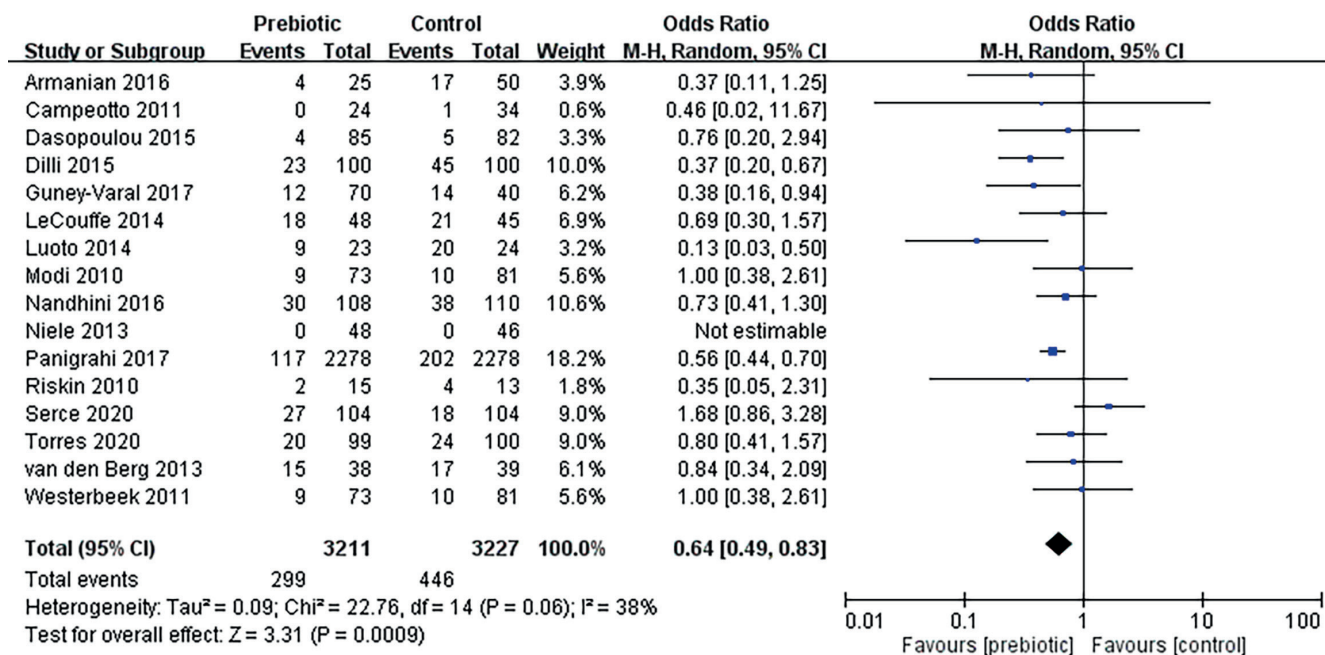


Fig. 4. Forest plot of odds ratio (OR) for sepsis events in infants (prebiotic compared to control). The prebiotic group of preterm infants had a significantly lower OR of sepsis events than the control group

and inhibitory effects on respiratory tract infections in infancy.⁴² Prebiotic supplementation has also been recommended if breast milk is unavailable. Therefore, treatment with prebiotics could be an economical choice for infants.

Limitations

This study had several limitations. First, some RCTs had small sample sizes, while others had appropriate sample sizes, and this imbalance could be a concern. Even though a weighting method was applied to decrease the bias, the impact of this issue should not be ignored.

There was also an imbalance in the sexes of the infants examined, which could influence the interpretation of the results. Similarly, there were variations in age, prebiotic content, doses, placebo used, and treatment duration, which are also potential sources of bias. The lack of patient-level data may be another concern and prevented us from fully evaluating patient-level covariates. Thus, possible subgroup effects could not be investigated.

Another limitation is that the definition and severity of sepsis in the included RCTs differed. Also, some RCTs were double-blinded, while some were single-blinded, and the timing of sepsis was variable between studies, which could affect the results. This issue required consideration when we reported such a significant result of lower sepsis (OR or RR) in this group of pediatric patients.

Conclusions

The results of this meta-analysis showed that prebiotic use could be associated with a reduction in sepsis rates

in infants, and prebiotics significantly lowered the sepsis risk in preterm infants. Therefore, they should be considered as an option in clinical practice. Fewer sepsis events under the use of prebiotics might potentially suggest that prebiotics might decrease the mortality and the damage to vulnerable organs. In addition, prebiotics might decrease the sequelae of infection, and the need for antibiotic use among preterm infants. Future clinical research should examine the standardized application of prebiotics in infant patients.

ORCID iDs

Yuejia Qin <https://orcid.org/0000-0003-0421-5255>

Linhui Pan <https://orcid.org/0009-0001-5577-9758>

References

- Shuai X, Li X, Wu Y. Prediction for late-onset sepsis in preterm infants based on data from East China. *Front Pediatr.* 2022;10:924014. doi:10.3389/fped.2022.924014
- Dierikx TH, Deianova N, Groen J, et al. Association between duration of early empiric antibiotics and necrotizing enterocolitis and late-onset sepsis in preterm infants: A multicenter cohort study. *Eur J Pediatr.* 2022;181(10):3715–3724. doi:10.1007/s00431-022-04579-5
- Goh GL, Lim CSE, Sultana R, De La Puerta R, Rajadurai VS, Yeo KT. Risk factors for mortality from late-onset sepsis among preterm very-low-birthweight infants: A single-center cohort study from Singapore. *Front Pediatr.* 2022;9:801955. doi:10.3389/fped.2021.801955
- Garg PM, Paschal JL, Ansari MAY, Block D, Inagaki K, Weitkamp JH. Clinical impact of NEC-associated sepsis on outcomes in preterm infants. *Pediatr Res.* 2022;92(6):1705–1715. doi:10.1038/s41390-022-02034-7
- Hibbert J, Strunk T, Nathan E, et al. Composition of early life leukocyte populations in preterm infants with and without late-onset sepsis. *PLoS One.* 2022;17(3):e0264768. doi:10.1371/journal.pone.0264768
- Johnston N, De Waal K. Clinical and haemodynamic characteristics of preterm infants with early onset sepsis. *J Paediatr Child Health.* 2022;58(12):2267–2272. doi:10.1111/jpc.16218
- Wang Z, Zhao Y, Jiang Y, Chu W. Prebiotic, antioxidant, and immunomodulatory properties of acidic exopolysaccharide from marine *Rhodotorula* RY1801. *Front Nutr.* 2021;8:710668. doi:10.3389/fnut.2021.710668

8. Thambiraj SR, Phillips M, Koyyalamudi SR, Reddy N. Yellow lupin (*Lupinus luteus* L.) polysaccharides: Antioxidant, immunomodulatory and prebiotic activities and their structural characterisation. *Food Chem*. 2018;267:319–328. doi:10.1016/j.foodchem.2018.02.111
9. Breton J, Plé C, Guerin-Deremaux L, et al. Intrinsic immunomodulatory effects of low-digestible carbohydrates selectively extend their anti-inflammatory prebiotic potentials. *BioMed Res Int*. 2015;2015:162398. doi:10.1155/2015/162398
10. Azagra-Boronat I, Massot-Cladera M, Mayneris-Perxachs J, et al. Immunomodulatory and prebiotic effects of 2'-fucosyllactose in suckling rats. *Front Immunol*. 2019;10:1773. doi:10.3389/fimmu.2019.01773
11. Eiwegger T, Stahl B, Haidl P, et al. Prebiotic oligosaccharides: In vitro evidence for gastrointestinal epithelial transfer and immunomodulatory properties. *Pediatr Allergy Immunol*. 2010;21(8):1179–1188. doi:10.1111/j.1399-3038.2010.01062.x
12. Pol K, De Graaf C, Meyer D, Mars M. The efficacy of daily snack replacement with oligofructose-enriched granola bars in overweight and obese adults: A 12-week randomized controlled trial. *Br J Nutr*. 2018;119(9):1076–1086. doi:10.1017/S0007114518000211
13. Chi C, Buys N, Li C, Sun J, Yin C. Effects of prebiotics on sepsis, necrotizing enterocolitis, mortality, feeding intolerance, time to full enteral feeding, length of hospital stay, and stool frequency in preterm infants: A meta-analysis. *Eur J Clin Nutr*. 2019;73(5):657–670. doi:10.1038/s41430-018-0377-6
14. Cumpston MS, McKenzie JE, Welch VA, Brennan SE. Strengthening systematic reviews in public health: Guidance in the *Cochrane Handbook for Systematic Reviews of Interventions*, 2nd edition. *J Public Health (Oxf)*. 2022;44(4):e588–e592. doi:10.1093/pubmed/fdac036
15. Knobloch K, Yoon U, Vogt PM. Preferred Reporting Items for Systematic Reviews and Meta-Analyses (PRISMA) statement and publication bias. *J Craniomaxillofac Surg*. 2011;39(2):91–92. doi:10.1016/j.jcms.2010.11.001
16. Armanian AM, Barekatin B, Hoseinzadeh M, Salehimehr N. Prebiotics for the management of hyperbilirubinemia in preterm neonates. *J Matern Fetal Neonatal Med*. 2016;29(18):3009–3013. doi:10.3109/14767058.2015.1113520
17. Campeotto F, Suau A, Kapel N, et al. A fermented formula in pre-term infants: Clinical tolerance, gut microbiota, down-regulation of faecal calprotectin and up-regulation of faecal secretory IgA. *Br J Nutr*. 2011;105(12):1843–1851. doi:10.1017/S0007114510005702
18. Dasopoulou M, Briana DD, Boutsikou T, et al. Motilin and gastrin secretion and lipid profile in preterm neonates following prebiotics supplementation. *J Parenter Enteral Nutr*. 2013;39(3):359–368. doi:10.1177/0148607113510182
19. Dilli D, Aydin B, Fettah ND, et al. The pro-pre-save study: Effects of probiotics and prebiotics alone or combined on necrotizing enterocolitis in very low birth weight infants. *J Pediatr*. 2015;166(3):545–551.e1. doi:10.1016/j.jpeds.2014.12.004
20. Güney-Varal İ, Köksal N, Özkan H, Bağcı O, Doğan P. The effect of early administration of combined multi-strain and multi-species probiotics on gastrointestinal morbidities and mortality in preterm infants: A randomized controlled trial in a tertiary care unit. *Turk J Pediatr*. 2017;59(1):13–19. doi:10.24953/turkjped.2017.01.003
21. LeCouffe N, Westerbeek E, Van Schie P, Schaaf V, Lafeber H, Van Elburg R. Neurodevelopmental outcome during the first year of life in preterm infants after supplementation of a prebiotic mixture in the neonatal period: A follow-up study. *Neuropediatrics*. 2014;45(1):22–29. doi:10.1055/s-0033-1349227
22. Luoto R, Ruuskanen O, Waris M, Kalliomäki M, Salminen S, Isolauri E. Prebiotic and probiotic supplementation prevents rhinovirus infections in preterm infants: A randomized, placebo-controlled trial. *J Allergy Clin Immunol*. 2014;133(2):405–413. doi:10.1016/j.jaci.2013.08.020
23. Modi M, Uthaya S, Fell J, Kulinskaya E. A randomised, double-blind, controlled trial of the effect of prebiotic oligosaccharides on enteral tolerance in preterm infants (ISRCTN77444690). *Pediatr Res*. 2010;68(5):440–445. doi:10.1203/PDR.0b013e3181f1cd59
24. Nandhini LP, Biswal N, Adhisivam B, Mandal J, Bhat BV, Mathai B. Synbiotics for decreasing incidence of necrotizing enterocolitis among preterm neonates: A randomized controlled trial. *J Matern Fetal Neonatal Med*. 2016;29(5):821–825. doi:10.3109/14767058.2015.1019854
25. Niele N, Van Zwol A, Westerbeek EA, Lafeber HN, Van Elburg RM. Effect of non-human neutral and acidic oligosaccharides on allergic and infectious diseases in preterm infants. *Eur J Pediatr*. 2013;172(3):317–323. doi:10.1007/s00431-012-1886-2
26. Panigrahi P, Parida S, Nanda NC, et al. A randomized synbiotic trial to prevent sepsis among infants in rural India. *Nature*. 2017;548(7668):407–412. doi:10.1038/nature23480
27. Riskin A, Hochwald O, Bader D, et al. The effects of lactulose supplementation to enteral feedings in premature infants: A pilot study. *J Pediatr*. 2010;156(2):209–214. doi:10.1016/j.jpeds.2009.09.006
28. Serce Pehlevan O, Benzer D, Gursoy T, Karatekin G, Ovali F. Synbiotics use for preventing sepsis and necrotizing enterocolitis in very low birth weight neonates: A randomized controlled trial. *Clin Exp Pediatr*. 2020;63(6):226–231. doi:10.3345/cep.2019.00381
29. Torres Roldan VD, Urtecho SM, Gupta J, et al. Human milk oligosaccharides and their association with late-onset neonatal sepsis in Peruvian very-low-birth-weight infants. *Am J Clin Nutr*. 2020;112(1):106–112. doi:10.1093/ajcn/nqaa102
30. Van Den Berg JP, Westerbeek EAM, Van Der Klis FRM, Berbers GAM, Lafeber HN, Van Elburg RM. Neutral and acidic oligosaccharides supplementation does not increase the vaccine antibody response in preterm infants in a randomized clinical trial. *PLoS One*. 2013;8(8):e70904. doi:10.1371/journal.pone.0070904
31. Westerbeek EAM, Hensgens RI, Mihatsch W, Boehm G, Lafeber HN, Van Elburg RM. The effect of neutral and acidic oligosaccharides on stool viscosity, stool frequency and stool pH in preterm infants. *Acta Paediatr*. 2011;100(11):1426–1431. doi:10.1111/j.1651-2227.2011.02295.x
32. Tulumoğlu Ş, Erdem B, Şimşek Ö. The effects of inulin and fructooligosaccharide on the probiotic properties of *Lactobacillus* spp. isolated from human milk. *Z Naturforsch C J Biosci*. 2018;73(9–10):367–373. doi:10.1515/znc-2018-0001
33. Di R, Vakkalanka MS, Onumpai C, et al. Pectic oligosaccharide structure-function relationships: Prebiotics, inhibitors of *Escherichia coli* O157:H7 adhesion and reduction of Shiga toxin cytotoxicity in HT29 cells. *Food Chem*. 2017;227:245–254. doi:10.1016/j.foodchem.2017.01.100
34. Vieira ADS, Bedani R, Albuquerque MAC, Biscola V, Saad SMI. The impact of fruit and soybean by-products and amaranth on the growth of probiotic and starter microorganisms. *Food Res Int*. 2017;97:356–363. doi:10.1016/j.foodres.2017.04.026
35. Abasubong KP, Li X, Adjoumani JY, Jiang G, Desouky HE, Liu W. Effects of dietary xylooligosaccharide prebiotic supplementation on growth, antioxidant and intestinal immune-related genes expression in common carp *Cyprinus carpio* fed a high-fat diet. *J Anim Physiol Anim Nutr (Berl)*. 2022;106(2):403–418. doi:10.1111/jpn.13669
36. Mio K, Otake N, Nakashima S, Matsuoka T, Aoe S. Ingestion of high beta-glucan barley flour enhances the intestinal immune system of diet-induced obese mice by prebiotic effects. *Nutrients*. 2021;13(3):907. doi:10.3390/nu13030907
37. Lee HB, Son SU, Lee JE, et al. Characterization, prebiotic and immune-enhancing activities of rhamnogalacturonan-I-rich polysaccharide fraction from molokhia leaves. *Int J Biol Macromol*. 2021;175:443–450. doi:10.1016/j.ijbiomac.2021.02.019
38. Ferret-Bernard S, Le Normand L, Romé V, et al. Maternal supplementation of food ingredient (prebiotic) or food contaminant (mycotoxin) influences mucosal immune system in piglets. *Nutrients*. 2020;12(7):2115. doi:10.3390/nu12072115
39. Leong A, Liu Z, Almshawit H, et al. Oligosaccharides in goats' milk-based infant formula and their prebiotic and anti-infection properties. *Br J Nutr*. 2019;122(4):441–449. doi:10.1017/S000711451900134X
40. Kukkonen K, Savilahti E, Haahtela T, et al. Long-term safety and impact on infection rates of postnatal probiotic and prebiotic (synbiotic) treatment: Randomized, double-blind, placebo-controlled trial. *Pediatrics*. 2008;122(1):8–12. doi:10.1542/peds.2007-1192
41. Rätsep M, Kõljalg S, Sepp E, et al. A combination of the probiotic and prebiotic product can prevent the germination of *Clostridium difficile* spores and infection. *Anaerobe*. 2017;47:94–103. doi:10.1016/j.anaerobe.2017.03.019
42. Shahramian I, Kalvandi G, Javaherizadeh H, et al. The effects of prebiotic supplementation on weight gain, diarrhoea, constipation, fever and respiratory tract infections in the first year of life. *J Paediatr Child Health*. 2018;54(8):875–880. doi:10.1111/jpc.13906

PPAR γ , NF- κ B and the UPR pathway as new molecular targets in the anti-inflammatory actions of NSAIDs: Novel applications in cancers and central nervous system diseases?

Paulina Sokołowska^{1,A,B,D–F}, Layla Bleibel^{2,D,E}, Jacek Owczarek^{3,E}, Anna Wiktorowska-Owczarek^{1,A,B,D–F}

¹ Department of Pharmacology and Toxicology, Medical University of Lodz, Poland

² Students' Research Club, Department of Pharmacology and Toxicology, Medical University of Lodz, Poland

³ Laboratory of Pharmacogenetics, Department of Hospital Pharmacy, Medical University of Lodz, Poland

A – research concept and design; B – collection and/or assembly of data; C – data analysis and interpretation; D – writing the article; E – critical revision of the article; F – final approval of the article

Advances in Clinical and Experimental Medicine, ISSN 1899–5276 (print), ISSN 2451–2680 (online)

Adv Clin Exp Med. 2024;33(9):1007–1022

Address for correspondence

Anna Wiktorowska-Owczarek

E-mail: anna.wiktorowska-owczarek@umed.lodz.pl

Funding sources

This research was funded with grants from the Medical University of Lodz (No. 503/1-108-01/503-11-001 and No. 503/3-011-03/503-31-001-19-00).

Conflict of interest

None declared

Received on October 18, 2022

Reviewed on October 13, 2023

Accepted on October 17, 2023

Published online on January 5, 2024

Abstract

Non-steroidal anti-inflammatory drugs (NSAIDs) such as aspirin, diclofenac, ibuprofen, or celecoxib have a well-established and unquestionable role in the human therapeutic arsenal, but still new perspectives are being discovered. This review presents new anti-inflammatory mechanisms of NSAIDs action, other than the classical one, i.e., the inhibition of cyclooxygenase (COX) isoforms leading to the prostanoids synthesis blockage. Literature data show that this group of drugs can activate anti-inflammatory peroxisome proliferator-activated receptor gamma (PPAR γ), inhibit pro-inflammatory nuclear factor- κ B (NF- κ B) activation or modulate the components of the unfolded protein response (UPR) pathway. These alternative pathways induced by NSAIDs may not only enhance their basic anti-inflammatory mechanism of action but also promote other effects of the drugs such as anti-cancer. It was also proved that neuroinflammation, with the involvement of NF- κ B, PPAR γ and the components of the UPR pathway has an essential impact on the development of central nervous system (CNS) diseases. Thus, it seems possible that these new molecular targets may expand the use of NSAIDs, e.g., in the treatment of cancers and/or CNS disorders.

Key words: NF- κ B, PPAR γ , NSAIDs, UPR pathway, cancers, CNS diseases

Cite as

Paulina Sokołowska P, Layla Bleibel L, Owczarek J, Wiktorowska-Owczarek A. PPAR γ , NF- κ B and the UPR pathway as new molecular targets in the anti-inflammatory actions of NSAIDs: Novel applications in cancers and central nervous system diseases? *Adv Clin Exp Med.* 2024;33(9):1007–1022. doi:10.17219/acem/174243

DOI

10.17219/acem/174243

Copyright

Copyright by Author(s)

This is an article distributed under the terms of the Creative Commons Attribution 3.0 Unported (CC BY 3.0) (<https://creativecommons.org/licenses/by/3.0/>)

Introduction

Non-steroidal anti-inflammatory drugs (NSAIDs) such as aspirin, diclofenac, ibuprofen, or celecoxib are popular drugs available both with and without prescription and are commonly used by patients with various ailments/diseases. For these reasons, questions arise as to how NSAIDs affect comorbidities such as neurodegenerative diseases, depression disorders, cardiovascular diseases, diabetes, cancers, and others. Moreover, the scientific interest may also result from the fact that NSAIDs are a heterogeneous group of drugs (chemical structure of NSAIDs is presented in Table 1), which means that each of them may show additional properties, related not only to their effects on cyclooxygenase (COX) isoforms.

Objectives

While NSAIDs have been used for many years, their mechanisms of action are still being explored, and other anti-inflammatory molecular targets that may expand their use or explain adverse effects are being investigated. Anti-inflammatory effects of NSAIDs, in addition to the basic mechanism of action, i.e., COX inhibition, may also

Table 1. Division of non-steroidal anti-inflammatory drugs (NSAIDs) based on their chemical structure and the effect on COX isoforms

Chemical group	Mechanism of action	
	non-selective COX-1 & COX-2	selective COX-2
Salicylates	acetylsalicylic acid (aspirin), sodium salicylate	–
Acetic acid derivatives	indomethacin, diclofenac, sulindac sulfide	–
Heteroaryl acetic acid derivatives	ibuprofen, naproxen	–
Enolic acid (oxicams)	piroxicam, meloxicam	–
Diaryl heterocycles (coxibs)	–	celecoxib, rofecoxib, parecoxib

COX-1 – cyclooxygenase-1; COX-2 – cyclooxygenase-2.

result from their impact on other pathways, such as oxidative stress¹ or kynurenine,² but they have been widely discussed elsewhere.^{1,2} This work offers a complex overview of selected but mutually related mechanisms of action of NSAIDs, namely peroxisome proliferator-activated receptor gamma (PPAR γ), nuclear factor- κ B (NF- κ B) and the unfolded protein response (UPR) pathways. There is a growing interest in these signaling molecules

Table 2. Effects of NSAIDs on PPAR γ , NF- κ B and UPR pathways. Within the mechanisms of action of NSAIDs, the literature is arranged alphabetically in relation to the drug under investigation.

Experimental model	Dose/concentration of NSAIDs and scheme of administration	Effects of NSAIDs on the signaling pathways	Role of NSAIDs action	Ref.
NSAIDs – the anti-inflammatory mechanism of action through the PPAR γ receptor				
Carrageenan-induced paw edema in rats – an acute inflammation model	celecoxib (0.3–30 mg/kg; ip.)	Activation of PPAR γ receptor and anti-inflammatory IL-10. Decrease in inflammatory cytokines.	anti-inflammatory	3
Lewis lung carcinoma cells	celecoxib (50–200 μ M for 24 h)	Increased AA level and decreased PGE ₂ production through upregulation and downregulation of cPLA2 and COX-2 proteins, respectively. Increased expression of PPAR γ protein.	pro-apoptotic	4
3T3-L1 preadipocytes	indomethacin (10 μ M) ibuprofen (75 μ M) sodium diclofenac (25 μ M)	Stimulation of PPAR γ activity. Regulation of PPAR γ -dependent target genes.	adipocyte differentiation	5
C3H10T1/2 clone 8 murine fibroblasts	indomethacin (10 ⁻⁴ M)	Inhibition of COX activity and activation of PPAR γ .	adipocyte differentiation	6
Rat hepatoma cell line H4-II-E-C3 and CV-1 cells co-transfected with rat PPAR α and PPAR γ	ibuprofen, indomethacin and naproxen (10 ⁻⁸ –10 ⁻³ M)	Activation of PPAR α and PPAR γ isoforms at concentrations of 10 ⁻⁴ –10 ⁻³ M.	potential angiostatic and anti-cancer effect	7
Preadipocytes (3T3-L1) and prostate cancer cells (DU-145)	diclofenac (25 μ M)	Activation of PPAR (partial agonist) and inhibition of PPAR trans-activation by rosiglitazone (competitive antagonist).	Antagonism of PPAR signaling by diclofenac resulted in the inhibition of adipocyte differentiation and increased proliferation of prostate cancer cells.	8
In vitro: hemangioma-derived mesenchymal stem cells (Hem-MSCs) obtained from patients. In vivo: 6-week-old, male, mice with xenograft tumors from Hem-MSCs	celecoxib (0.1–1000 μ g/mL for 24 h) celecoxib (0.1 mg/g/day) administered to the mice via oral intake for 4 weeks	Increased expression levels of genes involved in adipogenic differentiation: COX-2, human-CCAAT-enhancer-binding protein (CEBPa) and PPAR- γ .	Inhibition of the proliferation and stimulation of the adipogenic differentiation of Hem MSCs in vitro and in the xenograft tumors.	9

Table 2. Effects of NSAIDs on PPAR γ , NF- κ B and UPR pathways – cont.

Experimental model	Dose/concentration of NSAIDs and scheme of administration	Effects of NSAIDs on the signaling pathways	Role of NSAIDs action	Ref.
Breast cancer MCF7 cells	celecoxib (0.02 mM) diclofenac (0.375 mM) ibuprofen (0.75 mM) indomethacin (0.5 mM) sulindac (0.06 mM) for 24 h	Upregulation of the PPAR γ expression and its translocation to the nucleus.	proapoptotic activity	10
NSAIDs – the anti-inflammatory mechanism of action through the NF- κ B pathway				
Human non-small cell lung carcinoma (H1299)	celecoxib (100 μ M) with TNF (0.1 nM) for 24 h	Inhibited activation of IKK and NF- κ B as well as related signaling kinases, i.e., JNK, p38 MAPK and ERK in cancer cells.	anti-inflammatory antiproliferative	11
Murine fibroblast cell line (NIH-3T3)	celecoxib – 25 μ M for 1 h with TNF- α (10 ng/mL)	Inhibition of the TNF- α -induced nuclear accumulation of the NF- κ B p65 subunit.	anti-inflammatory	12
Osteoclasts derived from mouse hematopoietic stem cells	diclofenac (10–500 nM) for 30 min	Inhibition of the I κ B degradation, which maintained inactive NF- κ B in the cytosol.	regulation of the osteoclast differentiation	13
Model of cystic fibrosis using respiratory epithelium cells	ibuprofen (480 μ M) for 30 min before stimulating cells with 10 ng/mL TNF- α	Modest suppression of TNF- α -induced NF κ B activation.	anti-inflammatory	14
RAW 264.7 mouse macrophages	etoricoxib and lumiracoxib (1/10/100 μ M) for 30 min and then stimulated for 30 min with 10 μ g/mL LPS	Inhibition of the LPS-induced NF- κ B activation by etoricoxib and lumiracoxib at highest concentration of 100 μ M. Etoricoxib additionally inhibited CREB activation, which contributed to a reduced expression of iNOS and COX-2 expression.	anti-inflammatory	15
Human leukemic cell line KBM-5	aspirin (1–10 mM) ibuprofen (1–5 mM) indomethacin (0.1–1 mM) diclofenac (0.2–1 mM) celecoxib (10–50 mM) for 4 h or 8 h and before stimulating cells with 0.1 nM TNF for 30 min	Tested NSAIDs suppressed activation of NF- κ B by inhibiting IKK activation and I κ B α degradation.	anti-inflammatory and antiproliferative	16
Human vulvar squamous cell carcinoma (A431 cells)	ibuprofen and diclofenac combined with cannabidiol equimolar to 20 μ M	Decreased level of NF- κ B p50 and p65 proteins and their ability to bind to DNA by combinations of cannabidiol with NSAIDs.	anti-inflammatory and antiproliferative	17
Rats with collagen-induced arthritis (CIA)	ibuprofen (30 mg/kg) given twice daily to CIA rats for 2 weeks	Attenuation of elevated levels of phosphorylated p38, JNK and NF- κ B p65 in the hippocampus of CIA rats. In addition, normalization of the decreased excitatory amino acid transporter 2 (EAAT2) level, the increased extracellular glutamate, and the upregulated hippocampal NMDA receptor 2B of CIA rats.	inhibition of neuroinflammation memory improvement	18
Human ovarian cancer cell lines SKOV3 and OVCAR3 In vivo: mice inoculated subcutaneously with cells SKOV3	celecoxib (100 mM)	diminished NF- κ B p65 expression	Celecoxib and chemotherapy drugs can enhance the inhibition of ovarian cancer cells in vivo.	19
NSAIDs – the anti-inflammatory mechanism of action through the UPR pathway				
Primary human coronary artery endothelial cells (HCAEC) Human umbilical vein endothelial cells (HUVEC) Human pulmonary artery endothelial cells (HPAEC)	In the presence of tunicamycin (1.0 μ M) or high-dextrose (27.5 mM) the cells were treated with different concentrations of celecoxib and rofecoxib (0–10,000 nM)	Celecoxib, but not rofecoxib inhibited ER stress in endothelial cells. It downregulated the ATF6 and GRP78 expression and phosphorylation of IRE1 α and PERK.	ER stress involved in unfavorable effects of rofecoxib on cardiovascular outcomes.	20

Table 2. Effects of NSAIDs on PPAR γ , NF- κ B and UPR pathways – cont.

Experimental model	Dose/concentration of NSAIDs and scheme of administration	Effects of NSAIDs on the signaling pathways	Role of NSAIDs action	Ref.
Human colorectal cancer cell lines: HCT-8, HT-29, HCT-116	celecoxib (20 μ M) in sequential treatment followed by bortezomib (20 nM)	Enhanced activation of apoptotic markers (i.e., caspase-9, caspase-3 and PARP, Bax, p53, and PUMA) through the ER stress-mediated mitochondrial dysfunction and increased cytosolic and mitochondrial Ca $^{2+}$ and increased induction of CHOP. Additionally, celecoxib followed by bortezomib enhanced the ER stress-mediated autophagy-associated cell death (induced expression of Beclin-1 and autophagosome-associated LC3-I/II proteins).	pro-apoptotic induction of autophagy-associated cell death	21
Hepatoma HepG2 cells	celecoxib (80 μ M) for 24 h and 48 h	Increased the mRNA and protein levels of ATF4, ATF6, sXBP-1, unspliced XBP1 (uXBP1), and CHOP.	pro-apoptotic	22
Human neuroblastoma SH-SY5Y cells	diclofenac (100–300 μ M) added 2 h before the stimulation by 100 nM thapsigargin or by 3 mg/mL tunicamycin for 24 h	Inhibition of caspase-2, caspase-9 and caspase-3 activation and prevention from a decrease in mitochondrial membrane potential caused by ER stress.	anti-apoptotic	23
Endothelial EA.hy926 cells	diclofenac (75 μ M) concomitantly with tunicamycin 0.5 μ g/mL for 24 h	Inhibition of ER stress-responsive genes, i.e., CHOP/DIT3, GRP78/HSPA5 and DNAJB9. Additionally, the drug diminished the significant upregulation and release of the GRP78 protein.	anti-apoptotic	24
In vitro: gastric carcinoma cells In vivo: mice were inoculated subcutaneously with MKN-45 cells	celecoxib (10–100 μ M) celecoxib orally (100 or 200 mg/kg/day)	Activation of PERK and eIF2 α leading to ATF4 expression. The overexpression of GRP78. GRP78 upregulation.	pro-apoptotic inhibition of xenograft tumor growth	25
Human hepatoma Huh-7 cells	diclofenac (300 μ M) indomethacin (500 nM)	Activation of the PERK pathway followed by enhanced expression of the proapoptotic GADD153/CHOP protein.	pro-apoptotic	26
In vitro: glioblastoma, breast carcinoma, pancreatic carcinoma, Burkitt's lymphoma, multiple myeloma cell lines In vivo: 6-week-old male athymic nu/nu mice implanted with U87 glioblastoma cells	celecoxib (40–80 μ M) 2,5-dimethyl-celecoxib (20–60 μ M) 2,5-dimethyl-celecoxib (150 mg/kg, orally for 50 h)	Activation of ER stress-associated proteins GRP78, CHOP, and caspase-4 in cancer cell lines. Increase in CHOP protein expression in the tumor tissue.	pro-apoptotic reduced tumor growth	27
In vivo: Sprague Dawley male rats after middle cerebral artery occlusion	parecoxib (10 or 30 mg/kg, IP)	Inhibition of translocation of CHOP and Foxo1 and increase in GRP78 and ORP150 (oxygen-regulated protein 150) expression.	suppressed cerebral ischemic injury	28

AA – arachidonic acid; ATF4 – activating transcription factor 4; ATF6 – activating transcription factor 6; CEBP α – human-CCAAT-enhancer-binding protein; CHOP – C/EBP homologous protein; CIA – collagen-induced arthritis; COX – cyclooxygenase; PLA2 – cytosolic phospholipase A2; CREB – cAMP response element-binding protein; DIT3 – DNA damage inducible transcript 3; DNAJB9 – DnaJ heat shock protein family (Hsp40) member B9; EAAT2 – excitatory amino acid transporter 2; eIF2 α – eukaryotic translation initiation factor 2 α ; ER – endoplasmic reticulum; ERK – extracellular signal-regulated kinases; Foxo1 – Forkhead box protein O1; GADD153 – DNA damage-inducible gene 153; GRP78 – 78-kDa glucose-regulated protein; HSPA5 – heat shock protein family A; IKK – I κ B kinase; IL-10 – interleukin 10; iNOS – inducible nitric oxide synthase; IRE1 – inositol-requiring enzyme 1; I κ B – inhibitor of nuclear factor kappa B; JNK – c-Jun N-terminal kinase; LPS – lipopolysaccharide; NF- κ B – nuclear factor- κ B; NMDA – N-methyl-D-aspartate receptor; NSAIDs – non-steroidal anti-inflammatory drugs; ORP – oxygen-regulated protein; p38 MAPK – p38 mitogen-activated protein kinases; PARP – poly (ADP-ribose) polymerase; PERK – protein kinase R-like ER kinase; PGE $_2$ – prostaglandin E $_2$; PPAR α – peroxisome proliferators-activated receptor α ; PPAR γ – peroxisome proliferators-activated receptor γ ; PUMA – p53-upregulated modulator of apoptosis; sXBP-1 – spliced X-box binding protein 1; TNF- α – tumor necrosis factor alpha; uXBP1 – unspliced X-box binding protein 1.

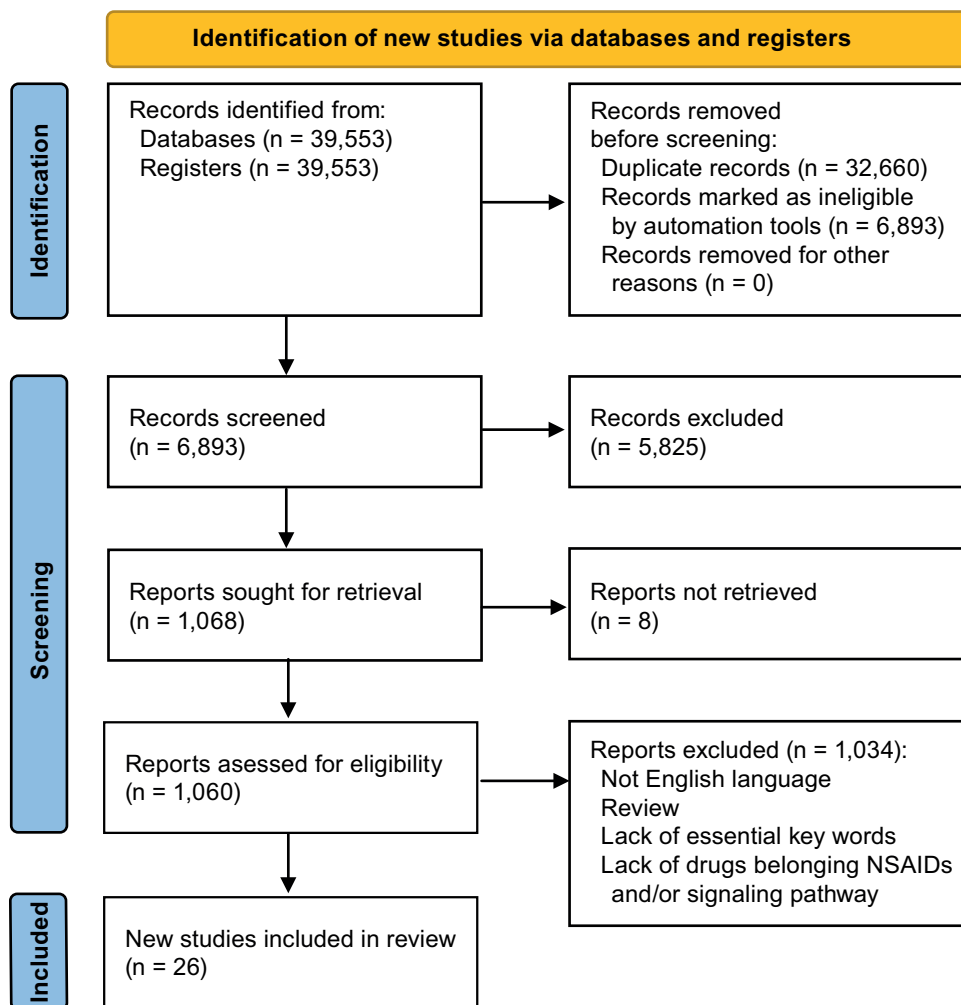


Fig. 1. The Preferred Reporting Items for Systematic Reviews and Meta-Analyses (PRISMA) flowchart

as mediators of the anti-inflammatory effects of NSAIDs in many diseases, i.e., cancer, neurodegenerative disorders and depression. Interestingly, these pathways may also underlie the mechanisms of action of NSAIDs on pathological processes other than inflammation, such as uncontrolled cancer cell proliferation or neuronal dysfunction. Herein, we will attempt to answer the question of how these new molecular targets may affect the therapeutic actions of NSAIDs pharmaceuticals.

Methodology

A literature search was carried out in the PubMed and Google Scholar databases on September 15, 2022, using the queries: “NSAIDs “and” mechanism of action”; “NSAIDs “and” PPARγ”; “NSAIDs “and” NF-κB”; “NSAIDs “and” ER stress (endoplasmic reticulum stress)”. We then selected key studies that examined both diverse cell lines and in vivo models. Their results are discussed in the text and presented in Table 2. The Preferred Reporting Items for Systematic Reviews and Meta-Analyses (PRISMA) flowchart is presented as Fig. 1.

Classical mechanism of action of NSAIDs

Non-steroidal anti-inflammatory drugs are among the most widely administered medications worldwide.²⁹ This is attributed to their variety of applications, including anti-inflammatory, antipyretic, analgesic, and anti-thrombotic effects for aspirin, along with their limited side effects. The inflammatory response is triggered by external stimuli, where membrane phospholipids activate phospholipase A₂ to release arachidonic acid, which is then converted to the precursor prostaglandin (PG)H₂ by COX isoforms. Following PGH₂ production, prostacyclin (PGI₂), prostaglandins, e.g., PGE₂, and thromboxane (TX) A₂ are formed.³⁰ TXA₂ causes vasoconstriction and platelet aggregation, while PGE₂ causes hyperalgesia, and both prostacyclin and prostaglandins (prostaglandin E₂ – PGE₂, prostaglandin I₂ – PGI₂, prostaglandin D₂ – PGD₂) cause vasodilation. These prostanoids mediate inflammation by contributing to pain, redness, and swelling.³¹ The main mechanism of NSAIDs, first discovered by Sir John Vane in 1971, works by inhibiting the synthesis of prostaglandins, specifically by blocking the COX enzymes COX-1

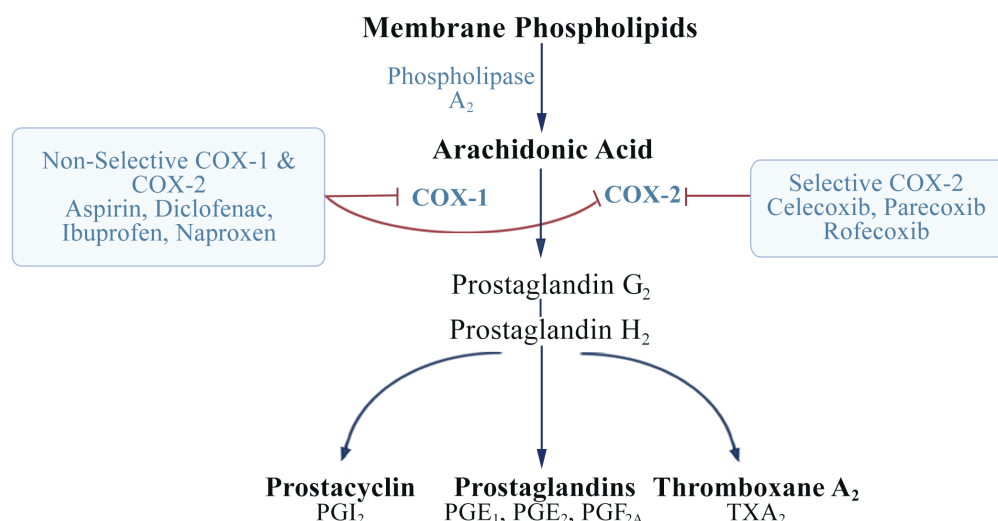


Fig. 2. Mechanism of action of non-steroidal anti-inflammatory drugs (NSAIDs). Membrane phospholipids produce arachidonic acid by phospholipase A₂. Arachidonic acid produces the first precursor prostaglandin G₂ by cyclooxygenase (COX)-1 and COX-2. Then, prostaglandin H₂ is produced from prostaglandin G₂, which by various enzymes produces prostacyclin (PGI₂), prostaglandins, e.g., PGE₁, PGE₂, and thromboxane A₂ (TXA₂). NSAIDs act as COX-1 and COX-2 inhibitors. Diclofenac, ibuprofen and naproxen reversibly inhibit COX-1 and COX-2, and aspirin irreversibly inhibits COX-1 and COX-2. Celecoxib is a COX-2 selective and reversible blocker

and COX-2, which prevents the formation of PGI₂, PGs and TXA₂²⁹ (Fig. 2). Blocking the effects of these prostaglandins results in the therapeutics and side effects of NSAIDs.³² As the use of NSAIDs has risen drastically over the years, the caution about their adverse effects has increased as well, including concerns regarding increased formation of gastrointestinal tract ulcers.³³ This, in turn, has halted NSAIDs as a medication for chronic pain, even though this was once a major indication for their use.³⁰

As the years progressed and scientific research advanced, the classification of NSAIDs has progressed from initially being based on their chemical structure to being differentiated according to their selectivity to cyclooxygenase inhibition.³³ Research has proven the presence of at least 2 COX isoforms until now. The 1st isoform of COX (COX-1) is constitutively expressed and carries out homeostatic functions in the body. It is regulated by development and highly expressed in platelets, renal collecting tubules, monocytes, and endothelial cells.³⁰ When COX-1 is activated, it promotes the protection of the gastric mucosa and platelet activation, and preserves kidney function.³² The 2nd isoform of COX (COX-2) is activated mostly by mediators of inflammation, such as tumor necrosis factor alpha (TNF- α), lipopolysaccharides (LPS) and interleukin-1 (IL-1). It acts on a vast range of cells and tissues, including rheumatoid synovial endothelial cells, vascular endothelial cells, macrophages, and monocytes.³⁰ Conversely, COX-2 has also been shown to express low-level physiological actions in tissues such as the uterus, brain and kidney.³⁴

There are also other isoforms of COX, such as COX-3, which is a splice variant of COX-1. It was identified in mice, rats and dogs. However, it remains controversial whether a COX-3 and 2 shorter variants without cyclooxygenase activity, i.e., PCOX-1a and PCOX-1b^{35,36} proteins, exist in humans, and their biological role is unknown.

Traditional NSAIDs non-selectively bind and inhibit COX-1 and COX-2 to varying degrees. However, due to the critical side effects of nonselective inhibition,

the difference in size between both COX isoform active sites was used to develop COX-2-specific inhibitors to gain the therapeutic uses of NSAIDs without their COX-1 inhibiting side effects. These side effects include small bowel and gastric mucosal injuries, renal injury, hepatotoxicity, and pulmonary complications.^{33,37} COX-2 selective inhibitors include meloxicam, rofecoxib and celecoxib,³² which demonstrate fewer gastrointestinal symptoms and complications compared to nonselective COX inhibitors, such as ibuprofen and diclofenac.³⁸ However, this is not to say that COX-2 selective inhibitors are void of concerning side effects. The most dangerous is the increase in cardiovascular risk.³⁹

Based on their chemical structure (Table 1), NSAIDs can be broadly classified into salicylates (e.g., sodium salicylate, acetylsalicylic acid), aryl, and heteroaryl acetic acid derivatives (e.g., ibuprofen, naproxen), indole/indene acetic acid derivatives (e.g., indomethacin, sulindac), anthranilates (e.g., diclofenac), and enolic acid derivatives (e.g., piroxicam, meloxicam).⁴⁰ However, a more common classification of NSAIDs is based on the type of COX interaction and selectivity, i.e., both COX enzymes can be inhibited equally (e.g., indomethacin, aspirin, diclofenac, naproxen, and ibuprofen), COX-2 can be inhibited with 5-50-fold selectivity (e.g., celecoxib, rofecoxib, parecoxib), COX-2 can be inhibited with greater than 50-fold selectivity (NS-398), and finally, some NSAIDs show poor selectivity for COX enzymes (e.g., sulfasalazine, sodium salicylate).^{33,41}

However, the mechanism of action of NSAIDs described above, which is based on the cascade of AA metabolite conversions, is only a small fragment of the myriad processes that occur within the organism during an inflammatory event.

At the onset of inflammation, different signaling pathways are activated by proinflammatory factors, and these may work to either reinforce or diminish their actions. During this process, proinflammatory and other factors are formed due to tissue damage and induce a cascade

of AA conversions, as well as COX and LOX activation. As a result of these conversions, reactive oxygen species (ROS) are being formed, leading to the activation of NF- κ B, a factor responsible for the promotion of proinflammatory signaling pathways. Conversely, AA, other polyunsaturated fatty acids (PUFA), and prostanoid conversion products, e.g., 15d-PGJ2, activate the anti-inflammatory factor PPAR γ .^{42–44} Thus, endogenous proinflammatory and anti-inflammatory systems can be activated and modulated by these pathways.

The anti-inflammatory mechanism of NSAIDs action through the PPAR γ receptor

The peroxisome proliferator-activated receptor (PPAR) belongs to the family of ligand-inducible nuclear receptors acting as transcription factors. The family of PPARs comprise 3 isoforms, namely PPAR α , PPAR δ/β and PPAR γ . The latter isoform is present in adipose tissue, the liver, the kidney, and the immune system, including bone marrow, lymphocytes, monocytes, and macrophages,^{45–47} and also in the central nervous system (CNS) cells, namely neurons, microglia, astrocytes, and oligodendrocytes.^{48,49} Peroxisome proliferator-activated receptor gamma plays an important role in lipid and glucose metabolism, and insulin sensitivity. Therefore, agonists of this receptor are called insulin-sensitizing medications, and they are used in the treatment of type 2 diabetes (e.g., pioglitazone). Previous studies indicate that PPAR γ agonists⁴³ stimulate the differentiation of monocytes to macrophages in peripheral tissue, control brain inflammation through inhibition of the proinflammatory function of microglia, and suppress the expression of inducible nitric oxide synthase (iNOS), matrix metalloproteinase (MMP-9) and proinflammatory cytokines, IL-1 β , IL-6 and TNF- α .^{47,50,51} Therefore, PPAR γ is the most intensively studied of the 3 isoforms. Stimulation of PPAR γ antagonizes the activity of NF- κ B and consequently inhibits the formation of proinflammatory cytokines.^{50,51} There are numerous natural PPAR γ ligands, including polyunsaturated fatty acids, e.g., linoleic acid, docosahexaenoic acid, exogenous agonists such as flavonoids⁵² (e.g., curcumin) and drugs such as glitazones,^{53,54} and NSAIDs⁴³ that are responsible for an anti-inflammatory effect. Several members of the heterogenous non-steroidal anti-inflammatory family of drugs have been described as ligands for PPAR γ according to their affinities and activity for PPAR γ . These anti-inflammatory drugs were divided into 3 groups: 1. Those with high affinity (indomethacin and diclofenac); 2. Those with moderate affinity (ibuprofen, fenoprofen, flufenamic acid); and 3. Those without agonistic effect (aspirin, piroxicam).^{47,55} The studies mentioned above^{47,55} were conducted *in vitro* and determined the affinity of NSAIDs to the PPAR γ receptor

without formulating a conclusion about possible therapeutic properties of the effects.⁵⁵ Puhl et al.⁵ found that NSAIDs bind to PPAR γ with a range of affinities as follows: sulindac sulfide > diclofenac > indomethacin > ibuprofen. Additionally, it was demonstrated that diclofenac is a weak partial agonist of PPAR γ , ibuprofen shows an intermediate agonistic activity, and indomethacin is a strong agonist of the receptor. Moreover, full agonists include thiazolidinediones, such as rosiglitazone, and stimulation of PPAR γ activity by NSAIDs has been shown to contribute to adipocyte differentiation. However, other studies indicate that activation of PPAR γ follows a different order, namely S-naproxen > indomethacin > S-ibuprofen > R-ibuprofen.⁷ The work of Adamson et al.⁸ has demonstrated that diclofenac shows an affinity for PPAR γ 50 times greater than other NSAIDs and 10 times lower than full agonist rosiglitazone, but similar to pioglitazone. Diclofenac is a partial agonist; therefore, it may function as a competitive antagonist in the presence of a full agonist, and consequently can displace other drugs, e.g., rosiglitazone, from the binding site of the receptor. Therefore, diabetic patients whose blood glucose is controlled using thiazolidinedione drugs may experience poorer glycemic control in the presence of diclofenac. Table 2 summarizes the effects of selected anti-inflammatory drugs on the PPAR γ receptor and the significance of these actions.

It is worth mentioning that NSAIDs bind to the PPAR γ at micromolar concentrations, and this is a higher concentration than what is needed to inhibit COXs.^{6,7} However, such a concentration can be achieved during rheumatoid disease when NSAIDs are used at high doses to obtain therapeutic effect.⁸

NSAIDs anti-inflammatory mechanism of action through the NF- κ B

Nuclear factor- κ B consists of a family of transcription factors that play essential roles in inflammation, immunity, cell proliferation, differentiation, and survival.^{56–58} Under normal conditions, NF- κ B as the heterodimer p50/p65 interacts with I κ B to remain in an inactive state in the cytosol. However, proinflammatory cytokines (e.g., TNF- α and IL-1), bacterial and viral products, and cellular stress (oxygen and ER stress) lead to the phosphorylation of I κ B protein by the activated IKK (I κ B kinase) complex.^{56–58} Interestingly, the I κ B protein acts as the natural inhibitor of NF- κ B. Thus, phosphorylation of I κ B results in its degradation, leading to the release of NF- κ B (p50/p65) that is then able to translocate into the nucleus and regulate multiple target genes encoding proinflammatory cytokines, chemokines, cell adhesion molecules, and enzymes that produce proinflammatory factors, such as nitric oxide and prostaglandins.^{56–58}

The impact of NSAIDs on NF- κ B was confirmed in studies on different cell lines and animal models (Table 2).^{11–16} All NSAIDs inhibit NF- κ B signaling, but the mechanisms of their actions and the potency of inhibition can differ between drugs. For example, a study by Takada et al.¹⁶ showed a comparison indicating that the most potent inhibitor of NF- κ B is celecoxib, followed by diclofenac > indomethacin > naproxen > ibuprofen > aspirin. There are also studies on the development of diclofenac⁵⁹ and ibuprofen⁶⁰ derivatives that demonstrate better effectiveness than reference drugs.

Non-steroidal anti-inflammatory drugs suppress the transcription factor NF- κ B, which controls the gene expression of proinflammatory factors, including COX-2, which is not only responsible for inflammation but is also implicated in tumor cell proliferation. This effect is obtained by the inhibition of IKK and the subsequent inhibition of I κ B degradation.^{11–14,16} Interestingly, diclofenac appeared to regulate osteoclast differentiation by stabilizing the inactive form of NF- κ B,¹³ whereas ibuprofen given to rats with collagen-induced arthritis inhibited neuroinflammation in the hippocampus by attenuating the NF- κ B cascade, and contributed to the memory improvement.¹⁸ This latter example shows that the presence of inflammatory processes and activation of the immune system may affect the CNS and trigger or exacerbate neuroinflammation. It was further demonstrated that inflammatory mediators are implicated in depressive symptoms by directly affecting brain tissue, modulating the monoaminergic system and initiating neurotoxic processes in brain areas responsible for emotions and emotional memories.⁶¹

PPAR γ compared to NF- κ B

As mentioned above, PPAR γ shows an anti-inflammatory effect in contrast to the proinflammatory NF- κ B. Previous studies demonstrate that PPAR γ modulates the inflammatory response initiated by activation of NF- κ B-dependent Toll-like receptors (TLRs). The activation of PPAR γ stimulates the expression of the genes and proteins that negatively regulate NF- κ B, such as I κ B.^{44,62} Moreover, potent exogenous agonists of PPAR γ , such as pioglitazone or rosiglitazone, used alone or in the presence of LPS (an inflammatory stimulator), significantly reduced the activation of NF- κ B in a mouse cystic fibrosis biliary epithelium.⁶² This effect results from the upregulation of I κ B, a negative regulator of NF- κ B.⁶² Peroxisome proliferator-activated receptor gamma also has enzymatic properties, being an E3 ubiquitin ligase. Therefore, the effect of PPAR γ on NF- κ B is also a result of the ubiquitination and degradation of p65, which appears to be critical to the NF- κ B signaling pathway.⁶³

Thus, NSAIDs stimulate PPAR γ -mediated inhibition of the proinflammatory transcription factor NF- κ B, while also potentially directly inhibiting NF- κ B. Further research

is required in this regard to define whether the inhibitory effects of NSAIDs on NF- κ B are indirect, direct, or if both mechanisms are interrelated.

NSAIDs anti-inflammatory mechanism of action through the UPR pathway

Endoplasmic reticulum (ER) is involved in many different cellular functions, such as regulating the synthesis, folding, maturation, and transport of proteins, the synthesis and storage of lipids, acting as the main cellular storage for Ca²⁺, contributing to glucose metabolism, and serving as a platform for signaling and communication between organelles. Endoplasmic reticulum stress homeostasis is constantly challenged by physiological demands or pathological factors that affect its multiple functions. Physiological and/or pathological processes that disturb proper protein folding resulting in the accumulation of unfolded or misfolded proteins, cause a cellular state known as ER stress. The UPR involves the reduction of new protein synthesis, and the elimination of misfolded proteins through the ER-associated protein degradation (ERAD) pathways and autophagy. Another possibility to restore ER homeostasis can be by enhancing the capacity of the ER to fold proteins. Depending on the strength or duration of the factor triggering ER stress, the UPR can have contrasting effects, being either cell-protective or cell-destructive. When attempts to restore proper homeostasis fail, and ER stress cannot be arrested, the signaling pathways switch from pro-survival to pro-apoptotic.^{64–70} The accumulation of unfolded/misfolded proteins is sensed by 3 ER transmembrane effector proteins, namely inositol requiring enzyme 1 (IRE1), protein kinase R-like ER kinase (PERK) and the activating transcription factor 6 (ATF6). Under physiological conditions, these 3 proteins are stored in inactive forms by binding to reticular chaperones 78-kDa glucose-regulated protein (GRP78) and 94-kDa glucose-regulated protein (GRP94). When ER stress is induced, GRP78 and GRP94 disassociate from PERK, IRE1 and ATF6, thereby activating their intracellular pro-survival and/or pro-apoptotic functions.^{64–70}

Protein kinase R-like ER kinase inhibits protein translation in the cell by phosphorylation of eukaryotic initiation factor 2 α (eIF2 α), leading to the transient attenuation of protein synthesis and the reduced influx of newly synthesized proteins into the ER. This marks one of the first responses of the cell to ER stress. Inhibition of protein synthesis supports cell survival by blocking the accumulation of unfolded nascent proteins. However, sustained stress again changes the pro-survival response to pro-apoptotic. This is accomplished by the promotion of increased activating transcription factor 4 (ATF4) expression, which is responsible for the transcription of different pro-apoptotic factors such as 1) growth arrest and

DNA damage-inducible 34 (GADD34), and 2) transcription factor C/EBP homologous protein (CHOP), as well as 3) the pro-apoptotic BCL-2 family proteins. The *CHOP* is one of the most potently upregulated genes during prolonged ER stress, and the interplay of GADD34, ATF4 and CHOP results in the activation of genes involved in cell death, cell-cycle arrest and senescence.^{64–70}

Inositol requiring enzyme 1, having an endoribonuclease activity, is responsible for the splicing of X-box binding protein 1 (XBP1) mRNA, resulting in the generation of an active (spliced) transcription factor XBP1s. Once generated, XBP1s induce expression of ER stress-responsive genes involved in the increased protein folding capacity and degradation of misfolded proteins to restore homeostasis and increase cell survival following stress.^{64–71}

Upon ER stress, ATF6 is transported to the Golgi apparatus, where it is cleaved by site-1 and site-2 proteases to release a fragment containing a basic leucine zipper (bZIP) transcription factor, termed “ATF6p50”. This 50 kDa ATF6 fragment translocates to the nucleus where it increases transcription of UPR-responsive genes, i.e., gene expression of ER chaperones, and ERAD components.^{64–71}

It is important to note that there is extensive crosstalk between PERK, IRE1 and ATF6 signaling pathways. For example, ATF4, which is regulated via the PERK pathway, increases the transcription of IRE1, whereas ATF6 can also induce the expression of XBP1 and CHOP to enhance UPR signaling. All 3 UPR pathways contribute to inducing cell apoptosis when the cell protective measures mediated by the UPR fail to restore folding capacity.^{64–71}

The ER stress-induced UPR not only maintains cellular homeostasis but can also directly regulate the inflammatory pathways.⁷¹ The principal inflammatory signaling proteins whose expression is directly initiated during the UPR are 1) NF- κ B and 2) mitogen-activated protein kinase (MAPK) family proteins consisting of A) stress-inducible kinases including JNK and p38 MAPK, and B) extracellular signal-regulated kinase (ERK). During ER stress, the IRE1-TRAF2 pathway has been shown to promote the NF- κ B-mediated inflammatory response by triggering the recruitment of IKK, the phosphorylation and subsequent degradation of I κ B, resulting in the activation of NF- κ B (the IKK-I κ B pathway). Additionally, PERK and ATF6 have been reported to promote NF- κ B activation. In response to ER stress, activation of the PERK-eIF2 α signaling pathway results in the attenuation of global mRNA translation and decreased translation of both I κ B and NF- κ B. Due to a shorter half-life of I κ B compared to NF- κ B, the higher proportion of NF- κ B to I κ B favors NF- κ B-mediated inflammatory responses.^{71,72} Moreover, the ATF6-mediated arm of the UPR has been demonstrated to activate NF- κ B.⁷¹ Therefore, this data highlights that ATF6 directly participates in regulating the inflammatory response as a transcription factor.

The effect of NSAIDs on UPR signaling was first described in a search for mechanisms underlying the adverse effects of these drugs. For example, studies carried

out by Tsutsumi et al.⁷³ showed that cultured guinea pig gastric mucosal cells treated with NSAIDs (indomethacin, diclofenac, ibuprofen, and celecoxib) decreased cell viability, increased DNA fragmentation, and displayed elevated CHOP mRNA and protein. Additionally, indomethacin was shown to induce the expression of other components of the UPR pathway, such as GRP78, ATF6, ATF4, and XBP1. In those studies, NSAIDs elicited ER stress-dependent apoptosis of cultured gastric mucosal cells, which was particularly related to the expression of CHOP.⁷³

NSAIDs effect on UPR signaling and cancer

Other studies have shown that the UPR-dependent induction of apoptosis by NSAIDs has important anti-cancer actions²⁷; therefore, the anti-neoplastic effect of NSAIDs has been widely studied in various types of cancer and was found to be associated with COX-dependent mechanisms, as well as with anti-apoptotic properties resulting from ER stress stimulation (Table 2).

Endoplasmic reticulum (ER) stress is an important factor in cancer development as increased expression of the main components of UPR pathways was observed in tissue sections from a variety of human tumors. In different cancer cell types, such as glioblastoma, breast and pancreatic carcinoma, Burkitt's lymphoma, and multiple myeloma, celecoxib was shown to induce activation of ER stress-associated proteins GRP78, CHOP and caspase-4, resulting in cancer cell death.^{27,74} In gastric carcinoma cells, the pro-apoptotic action of celecoxib was demonstrated to be related to PERK and eIF2 α phosphorylation, leading to ATF4 expression. However, silencing of ATF4 partially reversed the overexpression of GRP78, which was also induced by celecoxib, suggesting that ATF4 was one of the UPR arms responsible for GRP78 upregulation after celecoxib treatment.²⁵ A recent meta-analysis of studies focusing on the molecular mechanisms of celecoxib in tumor development further highlighted its various anti-cancer actions.⁷⁵ It was shown that celecoxib mainly regulates the proliferation, migration and invasion of tumor cells by inhibiting the COX-2/prostaglandin E2 signal axis, thereby inhibiting the phosphorylation of NF- κ B gene binding Akt, a signal transducer and activator of transcription, and the expression of MMP-2 and MMP-9. Likewise, diclofenac and indomethacin also efficiently activated the PERK pathway of the UPR, which enhanced the expression of the pro-apoptotic GADD153/CHOP protein in Huh7 hepatoma cells.²⁶

However, NSAIDs do not always cause ER stress-dependent apoptosis in cancer cells. Yamazaki et al.²³ were the first to demonstrate that diclofenac, indomethacin, ibuprofen, aspirin, and ketoprofen have protective effects against ER-stress-induced apoptosis of human neuroblastoma SH-SY5Y cells, and this is independent of its COX-inhibitory activity.

NSAIDs and the UPR signaling in other experimental models

The role of UPR signaling in the mechanism of action of NSAIDs has been widely studied in cancer cells. However, limited data are available for other experimental models (Table 2). For example, in endothelial cells, diclofenac significantly inhibited the activation of ER stress-responsive genes, i.e., *CHOP/DIT3*, *GRP78/HSPA5* and *DNAJB9*. Additionally, the drug diminished the significant upregulation and release of the GRP78 protein in endothelial cells.²⁴ Similar effects in endothelial cells (e.g., HCAEC, HPAEC and HUVECs) were obtained after the application of meloxicam, ibuprofen and acetylsalicylic acid, although notably not for celecoxib. Celecoxib downregulated ATF6 and GRP78 expression, as well as IRE1 α and PERK phosphorylation stimulated by ER-stress inducer tunicamycin.²⁰ There is also a study on a model of cerebral ischemic injury, in which parecoxib significantly suppressed cerebral ischemic injury-induced nuclear translocation of CHOP and Foxo1, and attenuated the immunoreactivity of caspase-12 in ischemic penumbra. Furthermore, the protective effect of parecoxib was accompanied by an increased GRP78 and 150-kDa oxygen-regulated protein (ORP150) expression. This study suggested that elevated GRP78 and ORP150, and suppression of CHOP and Foxo1 nuclear translocation may contribute to parecoxib-mediated neuroprotection during ER stress responses.²⁸ The effects of NSAIDs on components of the UPR pathway in different experimental models are summarized in Table 2.

PPAR γ compared to NF- κ B compared to the UPR pathway

This paper presents a certain outline of anti- and pro-inflammatory processes that might be modified by NSAIDs that involve 3 different pathways related to PPAR γ , NF- κ B and UPR signaling. While they appear closely related, there are currently only limited data on their interrelation (Fig. 3). For example, it was demonstrated that inflammatory stimuli can induce NF- κ B, and early activation of NF- κ B stimulates 3 branches of the UPR, being PERK, ATF and IRE1. Conversely, prolonged ER stress results

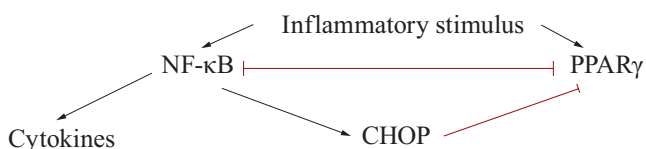


Fig. 3. Relations between peroxisome proliferator-activated receptor gamma (PPAR γ), nuclear factor- κ B (NF- κ B) and unfolded protein response (UPR) pathways. Inflammatory stimulus induces pro-inflammatory pathways such as NF- κ B and anti-inflammatory mechanism of action through the PPAR γ . These transcription factors can inhibit each other. NF- κ B induces the UPR pathway and the release of cytokines. During chronic inflammation and prolonged endoplasmic reticulum (ER) stress, the expression of CHOP is stimulated. CHOP inhibits PPAR γ .

in CHOP expression, that is responsible for the low level of PPAR γ . In the absence of CHOP, PPAR γ was strongly upregulated in epithelial cells.⁷⁰ Okamura et al.⁷⁶ showed that the anti-inflammatory potential of the UPR may be mediated, at least in part, by the induction of GRP78, leading to diminished activation of NF- κ B. The ER chaperone GRP78 also has anti-inflammatory and immunomodulatory properties when present in the extracellular environment.⁷² However, in some cell types, e.g., in human prostate cancer cells, GRP78 may be involved in the activation of NF- κ B by suppressing the activation of IKK.⁷⁷ Thus, the role of GRP78 and other factors of the UPR pathway in the regulation of NF- κ B is complex and is likely to be cell type-dependent.

Potential new therapeutic applications of non-steroidal anti-inflammatory drugs (NSAIDs) in cancer

As shown in Table 2, many studies on the impact of NSAIDs on PPAR, NF- κ B and UPR pathways have been conducted on cancer cells or in xenograft tumors. The reason for this is that the classical mechanism of action of NSAIDs, responsible for their anti-inflammatory effects, i.e., inhibition of COX-1 and COX-2 enzymes, also contributes to cancer development. Particularly, COX-2 expressed in response to inflammation seems to play a leading role in most cancers. This discovery has led to the investigation of further mechanisms underlying the involvement of COX enzymes in cancer development, aiming to clarify this phenomenon. For example, it has been shown that PGE₂, which is a product of COX action, is involved in cancer cell proliferation, invasion, migration, and angiogenesis. For these reasons, NSAIDs, by inhibiting COX-2, may show anti-cancer action, and this new property of the drugs has become the subject of intensive research.¹⁹ In this review, it was demonstrated that alternative pathways induced by NSAIDs, i.e., PPAR γ stimulation, inhibition of NF- κ B activation, or modulatory effects on different components of the UPR pathway, on the one hand, may enhance the basic anti-inflammatory mechanism of action of the drugs, and on the other hand, may be directly involved in different, e.g., anti-cancer effects of NSAIDs.

Promising results of the in vitro studies contributed to the administration of NSAIDs to cancer patients, leading to the analysis of the relationship between taking these drugs and the incidence of cancer. The use of NSAIDs in patients showed different effects, not always as spectacular as in experiments in vitro. Therefore, in most of the studies (Table 3), the need for further research and analysis regarding dosage, treatment duration, and, most importantly, the selection of the drug from the group

Table 3. Examples of potential new therapeutic applications of NSAIDs. The order of research presented is arranged alphabetically by disease, i.e., tissue origin of cancer, next: degree of advancement, next: neurodegenerative diseases, next: neurological disorder

Disease	Type of study	Methodology	Results	Ref.
Cancer				
Bladder cancer	epidemiological study	1,514 cases of incident bladder cancer	All classes of NSAIDs, except pyrazolon derivatives, were negatively associated with bladder cancer risk. Protective effect varied in strength by subcategories of formulation: the strongest for acetic acids and the weakest for aspirin/other salicylic acids and oxicam.	79
Breast cancer	meta-analysis	16 studies with 23,813 participants	The use of NSAIDs may be associated with a small decrease in the risk of breast cancer. However, the available data are insufficient to estimate the dose–response effect for duration and frequency of use of any particular types of NSAID.	80
Colorectal cancer	systematic reviews and meta-analyses	986 participants with low dose of aspirin (81–325 mg/day) 2,289 participants with celecoxib (400–800 mg/day) 1,277 participants with rofecoxib (25 mg/day)	The beneficial effect of low-dose aspirin on recurrence of any adenomas. The effect on advanced adenomas was inconclusive. Possible increased risk of recurrence of adenomas observed after discontinuing regular use of NSAIDs.	81
Ovarian cancer	systematic review and meta-analysis of observational studies	380,277 participants	The use of aspirin significantly reduced the risk of invasive ovarian cancer. A similar tendency was observed for non-aspirin NSAIDs, but the results were not significant.	82
Prostate cancer	systematic review and meta-analysis	108,136 cases from 39 observational studies (20 case-control and 19 cohort studies)	No association with the use of non-aspirin NSAIDs and the development of prostate cancer. Aspirin provided potential benefits in the reduction of prostate cancer incidence.	83
Advanced cancer	meta-analysis of 11 randomized clinical trials	11 randomized clinical trials consisting of 2,570 patients with advanced cancer	Celecoxib showed a benefit in the treatment of advanced cancers but with increased risk of cardiovascular events. Benefit compared to harm needs to be carefully considered when celecoxib is recommended in patients with advanced cancers.	84
Neurodegenerative diseases				
Alzheimer's disease (AD)	systematic review and meta-analysis of observational studies	14,654 participants	NSAIDs offered some protection against the AD development. The appropriate dosage and duration of drug use and the ratio of risk to benefit are unclear.	85
	systematic review prospective and non-prospective studies	7 non-prospectives studies with 1,500 AD cases and 3 prospectives studies with 475 AD cases	NSAIDs exposure was associated with decreased risk of AD.	86
	meta-analysis based on the preferred reporting items for systematic reviews and meta-analysis checklist	236,022 participants	NSAIDs exposure might be significantly associated with reduced risk of AD.	87
Parkinson's disease (PD)	systemic review meta-analysis of observational studies random-effects meta-analyses	301,420 participants	Protective effect of non-aspirin, non-steroidal anti-inflammatory drugs on the risk of PD possibly by influencing a neuroinflammatory pathways in the pathogenesis of PD.	89
	meta-analysis, cohort, case-control	17 articles with 14,713 patients with PD	No association between NSAIDs and the risk of PD.	89
	systematic review and meta-analysis of observational studies	11 studies with 1,020,379 participants	NSAIDs as a class did not seem to modify the risk of PD. Ibuprofen may have a slight protective effect in lowering the risk of PD.	91
	meta-analyses of prospective studies	136,197 participants	Ibuprofen but not other NSAIDs lowered the risk of PD.	91

Table 3. Examples of potential new therapeutic applications of NSAIDs – cont.

Disease	Type of study	Methodology	Results	Ref.
Neurological disorders				
Depression	randomized double-blind placebo-controlled study	40 patients with MDD received celecoxib (200 mg twice daily) or placebo in addition to sertraline (200 mg/day) for 6 weeks.	Reduction of interleukin-6 by celecoxib. Celecoxib can be effective as an adjunctive antidepressant.	92
	double-blind randomized placebo control	40 patients with psychotic depression receiving reboxetine (4–10 mg/day) with celecoxib (400 mg/day) or reboxetine with placebo for 6 weeks	Additional treatment with celecoxib had significant positive effects on the therapeutic action of reboxetine with regard to depressive symptomatology.	93
	double-blind randomized placebo control	40 patients with depression received celecoxib (400 mg/day) or placebo with fluoxetine (40 mg)	The combination of fluoxetine and celecoxib showed a significant superiority effect over fluoxetine alone in the treatment of symptoms of major depression.	94
	review and meta-analysis randomized placebo-control trials	14 trials (6,262 participants) with subanalyses with celecoxib (200–400 mg/day)	Celecoxib decreased depressive symptoms without increased risks of adverse effects.	95
	review and meta-analysis randomized controlled trials	312 participants with bipolar depression, 53 patients received NSAIDs	A moderate antidepressant effect for adjunctive NSAIDs compared with conventional therapy alone in the treatment of bipolar depression.	96

NSAIDs – non-steroidal anti-inflammatory drugs; MDD – major depressive disorder.

is emphasized. Examples of epidemiologic studies have shown a diminished incidence of adenomatous polyps and lower colorectal cancer death rates in persons regularly taking NSAIDs. It suggests a possible protective effect of NSAIDs on the general population. Some recent randomized clinical trials showed that aspirin suppressed the recurrence of adenomatous polyps in patients with a previous polyp.⁷⁸ In turn, the use of all classes of NSAIDs, except pyrazolone derivatives, suppressed the bladder cancer risk; however, the protective effects varied in strength depending on the subcategories of the formulation.⁷⁹ More examples can be found in Table 3.

Potential new therapeutic applications of NSAIDs in CNS disorders

Central nervous system disorders, including those of a psychiatric or neurological nature, are a major challenge for medicine and public health worldwide. They are multifaceted disorders with diverse and ill-defined pathophysiological mechanisms, e.g., the development of inflammatory processes, ER stress and disturbance of neuronal–glial communication. The pathological processes are associated with specific signaling pathways, and their elements can become strategic points of development for new drugs and for new applications of those already approved. Therefore, NSAIDs have been used in epidemiological studies analyzing their therapeutic effectiveness as protective factors in CNS disorders.

Neuroinflammation with the involvement of NF- κ B, PPAR γ and the UPR pathways also has an impact

on the development of CNS disorders. Neuroinflammation is a defense mechanism that initially protects the brain by removing or inhibiting diverse pathogens, but persistent inflammation can induce microglia and astrocytes toward a proinflammatory phenotype, which causes the neurotoxic effect. The UPR dysfunction, which is characterized by the accumulation and aggregation of misfolded proteins, mediates neuronal death in Alzheimer's disease (AD), Parkinson's disease (PD), amyotrophic lateral sclerosis (ALS), Huntington's disease (HD), and psychiatric disorders such as schizophrenia, depression and post-traumatic stress disorder (PTSD).^{97,98} Considering all 3 trans-ER membrane stress sensors (IRE1, PERK and ATF6) are present in astrocytes, it is clear that the PERK-mediated arm of the UPR is most linked to the induction of inflammatory responses in astrocytes and may be a target to attenuate immune responses in neurological diseases. However, other signaling molecules may also contribute to the pathogenic activities of astrocytes.

Currently, there are several neuroprotective mechanisms of NSAIDs being investigated, including those resulting from the stimulation of the PPAR γ receptor and the reduction of microglia activation. It is believed that activation of these anti-inflammatory effects may contribute to the anti-amyloidogenic action of NSAID.^{85,99,100}

Various clinical trials have already revealed promising results using PPAR γ agonists and, therefore, may represent an attractive therapeutic target for the treatment of AD.¹⁰⁰ Many clinical trials and meta-analyses have shown that NSAID exposure may be significantly associated with a reduced risk of AD.^{85,86} However, this evidence was only based on observational studies, while other types of investigations did not find this association.⁸⁵

According to the analysis of prospective and retrospective studies, NSAID exposure was associated with a decreased risk of AD, slower progression and reduced severity of dementia.⁸⁶ Similar neuroprotective effects, although still controversial, were obtained in other neurodegenerative disorders such as PD. A meta-analysis presented by Gagne and Power⁸⁸ indicated that the use of non-aspirin NSAIDs, particularly ibuprofen, reduced the risk of PD by 15%, while the use of aspirin did not show any effect. The NSAIDs have demonstrated neuroprotective potential, but a meta-analysis by Poly et al.⁸⁹ showed that there is no association between NSAIDs and the risk of PD at the population level. Other research suggested that ibuprofen may have a slight protective effect in lowering the risk of PD, whereas NSAIDs as a class of drugs do not seem to modify the risk of PD.^{90,91}

Neuroinflammation is implicated in a variety of neurologic and somatic illnesses, including depression. It has been reported that a significant proportion of major depressive disorder (MDD) patients exhibit increased levels of TNF- α and IL-6 in plasma.^{101,102} Neuroinflammation also contributes to non-responsiveness to current antidepressant therapies. It has been shown that the response to conventional antidepressant medications is associated with a decrease in inflammatory biomarkers, whereas resistance to treatment is accompanied by increased inflammation.¹⁰³ For these reasons, there have been few successful trials investigating whether treatment with NSAIDs may show beneficial effects on MDD. Meta-analyses of randomized controlled trials (RCTs) of NSAIDs, given in monotherapy or as add-on therapy, indicated that these medications may be beneficial in treating depression.^{93,95} For example, a combination of celecoxib with sertraline or fluoxetine could exhibit a more efficacious antidepressant effect than sertraline or fluoxetine treatment alone.^{92,94} However, another meta-analysis of adjunctive use of NSAIDs in the treatment of bipolar depression showed only moderate antidepressant effects of the drugs compared with conventional therapy alone.⁹⁶ In a retrospective analysis of the association between NSAID use by adults with chronic inflammatory conditions and the presence of depression among them, no statistically significant results were observed.¹⁰⁴

Several studies have provided evidence that PPAR γ receptor expression or the levels of its endogenously produced modulators are downregulated in several neurological and psychiatric disorders such as depression,¹⁰⁵ schizophrenia¹⁰⁶ and PD.¹⁰⁷ Therefore, synthetic agonists should be investigated in the context of these disorders.¹⁰⁸

Conclusions

Non-steroidal anti-inflammatory drugs have a well-established role in the human therapeutic arsenal, but still, new perspectives are being discovered. This


review presents new anti-inflammatory molecular targets of NSAIDs involving actions on PPAR γ , NF- κ B and the components of the UPR pathway. More importantly, the effects of NSAIDs on these signaling molecules are observed in higher concentrations than those required for COX inhibition. However, it should be emphasized that it is difficult to compare concentrations used in laboratory studies, i.e., on cell lines, with effective doses necessary to obtain the effect in humans. Additionally, some literature shows derivatives of individual drugs from the anti-inflammatory group, which more potently affect the above-mentioned molecular targets, and thus they may become a valuable alternative to classic NSAIDs in the future.


Another aspect is the search for new drug targets for the therapy of neurological and neurodegenerative disorders or cancers. Many epidemiological prospective and retrospective studies show the beneficial contribution of NSAIDs in the prevention or treatment of these diseases, but the mechanisms of the observed effects remain mostly unknown. Nevertheless, searching for new applications and molecular targets of already approved drugs represents an important avenue of exploration and may contribute to the development of more effective therapies. However, the question of whether NSAIDs or other drugs affecting PPAR γ , NF- κ B or UPR pathways will be applied in the future in the treatment of cancers or neurodegenerative disorders still needs answering.

ORCID iDs

Paulina Sokółowska  <https://orcid.org/0000-0002-6290-7172>

Layla Bleibel  <https://orcid.org/0009-0008-8586-1462>

Jacek Owczarek  <https://orcid.org/0000-0001-5688-4819>

Anna Wiktorowska-Owczarek  <https://orcid.org/0000-0003-3452-5748>

References

- Kaplan Ö, Nazroğlu M, Güney M, Aykur M. Non-steroidal anti-inflammatory drug modulates oxidative stress and calcium ion levels in the neutrophils of patients with primary dysmenorrhea. *J Reprod Immunol*. 2013;100(2):87–92. doi:10.1016/j.jri.2013.10.004
- Zakrocka I, Załuska W. The influence of cyclooxygenase inhibitors on kynurenic acid production in rat kidney: A novel path for kidney protection? *Pharmacol Rep*. 2023;75(2):376–385. doi:10.1007/s43440-023-00460-w
- Houshmand G, Naghizadeh B, Ghorbanzadeh B, Ghafouri Z, Goudarzi M, Mansouri MT. Celecoxib inhibits acute edema and inflammatory biomarkers through peroxisome proliferator-activated receptor- γ in rats. *Iran J Basic Med Sci*. 2020;23(12):1544–1550. doi:10.22038/ijbms.2020.43995.10315
- Zhang M, Xu ZG, Shi Z, et al. Inhibitory effect of celecoxib in lung carcinoma by regulation of cyclooxygenase-2/cytosolic phospholipase A2 and peroxisome proliferator-activated receptor gamma. *Mol Cell Biochem*. 2011;355(1–2):233–240. doi:10.1007/s11010-011-0859-5
- Puhl AC, Milton FA, Cvorova A, et al. Mechanisms of peroxisome proliferator activated receptor γ regulation by non-steroidal anti-inflammatory drugs. *Nucl Recept Signal*. 2015;13:e004. doi:10.1621/nrs.13004
- Lehmann JM, Lenhard JM, Oliver BB, Ringold GM, Kliewer SA. Peroxisome proliferator-activated receptors alpha and gamma are activated by indomethacin and other non-steroidal anti-inflammatory drugs. *J Biol Chem*. 1997;272(6):3406–3410. doi:10.1074/jbc.272.6.3406
- Jaradat MS, Wongsud B, Phornchirasilp S, et al. Activation of peroxisome proliferator-activated receptor isoforms and inhibition of prostaglandin H2 synthases by ibuprofen, naproxen, and indomethacin. *Biochem Pharmacol*. 2001;62(12):1587–1595. doi:10.1016/S0006-2952(01)00822-X

8. Adamson DJA, Frew D, Tatoud R, Wolf CR, Palmer CNA. Diclofenac antagonizes peroxisome proliferator-activated receptor-gamma signaling. *Mol Pharmacol*. 2002;61(1):7–12. doi:10.1124/mol.61.1.7
9. Wang Y, Kong L, Sun B, Cui J, Shen W. Celecoxib induces adipogenic differentiation of hemangioma-derived mesenchymal stem cells through the PPAR- γ pathway in vitro and in vivo. *Exp Ther Med*. 2022;23(6):375. doi:10.3892/etm.2022.11303
10. Kazberuk A, Chalecka M, Palka J, Surazynski A. Nonsteroidal anti-inflammatory drugs as PPAR γ agonists can induce PRODH/POX-dependent apoptosis in breast cancer cells: New alternative pathway in NSAID-induced apoptosis. *Int J Mol Sci*. 2022;23(3):1510. doi:10.3390/ijms23031510
11. Shishodia S, Koul D, Aggarwal BB. Cyclooxygenase (COX)-2 inhibitor celecoxib abrogates TNF-induced NF- κ B activation through inhibition of activation of I kappa B alpha kinase and Akt in human non-small cell lung carcinoma: Correlation with suppression of COX-2 synthesis. *J Immunol*. 2004;173(3):2011–2022. doi:10.4049/jimmunol.173.3.2011
12. Funakoshi-Tago M, Shimizu T, Tago K, et al. Celecoxib potently inhibits TNF α -induced nuclear translocation and activation of NF- κ B. *Biochem Pharmacol*. 2008;76(5):662–671. doi:10.1016/j.bcp.2008.06.015
13. Karakawa A, Fukawa Y, Okazaki M, et al. Diclofenac sodium inhibits NF κ B transcription in osteoclasts. *J Dent Res*. 2009;88(11):1042–1047. doi:10.1177/0022034509346147
14. Daultbaev N, Lam J, Eklove D, Iskandar M, Lands LC. Ibuprofen modulates NF- κ B activity but not IL-8 production in cystic fibrosis respiratory epithelial cells. *Respiration*. 2010;79(3):234–242. doi:10.1159/000255342
15. Niederberger E, Manderscheid C, Geisslinger G. Different COX-independent effects of the COX-2 inhibitors etoricoxib and lumiracoxib. *Biochem Biophys Res Commun*. 2006;342(3):940–948. doi:10.1016/j.bbrc.2006.02.040
16. Takada Y, Bhardwaj A, Potdar P, Aggarwal BB. Nonsteroidal anti-inflammatory agents differ in their ability to suppress NF- κ B activation, inhibition of expression of cyclooxygenase-2 and cyclin D1, and abrogation of tumor cell proliferation. *Oncogene*. 2004;23(57):9247–9258. doi:10.1038/sj.onc.1208169
17. Krajka-Kuźniak V, Papierska K, Narożna M, Jelińska A, Majchrzak-Celińska A. Cannabidiol and its combinations with nonsteroidal anti-inflammatory drugs induce apoptosis and inhibit activation of NF- κ B signaling in vulvar squamous cell carcinoma. *Molecules*. 2022;27(24):8779. doi:10.3390/molecules27248779
18. Zhang NY, Wang TH, Chou CH, et al. Ibuprofen treatment ameliorates memory deficits in rats with collagen-induced arthritis by normalizing aberrant MAPK/NF- κ B and glutamatergic pathways. *Eur J Pharmacol*. 2022;933:175256. doi:10.1016/j.ejphar.2022.175256
19. Zhang X, Yan K, Deng L, et al. Cyclooxygenase 2 promotes proliferation and invasion in ovarian cancer cells via the PGE $_2$ /NF- κ B pathway. *Cell Transplant*. 2019;28(1_suppl):1S–13S. doi:10.1177/0963689719890597
20. Haas MJ, Warda F, Bikkina P, et al. Differential effects of cyclooxygenase-2 (COX-2) inhibitors on endoplasmic reticulum (ER) stress in human coronary artery endothelial cells. *Vascul Pharmacol*. 2022;142:106948. doi:10.1016/j.vph.2021.106948
21. Park G, Jin D, Kim D. Sequential treatment with celecoxib and bortezomib enhances the ER stress-mediated autophagy-associated cell death of colon cancer cells. *Oncol Lett*. 2018;16(4):4526–4536. doi:10.3892/ol.2018.9233
22. Maeng HJ, Song JH, Kim GT, et al. Celecoxib-mediated activation of endoplasmic reticulum stress induces de novo ceramide biosynthesis and apoptosis in hepatoma HepG2 cells. *BMB Rep*. 2017;50(3):144–149. doi:10.5483/BMBRep.2017.50.3.197
23. Yamazaki T, Muramoto M, Oe T, et al. Diclofenac, a non-steroidal anti-inflammatory drug, suppresses apoptosis induced by endoplasmic reticulum stresses by inhibiting caspase signaling. *Neuropharmacology*. 2006;50(5):558–567. doi:10.1016/j.neuropharm.2005.10.016
24. Sokołowska P, Siatkowska M, Józwiak-Bębenista M, et al. Diclofenac diminished the unfolded protein response (UPR) induced by tunicamycin in human endothelial cells. *Molecules*. 2022;27(11):3449. doi:10.3390/molecules27113449
25. Tsutsumi S, Namba T, Tanaka KI, et al. Celecoxib upregulates endoplasmic reticulum chaperones that inhibit celecoxib-induced apoptosis in human gastric cells. *Oncogene*. 2006;25(7):1018–1029. doi:10.1038/sj.onc.1209139
26. Franceschelli S, Moltedo O, Amodio G, Tajana G, Remondelli P. In the Huh7 hepatoma cells diclofenac and indomethacin activate differently the unfolded protein response and induce ER stress apoptosis. *Open Biochem J*. 2011;5:45–51. doi:10.2174/1874091X01105010045
27. Pyrko P, Kardosh A, Liu YT, et al. Calcium-activated endoplasmic reticulum stress as a major component of tumor cell death induced by 2,5-dimethyl-celecoxib, a non-coxib analogue of celecoxib. *Mol Cancer Ther*. 2007;6(4):1262–1275. doi:10.1158/1535-7163.MCT-06-0629
28. Ye Z, Wang N, Xia P, Wang E, Liao J, Guo Q. Parecoxib suppresses CHOP and Foxo1 nuclear translocation, but increases GRP78 levels in a rat model of focal ischemia. *Neurochem Res*. 2013;38(4):686–693. doi:10.1007/s11064-012-0953-4
29. Grosser T, Ricciotti E, FitzGerald GA. The cardiovascular pharmacology of nonsteroidal anti-inflammatory drugs. *Trends Pharmacol Sci*. 2017;38(8):733–748. doi:10.1016/j.tips.2017.05.008
30. Rao P, Knaus EE. Evolution of nonsteroidal anti-inflammatory drugs (NSAIDs): Cyclooxygenase (COX) inhibition and beyond. *J Pharm Pharm Sci*. 2008;11(2):815–110s. doi:10.18433/J3T886
31. Davies JA. Arachidonic acid. In: *xPharm: The Comprehensive Pharmacology Reference*. Amsterdam, the Netherlands: Elsevier; 2008:1–4. doi:10.1016/B978-008055232-3.63337-9
32. Vane JR, Botting RM. The mechanism of action of aspirin. *Thromb Res*. 2003;110(5–6):255–258. doi:10.1016/S0049-3848(03)00379-7
33. Bindu S, Mazumder S, Bandyopadhyay U. Non-steroidal anti-inflammatory drugs (NSAIDs) and organ damage: A current perspective. *Biochem Pharmacol*. 2020;180:114147. doi:10.1016/j.bcp.2020.114147
34. Faki Y, Er A. Different chemical structures and physiological/pathological roles of cyclooxygenases. *Rambam Maimonides Med J*. 2021;12(1):e0003. doi:10.5041/RMMJ.10426
35. Zarghi A, Arfaei S. Selective COX-2 inhibitors: A review of their structure-activity relationships. *Iran J Pharm Res*. 2011;10(4):655–683. PMID:24250402. PMCID:PMC3813081.
36. Chandrasekharan NV, Dai H, Roos KLT, et al. COX-3, a cyclooxygenase-1 variant inhibited by acetaminophen and other analgesic/antipyretic drugs: Cloning, structure, and expression. *Proc Natl Acad Sci U S A*. 2002;99(21):13926–13931. doi:10.1073/pnas.162468699
37. Zidar N, Odar K, Glavac D, Jerse M, Zupanc T, Stajer D. Cyclooxygenase in normal human tissues: Is COX-1 really a constitutive isoform, and COX-2 an inducible isoform? *J Cell Mol Med*. 2009;13(9B):3753–3763. doi:10.1111/j.1582-4934.2008.00430.x
38. Silverstein FE, Faich G, Goldstein JL, et al. Gastrointestinal toxicity with celecoxib vs nonsteroidal anti-inflammatory drugs for osteoarthritis and rheumatoid arthritis: The CLASS study. A randomized controlled trial. Celecoxib Long-Term Arthritis Safety Study. *JAMA*. 2000;284(10):1247–1255. doi:10.1001/jama.284.10.1247
39. Ritter J, Flower R, Henderson G, Loke YK, MacEwan D, Rang HP. *Rang & Dale's Pharmacology*. 9th ed. Edinburgh–London–New York: Elsevier; 2020. ISBN:978-0-7020-7448-6.
40. Kowalski ML, Makowska JS. Seven steps to the diagnosis of NSAIDs hypersensitivity: How to apply a new classification in real practice? *Allergy Asthma Immunol Res*. 2015;7(4):312–320. doi:10.4168/aaair.2015.7.4.312
41. Vane JR, Botting RM. Anti-inflammatory drugs and their mechanism of action. *Inflamm Res*. 1998;47(Suppl 2):S78–S87. doi:10.1007/s00011050284
42. Kaduševičius E. Novel applications of NSAIDs: Insight and future perspectives in cardiovascular, neurodegenerative, diabetes and cancer disease therapy. *Int J Mol Sci*. 2021;22(12):6637. doi:10.3390/ijms22126637
43. Marion-Letellier R, Savoye G, Ghosh S. Fatty acids, eicosanoids and PPAR gamma. *Eur J Pharmacol*. 2016;785:44–49. doi:10.1016/j.ejphar.2015.11.004
44. Korbecki J, Bobiński R, Dutka M. Self-regulation of the inflammatory response by peroxisome proliferator-activated receptors. *Inflamm Res*. 2019;68(6):443–458. doi:10.1007/s00011-019-01231-1
45. Schoonjans K, Staels B, Auwerx J. The peroxisome proliferator activated receptors (PPARs) and their effects on lipid metabolism and adipocyte differentiation. *Biochim Biophys Acta*. 1996;1302(2):93–109. doi:10.1016/0005-2760(96)00066-5
46. Grygiel-Górniak B. Peroxisome proliferator-activated receptors and their ligands: Nutritional and clinical implication. A review. *Nutr J*. 2014;13:17. doi:10.1186/1475-2891-13-17

47. Bernardo A, Minghetti L. PPAR-gamma agonists as regulators of microglial activation and brain inflammation. *Curr Pharm Des.* 2006;12(1): 93–109. doi:10.2174/138161206780574579
48. Bernardo A, Minghetti L. Regulation of glial cell functions by PPAR- natural and synthetic agonists. *PPAR Res.* 2008;2008:864140. doi:10.1155 /2008/864140
49. Moreno S, Farioli-Vecchioli S, Cerù MP. Immunolocalization of peroxisome proliferator-activated receptors and retinoid x receptors in the adult rat CNS. *Neuroscience.* 2004;123(1):131–145. doi:10.1016/j. neuroscience.2003.08.064
50. Tsuji T, Asanuma M, Miyazaki I, Miyoshi K, Ogawa N. Reduction of nuclear peroxisome proliferator-activated receptor γ expression in methamphetamine-induced neurotoxicity and neuroprotective effects of ibuprofen. *Neurochem Res.* 2009;34(4):764–774. doi:10.1007/ s11064-008-9863-x
51. Ricote M, Li AC, Willson TM, Kelly CJ, Glass CK. The peroxisome proliferator-activated receptor- γ is a negative regulator of macrophage activation. *Nature.* 1998;391(6662):79–82. doi:10.1038/34178
52. Mazidi M, Karimi E, Meydani M, Ghayour-Mobarhan M, Ferns GA. Potential effects of curcumin on peroxisome proliferator-activated receptor- γ in vitro and in vivo. *World J Methodol.* 2016;6(1):112–117. doi:10.5662/wjm.v6.i1.112
53. Liu Y, Qu Y, Liu L, et al. PPAR- γ agonist pioglitazone protects against IL-17 induced intervertebral disc inflammation and degeneration via suppression of NF- κ B signaling pathway. *Int Immunopharmacol.* 2019;72:138–147. doi:10.1016/j.intimp.2019.04.012
54. Yu H, Wang L, Huang K, et al. PPAR- γ agonist pioglitazone alleviates inflammatory response induced by lipopolysaccharides in osteoblast cells. *J Orthop Res.* 2022;40(11):2471–2479. doi:10.1002/jor.25279
55. Kojo H, Fukagawa M, Tajima K, et al. Evaluation of human peroxisome proliferator-activated receptor (PPAR) subtype selectivity of a variety of anti-inflammatory drugs based on a novel assay for PPAR delta(beta). *J Pharmacol Sci.* 2003;93(3):347–355. doi:10.1254/ jphs.93.347
56. Oeckinghaus A, Ghosh S. The NF- κ B family of transcription factors and its regulation. *Cold Spring Harb Perspect Biol.* 2009;1(4): a000034. doi:10.1101/cshperspect.a000034
57. Liu T, Zhang L, Joo D, Sun SC. NF- κ B signaling in inflammation. *Sig Transduct Target Ther.* 2017;2:17023. doi:10.1038/sigtrans.2017.23
58. Lawrence T. The nuclear factor NF- κ B pathway in inflammation. *Cold Spring Harb Perspect Biol.* 2009;1(6):a001651. doi:10.1101/cshperspect.a001651
59. Frantzas J, Logan J, Mollat P, et al. Hydrogen sulphide-releasing diclofenac derivatives inhibit breast cancer-induced osteoclastogenesis in vitro and prevent osteolysis ex vivo. *Br J Pharmacol.* 2012; 165(6):1914–1925. doi:10.1111/j.1476-5381.2011.01704.x
60. Shin JS, Baek SR, Sohn SI, Cho YW, Lee KT. Anti-inflammatory effect of pelubipirofen, 2-[4-(oxocyclohexylidene)methyl]-phenyl]propionic acid, mediated by dual suppression of COX activity and LPS-induced inflammatory gene expression via NF- κ B inactivation. *J Cell Biochem.* 2011;112(12):3594–3603. doi:10.1002/jcb.23290
61. Galecki P, Talarowska M. The evolutionary theory of depression. *Med Sci Monit.* 2017;23:2267–2274. doi:10.12659/MSM.901240
62. Scirpo R, Fiorotto R, Villani A, Amenduni M, Spirli C, Strazzabosco M. Stimulation of nuclear receptor peroxisome proliferator-activated receptor- γ limits NF- κ B-dependent inflammation in mouse cystic fibrosis biliary epithelium. *Hepatology.* 2015;62(5):1551–1562. doi:10.1002/hep.28000
63. Hou Y, Moreau F, Chadee K. PPAR γ is an E3 ligase that induces the degradation of NF κ B/p65. *Nat Commun.* 2012;3:1300. doi:10.1038/ncomms2270
64. Almanza A, Carlesso A, Chintha C, et al. Endoplasmic reticulum stress signalling: From basic mechanisms to clinical applications. *FEBS J.* 2019;286(2):241–278. doi:10.1111/febs.14608
65. Read A, Schröder M. The unfolded protein response: An overview. *Biology (Basel).* 2021;10(5):384. doi:10.3390/biology10050384
66. Wang J, Lee J, Liem D, Ping P. HSPA5 gene encoding Hsp70 chaperone BiP in the endoplasmic reticulum. *Gene.* 2017;618:14–23. doi:10.1016/j. gene.2017.03.005
67. Schröder M, Kaufman RJ. ER stress and the unfolded protein response. *Mutat Res.* 2005;569(1–2):29–63. doi:10.1016/j.mrfmmm.2004.06.056
68. Ron D, Walter P. Signal integration in the endoplasmic reticulum unfolded protein response. *Nat Rev Mol Cell Biol.* 2007;8(7):519–529. doi:10.1038/nrm2199
69. Rutkowski DT, Kaufman RJ. A trip to the ER: Coping with stress. *Trends Cell Biol.* 2004;14(1):20–28. doi:10.1016/j.tcb.2003.11.001
70. Hetz C. The biological meaning of the UPR. *Nat Rev Mol Cell Biol.* 2013;14(7):404. doi:10.1038/nrm3606
71. Shi M, Chai Y, Zhang J, Chen X. Endoplasmic reticulum stress-associated neuronal death and innate immune response in neurological diseases. *Front Immunol.* 2022;12:794580. doi:10.3389/fimmu.2021. 794580
72. Sprenkle NT, Sims SG, Sánchez CL, Meares GP. Endoplasmic reticulum stress and inflammation in the central nervous system. *Mol Neurodegener.* 2017;12(1):42. doi:10.1186/s13024-017-0183-y
73. Tsutsumi S, Gotoh T, Tomisato W, et al. Endoplasmic reticulum stress response is involved in nonsteroidal anti-inflammatory drug-induced apoptosis. *Cell Death Differ.* 2004;11(9):1009–1016. doi:10.1038/sj.cdd. 4401436
74. Mügge FLB, Silva AM. Endoplasmic reticulum stress response in the roadway for the effects of non-steroidal anti-inflammatory drugs. *Endoplasm Reticul Stress Dis.* 2015;2(1):1–17. doi:10.1515/ersc-2015-0001
75. Wen B, Wei YT, Mu LL, Wen GR, Zhao K. The molecular mechanisms of celecoxib in tumor development. *Medicine (Baltimore).* 2020;99(40): e22544. doi:10.1097/MD.00000000000022544
76. Okamura M, Takano Y, Hiramatsu N, et al. Suppression of cytokine responses by indomethacin in podocytes: A mechanism through induction of unfolded protein response. *Am J Physiol Renal Physiol.* 2008;295(5):F1495–F1503. doi:10.1152/ajprenal.00602.2007
77. Misra UK, Deedwania R, Pizzo SV. Activation and cross-talk between Akt, NF- κ B, and unfolded protein response signaling in 1-LN prostate cancer cells consequent to ligation of cell surface-associated GRP78. *J Biol Chem.* 2006;281(19):13694–13707. doi:10.1074/jbc. M511694200
78. Maniewska J, Jeżewska D. Non-steroidal anti-inflammatory drugs in colorectal cancer chemoprevention. *Cancers (Basel).* 2021;13(4):594. doi:10.3390/cancers13040594
79. Castela JE, Yuan JM, Gago-Dominguez M, Yu MC, Ross RK. Non-steroidal anti-inflammatory drugs and bladder cancer prevention. *Br J Cancer.* 2000;82(7):1364–1369. doi:10.1054/bjoc.1999.1106
80. Khuder SA, Mutgi AB. Breast cancer and NSAID use: A meta-analysis. *Br J Cancer.* 2001;84(9):1188–1192. doi:10.1054/bjoc.2000.1709
81. Veetil SK, Lim KG, Ching SM, Saokaew S, Phisalprapa P, Chaiyakunapruk N. Effects of aspirin and non-aspirin nonsteroidal anti-inflammatory drugs on the incidence of recurrent colorectal adenomas: A systematic review with meta-analysis and trial sequential analysis of randomized clinical trials. *BMC Cancer.* 2017;17(1):763. doi:10.1186/s12885-017-3757-8
82. Baandrup L, Faber MT, Christensen J, et al. Nonsteroidal anti-inflammatory drugs and risk of ovarian cancer: Systematic review and meta-analysis of observational studies. *Acta Obstet Gynecol Scand.* 2013;92(3):245–255. doi:10.1111/aogs.12069
83. Liu Y, Chen JQ, Xie L, et al. Effect of aspirin and other non-steroidal anti-inflammatory drugs on prostate cancer incidence and mortality: A systematic review and meta-analysis. *BMC Med.* 2014;12:55. doi:10.1186/1741-7015-12-55
84. Chen J, Shen P, Zhang XC, Zhao MD, Zhang XG, Yang L. Efficacy and safety profile of celecoxib for treating advanced cancers: A meta-analysis of 11 randomized clinical trials. *Clin Ther.* 2014;36(8):1253–1263. doi:10.1016/j.clinthera.2014.06.015
85. Etminan M, Gill S, Samii A. Effect of non-steroidal anti-inflammatory drugs on risk of Alzheimer's disease: Systematic review and meta-analysis of observational studies. *BMJ.* 2003;327(7407):128. doi:10.1136/bmj.327.7407.128
86. Szekely CA, Thorne JE, Zandi PP, et al. Nonsteroidal anti-inflammatory drugs for the prevention of Alzheimer's disease: A systematic review. *Neuroepidemiology.* 2004;23(4):159–169. doi:10.1159/000078501
87. Zhang C, Wang Y, Wang D, Zhang J, Zhang F. NSAID exposure and risk of Alzheimer's disease: An updated meta-analysis from cohort studies. *Front Aging Neurosci.* 2018;10:83. doi:10.3389/fnagi.2018.00083
88. Gagne JJ, Power MC. Anti-inflammatory drugs and risk of Parkinson disease: A meta-analysis. *Neurology.* 2010;74(12):995–1002. doi:10.1212 /WNL.0b013e3181d5a4a3

89. Poly TN, Islam MdM, Yang HC, Li YCJ. Non-steroidal anti-inflammatory drugs and risk of Parkinson's disease in the elderly population: A meta-analysis. *Eur J Clin Pharmacol*. 2019;75(1):99–108. doi:10.1007/s00228-018-2561-y
90. Samii A, Etmnan M, Wiens MO, Jafari S. NSAID use and the risk of Parkinson's disease: Systematic review and meta-analysis of observational studies. *Drugs Aging*. 2009;26(9):769–779. doi:10.2165/11316780-000000000-00000
91. Gao X, Chen H, Schwarzschild MA, Ascherio A. Use of ibuprofen and risk of Parkinson disease. *Neurology*. 2011;76(10):863–869. doi:10.1212/WNL.0b013e31820f2d79
92. Abbasi SH, Hosseini F, Modabbernia A, Ashrafi M, Akhondzadeh S. Effect of celecoxib add-on treatment on symptoms and serum IL-6 concentrations in patients with major depressive disorder: Randomized double-blind placebo-controlled study. *J Affect Disord*. 2012;141(2–3):308–314. doi:10.1016/j.jad.2012.03.033
93. Müller N, Schwarz MJ, Dehning S, et al. The cyclooxygenase-2 inhibitor celecoxib has therapeutic effects in major depression: Results of a double-blind, randomized, placebo controlled, add-on pilot study to reboxetine. *Mol Psychiatry*. 2006;11(7):680–684. doi:10.1038/sj.mp.4001805
94. Akhondzadeh S, Jafari S, Raisi F, et al. Clinical trial of adjunctive celecoxib treatment in patients with major depression: A double blind and placebo controlled trial. *Depress Anxiety*. 2009;26(7):607–611. doi:10.1002/da.20589
95. Köhler O, Benros ME, Nordentoft M, et al. Effect of anti-inflammatory treatment on depression, depressive symptoms, and adverse effects: A systematic review and meta-analysis of randomized clinical trials. *JAMA Psychiatry*. 2014;71(12):1381–1391. doi:10.1001/jama.psychiatry.2014.1611
96. Rosenblat JD, Kakar R, Berk M, et al. Anti-inflammatory agents in the treatment of bipolar depression: A systematic review and meta-analysis. *Bipolar Disord*. 2016;18(2):89–101. doi:10.1111/bdi.12373
97. Xiang C, Wang Y, Zhang H, Han F. The role of endoplasmic reticulum stress in neurodegenerative disease. *Apoptosis*. 2017;22(1):1–26. doi:10.1007/s10495-016-1296-4
98. Kwon HS, Koh SH. Neuroinflammation in neurodegenerative disorders: The roles of microglia and astrocytes. *Transl Neurodegener*. 2020;9(1):42. doi:10.1186/s40035-020-00221-2
99. Heneka MT, Kummer MP, Weggen S, et al. Molecular mechanisms and therapeutic application of NSAIDs and derived compounds in Alzheimer's disease. *Curr Alzheimer Res*. 2011;8(2):115–131. doi:10.2174/156720511795256099
100. Kummer MP, Heneka MT. PPARs in Alzheimer's disease. *PPAR Res*. 2008;2008:403896. doi:10.1155/2008/403896
101. Yoshimura R, Hori H, Ikenouchi-Sugita A, Umene-Nakano W, Ueda N, Nakamura J. Higher plasma interleukin-6 (IL-6) level is associated with SSRI- or SNRI-refractory depression. *Prog Neuropsychopharmacol Biol Psychiatry*. 2009;33(4):722–726. doi:10.1016/j.pnpbp.2009.03.020
102. Motivala SJ, Sarfatti A, Olmos L, Irwin MR. Inflammatory markers and sleep disturbance in major depression. *Psychosom Med*. 2005;67(2):187–194. doi:10.1097/01.psy.0000149259.72488.09
103. Adzic M, Brkic Z, Mitic M, et al. Therapeutic strategies for treatment of inflammation-related depression. *Curr Neuropharmacol*. 2018;16(2):176–209. doi:10.2174/1570159X15666170828163048
104. Shaikh NF, Sambamoorthi U. Prescription non-steroidal anti-inflammatory drugs (NSAIDs) and depression among adults with inflammatory chronic conditions in the United States. *Psychiatr Q*. 2020;91(1):209–221. doi:10.1007/s11126-019-09693-6
105. Rosa AO, Kaster MP, Binfaré RW, et al. Antidepressant-like effect of the novel thiazolidinone NP031115 in mice. *Prog Neuropsychopharmacol Biol Psychiatry*. 2008;32(6):1549–1556. doi:10.1016/j.pnpbp.2008.05.020
106. Sullivan CR, Mielnik CA, O'Donovan SM, et al. Connectivity analyses of bioenergetic changes in schizophrenia: Identification of novel treatments. *Mol Neurobiol*. 2019;56(6):4492–4517. doi:10.1007/s12035-018-1390-4
107. Quinn LP, Crook B, Hows ME, et al. The PPAR γ agonist pioglitazone is effective in the MPTP mouse model of Parkinson's disease through inhibition of monoamine oxidase B. *Br J Pharmacol*. 2008;154(1):226–233. doi:10.1038/bjpp.2008.78
108. Tufano M, Pinna G. Is there a future for PPARs in the treatment of neuropsychiatric disorders? *Molecules*. 2020;25(5):1062. doi:10.3390/molecules25051062

Investigation of cerebellar damage in adult amyotrophic lateral sclerosis patients using magnetic resonance imaging and diffusion tensor imaging

Marta Nowakowska-Kotas^{1,A–F}, Adrian Korbecki^{2,B–D,F}, Sławomir Budrewicz^{1,C,E,F}, Joanna Bładowska^{3,A,C,E,F}

¹ Department of Neurology, Wrocław Medical University, Poland

² Chair of Radiology, Department of General Radiology, Interventional Radiology and Neuroradiology, Wrocław Medical University, Poland

³ Department of Radiology, 4th Military Clinical Hospital, Wrocław, Poland

A – research concept and design; B – collection and/or assembly of data; C – data analysis and interpretation; D – writing the article; E – critical revision of the article; F – final approval of the article

Advances in Clinical and Experimental Medicine, ISSN 1899–5276 (print), ISSN 2451–2680 (online)

Adv Clin Exp Med. 2024;33(9):1023–1028

Address for correspondence

Marta Nowakowska-Kotas

E-mail: marta.nowakowska-kotas@umw.edu.pl

Funding sources

None declared

Conflict of interest

None declared

Received on March 26, 2023

Reviewed on May 12, 2023

Accepted on September 21, 2023

Published online on November 14, 2023

Cite as

Nowakowska-Kotas M, Korbecki A, Budrewicz S, Bładowska J. Investigation of cerebellar damage in adult amyotrophic lateral sclerosis patients using magnetic resonance imaging and diffusion tensor imaging. *Adv Clin Exp Med.* 2024;33(9):1023–1028. doi:10.17219/acem/172698

DOI

10.17219/acem/172698

Copyright

Copyright by Author(s)

This is an article distributed under the terms of the Creative Commons Attribution 3.0 Unported (CC BY 3.0) (<https://creativecommons.org/licenses/by/3.0/>)

Abstract

Background. Research on amyotrophic lateral sclerosis (ALS) reveals that the disorder is not restricted to motor neurons.

Objectives. This neuroimaging study aimed to investigate the presence of cerebellar damage in adult ALS patients.

Materials and methods. The study retrospectively analyzed magnetic resonance imaging (MRI) examinations performed on a 1.5T MR unit of 33 patients (17 men and 16 women with a mean age of 59.3 years) diagnosed with ALS. Cerebellar and posterior fossa dimensions were calculated using plain MR images. In addition, diffusion tensor imaging (DTI) was used to obtain white matter integrity measurements, represented as fractional anisotropy (FA) values, in the posterior limbs of internal capsules (PLIC) and middle cerebellar peduncles (MCPs). These measurements were compared to 36 healthy volunteers (11 men and 25 women with a mean age of 55.3 years). The study also assessed clinical data for correlations with cerebellar imaging findings.

Results. The linear measurements of the cerebellum did not differ between groups. However, the transverse cerebellar dimension (TCD) ratio to the maximum length of the posterior fossa (0.973 compared to 0.982, $t = -2.76$, $p < 0.01$) and FA value in both MCPs (0.67 compared to 0.65 and 0.69 compared to 0.67, $p < 0.05$) were significantly lower in ALS patients. No significant differences were found in FA value in the PLIC, and no significant correlations were observed between patient clinical characteristics and cerebellar damage.

Conclusions. This study provides evidence of cerebellar damage in adult ALS patients. These findings contribute to ALS understanding and highlight the importance of considering cerebellar involvement in the disease process. The results suggest that measuring the TCD ratio and FA value in both MCPs could be potential biomarkers for cerebellar damage in ALS patients.

Key words: cerebellum, magnetic resonance imaging, amyotrophic lateral sclerosis, fractional anisotropy, transverse cerebellar diameter

Background

Amyotrophic lateral sclerosis (ALS) affects both upper and lower motor neurons. Some non-motor symptoms may also be present, including extrapyramidal symptoms,¹ cerebellar signs² and dementia.^{3,4} This condition is characterized by the loss of cortical motor neurons and cortical atrophy of the motor cortex,⁵ leading to motor preparation and initiation difficulties. Compensation mechanisms are then activated in the premotor area, cerebellum and basal ganglia.^{6–8}

The cerebellum plays a crucial role in ALS, extending beyond motor control to various cognitive processes such as working memory, verbal fluency and emotion-affect control.^{9,10} Imaging studies have shown inconsistent data on cerebellar changes in ALS, with atrophy of the whole cerebellum, focal changes in specific lobules, changes in the integrity of cerebellar peduncles, and increased metabolism in various cerebellar regions being reported.^{2,11–15} Advanced magnetic resonance imaging (MRI) techniques, such as diffusion tensor imaging (DTI), enable the measurement of anisotropic diffusion of water molecules within tissue. By calculating the fractional anisotropy (FA) parameter, characteristic changes in brain tissues at the level of cellular microarchitecture can be depicted, as well as changes in apparently normal white matter that are not visible on conventional MRI.¹⁶

Objectives

The objective of this investigation was to ascertain the linear dimensions of the cerebellum and the posterior cranial fossa, and assess the association between these parameters and white matter integrity, gender, disease duration, and age in patients with ALS compared to healthy controls.

Materials and methods

This investigation employed a retrospective case-control design, utilizing standard diagnostic data documented in all patients diagnosed with ALS at the Department of Neurology of the University Clinical Hospital (Wrocław, Poland). The MRI examinations were conducted at the Department of Radiology of the same hospital. All participants provided informed consent. The approval of the local Bioethics Committee of Wrocław Medical University was obtained (approval No. 885/2022).

The study group

The study group consisted of 33 subsequent patients (16 women and 17 men with a mean age of 59.3 years, standard deviation (SD) ± 11.2 years) from the Department of Neurology, diagnosed with ALS between 2017 and 2018 based on the El Escorial criteria.¹⁷ Disease-related variables (type and duration of the disease and first symptoms)

were established based on medical records. The mean time of disease duration until the MRI examination was noted as 1.43 years (median: 1 year, range: 0.5–4 years).

Exclusion criteria included cerebrovascular events, neoplasm or paraneoplastic syndromes in a patient's medical history, present overt dementia, or extrapyramidal and cerebellar signs in the neurological examination.

Magnetic resonance imaging protocol

The MRI examinations for ALS patients and controls were conducted using a Signa HDx 1.5 Tesla MRI unit (GE Medical Systems, Chicago, USA) and a 16-channel head and spine (HNS) coil. A conventional brain MRI protocol was initially performed with the following sequences: sagittal and coronal T2 fast recovery spin echo (FRFSE), axial T1 spin echo (SE), axial T2 fast spin-echo (FSE), axial fluid-attenuated inversion recovery (FLAIR), axial diffusion-weighted imaging (DWI) SE-echo-planar imaging (EPI) sequences, and a gadolinium-enhanced three-dimensional-fast spoiled gradient-echo (3D-FSPGR) T1 sequence. Subsequently, linear measurements of the cerebellum were obtained from axial and sagittal T2-FSE sequences (Fig. 1). The transverse cerebellar diameter (TCD) and the maximum length of the posterior fossa were measured twice. To standardize the TCD to the head size, the ratio between 2 parameters (TCD and the maximum width of the posterior cranial fossa) was calculated and used as the fundamental parameter for further analyses.

Diffusion tensor imaging

Diffusion tensor imaging (DTI) examinations were performed using a single-shot (SS) EPI sequence in 25 different diffusion-encoding directions, with the following parameters: b-values = 0 and 1000 s/mm², transfer ratio (TR) = 8500 ms, time to echo (TE) = 100 ms, field of view (FOV) = 24 × 24 cm, and a matrix = 128 × 128 mm, with 2.5 mm-thick axial slices obtained parallel to the anterior and posterior commissures. The DTI data were post-processed on the Advantage Workstation 4.6 (GE Medical Systems) using Ready View software provided by the manufacturer. The FA values were evaluated bilaterally in the following white matter tracts: posterior limbs of internal capsules (PLIC) and middle cerebellar peduncles (MCP) in small, fixed-in-size and circular regions of interest (ROIs; size 25–30 mm²) were assessed by means of color-coded maps. The mean FA values out of 3 measurements were calculated.

The control group

Thirty-six healthy age-matched controls (25 women and 11 men with a mean age of 55.4 \pm 15.9 years) were recruited (volunteers, mainly hospital staff members) to obtain normal values for neuroimaging measurements.

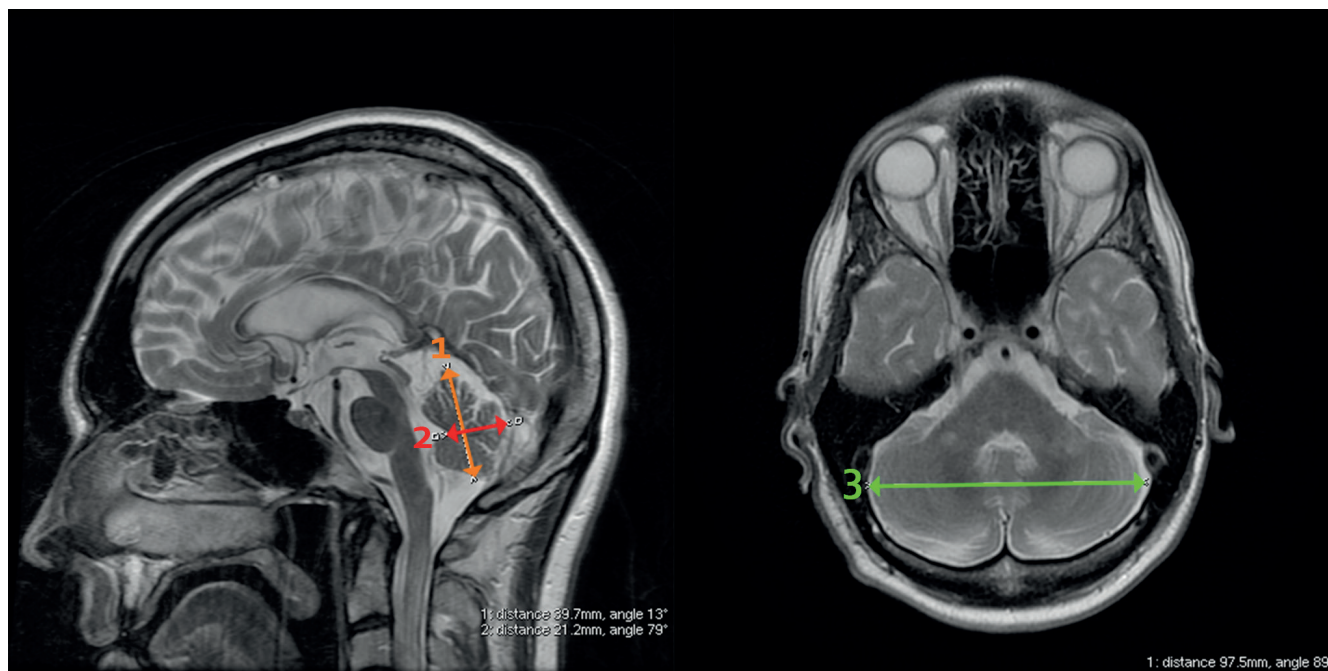


Fig. 1. Cerebellum linear measurements on T2-weighted sagittal and axial plains cerebellum height (1 – orange arrow), cerebellum width (2 – red arrow) and transverse cerebellar diameter (3 – green arrow).

Clinical–neuroimaging correlations

Measurements of the cerebellum and posterior fossa and DTI parameters were compared between patient and control groups. The ALS characteristics (onset of symptoms and disease duration) and the abovementioned variables were analyzed to identify potential correlations with cerebellar dimensions.

Statistical analyses

Statistical analyses employed STATISTICA PL v. 8 software (StatSoft Polska, Cracow, Poland). A p-value <0.05 was considered statistically significant. The normality of distribution for all continuous variables was verified with a Shapiro–Wilk test to select appropriate statistical methods. Comparisons between 2 independent groups were performed using Student’s t-test and the Mann–Whitney U test (Supplementary Table 1). A Kruskal–Wallis

analysis of variance (ANOVA) rank test compared categorical independent variables. Pearson’s correlation was used to assess clinical–radiological correlations.

Results

The measurements of the cerebellum in both groups are presented in Table 1. Although the posterior fossa dimension and transcerebellar diameter did not differ statistically, the calculated ratio (TCD/posterior fossa dimension) revealed a significant difference between ALS patients and controls (median: 0.978 compared to 0.984, U = 845.0, p = 0.002). The dimensions of the posterior fossa and TCD differed between male and female patients (107.7 mm compared to 103.3 mm, p < 0.005, and 104.5 mm compared to 100.8 mm, p < 0.01, respectively). The TCD showed a significant correlation with age (r = –0.38, p < 0.05). The ratio of the TCD/posterior

Table 1. Basic characteristics of the cerebellar linear measurements in patient and control groups

Parameter	Patients (n = 33)			Controls (n = 36)			p-value (used test)
	mean [mm]	median [mm]	95% CI/Q1–Q3	mean [mm]	median [mm]	95% CI/Q1–Q3	
Posterior fossa dimension	105.5	105.3	103.99; 107.07	106.5	105.5	105.1; 108.0	0.33 (Student’s t)
Transcerebellar diameter (TCD)	102.7	103.0	101.3; 104.2	104.4	104.8	103.0; 105.8	0.1 (Student’s t)
Cerebellar width	46.4	47.0	45.2; 47.2	46.4	46.7	45.5; 47.3	0.95 (Student’s t)
Cerebellar height	25.8	25.1	23.9–26.9	26.0	26.2	23.9–27.9	0.42 (Mann–Whitney U)

95% CI – 95% confidence interval; Q1 – 1st quartile; Q3 – 3rd quartile; TCD – transverse cerebellar dimension.

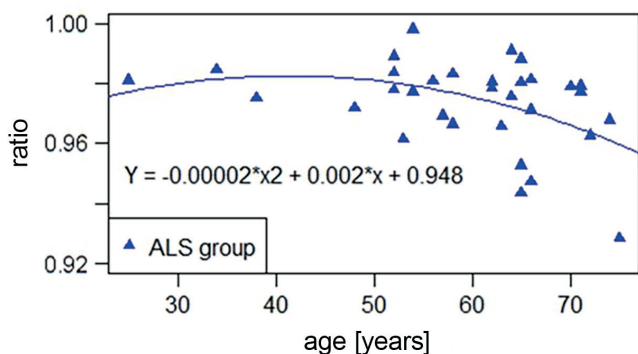


Fig. 2. Correlation of the ratio of transverse cerebellar dimension (TCD) measurements to the posterior fossa dimension in relation to age in amyotrophic lateral sclerosis (ALS) patients

fossa dimension significantly correlated with the age of the patients ($S = -0.370$, $p < 0.05$) (Fig. 2). Analysis of the correlation between age and TCD/posterior fossa ratio was significant only in the ALS group. As the ratio of the TCD/posterior fossa dimension did not have a normal distribution in either group, a Spearman's rank correlation test was used. In the control group, the rho value was -0.324 , corresponding to a p-value of 0.053, slightly above the assumed significance level of 0.05. In the ALS group, Spearman's rank correlation rho was -0.370 , corresponding to a p-value of 0.034. A series of fitting several polynomial regression models, from 1 up to 5 degrees, were conducted to assess the nature of the relationship. The calculated adjusted R^2 of each model was the highest for the second-degree polynomial, which had an adjusted R^2 of 0.132. The p-value for the selected model as a whole was 0.046. The coefficient estimates and 95% confidence intervals (95% CIs) are presented in Supplementary Table 2. No other correlations for cerebellar linear measurements and sex, age or duration of the disease and its first symptoms were found.

The FA values were significantly different between controls and patients in both MCPs but not at the level of the internal capsules (Table 2). Strong correlations were found between FA values in the PLIC on both sides ($S = 0.49$, $p < 0.005$ (Spearman's correlation)) and FA in MCP on both sides. No correlation was found between linear cerebellum measurements and FA values in ALS patients.

Discussion

The method used in this study (i.e., linear measurements were easily performed on axial and sagittal T2-FSE) proved simple, effective and feasible for all subjects. The TCD alone showed sexual dimorphism, a typical observation during the developmental period but not uniformly found in mature brains.^{18,19} In turn, the TCD/posterior fossa dimension ratio had a nonlinear correlation with age in healthy and patient groups. Since TCD correlated significantly with age, a change in the ratio occurred due to atrophy of the cerebellum, which has also been described by other authors using both linear and volumetric measurements.^{20–23}

The TCD/posterior fossa ratio decreased with age significantly faster in patients than in controls, which would be consistent with observations of most authors describing the decrease in the cerebellum or individual cerebellar lobes and brainstem size or volume, with the degree of atrophy varying according to the form of motor neuron disease, the severity of motor disturbances, and the presence of behavioral and cognitive dysfunctions.^{24–27} In contrast, some authors report no significant abnormalities in cerebellar volumetric measurements.^{28,29} Several factors contribute to the variability of our findings, with emerging evidence that genetic and sporadic ALS differ in their imaging signature.^{2,13} There is a significant association between cerebellar atrophy in ALS combined with frontotemporal dementia (FTD) or carrying C9orf72 hexanucleotide repeat expansion in patients who already show some cognitive impairment (ALSci), as opposed to patients presenting with more behavioral abnormalities (ALSbi).^{13,30,31} Patients with ALS-ataxia continuum symptoms do not display such abnormalities.¹³

The various patterns of white matter integrity change observed using DTI in ALS patients need to be emphasized because they may offer unique insights into the neurodegeneration processes and ALS pathophysiology. The measurements of FA values in the PLIC and MCP, which include the corticopontocerebellar pathway, showed significant differences between patients and healthy controls in the MCP but not at the level of the PLIC. Other authors have demonstrated a significantly decreased FA value at the pyramidal pathways and, in some cases, at the MCP

Table 2. Diffusion tensor imaging (DTI) measurements of fractional anisotropy (FA) on both sides of posterior limbs of internal capsules (PLIC) and middle cerebellar peduncles (MCP) in patients and controls

Region	Patients (n = 33)			Controls (n = 36)			p-value (used test)
	mean FA	median	95% CI/Q1–Q3	mean FA	median	95% CI/Q1–Q3	
MCP right	0.67	0.68	0.66; 0.69	0.65	0.64	0.64; 0.66	<0.001 (Student's t)
MCP left	0.69	0.69	0.67; 0.71	0.67	0.67	0.66; 0.68	0.052 (Welch's t)
PLIC right	0.62	0.62	0.61; 0.63	0.63	0.63	0.62; 0.64	0.23 (Student's t)
PLIC left	0.64	0.63	0.62; 0.65	0.64	0.64	0.62; 0.66	0.29 (Mann–Whitney U)

95% CI – 95% confidence interval; Q1 – 1st quartile; Q3 – 3rd quartile.

level.^{32–38} Our findings, together with the atrophy phenomenon discussed earlier, suggest the simultaneous occurrence of cerebellar degeneration and loss of the integrity of pathways connecting this structure with other brain regions. Our study also indicates that this process occurs at a different rate and somewhat independently of pyramidal tract degeneration, consistent with coexisting degenerative and compensatory processes postulated in other papers.^{6,8,39} This alternation of cerebrocerebellar connectivity^{8,28,36,40–42} underscores the importance of understanding the complex and multifactorial nature of ALS pathology.

Limitations

Although our results are easily accessible and encouraging, the study had some limitations. First, the retrospective design and relatively small number of patients included in our study limited the number of examination techniques. Second, the patients could have diverse clinical phenotypes and severity levels of the disease, which may have resulted in various predispositions to cerebellar abnormalities.^{13,43,44} Third, the measurements were done using certified software provided by the MRI manufacturer, reducing the potential number of measurements to those that are relatively simple. Despite these limitations, our study provides important insights into the specific patterns of cerebellar damage in ALS patients. Our method was simple and can be improved in further longitudinal projects.

Conclusions

This study shows that a simple MRI measurement might reveal accelerated cerebellar atrophy in ALS patients, which correlates with reduced white matter integrity in the cerebellar afferent pathways. Our results highlight the importance of cerebellar pathology in these patients.

Supplementary data

The Supplementary materials are available at <https://doi.org/10.5281/zenodo.8321084>. The package consists of the following files:


Supplementary Table 1. Normality and variance tests.


Supplementary Table 2. Coefficient estimates together with 95% CI for polynomial regression models of correlation of the age and ratio of the TCD to the dimension of the posterior fossa.

ORCID iDs

Marta Nowakowska-Kotas  <https://orcid.org/0000-0002-3173-8337>

Adrian Korbecki  <https://orcid.org/0000-0003-0047-9819>

Sławomir Budrewicz  <https://orcid.org/0000-0002-2044-6347>

Joanna Bladowska  <https://orcid.org/0000-0003-0597-8457>

References

- Pradat PF, Bruneteau G, Munerati E, et al. Extrapyramidal stiffness in patients with amyotrophic lateral sclerosis. *Mov Disord*. 2009;24(14):2143–2148. doi:10.1002/mds.22762
- Prell T, Grosskreutz J. The involvement of the cerebellum in amyotrophic lateral sclerosis. *Amyotroph Lateral Scler Frontotemporal Degener*. 2013;14(7–8):507–515. doi:10.3109/21678421.2013.812661
- Mackenzie IRA, Frick P, Neumann M. The neuropathology associated with repeat expansions in the *C9ORF72* gene. *Acta Neuropathol*. 2014;127(3):347–357. doi:10.1007/s00401-013-1232-4
- Strong MJ, Abrahams S, Goldstein LH, et al. Amyotrophic lateral sclerosis-frontotemporal spectrum disorder (ALS-FTSD): Revised diagnostic criteria. *Amyotroph Lateral Scler Frontotemporal Degener*. 2017;18(3–4):153–174. doi:10.1080/21678421.2016.1267768
- Bede P, Bokde A, Elamin M, et al. Grey matter correlates of clinical variables in amyotrophic lateral sclerosis (ALS): A neuroimaging study of ALS motor phenotype heterogeneity and cortical focality. *J Neurol Neurosurg Psychiatry*. 2013;84(7):766–773. doi:10.1136/jnnp-2012-302674
- Proudfoot M, Bede P, Turner MR. Imaging cerebral activity in amyotrophic lateral sclerosis. *Front Neurol*. 2019;9:1148. doi:10.3389/fneur.2018.01148
- Mohammadi B, Kollwe K, Cole DM, et al. Amyotrophic lateral sclerosis affects cortical and subcortical activity underlying motor inhibition and action monitoring. *Hum Brain Mapp*. 2015;36(8):2878–2889. doi:10.1002/hbm.22814
- Abidi M, De Marco G, Couillandre A, et al. Adaptive functional reorganization in amyotrophic lateral sclerosis: Coexisting degenerative and compensatory changes. *Eur J Neurol*. 2020;27(1):121–128. doi:10.1111/ene.14042
- Argyropoulos GPD, Van Dun K, Adamaszek M, et al. The cerebellar cognitive affective/Schmahmann syndrome: A Task Force paper. *Cerebellum*. 2020;19(1):102–125. doi:10.1007/s12311-019-01068-8
- Kozioł LF, Budding D, Andreasen N, et al. Consensus paper: The cerebellum's role in movement and cognition. *Cerebellum*. 2014;13(1):151–177. doi:10.1007/s12311-013-0511-x
- Christidi F, Karavasilis E, Riederer F, et al. Gray matter and white matter changes in non-demented amyotrophic lateral sclerosis patients with or without cognitive impairment: A combined voxel-based morphometry and tract-based spatial statistics whole-brain analysis. *Brain Imaging Behav*. 2018;12(2):547–563. doi:10.1007/s11682-017-9722-y
- Cistaro A, Valentini MC, Chiò A, et al. Brain hypermetabolism in amyotrophic lateral sclerosis: A FDG PET study in ALS of spinal and bulbar onset. *Eur J Nucl Med Mol Imaging*. 2012;39(2):251–259. doi:10.1007/s00259-011-1979-6
- Bede P, Chipika RH, Christidi F, et al. Genotype-associated cerebellar profiles in ALS: Focal cerebellar pathology and cerebro-cerebellar connectivity alterations. *J Neurol Neurosurg Psychiatry*. 2021;92(11):1197–1205. doi:10.1136/jnnp-2021-326854
- Prudlo J, Bißbort C, Glass A, et al. White matter pathology in ALS and lower motor neuron ALS variants: A diffusion tensor imaging study using tract-based spatial statistics. *J Neurol*. 2012;259(9):1848–1859. doi:10.1007/s00415-012-6420-y
- Trojsi F, Di Nardo F, D'Alvano G, et al. Resting state fMRI analysis of pseudobulbar affect in amyotrophic lateral sclerosis (ALS): Motor dysfunction of emotional expression. *Brain Imaging Behav*. 2023;17(1):77–89. doi:10.1007/s11682-022-00744-4
- Bladowska J, Zimny A, Kołtowska A, et al. Evaluation of metabolic changes within the normal appearing gray and white matters in neurologically asymptomatic HIV-1-positive and HCV-positive patients: Magnetic resonance spectroscopy and immunologic correlation. *Eur J Radiol*. 2013;82(4):686–692. doi:10.1016/j.ejrad.2012.11.029
- Brooks BR, Miller RG, Swash M, Munsat TL. El Escorial revisited: Revised criteria for the diagnosis of amyotrophic lateral sclerosis. *Amyotroph Lateral Scler Other Motor Neuron Disord*. 2000;1(5):293–299. doi:10.1080/146608200300079536
- Imamoglu EY, Gursoy T, Ovali F, Hayran M, Karatekin G. Nomograms of cerebellar vermis height and transverse cerebellar diameter in appropriate-for-gestational-age neonates. *Early Hum Dev*. 2013;89(12):919–923. doi:10.1016/j.earlhumdev.2013.10.001
- Co E, Raju TN, Aldana O. Cerebellar dimensions in assessment of gestational age in neonates. *Radiology*. 1991;181(2):581–585. doi:10.1148/radiology.181.2.1924808

20. Captier G, Boë LJ, Badin P, Guihard-Costa AM, Canovas F, Larroche JC. Modèles géométriques de croissance du cerveau, cervelet, tronc cérébral et modification des angles de la base du crâne au cours de la période foétale. *Morphologie*. 2013;97(317):38–47. doi:10.1016/j.morpho.2012.12.002
21. Luft AR. Patterns of age-related shrinkage in cerebellum and brainstem observed in vivo using three-dimensional MRI volumetry. *Cereb Cortex*. 1999;9(7):712–721. doi:10.1093/cercor/9.7.712
22. Raz N, Schmiedek F, Rodrigue KM, Kennedy KM, Lindenberger U, Lövdén M. Differential brain shrinkage over 6 months shows limited association with cognitive practice. *Brain Cogn*. 2013;82(2):171–180. doi:10.1016/j.bandc.2013.04.002
23. Han S, An Y, Carass A, Prince JL, Resnick SM. Longitudinal analysis of regional cerebellum volumes during normal aging. *NeuroImage*. 2020;220:117062. doi:10.1016/j.neuroimage.2020.117062
24. Bede P, Chipika RH, Finegan E, et al. Brainstem pathology in amyotrophic lateral sclerosis and primary lateral sclerosis: A longitudinal neuroimaging study. *NeuroImage Clin*. 2019;24:102054. doi:10.1016/j.nicl.2019.102054
25. Querin G, El Mendili MM, Lenglet T, et al. Spinal cord multi-parametric magnetic resonance imaging for survival prediction in amyotrophic lateral sclerosis. *Eur J Neurol*. 2017;24(8):1040–1046. doi:10.1111/ene.13329
26. Whitwell JL, Weigand SD, Boeve BF, et al. Neuroimaging signatures of frontotemporal dementia genetics: C9ORF72, tau, progranulin and sporadics. *Brain*. 2012;135(3):794–806. doi:10.1093/brain/aws001
27. Consonni M, Dalla Bella E, Nigri A, et al. Cognitive syndromes and C9orf72 mutation are not related to cerebellar degeneration in amyotrophic lateral sclerosis. *Front Neurosci*. 2019;13:440. doi:10.3389/fnins.2019.00440
28. Bharti K, Khan M, Beaulieu C, et al. Involvement of the dentate nucleus in the pathophysiology of amyotrophic lateral sclerosis: A multi-center and multi-modal neuroimaging study. *NeuroImage Clin*. 2020;28:102385. doi:10.1016/j.nicl.2020.102385
29. Schönecker S, Neuhofer C, Otto M, et al. Atrophy in the thalamus but not cerebellum is specific for C9orf72 FTD and ALS patients: An Atlas-based volumetric MRI study. *Front Aging Neurosci*. 2018;10:45. doi:10.3389/fnagi.2018.00045
30. Kim HJ, Oh SI, De Leon M, et al. Structural explanation of poor prognosis of amyotrophic lateral sclerosis in the non-demented state. *Eur J Neurol*. 2017;24(1):122–129. doi:10.1111/ene.13163
31. Shen D, Hou B, Xu Y, et al. Brain structural and perfusion signature of amyotrophic lateral sclerosis with varying levels of cognitive deficit. *Front Neurol*. 2018;9:364. doi:10.3389/fneur.2018.00364
32. Cosottini M, Giannelli M, Siciliano G, et al. Diffusion-tensor MR imaging of corticospinal tract in amyotrophic lateral sclerosis and progressive muscular atrophy. *Radiology*. 2005;237(1):258–264. doi:10.1148/radiol.2371041506
33. Li J, Pan P, Song W, Huang R, Chen K, Shang H. A meta-analysis of diffusion tensor imaging studies in amyotrophic lateral sclerosis. *Neurobiol Aging*. 2012;33(8):1833–1838. doi:10.1016/j.neurobiolaging.2011.04.007
34. Verstraete E, Polders DL, Mandl RCW, et al. Multimodal tract-based analysis in ALS patients at 7T: A specific white matter profile? *Amyotroph Lateral Scler Frontotemporal Degener*. 2014;15(1–2):84–92. doi:10.3109/21678421.2013.844168
35. Zhang F, Chen G, He M, et al. Altered white matter microarchitecture in amyotrophic lateral sclerosis: A voxel-based meta-analysis of diffusion tensor imaging. *NeuroImage Clin*. 2018;19:122–129. doi:10.1016/j.nicl.2018.04.005
36. Menke RAL, Proudfoot M, Wu J, et al. Increased functional connectivity common to symptomatic amyotrophic lateral sclerosis and those at genetic risk. *J Neurol Neurosurg Psychiatry*. 2016;87(6):580–588. doi:10.1136/jnnp-2015-311945
37. De Marchi F, Stecco A, Falaschi Z, et al. Detection of white matter ultrastructural changes for amyotrophic lateral sclerosis characterization: A diagnostic study from Dti-derived data. *Brain Sci*. 2020;10(12):996. doi:10.3390/brainsci10120996
38. Budrewicz S, Szewczyk P, Bładowska J, et al. The possible meaning of fractional anisotropy measurement of the cervical spinal cord in correct diagnosis of amyotrophic lateral sclerosis. *Neurol Sci*. 2016;37(3):417–421. doi:10.1007/s10072-015-2418-4
39. Qiu T, Zhang Y, Tang X, et al. Precentral degeneration and cerebellar compensation in amyotrophic lateral sclerosis: A multimodal MRI analysis. *Hum Brain Mapp*. 2019;40(12):3464–3474. doi:10.1002/hbm.24609
40. Tu S, Menke RAL, Talbot K, Kiernan MC, Turner MR. Cerebellar tract alterations in PLS and ALS. *Amyotroph Lateral Scler Frontotemporal Degener*. 2019;20(3–4):281–284. doi:10.1080/21678421.2018.1562554
41. Keil C, Prell T, Peschel T, Hartung V, Dengler R, Grosskreutz J. Longitudinal diffusion tensor imaging in amyotrophic lateral sclerosis. *BMC Neurosci*. 2012;13(1):141. doi:10.1186/1471-2202-13-141
42. Barry RL, Babu S, Anteraper SA, et al. Ultra-high field (7T) functional magnetic resonance imaging in amyotrophic lateral sclerosis: A pilot study. *NeuroImage Clin*. 2021;30:102648. doi:10.1016/j.nicl.2021.102648
43. Bede P, Bokde ALW, Byrne S, et al. Multiparametric MRI study of ALS stratified for the C9orf72 genotype. *Neurology*. 2013;81(4):361–369. doi:10.1212/WNL.0b013e31829c5eee
44. DeJesus-Hernandez M, Mackenzie IR, Boeve BF, et al. Expanded GGGGCC hexanucleotide repeat in noncoding region of C9ORF72 causes chromosome 9p-linked FTD and ALS. *Neuron*. 2011;72(2):245–256. doi:10.1016/j.neuron.2011.09.011